Conventional Concentrically Braced Frames with I-shape Braces and Bolted Brace Connections

by

CHEN WANG

Department of Civil Engineering

McGill University

Montréal, Québec, Canada

April 2021

A thesis submitted to McGill University in partial fulfillment of the requirements of the degree of

Doctor of Philosophy

ABSTRACT

In low and moderate seismic regions, low-ductility concentrically braced frames (CBFs) are widely used as the seismic force-resisting system for steel structures. Unlike high-ductility CBFs, the capacity-based design principle and additional seismic detailing are not required for such systems, which are referred to as conventional CBFs (CCBFs) in this study. In CCBFs, the brace-to-gusset connections are inherently weaker than the adjoining gusset plates and braces when loaded in tension. This occurs because both the gusset plates and the braces are most often selected based on their respective compressive buckling resistances, and hence, typically have a much greater resistance in tension. As such, brace connections are critical for the seismic behaviour and collapse prevention performance of CCBFs. However, brace connections have received little research attention because they are usually assumed to remain elastic in most capacity-based designs, and as such, their inelastic behaviour is not fully understood at a fundamental level. This is reflected in the different code provisions: in Canada, the seismic design force must be amplified by 1.5 for brace connections in CCBFs unless these connections are proven to be ductile as per CSA S16-19; in New Zealand, for connections in CCBFs, a structural performance factor of 1.0 is required, compared with 0.9 for structural members, which effectively increases the seismic design force demand on connections as per NZS 3404; no analogous requirements exist for CCBFs in the USA as per ANSI/AISC 341-16 or in Europe as per Eurocode 8.

The inelastic behaviour of and the seismic deformation demand on CCBF brace connections were studied through a two-level numerical simulation approach, which is presented in this thesis. The bolted flange plate connection of the I-shape brace, which is a common design choice for CCBFs, was selected as the subject of this study.

At the connection level, a high-fidelity finite element (FE) simulation procedure was developed for the bolted flange plate connection and validated against laboratory test results. The force transfer mechanism within the branches of the connection was characterized. Subsequently, a parametric study based on the validated numerical simulation procedure was carried out. Three key design parameters, namely, the gusset plate thickness, the flange lap plate thickness, and the web lap plate thickness, were varied to study their effects on both the compressive and tensile behaviour of the brace and the connection assembly. Various deformation mechanisms and failure modes were revealed under both compression and tension. Design recommendations are proposed with regards to attaining better deformation capacity.

Based on the knowledge gained from the high-fidelity numerical simulations, a computationally efficient component-based modeling method was developed for the bolted brace connection. The connection was discretized into individual components, and modeled by means of organized springs, which each simulate the behaviour of a component. After validation against experimental test results, the component-based connection model was incorporated into a system-level numerical model for a series of prototype CCBFs. Through nonlinear static and dynamic structural analyses, the seismic behaviour and collapse prevention performance of CCBFs were studied. When loaded in tension, the brace connections deformed much more than the brace, and amplifying the design force by 1.5 was effective in reducing the seismic deformation demand on brace connections. In some cases, a secondary seismic force-resisting mechanism developed and prevented the system from collapse after the primary seismic force-resisting mechanism had failed.

RÉSUMÉ

Dans les régions à bas et modéré aléa sismique, les cadres à contreventement concentrique (CCC) à basse ductilité sont souvent employés comme système de reprise des charges latérales des structures en acier. Contrairement aux CCC à haute ductilité, ce type de cadre, appelé ici CCC conventionnel (CCCC), ne requiert pas l'application des principes de conception par capacité ni de détails parasismiques additionnels. Dans les CCCC, les connexions entre les diagonales et les goussets sont moins résistantes que les diagonales lorsque soumises à des charges de traction. Ceci est dû au fait que les dimensions des goussets et des diagonales sont définies en fonction de leur résistance au flambement, ce qui leur confère une résistance plus haute à la traction. Les connexions des diagonales sont déterminantes en ce qui concerne la performance sismique et la prévention de l'écroulement des CCCC. Or, elles ont été délaissées par la recherche car il est souvent supposé que leur réponse est élastique, ce qui fait que leur comportement inélastique ne soit pas bien compris. Cela se reflète dans les normes de conception : au Canada, la charge sismique de conception des connexions des CCCC doit être amplifiée par un facteur de 1.5 à moins qu'il soit démontré qu'elles sont ductiles tel qu'établit par norme CSA S16-19; en Nouvelle-Zélande, la norme NZS 3404 requiert l'emploi d'un facteur de performance structurelle de 1.0 pour les connexions des CCCC, au lieu de 0.9 comme pour le reste de la structure, ce qui accroît les charges de conception sur les connexions. Ni la norme ANSI/AISC 341-16 aux États-Unis ni l'Eurocode 8 en Europe comportent de telles exigences pour les CCCC.

Dans cette thèse, le comportement inélastique et la demande en déformation des connexions des diagonales des CCCC ont été étudiés par l'entremise d'une approche de simulation numérique de

deux niveaux. Les connexions boulonnées de diagonales en profilés en I au moyen de plaques de renfort soudées aux ailes, un choix fréquent dans les CCCC, ont été choisies comme sujet d'étude.

Au niveau de la connexion, une procédure de simulation à éléments finis d'haute-fidélité a été développé pour la connexion boulonnée de l'aile avec plaque de renfort et validée contre des résultats d'essais. Le mécanisme de transfert des charges a été caractérisé. Ensuite, une étude paramétrique basée sur la procédure de simulation numérique a été menée. L'influence de trois paramètres sur la réponse de la diagonale et de l'assemblage de la connexion a été étudiée: l'épaisseur de la plaque du gousset, l'épaisseur de la plaque de renfort de l'aile et l'épaisseur de la plaque de renfort de l'âme. Plusieurs mécanismes de déformation et modes de défaillance. Des recommandations pour la conception sont proposées.

Dérivée de l'expérience acquise avec les simulations numériques, une méthode de modélisation basée sur les composants efficiente computationnellement a été développée pour la connexion boulonnée des diagonales. La connexion est discrétisée en composants individuels et modélisée par le biais de ressorts organisés, chacun simulant le comportement d'un des composants. Par suite d'une validation contre des données expérimentales, le modèle de connexion a été incorporé dans un modèle numérique au niveau-système pour une série de CCCC prototypes. Au moyen d'analyses structurelles non-linéaires statiques et dynamiques, la performance sismique et de prévention de l'écroulement des CCCC a été étudiée. Lorsque soumises à des charges de traction, les connexions ont présenté des déformations beaucoup plus hautes que la diagonale et l'amplification de la charge de conception par 1.5 a été effective pour réduire la demande en déformation sur les connexions. Dans certains cas, un mécanisme secondaire de résistance aux forces sismiques s'est développé et a évité l'écroulement du système à la suite de la défaillance du mécanisme primaire de résistance aux forces sismiques.

ACKNOWLEDGMENTS

First and foremost, I would like to express my deepest gratitude to my supervisor, Prof. Colin A. Rogers, for his patient guidance, encouragement, and support throughout this program. It has been definitely a privilege to have a supervisor who cares so much about my work and responds promptly to my questions and requests. I am also grateful to Prof. Robert Tremblay for his invaluable co-supervision on this study. This thesis would not be possible without his insightful knowledge, vision, and comments.

I would like to thank DPHV Structural Consultants and ADF Group Inc. for their generous technical and financial support, as well as the Natural Sciences and Engineering Research Council of Canada (NSERC), the Fonds de Recherche du Québec – Nature et Technologies (FRQ-NT), and the Centre d'Études Interuniversitare des Structures sous Charges Extrêmes (CEISCE). I would also like to thank China Scholarship Council (CSC) for the financial support.

I am very grateful to Calcul Quebec and Compute Canada for access to the high-performance supercomputer, which greatly enhanced my research progress.

I would like to thank my colleagues Andrés González Ureña and Mohamed Afifi for all the fruitful discussions and casual talks that made my time in the office enjoyable. A special thanks to Alina Rudman for sharing the experimental test data. I also appreciate the help from Bashar Hariri at Polytechnique Montreal in ground motion record selection and scaling.

Lastly but most importantly, I would like to thank my family for all the love and support they have provided. To my parents and sister, as I would not be where I am today without them. To my wife, Yue Chu, for always being supportive and believing in me.

PREFACE

This thesis is presented in a manuscript-based format in accordance with the Thesis Guidelines from Graduate and Postdoctoral Studies, McGill University. It comprises three journal papers, in addition to the chapters corresponding to the Introduction, Literature Review, and Summary and Conclusions. The contributions of each author to the included manuscripts are as follows.

Chapter 3:

Chen Wang, Alina Rudman, Robert Tremblay, Colin A. Rogers. Numerical Investigation into I-shape Brace Connections of Conventional Concentrically Braced Frames. *Engineering Structures*, Volume 236, 2021, 112091, ISSN 0141-0296, https://doi.org/10.1016/j.engstruct.2021.112091.

- Chen Wang conducted the numerical simulations and wrote the manuscript.
- Alina Rudman provided the laboratory test data for validation of numerical models.
- Robert Tremblay assisted in supervision of the research and provided editing of the manuscript.
- Colin A. Rogers provided supervision of the research and provided editing of the manuscript.

Chapter 4:

Chen Wang, Robert Tremblay, Colin A. Rogers. Parametric Study on the I-shape Brace Connection of Conventional Concentrically Braced Frames. *Journal of Constructional Steel Research*, Volume 182, 2021, 106669, ISSN 0143-974X, https://doi.org/10.1016/j.jcsr.2021.106669.

- Chen Wang conducted the numerical simulations and wrote the manuscript.

- Robert Tremblay assisted in supervision of the research and provided editing of the manuscript.
- Colin A. Rogers provided supervision of the research and provided editing of the manuscript.

Chapter 5:

Chen Wang, Robert Tremblay, Colin A. Rogers. Component-Based Model for Bolted Brace Connections in Conventional Concentrically Braced Frames. *Engineering Structures* (Submitted).

- Chen Wang proposed the modeling method, conducted the numerical simulations, and wrote the manuscript.
- Robert Tremblay assisted in supervision of the research and provided editing of the manuscript.
- Colin A. Rogers provided supervision of the research and provided editing of the manuscript.

The original scholarship and distinct contributions of this thesis are as follows:

- Characterization of seismic behaviour for the bolted I-shape brace connection specific to Conventional Concentrically Braced Frames (CCBFs)
- Comprehensive evaluation of the critical connection design parameters on both the tensile and compressive behaviour of the I-shape brace and bolted brace connections
- Development of recommendations to prevent bolt and weld failure and to promote inelastic deformation capacity for the bolted I-shape brace connection
- Development of the component-based modeling method for bolted brace connections

- Seismic performance evaluation of CCBFs with I-shape braces and bolted brace connections
- Quantification of bolted I-shape brace connection deformations in CCBFs under severe earthquakes

TABLE OF CONTENTS

LIST OF FIGURES

LIST OF TABLES

CHAPTER 1: INTRODUCTION

1.1. RESEARCH PROBLEM AND MOTIVATION

Steel concentrically braced frames (CBFs) are widely used as seismic force-resisting systems. Different design methods have been developed for the seismic design of steel CBFs with different levels of expected system ductility. In areas of low and moderate seismic hazard, low-ductility CBFs using a simple design method are permitted in many countries. Under the simple design framework, the earthquake load effects are calculated using a linear elastic structural analysis method; all the structural members and connections are designed to resist the calculated earthquake load effects; no capacity-based design or additional seismic detailing are required. In this study, such CBFs are referred to as Conventional Concentrically Braced Frames (CCBFs). CCBFs are expected to have low ductility, and therefore higher seismic design loads are generally assigned. However, due to the exemption of the capacity-based design and seismic detailing requirements, CCBFs are usually the more economical choice in low and moderate seismic regions compared to their more ductile counterparts. Furthermore, the elastic based design approach is much simpler and less time consuming compared with that used for the design of ductile CBFs, which allows for cost savings in terms of engineering hours.

Owning to the simple design and economy, CCBFs are readily used in low and moderate seismic regions around the world. In Canada, a type of CBF, namely Type Conventional Construction (CC) CBF, is permitted in CSA S16 (CSA, 2019). Capacity design and seismic detailing are not required for structural members of Type CC systems, but a 1.5-times amplification is required for the design seismic force of the brace connections if these connections are not proven to be ductile. In the USA, CBFs categorized as “systems not specifically detailed for seismic resistance” in ASCE/SEI

7-16 (ASCE, 2016) are prevalent in regions of low and moderate seismic hazard. A relatively lower seismic force reduction factor, R=3, is assigned to such systems to account for their low expected ductility. Similarly, in Europe, CBFs designed with Structural Ductility Class DCL (low) are permitted in low seismicity cases per Eurocode 8 (EN 1998-1, 2004). Due to the low dissipative structural behaviour, a country specific low behavioural factor ($1.5 \leq q \leq 2.0$) is recommended for such systems. For CBFs in New Zealand, the seismic design could be conducted with ductility classified as Category 4. A low level of structural ductility is expected from such systems; as such, a low structural ductility factor (μ=1) is assigned in NZS 3404 (NZS, 2007). For connections in Category 4 CBFs, a greater structural performance factor (S_p) of 1.0 is required, compared with 0.9 for structural members, which effectively increases the design force demand for connections. It is worth noting that in some countries, e.g. China (GB50017, 2017) and Japan (AIJ, 2012), the low-ductility CCBFs are not permitted in seismic design. CBFs are instead required to be designed as ductile systems having a hierarchy of resistances as dictated by capacity-based design provisions.

In CBFs, brace connections can be further divided into two parts: the brace-to-gusset connection and the gusset plate. The two parts work in series, and the failure of either of them will result in significant loss of the system's lateral stiffness and strength (Astaneh-Asl, 1998). Previous studies on brace connections have mainly focused on the gusset plates, as the brace-to-gusset connections usually will not fail with the protection of capacity design. The tensile behaviour of gusset plates has been extensively studied over the years, e.g. Whitmore (1952), Chakrabarti & Bjorhovde (1985), Huns et al. (2006), and Teh & Elliott (2019), among others. Under seismic loading, the gusset plates could also be subjected to compressive loads, and are prone to buckling. The compressive instability issue has been studied by Thornton (1984), Cheng et al. (1994), and Yam & Cheng (2002). The Whitmore effective width and the so-called Thornton model are still

commonly used in gusset plate design practice. To accommodate the brace end rotation upon brace buckling, Astaneh-Asl et al. (2006) proposed to leave a 2*t* (*t*=thickness of the gusset plate) clearance in the gusset plate. Lehman et al. (2008) pointed out that the 2*t* clearance might result in uneconomical gusset plate designs and inferior performance, and proposed the elliptical clearance model. From the perspective of the global system performance, a balanced design procedure was proposed by Roeder et al. (2011) for the gusset plate connection design, which aimed to maximize the system ductility by encouraging more desirable yielding mechanisms and suppressing undesirable failure modes.

However, in CCBFs, the brace-to-gusset connections are weaker than the adjoining gusset plates and braces, and vulnerable to fracture. This is because under the CCBF design framework, the brace-to-gusset connection, and the adjoining brace and gusset plate, are designed to resist the same force demand. Braces and gusset plates are generally selected and designed based on their compressive buckling resistances, while brace-to-gusset connections are not. As such, when loaded in tension, braces and gusset plates can usually sustain greater forces than the brace-to-gusset connections. Sen et al. (2016, 2017) experimentally studied older CBFs that were designed without the capacity-based design principle. The brace-to-gusset weld fracture was found at low storey drift; they concluded that the brace-to-gusset connection is of high priority in terms of the retrofit. The seismic performance of low-ductility CBFs in the USA (including the *R*=3 CBFs) was studied by Bradley et al. (2017) and Sizemore et al. (2017, 2019). They found that the brace-gusset weld fracture was the dominant limit state, and the as-built weld overstrength significantly affected the damage locations.

I-shape braces and bolted brace connections are commonly used in the design of CCBFs as more section choices are available and faster construction can be attained. To study the seismic

behaviour and performance of bolted I-shape brace connections in CCBFs, Rudman (2018) and Rudman et al. (2021) experimentally tested a series of full-scale I-shape brace and connection assemblies under reversed cyclic loading. Significant plasticity and ultimate failure occurred in the brace-to-gusset connections when the specimens were loaded in tension, which confirmed that the bolted brace-to-gusset connection was weaker in tension than the adjoining braces and gusset plates. Some specimens exhibited promising deformation capacities under cyclic loading. However, high variability of the connection deformation capacity (with the corresponding storey drift ratios ranging from 0.01 to 0.02) and various failure modes were observed. Most importantly, some observed failure modes were different from those predicted by the code prescribed design equations, which indicated that the behaviour of the tested brace connections was not fully understood. Due to the limitation of measurement instrumentation in the experimental tests, the seismic behaviour of the tested brace connections was still unclear, and as such, an accurate numerical study was needed to further examine the response of these CCBF systems to seismic loading.

Without the capacity-based design requirement, no individual component in a CCBF is explicitly designated to sustain plastic deformations under seismic loadings. Past system-level experimental tests of CCBFs (Sen et al., 2016; Bradley et al., 2017; Simpson & Mahin, 2018) exhibited various structural behaviour and failures in different locations. The reserve capacity, which refers to the lateral force-resisting capacity outside the primary seismic force-resisting system, has been shown to play a crucial role in the collapse prevention performance of CCBFs under severe earthquakes (Hines et al., 2009; Li et al., 2018; Sizemore et al., 2019). Through a numerical study of a 3-storey CCBF, Chu (2017) found that uncertainties in the design practice and structural properties have a noticeable effect on the collapse prevention capacity of low-ductility CBFs. All these studies

revealed the complexity of seismic behaviour of CCBFs. As such, experimental testing should not solely be relied upon to develop a comprehensive evaluation and understanding of CCBFs. In support of physical testing, the use of numerical structural analyses based on accurate nonlinear models is recommended.

As brace connections are considered to be the weak links in CCBFs, the accurate numerical modeling of the plastic behaviour and fracture of these connections in nonlinear structural models is critical for the reliable seismic performance evaluation of such systems. Most modeling of welded brace connections in structural analyses used a single spring (e.g., Sizemore, 2017). To capture the brace-to-gusset weld fracture and subsequent brace re-engagement behaviour, Chu et al. (2018) combined a linear elastic material, a gap material, and a fracture material to model each brace connection. Little research has been done on the numerical modeling of bolted brace connections. The high-fidelity continuum finite element analysis method could capture the brace connection behaviour accurately, but such an approach is extremely computationally demanding and not practical for structural seismic analyses, especially when extensive geometric and material nonlinearities are involved. There is an urgent need to develop an accurate and computationally efficient numerical modeling method to capture the full-range behaviour of brace connections for reliable structural analyses of CCBFs.

1.2. OBJECTIVES

The primary purpose of this thesis is to assess the seismic performance of CCBFs with I-shape braces and bolted brace connections. The focus is on the bolted brace connection, specifically, the flange plate connection. The main objectives of this thesis are as follows:

- Develop and validate a high-fidelity finite element (FE) modeling procedure that is able to capture the full-range behaviour of bolted brace connections, including the nonlinear deformation of each component and frictional slippage.
- Characterize the nonlinear force-deformation hysteretic behaviour of the bolted brace connection under reversed cyclic loading.
- Assess the effect of key brace connection design parameters on the behaviour and deformation capacity of brace connections through numerical parametric studies.
- Propose design recommendations for brace connections to achieve higher ductility.
- Develop a numerical modeling framework for bolted brace connections to capture the nonlinear force-deformation hysteretic behaviour, which can be efficiently implemented in system-level structural analyses under seismic loading.
- Investigate the seismic behaviour and collapse prevention performance of CCBFs, and assess the collapse risk under severe earthquakes.
- Quantify the deformation demand on brace connections to avoid brace connection fracture under severe earthquakes.
- Propose design recommendations for CCBFs to enhance the seismic performance under severe earthquakes.

1.3. THESIS OUTLINE

Chapter 2 provides a comprehensive literature review related to conventional concentrically braced frames (CCBFs) and brace connections. This chapter contains a summary of code specifications in different countries and an overview of experimental and numerical studies related to the low-ductility CCBFs. Studies related to brace connections subjected to monotonic and cyclic loading are presented. Subsequently, numerical structural analyses of braced frames, in which the

modeling of brace connections was incorporated, are summarized with the focus on the technique of brace connection modeling. Finally, the component-based modeling method for complex connection modeling is discussed. Mathematical models proposed in previous studies describing the force-deformation relationship of each component involved in the bolted flange plate brace connection are reviewed.

In Chapter 3, a presentation of the numerical study on the behaviour of the bolted flange plate brace connection is provided. A high-fidelity finite element (FE) simulation procedure was developed, in which the inelastic bolt deformation, bolt contacts, bolt pretension, and frictional slippage were modeled. The accuracy of the FE models was validated against test results of a prior Type CC I-shape brace connection test program. The force flow in each plate was extracted, and the force transfer mechanisms within the two branches of the connection were characterized. The shear force in each bolt was extracted and the shear force distribution within the bolt group in the flange lap plate was analyzed. The force imposed on each fillet weld was extracted and the loading condition was studied. Recommendations were then proposed regarding how to avoid brittle bolt shear rupture and premature weld fracture.

A parametric study on the bolted flange plate brace connection is described in Chapter 4. The validated FE modeling procedure developed in Chapter 3 was utilized to create the FE models. Three key design parameters, namely, the gusset plate thickness, the flange lap plate thickness, and the web lap plate thickness, were varied. For each model, the brace connection was loaded monotonically both in tension and compression to a large deformation level. Various possible failure modes of the brace connection were revealed, and all the deformation mechanisms were identified, which laid a foundation for the component-based modeling of the connection, which was detailed in Chapter 5. The effect of each studied design parameter on the connection

deformation capacity was discussed. Design recommendations are proposed with regards to attaining better deformation capacity of the brace connection.

The structural analyses and seismic evaluation of CCBFs with I-shape braces and bolted brace connections is documented in Chapter 5. An efficient nonlinear numerical modeling method, comprising the component-based modeling concept, was proposed for bolted brace connections. Mathematical models describing the force-deformation relationship of each component in the bolted flange plate brace connection were introduced. The component-based modeling of the bolted flange plate brace connection was implemented in OpenSees and validated through comparison with the laboratory test results of full-scale I-shape brace connection specimens. Eight single-storey CCBFs with the symmetric diagonal bracing configuration were designed with variation in seismic hazard level, brace connection seismic design force level, and beam orientation. A numerical model was constructed for each frame, incorporating the component-based modeling for all brace connections. Nonlinear static analyses were first conducted and the limit state evolution was studied up to large storey drift. A set of ground motion records were selected and scaled to match the target response spectrum in Canada with an exceedance probability of 2% in 50 years (a return period of 2475 years) for each building. Nonlinear response history analyses were then conducted for each building subjected to the selected and scaled ground motion records. The structural responses under the selected ground motions were examined, and the collapse prevention performance of the CCBFs was discussed. The maximum deformations of brace connections under each ground motion were extracted and statistically analyzed. The effect of the studied parameters (seismic hazard level, brace connection seismic design force level, and beam orientation) was discussed with the focus on the brace connection deformation.

A summary of the main conclusions and recommendations for design is found in Chapter 6. The limitations of this thesis and suggestions for future work are also presented.

CHAPTER 2: LITERATURE REVIEW

2.1. BACKGROUND AND SCOPE

The main objectives of this thesis are to evaluate the seismic behaviour and performance of low-ductility conventional concentrically braced frames (CCBFs) with I-shape braces and bolted brace connections, and to quantify the brace connection deformation demand in such systems, so as to establish the brace connection ductility acceptance criterion. Code specifications in different countries, and experimental and numerical studies related to the low-ductility CCBFs are first reviewed. Other key issues related to the quantification of brace connection deformations are identified including: a) the seismic behaviour of brace connections; b) the numerical modeling of brace connections in structural analyses of steel braced frames; c) the accurate and efficient numerical modeling method for complex connections, specifically the component-based modeling method. A comprehensive review of studies concerning the aforementioned issues is presented.

2.2. CODE SPECIFICATIONS AND STUDIES RELATED TO LOW DUCTILITY CCBFS

2.2.1. Code specifications on CCBFs in different countries

Canada

According to CSA S16 Design of Steel Structures Standard (CSA, 2019), CBFs can be designed as Type Conventional Construction (CC) systems with the ductility-related force modification factor R_d=1.5 and overstrength-related force modification factor R_o=1.3. Capacity-based design and seismic detailing are not required for structural members of Type CC systems. Such systems are expected to have minimal deformation capacity and dissipate earthquake-induced energy

through localized yielding and friction that inherently exists in traditional design and construction practices.

For connections in Type CC systems, however, the seismic design force has to be amplified by 1.5 if they are not proven to be ductile. It is noted that there is no criterion available yet regarding what qualifies as being ductile.

The United States of America

In ASCE/SEI 7-16 (ASCE, 2016), there is a seismic force-resisting system, 'Steel systems not specifically detailed for seismic resistance'. A response modification coefficient (*R*) of 3 is specified. The *R*=3 system is permitted to be designed and detailed only in accordance with the AISC 360 Specification (AISC, 2016), and is exempted from all seismic proportioning and detailing requirements in the AISC 341 Seismic Provisions (AISC, 2016). The *R*=3 system is permitted in areas of Seismic Design Category B and C, without limit on the structural height.

Moreover, before the introduction of the 1988 Uniform Building Code (UBC) (ICBO,1988), CBFs built in the USA did not need to be designed following capacity-based philosophy. These existing CBFs can also be grouped in the category of CCBF.

New Zealand

In the NZS 3404 Steel Structures Standard (NZS, 2007), there is a structural category called 'Elastic systems', also referred to as Category 4 systems (Clause 12.2.3.1). These systems are expected to respond with minimal structural displacement ductility demand under the design level ultimate earthquake loads, and must resist collapse under a maximum considered earthquake as directed by the Loadings Standard (NZS, 2004).

In accordance with Clause 12.12.5.4 ‘Seismic design procedures for category 4 systems’ (NZS, 2007), the capacity-based design is not required for such systems. The design procedure takes account of the force distribution in the elements of the CBF in the elastic mode of response. The structural performance factor, S_p, is taken as 0.9 for the category 4 structures. However, for the connections in such systems, S_p is set as 1.0 to calculate the design force, which effectively increases the design force compared to that applied to the structural members.

Europe

According to Clause 6.1.2 of Eurocode 8 (EN 1998-1, 2004), earthquake resistant steel buildings shall be designed in accordance with one of the following concepts: concept a), low-dissipative structural behaviour; concept b), dissipative structural behaviour. The low structural ductility class, DCL, is required assigned to the concept a) structures, with the reference range of the behaviour factor, $1.5 \leq q \leq 2.0$.

In concept a), the action effects may be calculated on the basis of an elastic global analysis without taking into account a significant non-linear material behaviour. The capacity-based design is not required for such systems. The resistance of the members and connections shall be evaluated in accordance with Eurocode 3 (EN 1993, 2005) without any additional requirements.

China and Japan

It is worth noting that in some countries, e.g. China (GB50017, 2017) and Japan (AIJ, 2012), the low-ductility CCBFs are not permitted in seismic design due to concern with their ability to adequately dissipate earthquake-induced energy. CBFs are instead required to be designed as ductile systems having a hierarchy of resistances as dictated by capacity-based design provisions.

2.2.2. Experimental and numerical studies on CCBFs with hollow steel braces and welded brace connections

Sloat (2014) and Sen et al. (2016) reported on existing pre-1988 CBF structures that were not designed following the capacity-based design concept. Twelve CBF structures, up to nine storeys in height, designed between 1974 and 1992, located on the West Coast of the USA and other seismically active regions of the country, were selected. By the standard of modern special CBFs (SCBFs) per AISC 341 Seismic Provisions (AISC, 2010), the deficiencies of the braced frame components were quantified. Among the most important findings are: 1) over 50% of brace-to-gusset plate welds or bolts had fracture demand-to-capacity ratios (DCRs) greater than 1.0; 2) all brace connections had inadequate clearance to accommodate brace end rotation.

Sen et al. (2016) subsequently conducted experimental tests of eight single-storey one-bay single-diagonal braced frames to examine common deficiencies in these pre-1988 nonductile CBFs. Specimen 1, of which no part was strengthened deliberately, exhibited brace-to-gusset weld fracture at a low storey drift ratio of 1.3%. It was found that deficient brace-to-gusset welds were common in nonductile CBFs because they were not designed for the expected capacity of the brace, and demand critical weld electrodes were not required. As such, they concluded that the brace-to-gusset weld is a high retrofit priority and should be addressed in a minimum retrofit. However, it was noted that despite the weld fracture at a low drift, the frame of Specimen 1 showed a stable post-fracture response due to frame action. The frame maintained between 40 and 60% of its peak shear resistance up to a drift range of 8.2%, implying the brace-to-gusset weld deficiency might not necessarily result in structural collapse.

To explore the possible retrofit schemes for the pre-1988 nonductile CBFs, Sen et al. (2017) conducted tests of 15 retrofitted single-storey one-bay CBFs with different retrofit details. In view

of the prevalence of brace-to-gusset weld deficiency, all tested specimens were retrofitted to have brace-to-gusset welds capable of resisting the yield strength of the respective brace. Four brace retrofit schemes were tested: 1) replacement with a more compact brace that buckled out of the plane of the frame; 2) replacement with a more compact brace that buckled in the plane of the frame; 3) replacement with a buckling-restrained brace (BRB); 4) concrete in-fill of the HSS brace to delay local buckling. The horizontal and/or vertical gusset plate interface welds were also strengthened in some specimens. The results showed that the rehabilitation of severe brace-to-gusset weld and HSS brace local slenderness deficiencies was beneficial to the deformation capacity regardless of the brace type. However, the extent of improvement varied significantly among the retrofitted specimens with different yielding mechanisms and failure modes. Moreover, the effect of the retrofits on the system-level performance of pre-1988 nonductile CBFs was unclear and warranted further structural nonlinear response history analyses.

Simpson and Mahin (2018) conducted an experimental and numerical study on pre-1988 existing CBFs, for which the capacity-based design was not required and for which restraints were not placed on the bracing member global/local slenderness. A nearly full-scale one-bay two-storey chevron braced frame—representative of a 1985 chevron CBF—was tested subjected to cyclic lateral loading of increased amplitudes. A soft storey mechanism formed early in the second storey after a brace buckled, and subsequently most damage concentrated in that storey. The high width-to-thickness ratios of the hollow structural steel (HSS) braces resulted in early severe inward local buckling, and the two braces in the second storey completely fractured after only a few small inelastic cycles (before the roof drift ratio reached ±1%). Before significant plasticity occurred elsewhere in the specimen, the test was stopped, and the specimen was upgraded with concrete-filled braces having the same sections and sizes as the previous ones. In the second test, weak-

storey response occurred again after the brace buckling, but in the first floor. Due to the fact that the beams were not designed for the unbalanced force caused by the brace post-buckling force on one side and the brace tension force on the other side, a seismic mechanism was formed, in which the first-floor east half-beam behaved like a long link in an eccentrically braced frame (EBF), and provided some reserve capacity. It is worth noting that due to the unavailability of non-notch tough weld electrodes matching those used in pre-1988 practice, notch tough weld metal was used in the fabrication of the test specimens, and thus weld-related failures were precluded, including the brace-to-gusset weld connection. Therefore, the test results should not be interpreted to rule out the existence of the brace-to-gusset weld connection deficiency.

To study the seismic behaviour and performance of the low-ductility steel CBFs that are widely used in moderate seismic regions of the USA, Bradley et al. (2017) conducted tests of two full-scale one-bay two-storey CBFs subjected to quasistatic cyclic loading. Of the two tested CBFs, one was designed in accordance with the requirements of the AISC 341 Seismic Provisions (AISC, 2005) for Ordinary CBFs (OCBFs) (R=3.25) with the split-x bracing configuration, while the other was designed with no seismic detailing (R=3) with the chevron bracing configuration. During the test of the R=3 CBF, the two braces in Storey 2 buckled at frame drift ratios of ±0.35%, resulting in a large reduction in the lateral strength and stiffness of Storey 2. To mobilize Storey 1, a brace-to-gusset weld fracture was deliberately induced at the Level 1 south connection. With the fracture of the weld group, a long-link EBF mechanism was formed, which provided a reserve capacity with a magnitude of 44% of the design base shear up to a 4% frame drift ratio.

Following the experimental program by Bradley et al. (2017), Sizemore et al. (2017) conducted a numerical parametric study on the low-ductility CBFs. Firstly, numerical models replicating the two full-scale two-storey CBF specimens were constructed and calibrated against the experimental

data. Subsequently, a parametric study of 12 three-storey frames was carried out to study the effect of two parameters (system type and bracing configuration) on the structural limit state evolution under cyclic static loading. They found that the brace-to-gusset weld failure was the dominant limit state in the analyses of low-ductility CBFs, and the as-built weld overstrength significantly affects the damage location and the progression of failure limit states. Moreover, it was found that the lateral force-resisting capacity outside the primary seismic mechanism, referred to as the reserve capacity, played a key role in the seismic performance of low-ductility CBFs under the maximum considered earthquake seismic hazard. Both the system type and bracing configuration would influence the system reserve capacity.

To evaluate current seismic provisions for low-ductility CBFs with the aim of revising them for improved seismic performance, Sizemore et al. (2019) performed a series of numerical simulations on typical 3-, 6-, and 9-storey buildings designed for Boston, Massachusetts, with current code-compliant R=3 CBFs and OCBFs. All systems were subjected to a suite of earthquake ground motions, and incremental dynamic analyses were used to assess the seismic performance within the framework of FEMA P695 (FEMA, 2009). It was found that none of the R=3 CBFs met the FEMA P695 basic collapse performance criterion. Based on the results, an R=4 system with modified seismic detailing and proportioning requirements was proposed for possible adoption in a future version of the AISC 341 Seismic Provisions.

2.2.3. Experimental study on bolted I-shape brace connections for CCBFs at McGill University

I-shape braces and bolted brace connections are a common design choice for CCBFs in practice. To study the seismic behaviour and performance of bolted I-shape brace connections in CCBFs, Rudman (2018) and Rudman et al. (2021) experimentally tested a series of full-scale I-shape brace

and connection assemblies under reversed cyclic loading. The test setup is shown in Figure 2.1. The flange plate connection configuration, as shown in Figure 2.2, was adopted in four specimens.

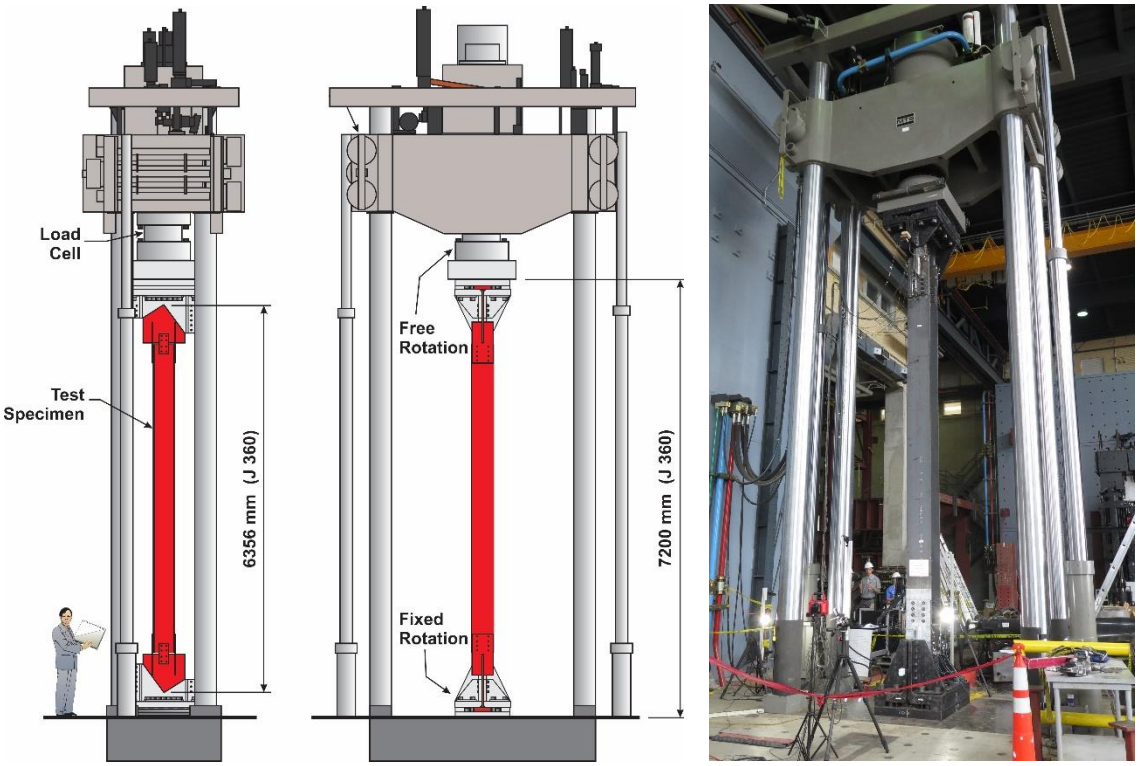

Figure 2.1: Test setup of the I-shape brace and bolted brace connection assemblies for CCBFs (From Rudman (2018) and Rudman et al. (2021))

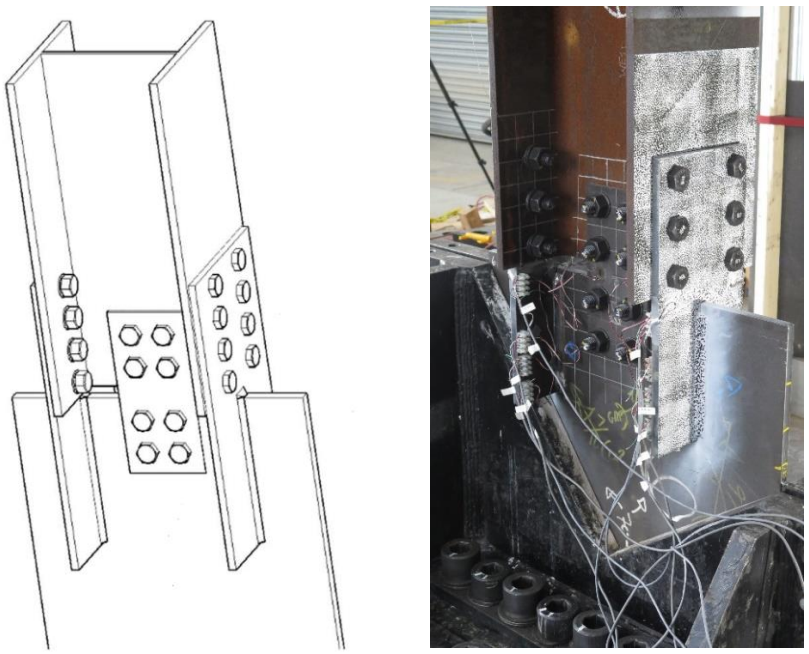

Figure 2.2: The flange plate brace connection (From Rudman (2018) and Rudman et al. (2021))

Some specimens exhibited promising deformation capacity under cyclic loading with corresponding storey drift ratios up to about 2%, although low ductility was expected; see Figure 2.3. However, various failure modes were observed, and significant variability existed in the specimen ultimate deformation capacities. When loaded in compression, either the gusset plate or the I-shape brace buckled, as shown in Figure 2.4. Significant plasticity, and ultimately failure, occurred in the brace-to-gusset connections when the specimens were loaded in tension, which confirmed that the bolted brace-to-gusset connection was weaker in tension than the adjoining braces and gusset plates; see Figure 2.5. Most importantly, some observed failure modes were different from those predicted by the code prescribed design equations, which indicated that the behaviour of the tested brace connections was not fully understood. Due to the limitation of measurement instrumentation in the experimental tests, the seismic behaviour of the tested brace connections was still unclear and an accurate numerical study was needed.

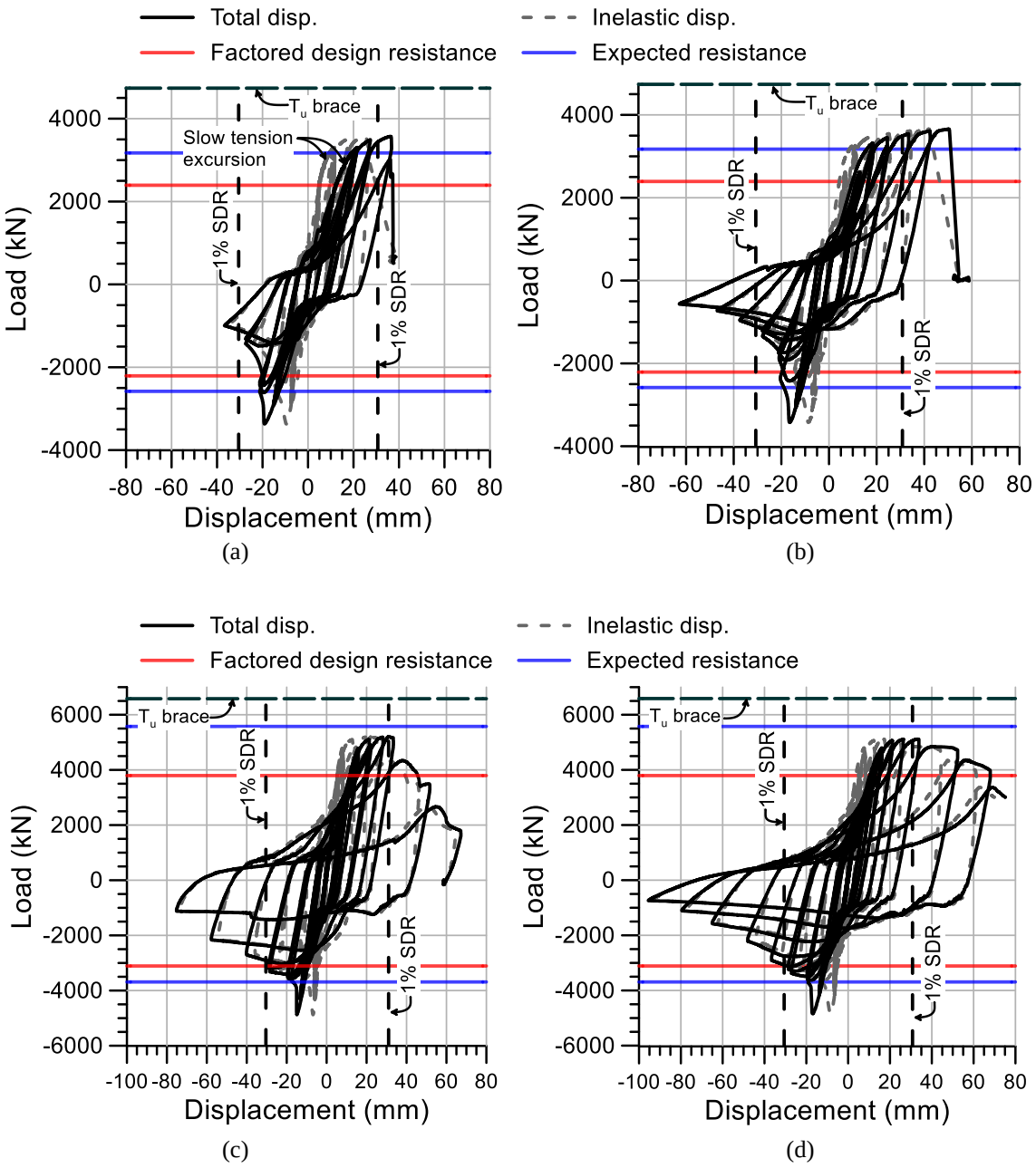

Figure 2.3: Axial load-deformation response: (a) J310-T; (b) J310-C; (c) J360-T; (d) J360-C (From Rudman (2018) and Rudman et al. (2021))

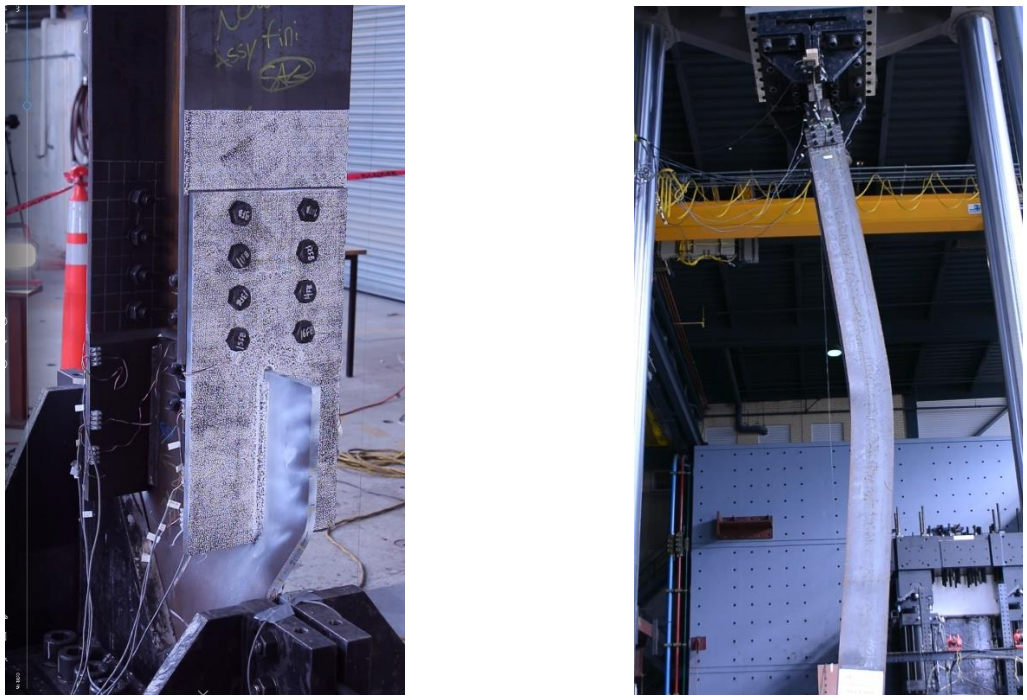

(a) (b)

Figure 2.4: Buckling mode: (a) gusset plate buckling; (b) brace buckling (From Rudman (2018) and Rudman et al. (2021))

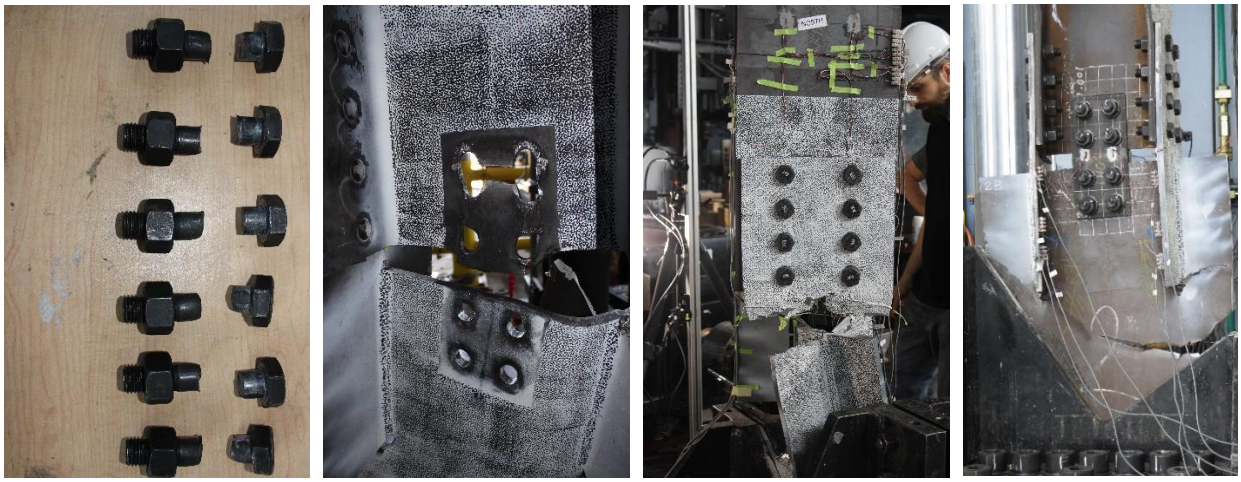

(a) (b) (c) (d)

Figure 2.5: Failure mode: (a) bolt shear rupture; (b) block shear of brace web; (c) tearing of the flange plate; (d) tearing of the gusset plate (From Rudman (2018) and Rudman et al. (2021))

From the review of previous studies on CCBFs, it was found that: a) most studies focused on CCBFs with HSS braces and welded brace connections; b) the brace-to-gusset connection (either bolted or welded) is deficient in strength and prone to inelastic deformation and ultimate failure; c) the inelastic behaviour of bolted brace connections is not well understood; d) various seismic

behaviour and failure modes were reported in studies of CCBFs, indicating the complexity in the evaluation of these framing systems.

2.3. RESEARCH RELATED TO THE SEISMIC BEHAVIOUR OF BRACE CONNECTIONS

In braced frames, bracing members are typically connected to other framing members (beams and columns) by means of gusset plates. More precisely, the brace connection can be further divided into brace-to-gusset connection, gusset plate, and gusset-to-frame connection. They work in series to transfer the brace force to and from the frame; failure of any one of them can cause essential loss in the structural lateral strength and stiffness, which in turn may result in a weak-storey mechanism. As weak links in CCBFs, brace connections play a critical role in the seismic performance of the entire system. In this section, past research in relation to the seismic design and behaviour of brace connections is summarized.

2.3.1. Performance of brace connections during past earthquakes

Failures of brace connections have been witnessed and reported in post-earthquake reconnaissance investigations, including in the 1985 Mexico (Astaneh-Asl, 1986), the 1994 Northridge (Tremblay et al., 1995; Astaneh-Asl et al., 1994), and the 1995 Kobe earthquakes (Tremblay et al., 1996). The failure modes are in the form of failure of the bolts, welds, and plates/angles connecting the gusset plate to other members, net section fracture of the gusset plate or bracing members, and buckling of the gusset plate.

2.3.2. Studies on brace connections under tension loading

Whitmore (1952) reported on the testing of a gusset plate connection made of high-strength aluminum. The specimen was representative of actual connections in a truss. Through the data

acquired by the strain gauges mounted on the test specimen, the stress contour in the gusset plate was obtained. It was found that the force distribution followed a dispersion angle of approximate 30 degrees with respect to the axis of the connected member. Accordingly, Whitmore proposed a practical method for calculation of the critical stress in the gusset plate: first, an effective area of gusset plate in the plane defined by the last points of connectors is established by drawing 30-degree dispersion lines with respect to the axis of the connected member from the first connectors; second, the critical stress is determined by dividing the force from the bracing member by the effective gusset plate area. The length of the effective gusset plate area is also known as the "Whitmore width", which is still commonly used in gusset plate design practice.

De Martino (1981) summarized a series of tests of x-bracing with end gusset plate, including both bolted and welded connections. It was found that the behaviour of the bolted joint was controlled by bolt slippage, which substantially contributed to the ductility of the joint, and therefore improved the dynamic response of the system.

Hardash and Bjorhovde (1985) described the results of 28 bolted gusset plate test connections subjected to tension, along with 14 similar tests conducted earlier at the University of Illinois and the University of Alberta. All specimens failed in the form of block shear failure, which consisted of tensile tearing across the last row of bolts and shear yielding along the outside lines of bolts. Based on the accumulated test data, they proposed an empirical equation to predict the block shear failure strength of gusset plates in tension, which accounted for the total connection length, and material yield and ultimate strengths.

Elliott and Teh (2019a) examined the validity of the Whitmore concept for the design of bolted gusset plates. In current design practice, both the Whitmore net section strength check and the block shear check are typically required. Firstly, they studied previously tested specimens that

failed in the form of block shear. It was found that the Whitmore criterion and the block shear criterion would yield similar results for standard connections having around 7 rows of bolts. However, for specimens having 2 or 3 bolt rows, the Whitmore criterion would yield highly conservative estimates of the tensile capacity. Conversely, for specimens having 9 bolt rows, it overestimates the tensile capacity. Through finite element (FE) analyses, they revealed that the commonly observed Whitmore tensile fracture only occurs when the tensile loading test continues long after the ultimate limit state of block shear. As such, they proposed that the Whitmore section check be made redundant since the block shear check could accurately predict the ultimate capacity under tension loading.

Subsequently, Elliott and Teh (2019b) further studied the behaviour of bolted gusset plates with the focus on the net section fracture through FE simulations (FE models validated against laboratory test results reported by Swanson and Leon (2000)). They found that the Whitmore width concept is not viable for the net section capacity check of bolted gusset plates. For a rectangular gusset plate subjected to loads that are parallel to the two edges, the net section tensile capacity can be calculated using the entire net width, rather than the Whitmore width, even if the Whitmore width is much smaller than the entire net width. For tapered gusset plates, the tensile failure may be in the form of inclined net section fracture, for which the Whitmore concept cannot predict accurately the resistance. Instead, they proposed a practical design equation that can predict the net section strength, with reasonable accuracy, of tapered bolted gusset plates.

Based on the recent findings in relation to the Whitmore section and the block shear mechanism for bolted gusset plates, Elliott and Teh (2020) proposed a new design equation for determining the yielding resistance of bolted gusset plates, which they refer to as the block shear yielding design equation. This equation is specifically for use in conjunction with the balanced design procedure

for SCBFs (Reoder et al., 2011), with the aim of promoting the block shear yielding as a secondary ductile yielding mechanism. Through a numerical example, it was illustrated that the proposed approach could yield a rational design outcome that is otherwise not possible using the Whitmore criterion.

2.3.3. Studies on brace connections under compression loading

Compared to being loaded in tension, the behaviour of brace connections becomes more complicated when loaded in compression as instability may develop in the gusset plate. Due to the large number of factors that may affect the gusset plate instability, e.g. gusset plate shape, brace connection configuration, brace angle, etc., it is difficult to accurately predict the compressive strength of gusset plates. Gusset plate buckling was reported in the experimental study on bolted brace connections of CCBFs by Rudman (2018) and Rudman et al. (2021). In this section, past research in relation to the brace connection compressive behaviour is summarized.

For the design of gusset plates under compression, Thornton (1984) proposed a practical approach. This approach considers an imaginary fixed-fixed column strip of unit width below the Whitmore section. The length of the column strip may be taken as the largest length under the Whitmore section. This strip is used to determine an equivalent slenderness ratio. The compressive buckling resistance of the gusset plate can be evaluated based on the Whitmore effective width and the compressive resistance of the imaginary column strip. Alternatively, a shorter length, such as the average of lengths under the Whitmore section, may give a more reasonable approximation of the buckling strength in some cases. Thornton states that this approach is conservative because it ignores plate action and the post-buckling strength of plates. The Thornton method is still widely used in current design practice because it is easy to use and no better alternative has emerged.

Gross (1990) conducted an experimental study, in which three k-shaped steel subassemblies designed for a prototype braced frame were tested. In Specimen No. 1, the axes of the two bracing members, beam and column intersected at one point, i.e. having no in-plane eccentricity. Specimen No. 2 was designed such that the axes of the two bracing members did not coincide with the intersection of the beam and column axes, therefore having in-plane eccentricity. Specimen No. 3 was similar to Specimen No. 2, except that the column was oriented in weak-axis bending. Both Specimens No. 1 and No. 2 failed in the form of gusset plate buckling. It was found that the Thornton method for predicting gusset plate buckling capacities was conservative and predicted capacities of 60% to 70% of the actual capacities. Gross also found that the compact specimens (with in-plane eccentricity) had a higher buckling load than the less compact specimen (having no in-plane eccentricity).

To investigate the compressive behaviour of brace connections, researchers at the University of Alberta conducted a series of laboratory tests on subassemblies consisting of bracing members, bolted brace-to-gusset connections, and gusset plates (Hu and Cheng, 1987; Yam and Cheng, 1993). The tested parameters included gusset plate size, gusset plate thickness, and the presence of out-of-plane restraint of the bracing member. The effect of frame action on the gusset plate was neglected in the tests. It was found that the primary failure mode of the brace connection when loaded in compression is gusset plate buckling. Without the presence of the out-of-plane restraint on the bracing member, the gusset buckling was in the form of sway buckling, while local buckling of the free edge would occur in the absence of the out-of-plane restraint. The buckling load was significantly affected by the gusset plate thickness (almost proportional to the cube of it) and the out-of-plane restraint on the bracing member. The Whitmore predictions produced unconservative estimates of the capacity of thin gusset plates loaded in compression.

To extend the findings obtained through laboratory tests, Cheng et al. (1994) carried out a numerical study based on FE models constructed in the program ANSYS. After validation of the FE models against test results, a parametric study was performed. The results indicated that the rotation restraint provided by the brace-to-gusset connection would notably affect the buckling strength of the gusset plates. Increasing the thickness of the splice plate increased the gusset plate buckling strength significantly. As such, they recommended that thick splice plates, tee-sections or back-to-back angles be used as the splicing member in the brace-to-gusset connection. Moreover, it was recommended that the splicing member should always be extended toward the beam and column boundary as close as possible to suppress the gusset plate buckling.

Yam and Cheng (2002) conducted thirteen full-scale tests to investigate the compressive behaviour and strength of gusset plate connections. Three gusset plate thicknesses (6.5, 9.8, and 13.3 mm), and two bracing angles (30 and 45°) were examined. All gusset plates were rectangular. During the tests, moments were applied on the beam and column studs to examine the possible effect on the gusset plate compressive behaviour. For the tested specimens, the buckling strengths were almost linearly proportional to the gusset plate thickness. Specimens having 30° bracing members showed slightly lower buckling strengths than specimens having 45° bracing members. The presence of moments in the adjacent beam and column did not affect the buckling strength of the gusset plates. Being consistent with previous studies, the Thornton method was conservative in predicting the buckling strength of gusset plates, with test-to-predicted ratios ranging from 1.51 to 1.87 with an average of 1.67. Based on the test observations and results, they proposed a modified Thornton method, based on a 45° dispersion angle, rather than the 30° originally proposed by Thornton (1984).

Sheng et al. (2002) performed a comprehensive numerical investigation of the compressive behaviour of gusset plate brace connections using the commercial FE program ABAQUS. The studied parameters included the length of free edge of gusset plates, gusset plate shapes, connection type between the splicing member and gusset plate (welded or bolted), splicing member type and stiffness, and the presence of gusset plate free edge stiffeners. The results showed that when the ratio of the gusset plate free edge length to its thickness exceeded $945/\sqrt{f_y}$, local buckling occurred along the unsupported edge. Compared to the bolted connection, a welded connection between the splicing member and the gusset plate increased the buckling strength by 10 to 20%. Adding stiffeners along the free edges of gusset plates would increase the buckling strength significantly, and would result in more stable post-buckling behaviour, which is beneficial for energy dissipation under seismic loading. Most notably, to provide more accurate predictions of the compressive strength of gusset plates, they proposed a design method accompanied by design charts based on the theoretical inelastic plate buckling equation. However, this method is only applicable to rectangular gusset plates with a 45° bracing angle.

2.3.4. Studies on brace connections under cyclic loading

Astaneh-Asl et al. (1982, 1984, 1985) conducted a test program, consisting of 17 full-scale double angle bracing members with end gusset plates. The research indicated that the cyclic behaviour of gusset plates was strongly dependent on the buckling direction of the bracing member. When the bracing member buckles in the plane of the frame, three hinges form in the member itself: one at mid-length, and one at each end of the member outside the gusset plate. In this case, the gusset plate can remain essentially elastic. Conversely, when the bracing member buckles out of the plane of the frame, two plastic hinges would form inside the gusset plate, in addition to the one at the mid-length of the bracing member. These plastic hinges in the gusset plates need to be free to

rotate; otherwise, early onset of fracture would occur due to the plastic strain concentration caused by the gusset plate deformation to accommodate the brace end rotation under brace buckling. Astaneh-Asl et al. (1985) proposed that a clearance of two times the gusset plate thickness ($2t$) should be provided between the brace end and the re-entrant corner of the gusset plate. The $2t$ clearance requirement was subsequently introduced in the 1990 AISC Seismic Provisions (AISC, 1990).

Lehman et al. (2008) reported on an experimental study to evaluate and improve the seismic response of SCBF gusset plate connections. Thirteen large-scale single-storey single-bay braced frames were included. The inclusion of beams and columns ensured simulation of realistic demand on the gusset plate brace connections. It was argued that the $2t$ linear clearance requirement in the gusset plate design may result in large and uneconomical brace connections. To address this issue, they proposed an elliptical clearance model; based on the test results, an elliptical clearance of $8t$ was recommended for the gusset plate design. Moreover, variation in the relative strength between the brace, gusset plate, and weld were considered, and recommendations were made for increased inelastic deformation capacity and improved seismic performance.

The balanced design concept, which seeks to control the sequence of yielding/failure and therefore increase the inelastic deformation capacity, has been proposed in seismic design, e.g. Prathuangsit et al. (1978). Roeder et al. (2011) implemented the balanced design concept in the design of brace connections for SCBFs, in which rational resistance checks and balance factors were used to balance each yield mechanism and failure mode. Based on the results of an extensive test program (Johnson, 2005; Herman, 2006; Kotulka, 2007; Clark, 2009; Lumpkin, 2009; Powell, 2010), the balance factors were calibrated. However, it is noted that the experimental data for bolted connections were limited, and therefore, relevant balance factors were not derived.

A parametric numerical study on the cyclic behaviour of brace and brace connection subassemblies was performed by Walbridge et al. (2005). Numerical models, which included the effect of initial imperfections and bolt slip, were constructed and validated against test results reported in Rabinovitch and Cheng (1993). The focus of the parametric study was on the interaction between the bracing member and the gusset plate under cyclic loading. The results showed that specimens, wherein the gusset plate buckled in compression, exhibited more stable post-buckling behaviour and better energy dissipation capacity than similar specimens in which bracing members buckled. As such, they proposed the weak gusset plate—strong bracing member concept for the seismic design of braced frames, in which the gusset plate is intended to buckle under compression rather than the bracing member. However, it is worth noting that fracture was not modeled in their FE models, and as such, the low-cycle fatigue performance of the gusset plate was not studied. The gusset plate buckling may result in early fracture compared to the bracing member buckling.

2.4. MODELING OF BRACE CONNECTIONS IN STRUCTURAL ANALYSES OF STEEL BRACED FRAMES

In most numerical studies of steel braced frames, the brace connections are usually designed to remain elastic under seismic loading based on the maximum probable capacity of the bracing members, i.e. a capacity-based design philosophy is followed. For the modeling of brace connections in these cases, the gusset plates were commonly modeled as rigid and the brace-to-gusset connections were defined as pinned or rigid, e.g. Del Gobbo et al. (2018) and Faytarouni et al. (2019). In contrast, brace connections in CCBFs are expected to sustain extensive plastic deformation and possibly fracture. Therefore, the accurate nonlinear inelastic modeling of the brace connections is crucial for reliable numerical structural analyses of CCBFs. In this section,

research related to the modeling of brace connections in numerical structural analyses of steel braced frames is reviewed.

Hsiao et al. (2012) found that the conventional modeling practice, in which the brace end connection was simplified as pinned or rigid, was not able to capture the full range of behaviours. Specifically, the brace connection could provide a certain level of rotational restraint to the brace, which in turn affects the compressive strength of the brace. To account for the end rotational restraint, they proposed a new connection model to simulate the brace connection behaviour, wherein a rotational spring is added between the bracing element and the rigid gusset plate element. The model parameters were derived based on the member sizes, material properties, and connection designs. Through comparison with the test results reported in Clark (2009) and Lumpkin (2009), a new model was demonstrated to be able to provide accurate simulation of both local and global behaviours. The model has been adopted in several studies to simulate brace connection behaviours (Hsiao et al., 2013; Asada et al., 2020; Tan et al., 2021).

Nonlinear static analysis was performed by Callister and Pekelnicky (2011) on a two-storey 1980s braced frame building located in California. The nonlinear static analysis procedure outlined in ASCE 41-06 (ASCE, 2007) was used. A three-dimensional model of the structure was created using ETABS v.9. For braces, both ductile and brittle hinges were added. Ductile hinges were defined to capture the possible brace yielding in tension and buckling in compression. Brittle hinges were defined to capture the sudden loss in strength caused by brace connection fracture. In the analysis, brace connection fracture occurred and resulted in a large loss in the structural stiffness and base shear. However, the gravity frames of the building and their connections exhibited sufficient reserve capacity and ductility to accommodate the earthquake-induced drift without incurring structural instability.

In CBFs, gusset plates that connect bracing members to the frame may create a strong zone at the intersection area of braces, beams and columns. The addition of gusset plates significantly affects the flexural behaviour of the beam-column connection. To quantify the cyclic flexural response of the brace-beam-column connection, eight full-scale beam-column connections with gusset plates were tested under reversed cyclic loading by Stoakes and Fahnestock (2011). An accompanying numerical parametric study was also undertaken to expand the database that covered a wider range of connection configurations (Stoakes and Fahnestock, 2012). Based on the combined experimental and numerical data set, a procedure was developed to estimate the flexural response of the beam-column connection with gusset plates, and a spring model was proposed.

Stoakes (2012) subsequently incorporated the developed spring model for the brace-beam-column connection into the modeling of a suite of CBFs. Moreover, to simulate the possible fracture of the brace-to-gusset welds, the force in each bracing member was monitored and compared with the weld capacity during the analysis. Once the force level exceeds the weld capacity, the brace would be removed from the analysis. Incremental dynamic analyses were conducted to evaluate the collapse prevention performance under maximum considered earthquakes. The results showed that after the brace-to-gusset welds fractured within a storey, the beam-column connection with gusset plates provided appreciable reserve capacity that significantly enhanced the structural collapse prevention performance.

To evaluate the seismic performance of non-ductile CBFs (equivalent to the CCBF in terms of design) across the USA, so as to develop efficient seismic retrofit solutions, Shen et al. (2015) conducted a numerical study on typical steel buildings using non-ductile CBFs as the main seismic force-resisting system. Most notably, before the modeling of the entire system, high-fidelity FE models were created for only the brace-gusset assembly using the program ABAQUS. The axial

force-axial deformation responses of the brace-gusset assemblies were extracted from the FE simulation. Thereafter, based on the numerical results and engineering judgment, the brace-gusset assembly was modeled by a lumped plastic hinge model in the structural analysis. To account for the possible fracture of the brace connections, a deformation limit of two times the deformation at first yielding was imposed on the plastic hinge. It is noted that the deformation limit was not rigorously determined based on experimental data. Instead, due to the lack of relevant test data, it was conservatively determined as two times the deformation at first yielding. The effect of gravity frames was included with the beam-to-column connections modeled using the analytical model proposed by Wen et al. (2013). The results showed that the life safety and collapse prevention performance of the buildings was significantly improved with the help of gravity frames after fracture occurred at the brace connections.

To examine the effect of the variation in design practice and uncertainty in structural properties on the seismic response of low-ductility CBFs, a numerical study was conducted by Chu (2017) and Chu et al. (2018). A 3-storey prototype low-ductility CBF was designed. Appropriate consideration of the uncertainties in design and structural properties was reflected in the numerical models by treating input model parameters as random variables and generating sample models through Monte Carlo Simulations. Corresponding numerical models were constructed in OpenSees. Different from other numerical studies, to capture the brace-to-gusset weld fracture and subsequent brace re-engagement behaviour reported in Sizemore et al. (2015), a linear elastic material, a gap material, and a fracture material were combined to define the spring element for brace connections. The model was calibrated and validated against the test results reported in Simpson et al. (2013) and Bradley et al. (2015). Incremental dynamic analysis was performed for all sample models and

the results revealed that uncertainties in the design practice and structural properties have a noticeable effect on the collapse prevention capacity of low-ductility CBFs.

To summarize, brace connections were not modeled in most structural analyses as they were assumed to remain elastic. In the few cases where brace connections were modeled, only the welded brace connection configuration was considered, and the behaviour of the entire brace connection was highly simplified. Therefore, there is an urgent need for accurate nonlinear numerical modeling of brace connections, especially bolted brace connections, that can be incorporated into the structural analyses of CCBFs.

2.5. COMPONENT-BASED MODELING OF CONNECTIONS

Numerical modeling of connections in steel structures is commonly carried out using either the high-fidelity FE method (Bursi & Jaspart, 1998; Citipitioglu et al., 2002; Bagheri Sabbagh et al., 2013; Motallebi et al., 2018) or the synthesized single-spring method (Lignos et al., 2011; Ma & Bocchini, 2019). The high-fidelity FE models can generally yield the most accurate and informative results. However, they are the most demanding in terms of model construction and computation (both computational hardware resources and time), especially when extensive material nonlinearity and geometric nonlinearity are involved. As such, the high-fidelity FE method is infeasible for the modeling and analysis of the entire structural system, e.g. the nonlinear response history analysis of the complete structure under earthquake ground shakings. In contrast, the synthesized single-spring method is simple and efficient in model construction and computation, as the overall response of the connection is characterized by a single spring. However, the development and calibration of an appropriate single-spring model require a large experimental database to account for the variation in connection parameters.

For complex connections, the component-based modeling concept provides a flexible numerical framework that lies between the high-fidelity FE method and the single-spring method in terms of model complexity and computational efficiency (Shen & Astaneh-Asl, 2000; Rassati et al., 2004). Under the component-based method, the connection is discretized into individual components that contribute to the global behaviour. Each component is modeled by a spring with the characteristic behavioural properties; the interactions between the components are captured by placing corresponding springs either in parallel or in series, as appropriate.

Extensive past research has been conducted to identify and characterize the response of individual mechanisms that may occur in steel connections. In this section, studies on characterizing the behaviour of the mechanisms that are related to the bolted flange plate connection are summarized.

2.5.1. Plate bearing behaviour

To develop a model for predicting the load-deformation response of plate bearing in bolted connections, Rex and Easterling (2003) conducted 48 tests of a single plate bearing on a single bolt. The studied parameters included the edge distance, plate thickness, bolt diameter, plate width, and edge conditions. In addition, 140 FE models were created to expand the data set. Firstly, they found that the stiffness associated with bearing, bending and shearing of the plate acted in combination to determine the overall initial stiffness, and as such, formulated a representative equation as follows:

$$K_i = \frac{1}{\frac{1}{K_{br}} + \frac{1}{K_b} + \frac{1}{K_v}} \tag{2.1}$$

where K_{br} = bearing stiffness, K_b = bending stiffness, K_v = shearing stiffness. Through regression and theoretical analyses, they quantified the individual stiffnesses as:

$$K_{br} = 120 t_p F_y \left(\frac{d_b}{25.4}\right)^{0.8} \tag{2.2}$$

$$K_b = 32 E t_p \left(\frac{L_e}{d_b} - \frac{1}{2}\right)^3 \tag{2.3}$$

$$K_v = 6.67 G t_p \left(\frac{L_e}{d_b} - \frac{1}{2}\right) \tag{2.4}$$

with t_p = thickness of the plate.

Subsequently, they normalized the load and deformation values following the equations:

$$\bar{R} = \frac{R}{R_n} \tag{2.5}$$

$$\bar{\Delta} = \frac{\Delta \beta K_i}{R_n} \tag{2.6}$$

where $\bar{R}$ is the normalized force, $\bar{\Delta}$ is the normalized deformation, R = plate load, R_n= plate ultimate bearing strength, Δ = hole elongation, β = steel correction factor (taken as one for typical steels), K_i = initial stiffness.

Finally, they conducted nonlinear regression analysis to fit the Richard equation (Richard & Abbott, 1975) to the data, and obtained the normalized load-deformation relationship:

$$\bar{R} = \frac{(\alpha_{kb} - \alpha_{kp})\bar{\Delta}}{\left[1 + \left|\frac{(\alpha_{kb} - \alpha_{kp})\bar{\Delta}}{\alpha_{rb}}\right|^n\right]^{\frac{1}{n}}} + \alpha_{kp}\bar{\Delta} = \frac{1.74\bar{\Delta}}{\left(1 + \bar{\Delta}^{\frac{1}{2}}\right)^2} - 0.009\bar{\Delta} \tag{2.7}$$

with $\alpha_{kb} = 1.731$, $\alpha_{kp} = -0.009$, $\alpha_{rb} = 1.740$, and $n = 0.5$.

2.5.2. Bolt behaviour

For a bolt subjected to shear loading in a lap plate joint, Sarraj (2007) proposed a model to describe the force-deformation relationship through numerical simulations. FE models of lap joints were created for S275 steel plates with Grade 8.8 high-strength bolts of diameters 12, 16, 20, and 24 mm. One plate was clamped at its end, while the other was displacement controlled to move axially. The relative deflection versus load data of the bolts were collected. The load-deformation relationship was mathematically expressed using a modified Ramberg-Osgood expression with all the parameters calibrated based on the numerically collected data:

$$\Delta = \frac{F}{K_{v,b}} + \Omega \left(\frac{F}{F_{v,Rd}} \right)^6 \tag{2.8}$$

where Δ = bolt shear deflection, F = shear force, $K_{v,b}$ = bolt shear stiffness, $F_{v,Rd}$ = bolt shear strength, Ω = parameter for curve fitting. Detailed information about these parameters is reported in Sarraj (2007). This model has been successfully used in the component-based modeling of bolted shear-tab connections to describe the bolt shearing behaviour by Yu et al. (2009) and Koduru and Driver (2014).

An alternative model was proposed by Weigand (2016) to describe the force-deformation relationship of bolts subjected to shear loading by means of the Richard equation:

$$R_{bolt} = \frac{\left(K_{i,bolt} - K_{p,bolt}\right)\Delta}{\left[1 + \left|\frac{\left(K_{i,bolt} - K_{p,bolt}\right)\Delta}{R_{v,bolt}}\right|^2\right]^{\frac{1}{2}}} + K_{p,bolt}\Delta \tag{2.9}$$

where R_{bolt} = transverse force, Δ = transverse deformation, $K_{i,bolt}$ = bolt initial stiffness, $K_{p,bolt}$ = bolt plastic stiffness, and $R_{v,bolt}$ = bolt shear capacity. The initial stiffness was calculated assuming that it is mainly affected by the bearing and shear deformation of the bolt as:

$$K_{i,bolt} = \frac{1}{\frac{1}{K_{br,bolt}} + \frac{1}{K_{v,bolt}}} \tag{2.10}$$

where $K_{br,bolt}$ is the bolt bearing stiffness, which was quantified by Nelson et al. (1983), and $K_{v,bolt}$ is the bolt shearing stiffness, which was determined by assuming that the bolt acts as a prismatic Timoshenko beam with circular cross section and fixed ends.

The accuracy of the proposed model was validated by comparison with the test data reported in Weigand (2014). For more information about the calculation of each parameter, please refer to Weigand (2016).

2.5.3. Fillet weld behaviour

Fillet welds are frequently used in steel connections loaded in shear. The deformation capacity of fillet welds generally deteriorates with increasing loading angle with respect to the longitudinal axis of the weld. Based on the test results for fillet welds loaded at different angles reported in Miazga and Kennedy (1989) and other relevant data collected from the literature, Lesik and Kennedy (1990) developed expressions to predict the deformation capacities of fillet welds at ultimate load and at fracture. Moreover, a nondimensional equation was proposed to characterize the force-deformation response for fillet welds under tension-induced shear at different angles:

$$P = P_0 f(\rho) \tag{2.11}$$

where P_0 is the ultimate strength of the longitudinal weld. The function $f(\rho)$ gives the variation of load with respect to deformation, and is defined as:

$$f(\rho) = 8.234\rho; \qquad 0 < \rho < 0.0325$$

$$f(\rho) = -13.29\rho + 457.32\rho^{\frac{1}{2}} - 3385.9\rho^{\frac{1}{3}} + 9054.29\rho^{\frac{1}{4}} - 9952.13\rho^{\frac{1}{5}} + 3840.71\rho^{\frac{1}{6}}; \quad \rho > 0.0325 \tag{2.12}$$

In Equation (2.12), ρ is the normalized deformation with respect to the deformation at ultimate strength,

$$\rho = \frac{\Delta}{\Delta_u} = \frac{\Delta}{0.209 \times 2^{-0.32D}} \tag{2.13}$$

where D is the fillet weld size.

2.6. SUMMARY

A comprehensive review of past studies related to low-ductility conventional concentrically braced frames (CCBFs) and brace connections was presented herein. In reviewing the research, four main conclusions were derived: (1) in CCBFs, the brace-to-gusset connection is weaker than the adjoining bracing member and gusset plate, and therefore, is critical for the behaviour of the entire system; (2) little research has been done on bolted brace connections, and hence, their inelastic behaviour is not fully understood; (3) numerical simulations are the most feasible method for seismic evaluation of CCBFs due to their complex nonlinear load-deformation behaviour, but no

accurate and computationally efficient model is available for bolted brace connections; (4) for complex connections, the component-based modeling concept provides a flexible numerical framework that can be easily incorporated into the nonlinear model for structural analyses.

Given the observation and conclusions, two critical tasks were identified for the seismic evaluation of CCBFs with I-shape braces and bolted brace connections: (1) conduct high-fidelity finite element simulations of the bolted brace connections to better understand their behaviour and to identify the influential deformation mechanisms; and (2) develop an accurate nonlinear numerical model for bolted brace connection based on the component-based concept, and incorporate it into the structural analyses to achieve a reliable evaluation of the seismic performance for CCBFs.

FOREWORD TO CHAPTER 3

The main objective of the research presented in this thesis is to evaluate the seismic response and performance of Conventional Concentrically Braced Frames (CCBFs) with I-shape braces and bolted brace connections. As described in Chapter 2, past experimental tests revealed that the bolted I-shape brace connections in CCBFs were prone to failure and their inelastic behaviour had not been well understood. As the first step of the present research study, the behaviour of the bolted I-shape brace connection, specifically the flange plate connection, was studied with the results being presented in Chapter 3. A high-fidelity finite element (FE) simulation procedure was developed, in which the inelastic bolt deformation, bolt contacts, bolt pretension, and frictional slippage were modeled. The accuracy of the FE models was validated against test results. The force flow in each plate was extracted, and the force transfer mechanisms of the connection were characterized. The loading conditions of the bolts and welds in the connections were analyzed. Recommendations were then proposed regarding how to avoid brittle bolt shear rupture and premature weld fracture. The validated FE simulation procedure provided the means for the more extensive parametric study of the bolted brace connections, which is presented in Chapter 4.

CHAPTER 3: NUMERICAL INVESTIGATION INTO I-SHAPE BRACE CONNECTIONS OF CONVENTIONAL CONCENTRICALLY BRACED FRAMES

Published in Engineering Structures, Volume 236, June 2021,

https://doi.org/10.1016/j.engstruct.2021.112091.

Chen Wang, Alina Rudman, Robert Tremblay, Colin A. Rogers

ABSTRACT

In many low and moderate seismic regions, a low-ductility concentrically braced frame (CBF) is used as the seismic force-resisting system for steel structures. The design of such CBFs is straightforward: all members and connections are designed based on the seismic force demand obtained through linear elastic structural analysis; capacity-based design and additional seismic detailing are not required. There is no designated energy-dissipating fuse in the lateral load-carrying path. Such CBFs are referred to as Conventional CBFs (CCBFs) in this study. In CCBFs, the brace-to-gusset connections are inherently weaker in tension than the adjoining gusset plates and braces. This occurs because both the gusset plates and the braces are selected on the basis of their respective compressive buckling resistances, and hence, typically have a much greater resistance in tension. Described herein is a numerical study of the popular flange plate bolted I-shape brace connection configuration. A high-fidelity finite element (FE) simulation procedure

was developed and validated against laboratory test results. The resulting numerical models were created with the objective of improving our understanding of the inelastic response of these brace connections. The force transfer mechanism within the two branches of the connection was characterized. Significant nonuniform shear distribution was found to exist within the bolt group in the flange branch, which may be detrimental to the safe functioning of these bolts in the seismic design context. The loading eccentricity on the weld group was quantified. Recommendations on how to avoid brittle bolt shear rupture and premature weld fracture are proposed.

Keywords: low ductility, no capacity design, bolted brace connections, FE simulation, force transfer mechanism

3.1. INTRODUCTION

Concentrically braced frames (CBFs) are widely used as the seismic force-resisting system for steel structures. Seismic design methods with different levels of expected system ductility have been developed for CBFs. In areas of low and moderate seismic hazard, the design of low-ductility CBFs using a simple approach is permitted in many countries. The earthquake action effects are calculated using linear elastic structural analysis. The structural members and connections are designed to resist the specified earthquake load effects; capacity-based design and additional seismic detailing are not required. As such, there is no designated energy-dissipating fuse in the lateral load-carrying path, which is unlike the configurations used for ductile CBF systems commonly found in high seismic zones. In this paper, such low-ductility CBFs are referred to as Conventional Concentrically Braced Frames (CCBFs). CCBFs are expected to have low ductility, and therefore, higher seismic design loads are generally assigned in comparison to their more ductile counterparts. However, due to the exemption for capacity design and seismic detailing, CCBFs are often the more economical choice in low and moderate seismic regions.

Owning to their simple design and economy, CCBFs are commonly used. In Canada, a type of CBF, known as the Type Conventional Construction (CC) CBF, is permitted as per CSA S16 [1]. Capacity-based design and seismic detailing are not required for structural members of Type CC systems, but a 1.5 amplification is compulsory for the design seismic force in the brace connections if they are not proven to be ductile. In the USA, CBFs categorized as “Systems not specifically detailed for seismic resistance” in ASCE/SEI 7-16 [2] are prevalent in regions of low and moderate seismic hazard, e.g. in the Midwest and Northeastern states. A relatively low seismic force reduction factor, R=3, is assigned to such systems to account for their expected ductility. Similarly, in Europe, CBFs described as being Structural Ductility Class Low (DCL) are permitted in low

seismicity regions as per Eurocode 8 [3]. Due to the anticipated limited ability to dissipate seismic energy, a behavioural factor $1.5 \leq q \leq 2.0$ is recommended for such systems. For CBFs in New Zealand, their seismic design may be conducted using a ductility classified as Category 4. A low level of structural ductility is expected from such systems; as such, a structural ductility factor of $\mu=1$ is assigned in NZS 3404 [4]. Furthermore, for connections in Category 4 CBFs, a structural performance factor (S_p) of 1.0 is required, compared with 0.9 for structural members, which effectively increases the design force demand on the connections. In contrast, the use of low-ductility CBF systems is not permitted in seismic design in other parts of the world, e.g. China [5] and Japan [6,7], due to concern with their ability to adequately dissipate seismically induced energy. Nonetheless, extensive use of these low-ductility CBFs occurs elsewhere in the world, and an improved understanding of their response to earthquake demands is warranted.

In CBFs, brace connections can be divided into two parts; the brace-to-gusset connection and the gusset plate. These two parts work in series; the failure of either may result in significant loss of the brace system's lateral stiffness and strength [8]. Previous studies on brace connections have mainly focused on the gusset plates, because the brace-to-gusset connections are typically protected in ductile framing systems through use of seismic capacity-based design provisions. The tensile behaviour of the gusset plates has been extensively studied [9-12]. Under seismic loading, the gusset plates may also be subjected to compressive loads, and are hence prone to buckling. The compressive instability issue has been studied by Thornton [13], Cheng et al. [14], and Yam & Cheng [15], among others. The Whitmore effective width [9] and the so-called Thornton model [13] are still commonly used in gusset plate design practice. To accommodate the brace end rotation at brace buckling, Astaneh-Asl et al. [16] proposed to leave a 2t (t=thickness of the gusset plate) clearance in the gusset plate. Lehman et al. [17] pointed out that the 2t clearance might result

in uneconomical gusset plate designs and inferior performance, and proposed the elliptical clearance model. From the perspective of the global system performance, a balanced design procedure was proposed by Roeder et al. [18] for the gusset plate connection design, which aimed to maximize the system ductility by encouraging more desirable yielding mechanisms and suppressing undesirable failure modes.

However, in CCBFs, the brace-to-gusset connections are not protected, and as such may become the weakest component in the lateral load carrying path, and further, be prone to fracture. This is because under the CCBF design framework, the brace-to-gusset connection, and the adjoining brace and gusset plate, are designed to resist the same force demand. Braces and gusset plates are generally selected based on their compressive buckling resistances, while brace-to-gusset connections are not. As such, when loaded in tension, braces and gusset plates can usually sustain greater forces than the brace-to-gusset connections. Sen et al. [19,20] experimentally studied older CBFs that were designed without the capacity-based design principle. Fracture of the brace-to-gusset welds was found at low storey drift. They concluded that the brace-to-gusset connection is of high priority in terms of retrofit in these existing structures. The seismic performance of low-ductility CBFs in the US (including the R=3 CBFs) was studied by Bradley et al. [21] and Sizemore et al. [22,23]. They found that the brace-gusset weld fracture was the dominant limit state; the as-built weld overstrength significantly affected the damage locations.

The brace connections, which are potentially the weak component of a CCBF, play a critical role in the seismic performance of such systems. Limited research has been conducted on the brace connections of CCBFs, especially in the case of I-shape braces and bolted end connections. To bridge the knowledge gap, a comprehensive experimental and numerical research project was launched at McGill University and Polytechnique Montréal. A series of full-scale reversed cyclic

tests of I-shape braces and bolted brace connections that were not capacity designed were first conducted [24,25]. Some specimens exhibited promising deformation capacities under cyclic loading. However, high variability of the connection deformation capacity (with the corresponding storey drift ratios ranging from 0.01 to 0.02) and various failure modes were observed. Most importantly, some observed failure modes were different from those predicted by the design equations, which is an indication that the behaviour of the tested brace connections is not at present fully understood. Due to the limitations of the measurement instrumentation employed in the laboratory tests, the seismic behaviour of the tested brace connections remained unclear, and as such, a numerical modelling study, as described herein, was needed.

This paper presents a numerical study on the flange plate connections of I-shape braces (Figure 3.1). A high-fidelity finite element (FE) simulation procedure was developed. The accuracy of the numerical models was validated through comparison with laboratory test results. By extracting the force development of individual components, the force transfer mechanism of the flange plate connection was characterized. Moreover, the behaviours of the bolt group and weld group were studied by analyzing the force and deformation of individual members.

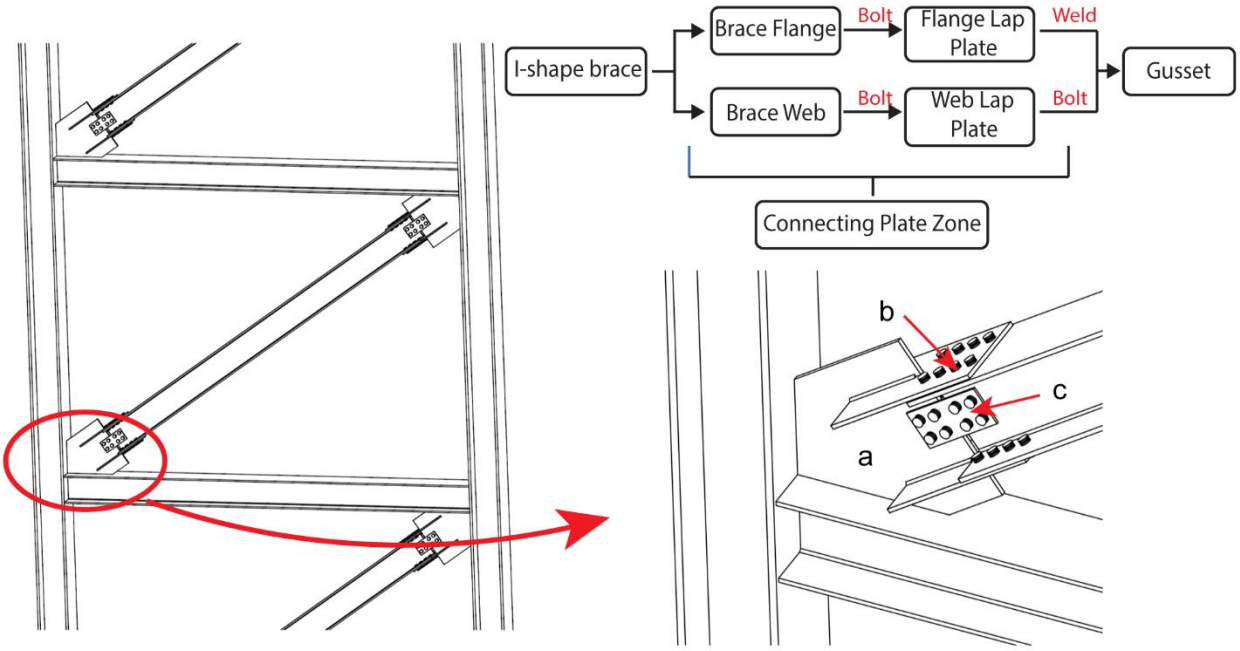

Figure 3.1: Schematic of CBF with I-shape braces and flange plate brace connections: (a) gusset plate; (b) flange lap plate; (c) web lap plate

3.2. SUMMARY OF DESIGN METHOD OF FLANGE PLATE CONNECTIONS AND LABORATORY TEST SPECIMENS

A summary of the design approach used for CCBFs is provided to familiarize the reader with the corresponding procedures used by engineers in practice. Further, a general overview of the previously conducted laboratory test program is provided, because the results of this work were used to establish and validate the numerical models described herein.

The main components of the flange plate connection are schematically presented in Figure 3.1. As shown, the connecting plate zone connects the brace and the gusset plate. In the connecting plate zone, axial forces are transferred by the flange lap plates acting in parallel with the web lap plates. In the absence of design guidance for the seismic design of such connections, practicing engineers usually assume that the force distribution between the flange lap plates and web lap plates is in

proportion to the ratio of the brace flange area to the brace web area. The design of the bolts and welds is also performed based on such force demand distribution.

To study the seismic behaviour of the flange plate brace connections in CCBFs, four full-scale assemblies of I-shape braces and flange plate connections were tested under reversed cyclic loading by Rudman [24] and Rudman et al. [25]. Both the brace connection and I-shape brace were designed based on the same preselected force demand; no additional seismic detailing or proportioning were considered. The connecting plate zones were designed following the force demand distribution as determined through comparison of the brace flange and brace web areas. The length of the test assembly was obtained from a representative 3.75 m high by 5.5 m wide braced frame (Figure 3.2). The corresponding storey drift ratios presented in Sections 3.4 and 3.5 of this paper were determined using the geometry of this frame.

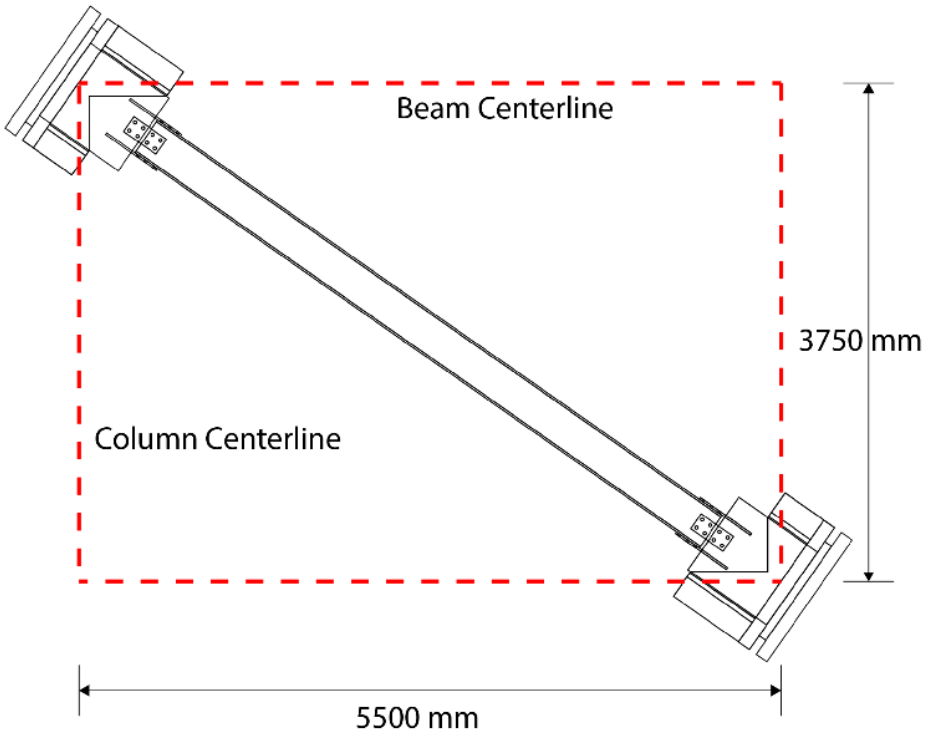

Figure 3.2: Prototype braced frame assembly considered in the test program

The testing assembly and an example test specimen are shown in Figure 3.3. The bottom end of the assembly was fixed to the base of the loading frame, while the upper grip applied axial displacements through the actuator's piston. This piston was allowed to rotate freely, which had to be accounted for in the FE modeling due to the axisymmetric support conditions of the opposing gusset plates.

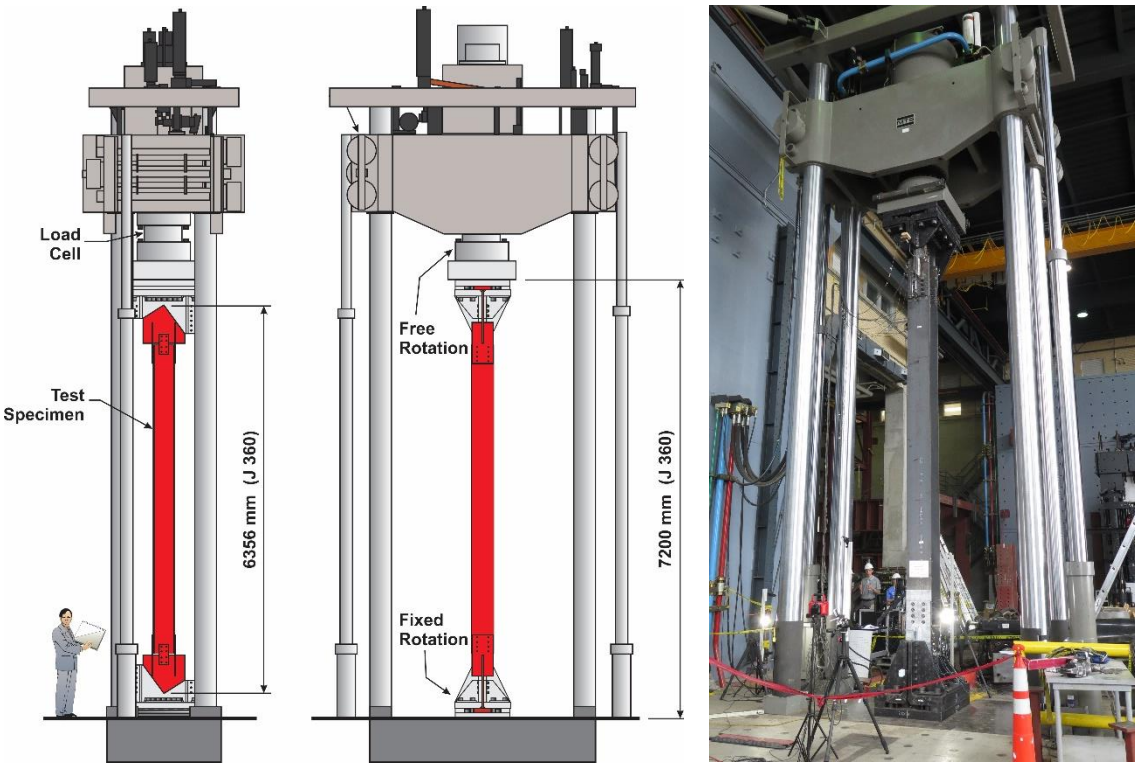

Figure 3.3: Test set-up of Type CC brace-connection assemblies [24,25]

Table 3.1 lists the predicted failure modes based on the calculated resistances using the design equations in the CSA S16 [1] and AISC 360 [26] standards. The test results exhibited significant variability in terms of failure modes and ductility. Most importantly, the discrepancy between the predicted failure modes and those observed during laboratory testing indicates that the behaviour of the brace connection is not fully understood. A thorough description of the design and testing of the Type CC brace-connection specimens can be found in the thesis of Rudman [24].

Table 3.1: Predicted and observed failure modes

Specimen ID	Compressive behaviour			Tensile behaviour		
	CSA S16	AISC 360	Experiment	CSA S16	AISC 360	Experiment
J310-C	Brace buckling	Brace buckling	Brace buckling	FLP fracture + BW block shear	FLP fracture + BW block shear	Bolt rupture in FLP + BW block shear
J310-T	Brace buckling	Brace buckling	Brace buckling	FLP fracture + BW block shear	FLP fracture + BW block shear	Bolt rupture in FLP + BW block shear
J360-C	Brace buckling	Brace buckling	Gusset buckling	FLP fracture + BW block shear	FLP fracture + BW block shear	Tearing of gusset and FLP + BW block shear
J360-T	Brace buckling	Brace buckling	Gusset buckling	FLP fracture + BW block shear	FLP fracture + BW block shear	Tearing of gusset + BW block shear

Note: FLP = flange lap plate; BW = brace web.

3.3. FINITE ELEMENT MODELING

A finite element (FE) modeling procedure was developed with the objectives of: (1) investigating the force transfer mechanisms within the I-shape brace flange plate connection; (2) investigating the possible brittle failure modes; and (3) proposing practical design recommendations or procedures to prevent brittle connection failure and improve deformation capacity. Finite element models replicating the brace-connection assembly tests by Rudman [24] and Rudman et al. [25] were developed in the commercial software package ABAQUS 6.14 [27].

Numerical simulation of bolted connections has long been a challenging topic, especially when extensive plasticity and cyclic bolt slippage are involved, because the algorithm is highly computationally demanding and prone to convergence problems [28,29]. However, because CCBF connections are designed without prescribed yielding and failure hierarchy, any yielding mechanism and failure mode could occur and, as such, had to be included in the FE model described herein. In addition, frictional bolt slippage is explicitly relied on to dissipate earthquake

induced energy for CCBFs, and has been experimentally found to constitute a significant part of the connection behaviour. Therefore, bolt deformations, bolt contacts, bolt pretension, and friction during slippage, were modeled in the numerical simulation. All analyses were conducted on the high-performance computers of Calcul Québec / Compute Canada.

3.3.1. Elements and meshes

As shown in Figure 3.3 the assembly is axisymmetric around its central point. Taking advantage of this axisymmetry, only half of the assembly was modeled for computational efficiency (Figure 3.4). First-order solid hexahedral elements with reduction (C3D8R) were used to model most parts, except fillet welds and K zone of the braces, for which wedge elements (C3D6) were used to facilitate regular meshes. The global mesh size was set as 10 mm. To obtain more accurate results and better convergence, through means of a mesh sensitivity study, more refined meshes were adopted in regions of extensive plastic deformation, e.g. bolts and bolt holes, for which the minimum mesh size was decreased to 2 mm. A set of three elements through the thickness of all plates was used, which was previously shown to capture their flexural behaviour [28,30]. All parts were partitioned to enable the structural meshing technique to have regular element shapes.

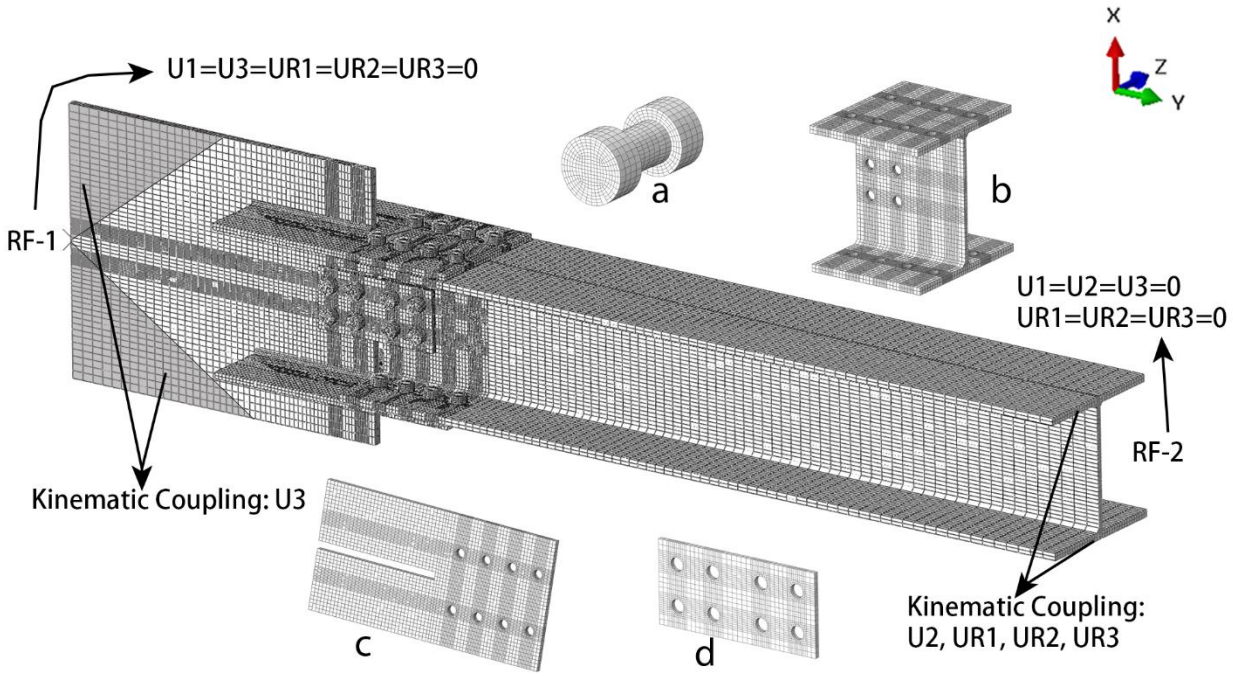

Figure 3.4: Brace connection FE model: (a) bolt; (b) brace end with fine mesh; (c) flange lap plate; (d) web lap plate

3.3.2. Material properties

The bilinear kinematic hardening model was adopted to depict the nonlinear steel behaviour. For the determination of key material parameters, mean properties from tension coupon (TC) tests conducted by Rudman [24] in accordance with ASTM A370 [31] were used for all components, except the bolts and welds. For the bolts (A325 and A490), the typical stress-strain curves presented in Kulak et al. [32] were adopted. The properties reported by Tousignant & Packer [33] were used to define the weld mechanical behaviour. The material properties used in this numerical study are listed in Table 3.2.

Table 3.2: Material properties used in FE models

Specimen number	Element	Yield stress (MPa)	Young's modulus (MPa)	Ultimate stress (MPa)	Ultimate strain
J360T J360C	Brace (W360X134)	355	200000	565	0.138
	Gusset plate	402	213000	540	0.146
	Flange lap plate	417	200000	564	0.108
	Web lap plate	430	199000	572	0.123
	Bolt (A490)	836	206000	1097	0.053
J310T J310C	Brace (W310X97)	352	216000	542	0.153
	Gusset plate	396	196500	557	0.113
	Flange lap plate	405	197000	566	0.108
	Web lap plate	400	180870	571	0.124
	Bolt (A325)	667	206000	867	0.044
	Weld	501	220000	571	0.100

3.3.3. Bolt pretension and contact modeling

There are three contacts in each bolted connection; contact between the connected plates, contact between the bolt shank and the bolt hole, and contact between the bolt nuts and the connected plates. These contacts were achieved using the 'surface-to-surface' contact algorithm provided in ABAQUS. Contact properties contain two aspects, tangential and normal. The 'hard contact' was used to reproduce the contact behaviour normal to surfaces.

In the laboratory tests all bolts were pretensioned with the turn-of-nut method. This pretension was simulated in ABAQUS by adding a 'cutting surface' in the bolts and subjecting it to a tensile load [27]. The pretension load tightens all components together and generates the frictional resistance preventing the components from slipping. Since the pretension of the bolts during assembly of the laboratory test specimens was not measured, the pretension load applied in the numerical models was set as 70% of the specified minimum tensile strength for each bolt. This is the assumed pretension load level through use of the turn-of-nut bolt installation method, as defined by the CSA S16 Standard [1]. The friction coefficient, back-calculated using the friction force at first slippage,

ranged from 0.29 to 0.38 for the test specimens. In the numerical models, the friction coefficient was set at 0.33, a value that was also recommended by Kulak et al. [32] for the surface conditions that existed for the laboratory tests. The slight misalignment inherent in the bolt hole arrangement was not modelled numerically, rather all bolts were placed in the middle of each bolt hole before loading.

3.3.4. Analysis procedures

Because of the axisymmetry around the centroid of the assembly in the brace midplane, all the nodes located on the brace midplane could move and deform freely as long as they remained in that plane. This boundary condition was achieved by coupling the translation in the y-direction (U2) and three rotational degrees of freedom (UR1, UR2, and UR3) to the control point (RP-2) defined at the centre of the brace midplane (Figure 3.4). The control point RP-2 was fixed throughout the whole process. At the other end of the model, the end surface of the gusset plate was set to fully follow the movement of the surface control point (RP-1) (Figure 3.4). The application of axial tension and compression to the assembly was achieved by defining the movement of control point RP-1 only along the longitudinal axis of the brace. The out-of-plane constraint provided by the loading grip to parts of the gusset plates was reproduced by coupling the out-of-plane movement (U3) of the constrained area to RP-1 (Figure 3.4).

A linear elastic buckling analysis was first conducted using the linear perturbation procedure to obtain the elastic buckling mode shapes, which were then introduced in the models to account for the possible geometric imperfection intrinsic to all components. An imperfection of an amplitude of 2 mm was introduced, which is within the permissible 1/1000 straightness variation specified by both ASTM A6/A6M [34] and CSA G40.20/G40.21 [35].

The reversed cyclic loading simulation of the four specimens was then performed. Given the complexity of the FE model and the number of elements, only one cycle of loading at each displacement (or force) magnitude was modeled to reduce the computational time. The loading cycles in which component fracture occurred during the tests were not modeled since steel fracture was not incorporated in the FE models.

3.4. VALIDATION OF THE NUMERICAL ANALYSES

To verify the accuracy of the FE analyses, the numerical predictions using the model described above were compared to the experimental results. Three response parameters were examined in that comparison: axial load vs. storey drift ratio hysteretic response, observed deformations, and the onset of fracture.

3.4.1. Comparison of load vs. storey drift ratio hysteretic curves

The numerical load-deformation results are plotted against the experimental load-deformation hysteretic curves in Figure 3.5. Note, the axial deformations of the brace connection assembly obtained from the laboratory tests and the FE models were converted to storey drift ratios using the dimensions of the representative braced bay illustrated in Figure 3.2. As the comparison shows, the cyclic loading simulation results agree well with the experimental results. The FE analyses accurately predicted the peak tensile and compressive strengths with an average numerical to experimental ratio of 1.02 and 1.03, respectively. The numerical and experimental load-deformation curves almost coincide at the start of the loading protocol, indicating comparable stiffness of the whole assembly. Moreover, the stiffnesses of all specimens upon load reversal also match well.

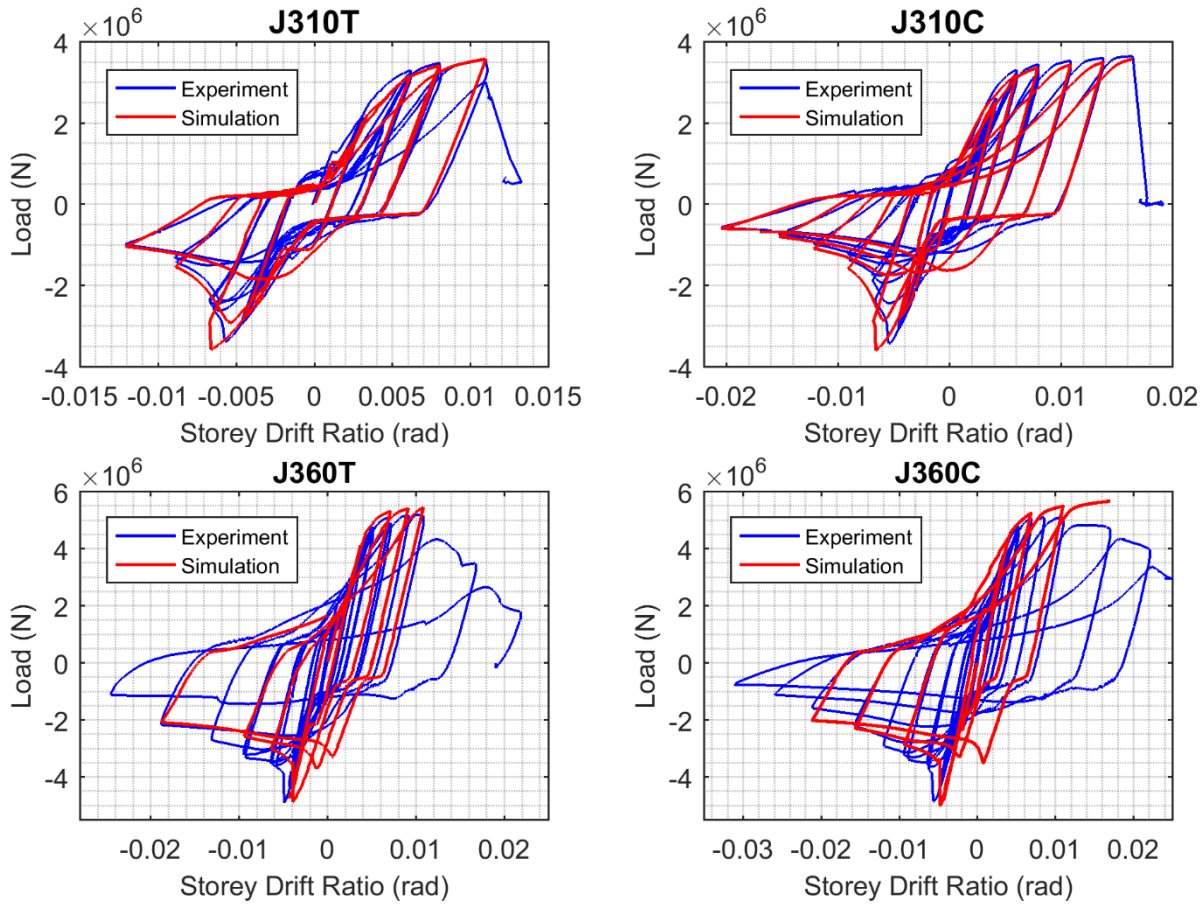

Figure 3.5: Comparison of FE simulation results with laboratory load vs. storey drift ratio hysteretic curves

In contrast, other than the prediction of the compressive strength upon first buckling, the compressive strengths in the second and subsequent cycles in the simulations are higher than those obtained from the tests. This is attributed to applying only one cycle at each displacement amplitude in the simulations to reduce the computational demands. In the laboratory tests more than one cycle was applied at each displacement level, and it is expected that the accumulated plasticity in the brace and connection due to multiple cycles of loading would have deteriorated the compressive strength. This behaviour could be seen in the test results, as revealed by the continuously decreasing compressive strengths at the same displacement level in the test hysteresis of Figure 3.5. However, since the post-buckling compressive resistance was not the focus of this research program, this simplification in modelling was considered to be acceptable.

3.4.2. Comparison of observed and simulated deformations

In the laboratory tests, specimens J360T and J360C suffered from gusset plate buckling, while specimens J310T and J310C were subjected to overall brace buckling during compression cycles. The FE simulation accurately predicted the buckling modes for all the specimens (Figure 3.6).

Extensive plastic deformation and fracture occurred within the brace connections during the tension loading cycles of each test specimen. Since the tension loading in tests of J360T and J360C was not stopped until the resistance dropped to almost zero, with significant fracture sequentially developing in different components, the simulated component deformation could not be compared with the observations at the end of the tests because fracture was not modelled. However, in tests of J310T and J310C, the bolts in the flange lap plates at one end of the brace ruptured at almost the same time, after which loading was stopped immediately. In this case, a comparison between the measured and predicted component deformations at the test end was possible. Two noticeable deformations were reported in these two tests: block shear in the brace web, and necking in the net section of the flange lap plate, both of which were predicted by the FE simulations with good agreement (Figure 3.7).

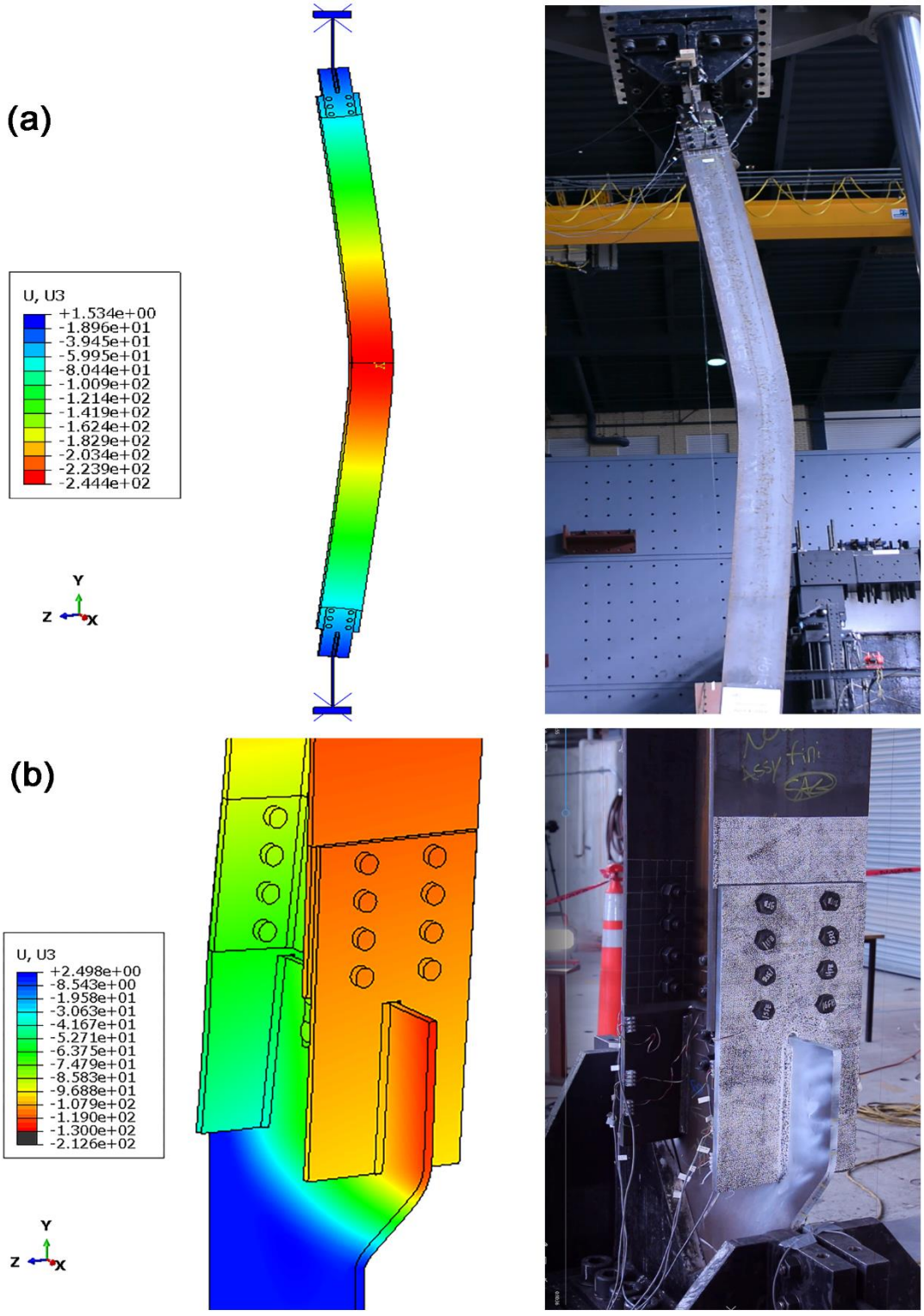

Figure 3.6: Comparison of observed and simulated buckling deformation: (a) overall brace buckling in J310T and J310C, (b) gusset plate buckling in J360T and J360C

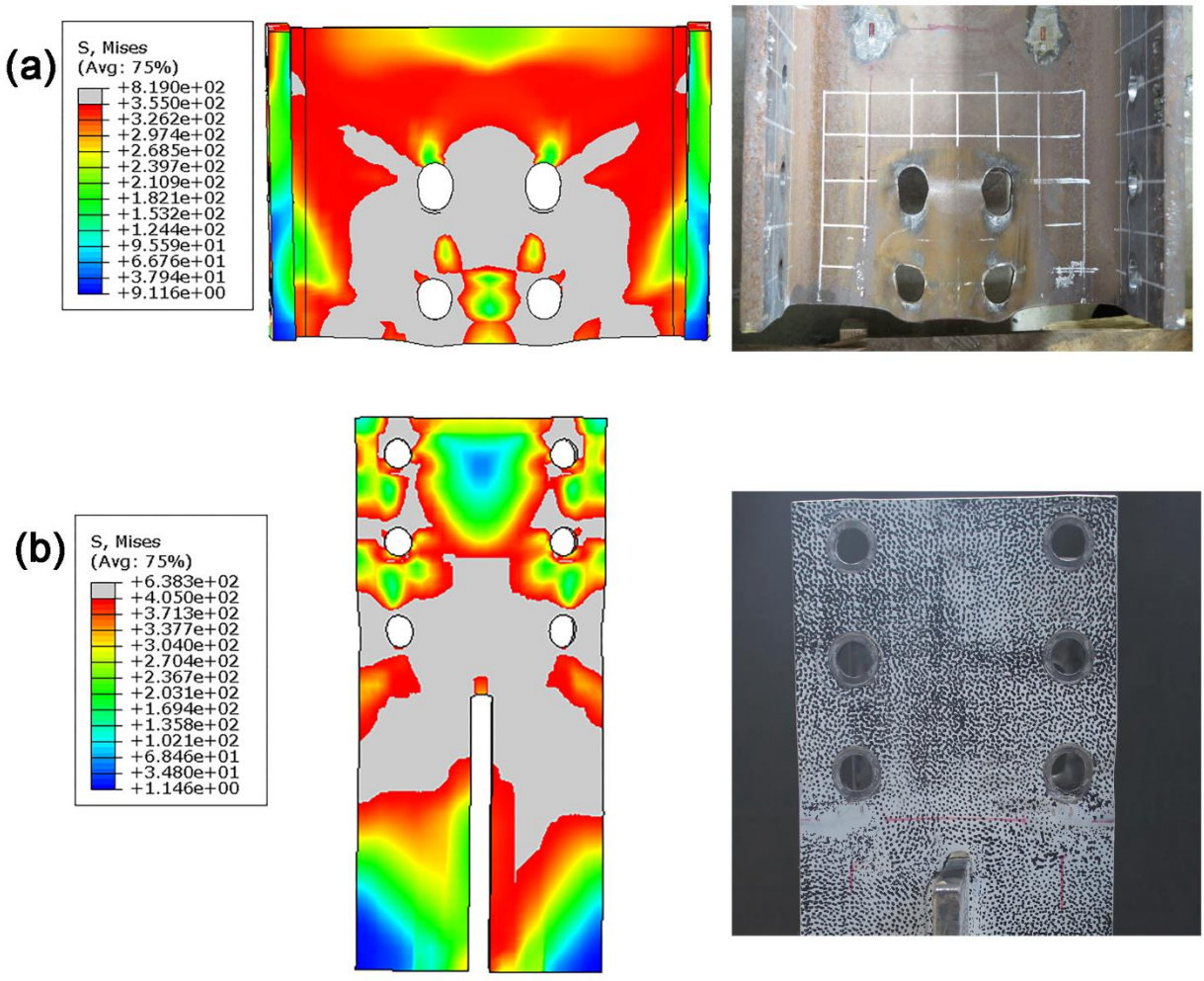

Figure 3.7: Comparison of simulated and observed local deformations in tests J310T and J310C: (a) block shear in the brace web, (b) necking in the flange lap plate. Note: the grey areas in the stress plots indicate yielded regions

3.4.3. Comparison of onset of fracture

Gusset buckling introduced large plastic strains in the gusset plates of specimens J360T and J360C, which initiated fracture that propagated upon continued cyclic loading of the test assembly. In the simulation, fracture could be predicted in a relative sense by means of the equivalent plastic strain (PEEQ) [36]. The PEEQ is the accumulated plastic strain; it is indicative of the void growth in the steel. A good correlation between the area of high PEEQ in the simulation and the fracture zone

in the test was found for specimen J360T, as shown in Figure 3.8. Similar comparison could be observed for specimen J360C.

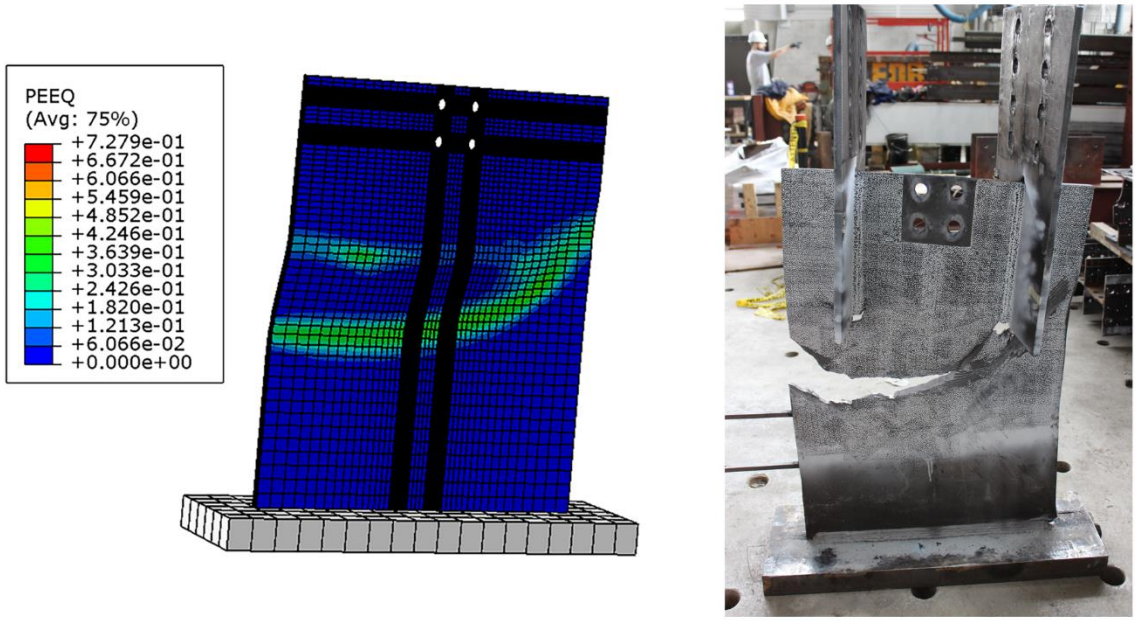

Figure 3.8: Comparison of observed fracture and predicted fracture onset for specimen J360T

Specimens J310T and J310C failed by shear rupture of all the bolts in the flange lap plates at one end of the brace. The steel in the high-strength bolts has less plastic deformation capacity compared to that of the regular structural steel used for the lap plates. The shear forces within the bolts were extracted from the simulations and compared to the nominal strengths determined by Kulak et al. [32]. The results showed that the bolt shear forces in specimens J310T and J310C exceeded the bolt shear strength, which will be discussed further in Section 3.5.2.

Above all, the proposed FE analysis procedure could give accurate predictions for the behaviour of the assembly of I-shape braces and flange plate brace connections, resulting in a powerful tool for further detailed investigation of the behaviour of connections used for CCBFs.

3.5. ANALYSIS AND DISCUSSION

3.5.1. Load transfer mechanisms within brace connections

Monotonic loading simulations are generally adopted to analyze the force transfer mechanism in connections. However, buckling response in compression can cause significant uneven plastic deformations in the buckling components, which can affect the tensile behaviour and ultimate tensile strengths after load reversal. In order to account for such effect, single-cycle loading simulations were conducted in which all specimens were initially loaded to their maximum compressive displacements imposed in the tests before fracture and then stretched to the test maximum tensile displacements before fracture. As shown in Figure 3.9, the compressive and tensile strengths obtained from the single-cycle loading simulations matched well the experimental results for all specimens.

To analyse the force development and distribution within the connection, the forces (friction force effect included) developed within the gusset plate, the flange lap plates, and the web lap plates were extracted from the simulations using the 'section output' function of ABAQUS [37]; the results are plotted in Figure 3.10. In the figure, the calculated yield strengths of the lap plates and the gusset, as determined from the measured steel yield strengths, are presented for reference purposes.

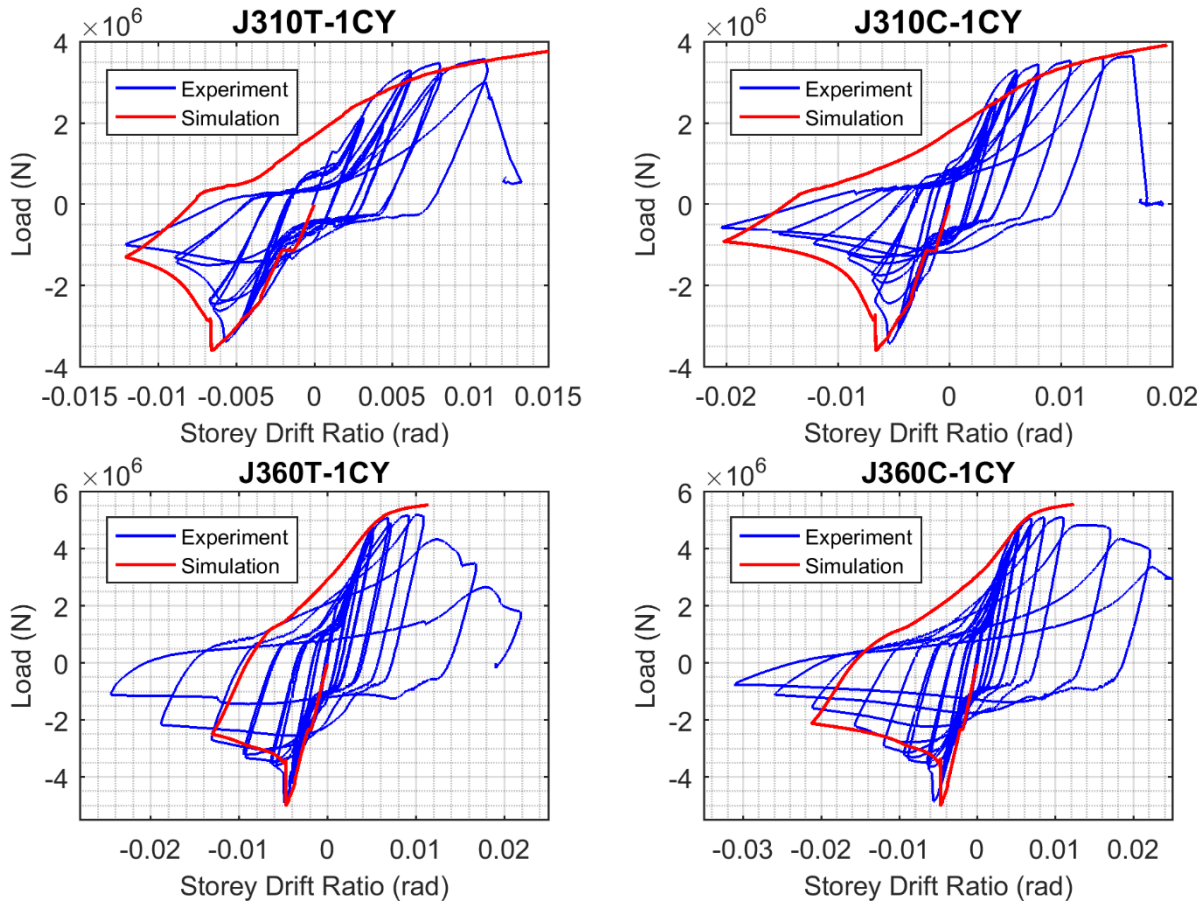

Figure 3.9: Comparison of single-cycle FE simulation results with laboratory load vs. storey drift ratio hysteretic curves

The force development in the flange lap plate and the web lap plate indicates that there are three stages in terms of force transfer within the connecting plate zone. Initially the force within the connecting plate zone was transferred by the frictional resistance between all components due to the clamping effect of the bolt pretension.

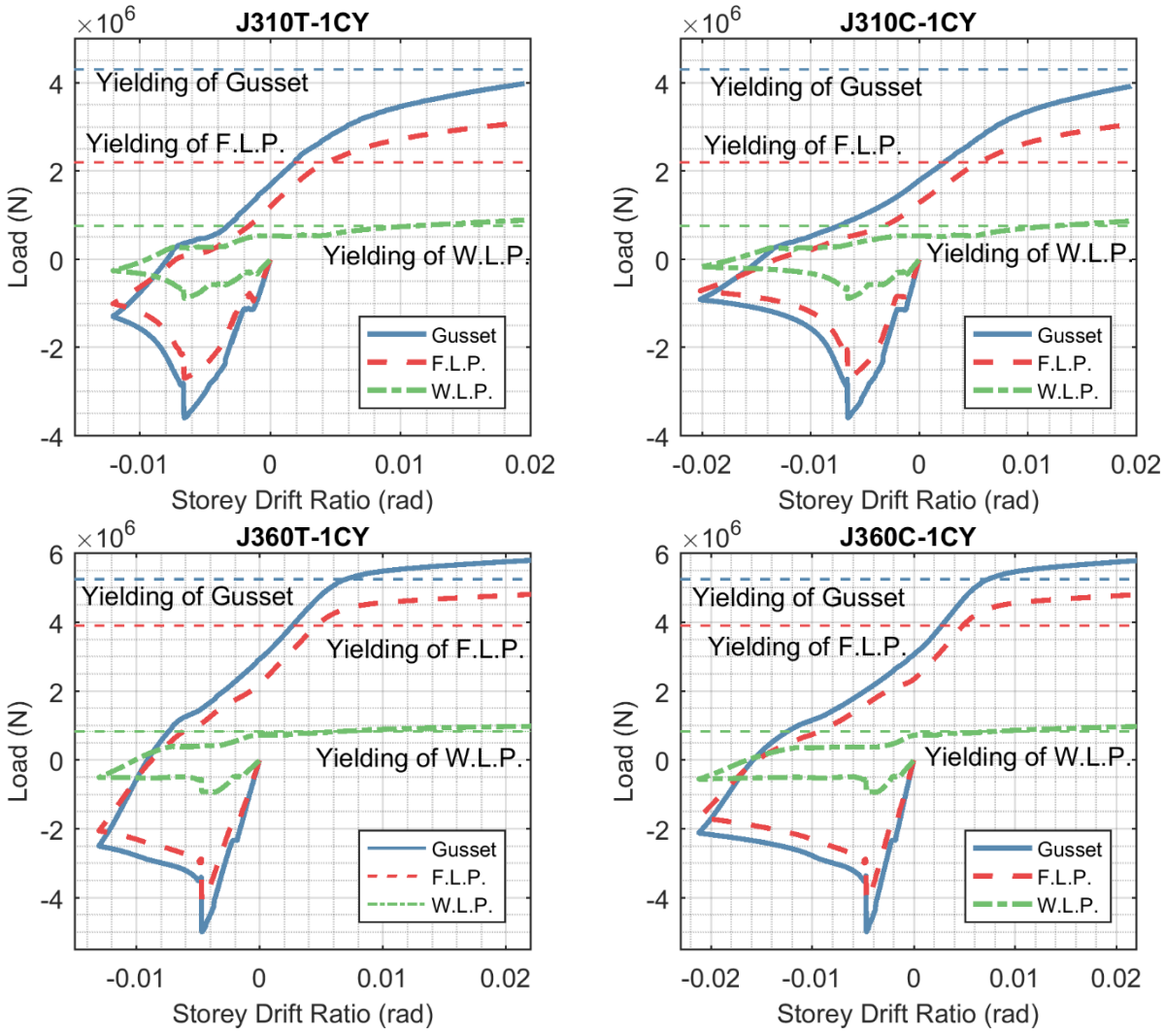

Figure 3.10: Force flow within connections: F.L.P. = flange lap plate, W.L.P. = web lap plate

As the force increased in compression, bolt slippage occurred in both the flange branch and the web branch. However, the bolt bearing in the two branches was not synchronized. Note that two major plateaus due to bolt slippage occurred in the force development of the web lap plates (WLP), while only one was found for the flange lap plates (FLP). This discrepancy was related to how the flange lap plates and the web lap plates were connected (Figure 3.1). The flange lap plates were bolted to the brace flange on one side and welded to the gusset plate on the other side, whereas the web lap plates were bolted on both sides to facilitate erection of the brace structure. For bearing-

type bolted connections, slip has to occur to reach their ultimate bearing condition; in contrast, welded components can develop their full resistance potential without the requirement for slip of the connection. Hence, theoretically the web lap plates (WLP) needed twice the bolt slippage to reach the bearing condition, which is indicated by the two plateaus shown for the WLP curves in Figure 3.10.

Therefore, following the first major bolt slippage, two stages will likely exist: the flange lap plates will start to develop their ultimate strengths by bolt bearing, while the force in the web branch is still a frictional force. Not until the flange branch deforms sufficiently to accommodate all bolt slippage in the web branch, will the ultimate bearing condition be attained in the web branch. This explains why the flange lap plates are always the first to yield and to develop their ultimate strength, as shown in Figure 3.10.

Moreover, when the brace connections are stretched in tension, Figure 3.10 shows that most plastic deformation concentrates in the connecting plate zone. The force in the gusset plate is determined as the sum of forces in the flange plates and the web lap plates. With the strain hardening of the flange plates after yielding and greater engagement of the web branch, the gusset plate might yield (the cases of J360T and J360C) or not (the cases of J310T and J310C).

In CCBFs, the connecting plate zone is usually the weakest link compared to its connected gusset plate and bracing member when subjected to tension. This is because the seismic design of CCBFs is based on an elastic structural analysis, and each component is only required to have a factored resistance equal to or greater than the factored load effects, without additional seismic detailing and proportioning requirements. The brace and its brace connection (including both the gusset plate and connecting plate zone) are selected using the same force demand, because they work in series. The tensile and compressive force demands obtained from a linear elastic structural analysis

are the same ($T_f = C_f$) since braces are often paired symmetrically. However, the braces and gusset plates are usually selected and designed based on their compressive resistances (C_r), because buckling normally leads to a lower axial resistance compared to that associated with tension loading ($C_r < T_r$). This generally results in a large overstrength in braces and gusset plates when they are loaded in tension. In contrast, since buckling behaviour is often not considered in the design of the connecting plate zone, the tensile overstrength for the plates is typically less.

3.5.2. Bolts in the connection

In bearing-type bolted joints, the forces are mainly transferred by bolt shear and bearing after slip. At the ultimate limit state, high-strength bolts in such 'bearing-type' joints may fail by shear rupture. This type of failure mode is known to have limited deformation capacity [32]. Hence, it is desirable to prevent bolt shear rupture if ductile connection behaviour is sought. As discussed in the previous section, within the connecting plate zone, the flange branch is always the first to develop its ultimate strength through bearing, which contradicts the common assumption in current design practice that the forces in the flange branch and web branch are in proportion to the ratio of the brace flange area to the brace web area. Moreover, the connecting plate zone is likely to develop its ultimate strength when loaded in tension, since it is usually the weakest compared to the connected brace and gusset plate. This places the bolts in the flange plate brace connections of CCBFs at risk of shear rupture. Bolt shear failure has been witnessed in the tests of Rudman [24] and Rudman et al. [25], and in the finite element modeling of Wang et al. [38]. To avoid bolt shear rupture, the bolt groups in the flange branch and the web branch should be designed to resist the predicted ultimate strength of the plates in each branch.

The connection of the brace web to the gusset plate with web lap plates is a typical double-shear bolted butt joint. The bolt group in such joints has been investigated by many researchers, e.g.,

Fisher & Rumpf [39] and Fisher & Kulak [40]. However, the behaviour of the single-shear bolt group in the flange lap plate is expected to be more complex. The shear force development in the bolts of the flange lap plates was extracted from the single-cycle loading FE simulation; the results are plotted in Figure 3.11. Uneven shear force distribution within the bolt group was found. The ratios of maximum to minimum shear forces in specimens J360T, J360C, J310T, and J310C, are 1.23, 1.23, 1.22, and 1.21, respectively. In all cases, the bolts in the row closest to the welds experience the minimum force, while the bolts in the middle row(s) were subjected to the maximum force. The uneven distribution of shear force in the bolt group comes from the requirement of deformation compatibility between the connected components; forces are shared in a way that the deformations of the two connected plates between any two adjacent transverse rows of bolts are compatible with each other. Past research has shown that the force partition within the 'bearing-type' bolt group is affected by a number of parameters, including connection length, relative stiffness of the connected components, pitches (the distance between centers of adjacent fasteners along the line of principal stress), bolt arrangement patterns, etc. [41].

In short connections, almost complete equalization of load is likely to take place before bolt failure occurs because the bolts' shear deformation allows for an even sharing of force between fasteners. Failure in this case appears as a simultaneous shearing of all the bolts. However, in situations where the force distribution between bolts is significant, the most highly loaded bolt will be the first to fail by shear rupture. The remaining bolts are usually not capable of carrying much additional load without incurring failure themselves in a sequential fashion. The sequential failure of fasteners is known as 'unbuttoning'. This phenomenon has been verified by both numerical and experimental research [40,42]. The unbuttoning behaviour was also observed in the tests of specimens J310T and J310C, in which the flange lap plate bolts in the middle row ruptured first,

followed by immediate rupture of all the remaining bolts connecting the flange lap plates. The process was so quick that the sequence of rupture could only be found by review of the video recording, as shown in Figure 3.12.

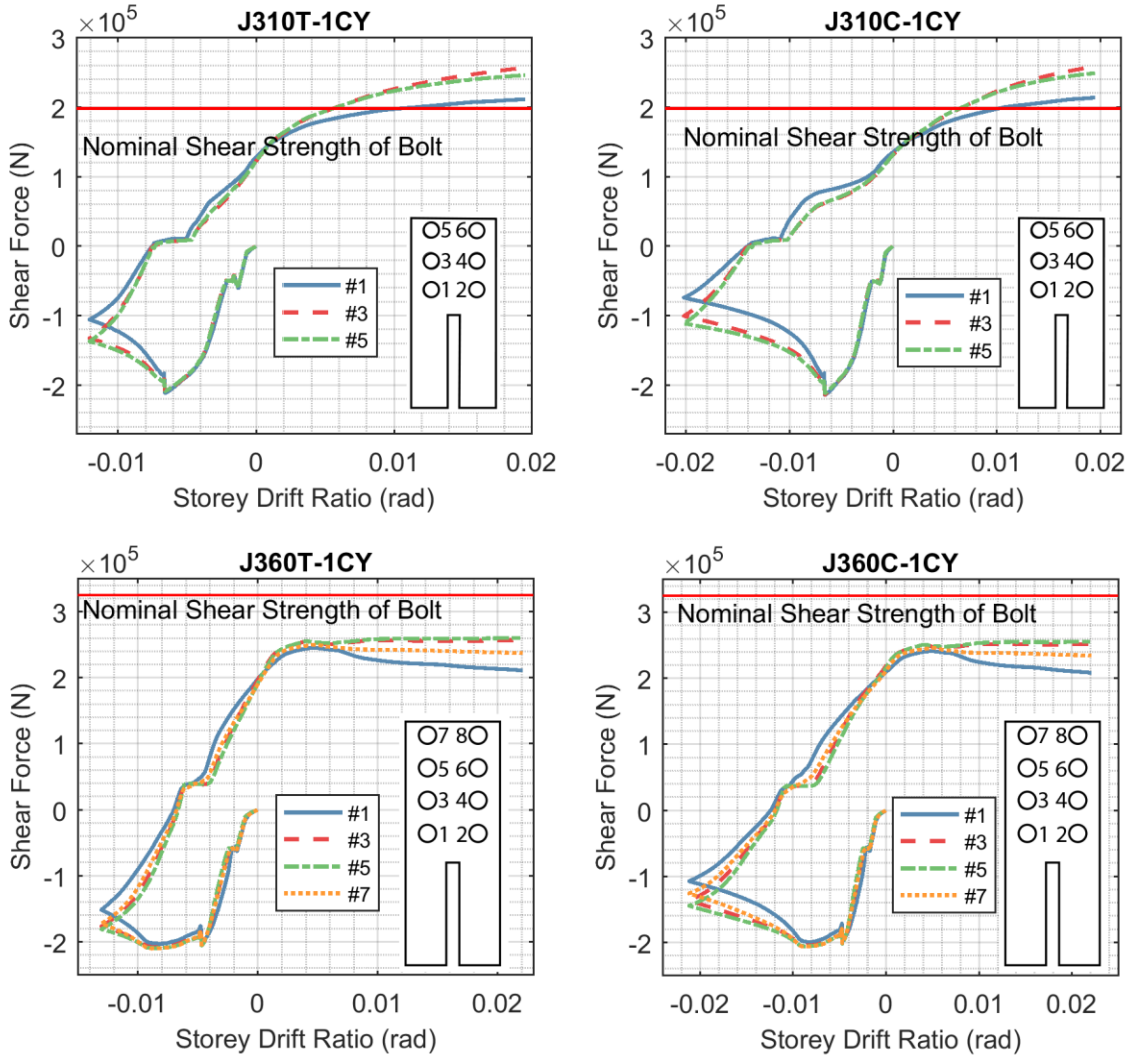

Figure 3.11: Individual bolt shear force development in flange lap plates

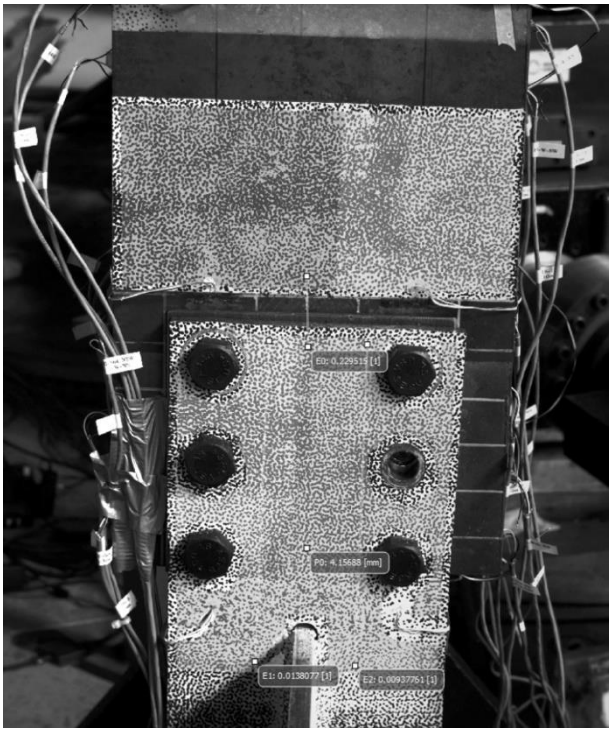

Figure 3.12: First ruptured bolt in the middle row

In order to avoid bolt shear rupture, the uneven distribution of shear forces within a bolt group should be taken into account in design. Current design practice is based on the assumption that each fastener carries an equal share of the load, and the shear resistance reduction due to the nonuniform distribution of force is generally accounted for by a reduction factor in a step-wise manner. In AISC 360 [26], the bolt shear resistance is reduced by 16.7% if the fastener pattern length is greater than 950 mm (38 in.). According to CSA S16 [1] (Clause 13.12.1.2), the bolt factored shear resistance has to be reduced by the same amount (16.7%) for lap splices with length L greater than 760 mm. However, the results indicate that for the bolts in the flange plates, significant variation in shear force distribution exists even in short connections, likely due to the extensive plastification of these plates. Further research is needed to quantify the nonuniform bolt shear forces in flange plates and to develop design guidelines.

To illustrate the effectiveness of the proposed design recommendations, whereby the bolts should be chosen to be able to carry the force associated with the predicted ultimate strength of the flange lap plates, new bolt designs were conducted for the tested specimens J310T and J310C. These configurations were chosen because all bolts in the flange branch failed in a brittle manner during laboratory testing [24, 25]. In the new design, eight 24 mm A325 bolts were used for each flange branch instead of the original six 22 mm A325 bolts. The shear force development of the individual bolts was extracted from the single-cycle loading simulation of the two modelled specimens (Figure 3.13). The results obtained from the numerical models illustrated that with the new design, bolt shear failure could be avoided.

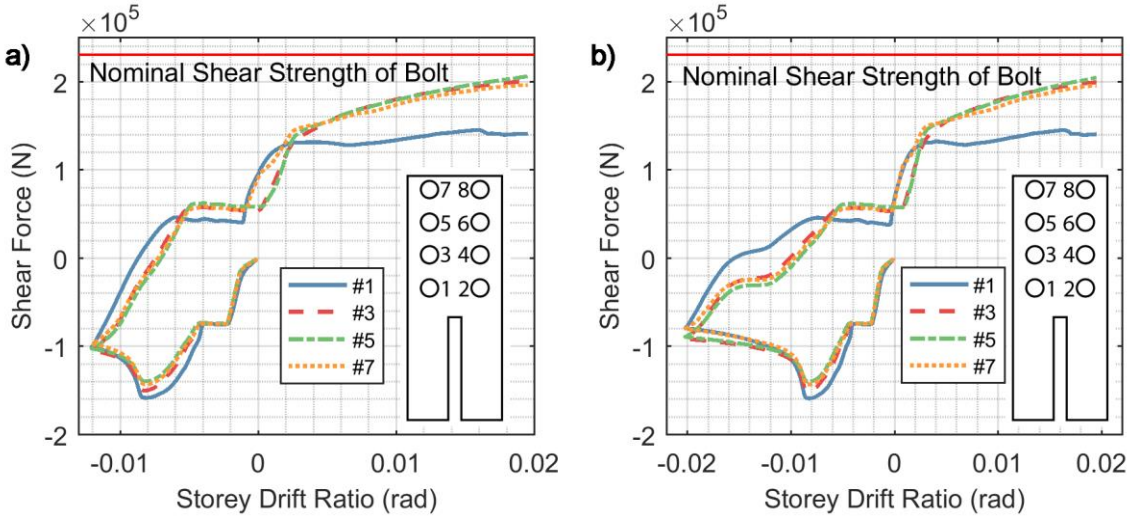

Figure 3.13: Individual bolt shear force development in flange lap plates with new bolt design: a) J310T; b) J310C

3.5.3. Welds in the connection

The connection of the flange lap plates to the gusset plate is made by slotting the flange plates longitudinally, inserting them onto the gusset plate, and then placing longitudinal fillet welds at the interface. The flange lap plate transfers the forces from the brace by bolt bearing and to the gusset plate by weld shear. As explained in Section 3.5.2, the flange branch in the connection is

always the first to develop its ultimate strength. As such, the weld group in the flange branch should have a resistance greater than the ultimate strength of this branch to avoid weld fracture.

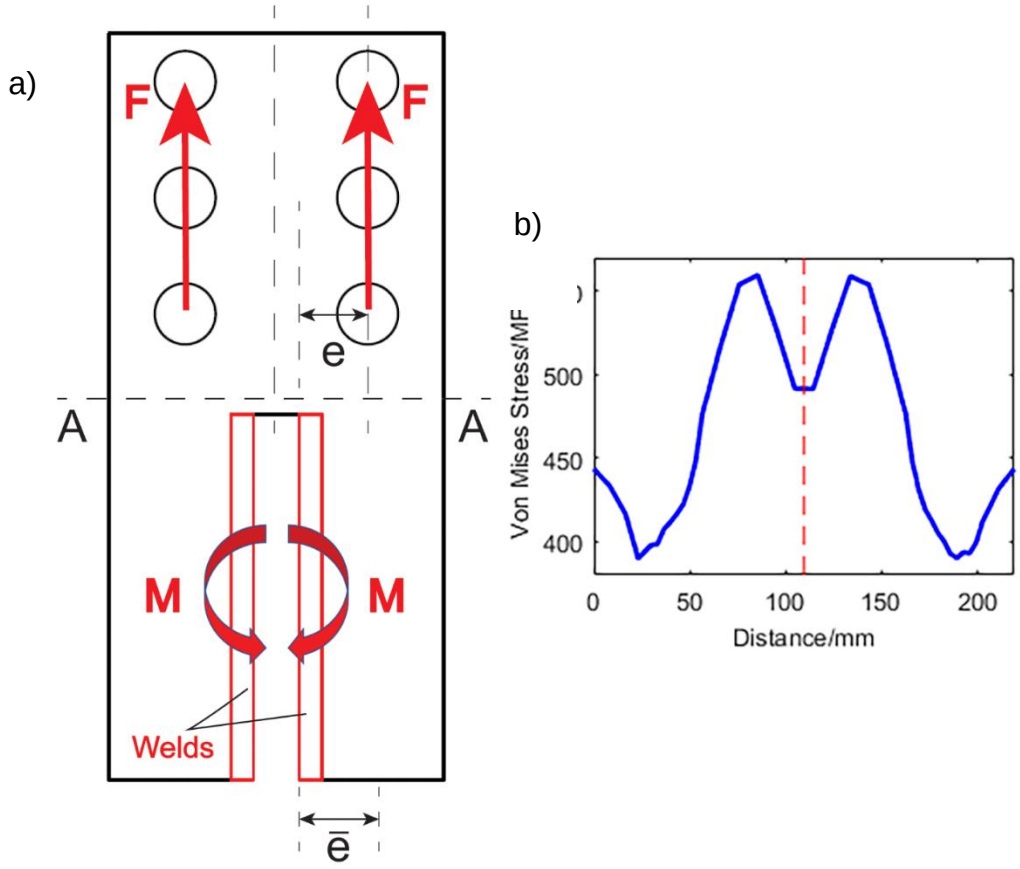

Figure 3.14: Forces in flange lap plates: (a) load eccentricity on welds, (b) simulated stress distribution along path A-A of J310T-1CY at storey drift ratio of 0.01

Since the distance between the bolts and welds of the flange lap plates is short, a significantly nonuniform stress distribution may occur in the area, as was observed in the numerical simulation (Figure 3.14b), which produces load eccentricity on the welds. The moment (M) acting on the weld-to-gusset plate interface and the force (F) transferred by each line of bolts were extracted from the single-cycle FE simulation. The value of the moment divided by the force (M/F) is plotted in Figure 3.15. For simplicity, only the results with positive stretch elongation of the assemblies are shown, since the most critical values occurred in this range. As the load transferred by the bolts

is increased, the eccentricity quickly reaches a peak and then slowly decreases. The slow reduction is believed to result from the plasticity that developed within the flange lap plate and the resulting stress redistribution. In all the specimens, the eccentricity peaks remained between e (distance between the weld-gusset interface and the centerline of bolts) and $\bar{e}$ (distance between the weld-gusset interface and the centerline of the leg of the flange lap plate) (Figure 3.14a).

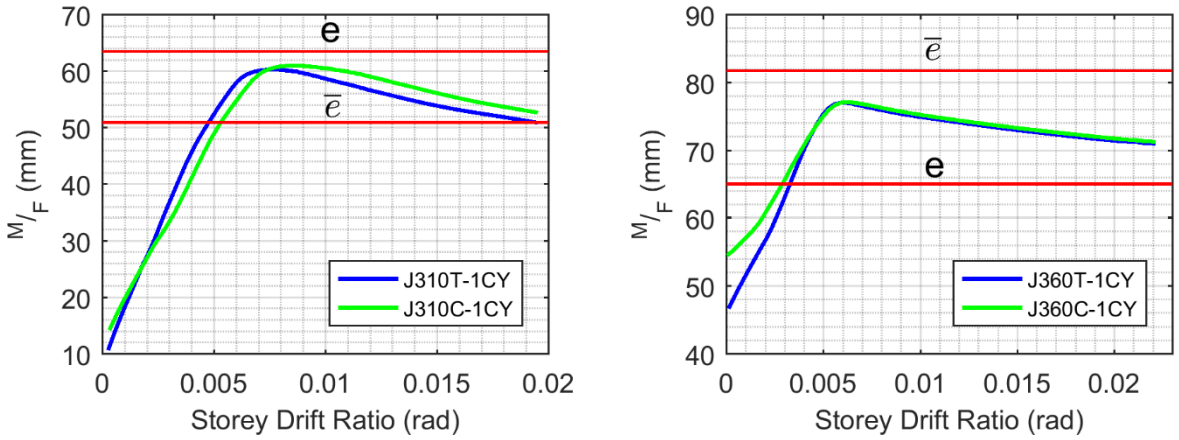

Figure 3.15: Loading eccentricity on welds about weld-gusset interface

3.6. CONCLUSIONS AND DESIGN RECOMMENDATIONS

A FE modeling procedure was developed to depict the behaviour of an assembly of CCBF I-shape braces and bolted brace connections subjected to cyclic inelastic loading. The model was validated against full-scale laboratory test results. It was found capable of predicting the brace and connection responses at both the global level (the global load-deformation relation) and the component level (the deformation of all parts). The developed FE model provides a powerful tool for the future parametric study of I-shape brace connections.

In the connections that were studied, the brace axial forces are transferred from the brace to the gusset by the flange lap plates (flange branch) and the web lap plates (web branch) acting in

parallel. The analyses revealed that three stages exist for the force transfer mechanism within the connecting plate zone: 1) before major bolt slippage occurs, the force is entirely transferred by means of friction resistance between all components; 2) following the first major bolt slippage, the flange lap plates start to develop their ultimate strength by bolt bearing, while the force in the web branch is still transferred by friction; and 3) not until the flange branch deforms to accommodate all bolt slippage in the web branch, will the ultimate bearing condition be attained in the web branch.

In CCBFs, gusset plates and braces are typically designed for compressive resistance, and therefore possess significant overstrength in tension. Connecting lap plates in the connections are designed for tensile resistance and, hence, the connecting plate zone is usually the weakest part compared to the gusset plate and the I-shape brace in terms of tensile strength. Both the flange branch and the web branch of the connecting plate zone are expected to develop their ultimate tensile strength. In order to avoid premature bolt shear rupture and weld fracture and to develop minimum ductility, it is recommended that the bolts and welds along the flange branch be designed based on the ultimate tensile strength of this branch (most likely the ultimate tensile strength of the flange lap plates). Likewise, the bolts in the web lap plates are recommended to be designed to resist a force equal to the ultimate tensile strength of the web branch (either the ultimate tensile strength of the web lap plates or the block shear strength of the I-shape brace web or gusset plate).

The tests and the numerical simulations revealed a nonuniform distribution of shear forces within the bolt group connecting the flange lap plates to the brace flanges, even if the connection length was short. This phenomenon may have detrimental consequences on the shear strength of the bolt group due to the ‘unbuttoning response’; this effect should be taken into account in the bolt design

to achieve a ductile connection response. Further studies are required to characterise the bolt shear distribution in this connection type and to propose guidance for design.

The study also showed that a pronounced loading eccentricity exists on the fillet welds connecting the flange lap plates to the gusset plate. For design, conservatively, the magnitude of the eccentricity can be taken as the larger of the distance between the weld-to-gusset plate interface and the centerline of bolts, and the distance between the weld-to-gusset plate interface and the centerline of the leg of the flange lap plates.

ACKNOWLEDGEMENTS

The authors would like to thank the ADF Group Inc. and DPHV Structural Consultants for their generous technical and financial support, as well as the Natural Sciences and Engineering Research Council of Canada (NSERC), the Fonds de recherche du Québec - Nature et technologies (FRQ-NT) and the Centre d'études interuniversitaire des structures sous charges extremes (CEISCE). The first author is supported in part through the China Scholarship Council (CSC). The finite element computations were conducted on the supercomputer Graham cluster, which is managed by Calcul Québec and Compute Canada. Operation of the supercomputer is funded by the Canada Foundation for Innovation (CFI), NanoQuébec, RMGA and the Fonds de recherche du Québec - Nature et technologies (FRQ-NT).

REFERENCES

[1] Canadian Standards Association (CSA) S16-19. (2019). Design of steel structures. Toronto, ON, Canada.

[2] American Society of Civil Engineers/Structural Engineering Institute (ASCE/SEI) 7-16. (2016). Minimum Design Loads and associated criteria for buildings and other structures. Reston, Virginia, USA.

[3] EN 1998-1. (2004). Eurocode 8: Design of Structures for Earthquake Resistance – Part 1: general Rules, Seismic Actions and Rules for Buildings. Brussels: European Committee for Standardization.

[4] Standards New Zealand (NZS). (2007). NZS 3404 Part 1:1997, Steel Structures Standard Incorporating Amendment No. 1 and Amendment No. 2., Wellington, NZ.

[5] GB50017-2017. (2017). Standards for Design of Steel Structures. Beijing, China: Ministry of Housing and Urban-Rural Development of the People's Republic of China. [in Chinese]

[6] National Institute for Land and Infrastructure Management & Building Research Institute. (2015). Manual for Structural Regulations for Building Design. All Japan Official Gazette Inc. [in Japanese]

[7] Architectural Institute of Japan. (2012). Recommendation for Design of Connections in Steel Structures. [in Japanese]

[8] Astaneh-Asl, A. (1998). Seismic behavior and design of gusset plates. Structural Steel Educational Council.

[9] Whitmore, R. E. (1952). Experimental investigation of stresses in gusset plates. MS thesis, Univ. of Tennessee, Knoxville, Tenn.

[10] Chakrabarti, S. K., & Bjorhovde, R. F. A. (1985). Tests of Full-Size Gusset Plate Connections. Journal of Structural Engineering, 111(3), 667-684. doi:10.1061/(ASCE)0733-9445(1985)111:3(667)

[11] Huns, B., Grondin, G., & Driver, R. (2006). Tension and shear block failure of bolted gusset plates. Canadian Journal of Civil Engineering, 33, 395–408.

[12] Teh, L. H., & Elliott, M. D. (2019). Ultimate tensile resistance of bolted gusset plates. Practice Periodical on Structural Design and Construction, 24(4). https://doi.org/10.1061/(ASCE)SC.1943-5576.0000454

[13] Thornton, W. A. (1984). Bracing connections for heavy construction. Engineering Journal, 21(3), 139-148.

[14] Cheng, J. J. R., Yam, M. C. H., & Hu, S. Z. (1994). Elastic buckling strength of gusset plate connections. Journal of Structural Engineering, 120(2), 538–559. https://doi.org/10.1061/(ASCE)0733-9445(1994)120:2(538)

[15] Yam, M. C. H., & Cheng, J. J. R. (2002). Behavior and design of gusset plate connections in compression. Journal of Constructional Steel Research, 58(5), 1143–1159. https://doi.org/10.1016/S0143-974X(01)00103-1

[16] Astaneh-Asl, A., Cochran, M., & Sabelli, R. (2006). Seismic detailing of gusset plates for special concentrically braced frames. Structural steel educational council.

[17] Lehman, D. E., Roeder, C. W., & Herman, D. (2008). Improved Seismic Performance of Gusset Plate Connections. Journal of Structural Engineering, 134(6), 890-901. doi:10.1061/(ASCE)0733-9445(2008)134:6(890)

[18] Roeder, C. W., Lumpkin, E. J., & Lehman, D. E. (2011). A balanced design procedure for special concentrically braced frame connections. Journal of Constructional Steel Research, 67(11), 1760-1772. doi:10.1016/j.jcsr.2011.04.016

[19] Sen, A. D., Roeder, C. W., Lehman, D. E., Berman, J. W., Sloat, D., Ballard, R., & Johnson, M. M. (2016). Experimental evaluation of the seismic vulnerability of braces and connections in older concentrically braced frames. Journal of Structural Engineering (United States), 142(9). doi:10.1061/(ASCE)ST.1943-541X.0001507

[20] Sen, A. D., Swatosh, M. A., Ballard, R., Sloat, D., Johnson, M. M., Roeder, C. W., Berman, J. W. (2017). Development and Evaluation of Seismic Retrofit Alternatives for Older Concentrically Braced Frames. Journal of Structural Engineering, 143(5), 04016232. doi:10.1061/(ASCE)ST.1943-541X.0001738

[21] Bradley, C. R., Fahnestock, L. A., Hines, E. M., & Sizemore, J. G. (2017). Full-Scale Cyclic Testing of Low-Ductility Concentrically Braced Frames. Journal of Structural Engineering, 143(6). doi:10.1061/(ASCE)ST.1943-541X.0001760

[22] Sizemore, J. G. S. M. A., Bradley, C. R. S. M. A., Fahnestock, L. A. P. D., & Hines, E. M. P. D. (2017). Parametric Study of Low-Ductility Concentrically Braced Frames under Cyclic Static Loading. Journal of Structural Engineering, 143(6). doi:10.1061/(ASCE)ST.1943-541X.0001761

[23] Sizemore, J. G., Fahnestock, L. A., & Hines, E. M. (2019). Seismic Performance Assessment of Low-Ductility Concentrically Braced Frames. Journal of Structural Engineering, 145(4). doi:10.1061/(ASCE)ST.1943-541X.0002276

[24] Rudman, A. (2018). Testing of conventional construction W-shape brace members and their bolted end connections undergoing reversed cyclic loading. Master's thesis, Department of Civil Engineering, McGill University, Montreal, QC, Canada.

[25] Rudman, A., Tremblay, R., Rogers, C.A. (2021). Conventional I-shape brace member bolted connections under seismic loading: Laboratory study. Journal of Constructional Steel Research, 184, 106795 .

[26] American Institute of Steel Construction (AISC) 360-16. (2016). Specification for Structural Steel Buildings. Chicago, IL, USA.

[27] Abaqus 6.14 Documentation (2014). Systèmes Dassault Simulia Corp., Providence, RI, USA.

[28] Citipitioglu, A. M., Haj-Ali, R. M., & White, D. W. (2002). Refined 3D finite element modeling of partially-restrained connections including slip. Journal of Constructional Steel Research, 58(5-8), 995-1013. doi:10.1016/s0143-974x(01)00087-6

[29] Bagheri Sabbagh, A., Petkovski, M., Pilakoutas, K., & Mirghaderi, R. (2013). Cyclic behaviour of bolted cold-formed steel moment connections: FE modelling including slip. Journal of Constructional Steel Research, 80, 100-108. doi:10.1016/j.jcsr.2012.09.010

[30] Bursi, O. S., & Jaspart, J. P. (1998). Basic issues in the finite element simulation of extended end plate connections. Computers & Structures, 69(3), 361-382. doi:10.1016/s0045-7949(98)00136-9

[31] American Society for Testing and Materials (ASTM) A370-17. (2017). Standard Test Methods and Definitions for Mechanical Testing of Steel Products. West Conshohocken, PA: ASTM International.

[32] Kulak, G. L., Fisher, J. W., & Struik, J. H. (2001). Guide to Design Criteria for Bolted and Riveted Joints Second Edition. Chicago, IL: AISC.

[33] Tousignant, K., & Packer, J. A. (2017). Numerical Investigation of Fillet Welds in HSS-to-Rigid End-Plate Connections. Journal of Structural Engineering, 143(12). doi:10.1061/(asce)st.1943-541x.0001889

[34] American Society for Testing and Materials (ASTM) A6/A6M-17. (2017). Standard Specification for General Requirements for Rolled Structural Steel Bars, Plates, Shapes, and Sheet Piling. West Conshohocken, PA: ASTM International.

[35] Canadian Standards Association (CSA) G40.20-13/G40.21-13. (2013). General requirements for rolled or welded structural quality steel/Structural quality steel. Toronto, ON: Canadian Standards Association.

[36] Wang, M., Shi, Y., Wang, Y., & Shi, G. (2013). Numerical study on seismic behaviors of steel frame end-plate connections. Journal of Constructional Steel Research, 90, 140-152. doi:10.1016/j.jcsr.2013.07.033

[37] Abaqus Analysis User's Guide. (2016). Systèmes Dassault Simulia Corp., Providence, RI, USA.

[38] Wang, C., González Ureña, A., Afifi, M., Rudman, A., Tremblay, R., Rogers, C. A. (2020) "Conventional construction steel braces with bearing plate energy dissipation", 17th World Conference on Earthquake Engineering, Sendai, Japan

[39] Fisher, J. W., & Rumpf, J. L. (1965). Analysis of bolted butt joints. Journal of the Structural Division, ASCE, Vol. 91, ST5.

[40] Fisher, J. W., & Kulak, G. L. (1968). Tests of bolted butt splices. Journal of the Structural Division, ASCE, Vol. 94, ST11.

[41] Kulak, G. L. (1967). The Analysis of Constructional Alloy Steel Bolted Plate Splices. Ph.D. Dissertation, Lehigh University, Bethlehem, Pennsylvania.

[42] Bendigo, R. A., Hansen, R. M., & Rumpf, J. L. (1963). Long bolted Joints. Journal of the Structural Division, Vol. 89, ST6.

FOREWORD TO CHAPTER 4

For CCBFs the capacity-based design method is typically not adopted, i.e. there are no designated yielding members and specified yielding/failure hierarchy. As such, the relative strength amongst components of the bolted brace connection is uncertain, and any component can be the weakest and fail under earthquake loading. To study the effect of the possible variability in the relative strength amongst components of the bolted brace connection, a parametric study was conducted and presented in Chapter 4. A series of high-fidelity FE models were constructed for the brace and connection assemblies following the validated modeling procedure developed in Chapter 3, in which three design parameters of the brace connection, namely, the flange lap plate thickness, the web lap plate thickness and the gusset plate thickness, were varied. The variation in the three parameters changed the relative strength between the flange branch and the web branch in the brace-to-gusset connection, and the relative strength between the brace-to-gusset connection and the gusset plate. The behaviour of the brace and connection assemblies under both tension and compression loadings was studied. Various possible failure modes of the brace connection were revealed, and all the deformation mechanisms were identified, which laid a foundation for the component-based modeling of the connection, which is detailed in Chapter 5. The effect of each studied design parameter on the connection deformation capacity was discussed. Design recommendations are proposed with regard to attaining better deformation capacity of the brace connection.

CHAPTER 4: PARAMETRIC STUDY ON THE I-SHAPE BRACE CONNECTION OF CONVENTIONAL CONCENTRICALLY BRACED FRAMES

Published in Journal of Constructional Steel Research, Volume 182, July 2021, https://doi.org/10.1016/j.jcsr.2021.106669

Chen Wang, Robert Tremblay, Colin A. Rogers

ABSTRACT

Concentrically braced frames (CBFs), designed using the conventional linear elastic method without seismic proportioning and detailing requirements, are referred to as Conventional CBFs (CCBFs) in this study. They are widely used in moderate and low seismic areas in North America due to the ease of design and economy. Without a code specified dedicated fuse member to dissipate earthquake induced energy, or a prescribed yield/failure hierarchy, the brace connection of a CCBF is usually the weakest link in the lateral load-carrying path and prone to fracture. The brace connection is therefore determinant for the structural seismic performance. In this paper, a parametric study based on a validated numerical simulation procedure was carried out on a typical I-shape brace connection, i.e. the flange plate connection. Three key design parameters, namely, the gusset plate thickness, the flange lap plate thickness, and the web lap plate thickness, were varied to study their effects on both the compressive and tensile behaviour of the brace and connection assembly. Various possible failure modes were revealed both in compression and in tension. The results showed that the brace end restraint provided by flange plate connections in

CCBFs was significant; the pinned-end assumption would lead to conservative estimation of the brace buckling resistance, which might trigger detrimental gusset plate buckling. The tensile overstrength of the flange lap plate, due to the presence of transverse tensile stress along the net section, was quantified using the von Mises criterion. Design recommendations are proposed with regards to attaining better deformation capacity.

Keywords**:** conventional CBFs, I-shape brace, flange plate connection, FE simulation, parametric study

4.1. INTRODUCTION

The choice of concentrically braced frames (CBFs) as the seismic force resisting system (SFRS) of steel buildings is prevalent in North America owing to their efficiency and economy in providing the required lateral strength and stiffness. In areas of high seismic hazard, the capacity design principle along with rigorous detailing and proportioning rules are generally required for the design of CBFs, e.g. the Special Concentrically Braced Frames (SCBFs) in the ASCE/SEI 7-16 [1] and the Moderately Ductile (Type MD) CBFs in the National Building Code of Canada (NBCC) [2]. The plastic behaviour in these systems is restricted to the bracing members, while all the other framing members and connections in the lateral load path are designed to remain essentially elastic when subjected to severe earthquake shaking [3].

However, in moderate or low seismic zones, CBFs designed following a conventional design method, in which the primary requirement is for the factored resistance of all components in the lateral load path to be greater than the factored load effect, are extremely popular. Such CBFs can easily be designed by practicing structural engineers based on a linear elastic analysis using commonly available software. Moreover, the ability to waive the rigorous seismic detailing and proportioning requirements may result in structures having less steel tonnage compared to CBFs designed with capacity design principles and more stringent detailing rules, despite the higher design seismic loads (lower seismic force reduction factor) [4]. There is no dedicated seismic fuse member in these CBFs; it is assumed that sufficient seismic energy dissipation can be provided through limited yielding in members and connections along the lateral load path, as well as through friction within the joints. In this paper, such CBFs are referred to as Conventional CBFs (CCBFs). CBFs of Conventional Construction (Type CC) category in the NBCC [2] and CBFs ‘not specifically detailed for seismic resistance’ in accordance with ASCE / SEI 7-16 [1] are two

examples of CCBF systems. Furthermore, existing CBFs that were designed prior to the adoption of the seismic design provisions in the 1988 Uniform Building Code [5] in the USA and the CSA S16.1-M89 Standard [6] in Canada were designed for reduced seismic loads with no regard for yield and failure hierarchy, or ductile detailing [7].

Bracing members are usually connected to other framing members by means of gusset plates. The focus of most past studies on brace connections has been placed on the design of the gusset plates, e.g. Chakrabarti & Bjorhovde [8], Lehman et al. [9] and Fang et al. [10]. However, another zone can be identified within the global brace connection, that is, the brace-to-gusset connection [11]. The bracing members, brace-to-gusset connections, and gusset plates work in series along the lateral load path. Under the conventional design principle, the brace-to-gusset connection is usually the weakest link, and thus is vulnerable to fracture when the brace is subjected to tension, because the compressive buckling resistance generally governs the design and selection of the bracing members and gusset plates. Greater tensile overstrength exists in the bracing members and gusset plates compared to the brace-to-gusset connection. The brace-to-gusset plate weld deficiency in CCBFs was found experimentally and proved highly detrimental for the drift capacity by Sen et al. [12]. Brace connection failures were also reported frequently in post-earthquake reconnaissance [13,14].

Unlike many structural steel members, which usually demonstrate a minimum level of ductility prior to failure, some failure modes of the brace connections, e.g. weld failure or bolt rupture, have very limited deformation capacity. Moreover, due to the low redundancy of CBFs, the failure of brace connections may severely diminish the structural integrity, i.e. very likely cause a soft-storey mechanism, and eventually lead to structural collapse [13].

Without a predefined yield and failure hierarchy in the design process, theoretically any failure mode could occur in CCBFs under a severe seismic event, resulting in high variance and unpredictability in the structural ductility and seismic performance. Recent research on CCBFs has revealed the high risk of their seismic behaviour and has indicated that brace connections are vulnerable to failure [15,16]. In order to prevent premature brace connection failure and early loss of structural integrity, the CSA S16 Standard [17] requires that the design seismic force for brace connections be amplified by 1.5 unless ductile connection behaviour can be guaranteed. Unfortunately, due to a lack of research on this issue, no code prescribed guidelines outlining how to achieve ductile connection behaviour are readily available.

I-shape sections are very common as bracing members, because they are available with a wider range of sizes compared to hollow structural sections (HSSs). However, the connection mechanism between an I-shape brace and its gusset plates is more complex than that of HSSs. A typical I-shape brace connection configuration is the flange plate connection, as shown in Figure 4.1. Although commonly specified in practice, the behaviour and performance of the I-shape brace connections are far from being well understood, which poses a high risk in the seismic performance of buildings using such connections. In order to gain insight into the behaviour of typical I-shape brace connections and to propose design guidelines to achieve ductile connection behaviour of CCBFs, a coordinated experimental and analytical research project was launched at McGill University and Polytechnique Montréal [18-21]. The study presented in this paper is a continuation of this research project.

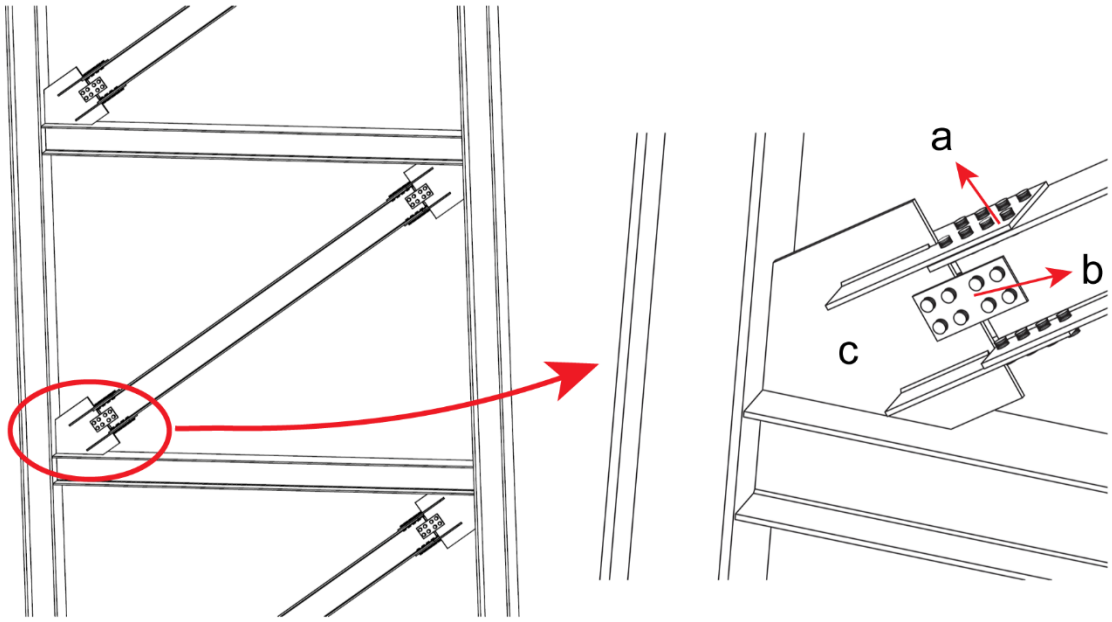

Figure 4.1: Schematic illustration of CCBF with I-shape braces and flange plate brace connections: (a) flange lap plate (FLP); (b) web lap plate (WLP); (c) gusset plate

A parametric study was conducted on the flange plate connection utilizing the validated finite element (FE) modelling procedure [21]. The specimens tested in the laboratory by Rudman et al. [18,19] served as the reference cases. Two I-shape sections were selected as the bracing members, to investigate the possible influence of section size. Three parameters, namely, gusset plate thickness, flange lap plate thickness, and web lap plate thickness, were varied, and their effects on both the tensile and compressive behaviour of the brace-connection assembly were studied. Recommendations are made based on the results of the parametric study, with the objective of achieving ductile behaviour of CCBFs.

4.2. RESEARCH PROJECT ON I-SHAPE BRACE CONNECTIONS

Currently, due to the lack of data on the seismic behaviour of CCBFs and the lack of code prescribed guidelines on how to attain ductile connection behaviour, practicing engineers in Canada will typically resort to the use of the 1.5 amplification factor in determining the seismic

design forces for brace connections (Cl. 27.11 CSA S16 [17]). This factor is equal to the ductility-related seismic force reduction factor, R_d, specified for CCBFs in the NBCC [2], with the objective of ensuring that the brace connections would remain essentially elastic under design level ground motions having a return period of 2475 years. A research project has been launched to investigate the seismic behaviour of CCBFs with I-shape braces. The objectives of this project include: to understand the behaviour of typical I-shape brace connections; to determine the force and deformation demands on brace connections; and eventually to propose design guidelines to achieve adequate structural seismic performance of CCBFs.

Under the research project, Rudman et al. [18, 19] and Wang et al. [20] conducted a series of full-scale tests on the assemblies of I-shape braces and brace connections subjected to reversed cyclic loading (Figure 4.2). Two brace connection configurations were tested—the flange plate connection and the flange angle connection. The assemblies were designed following conventional design principles without extra strengthening of the brace connections. As expected, highly variant behaviour was witnessed with different buckling modes, failure modes, and deformation capacities. However, even though the 1.5 force amplification was not applied in the design of these test specimens, all tested connections exhibited a measurable ductile response.

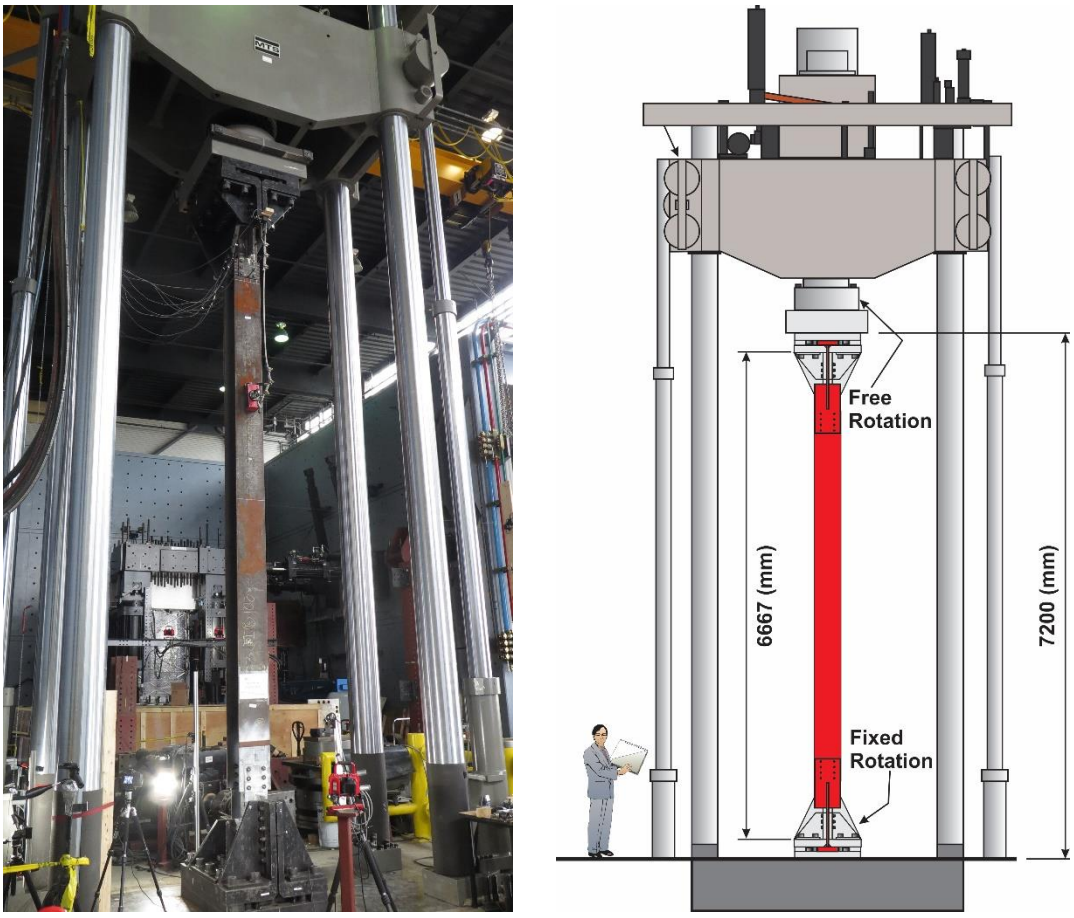

Figure 4.2: Test set-up of the full-scale I-shape brace and connection assembly [18,19]

A numerical simulation procedure based on 3D continuum elements was then developed by Wang et al. [21] for the flange plate brace connection. A typical FE model is shown in Figure 4.3. By making use of the axisymmetry, only half of the assembly was modeled for computational efficiency. The general-purpose 3D brick elements C3D8R in Abaqus were used to model most parts, except fillet welds and the K zones of braces for which wedge elements (C3D6) were used to facilitate regular meshes. The results of the steel tension coupon tests [18] were used as the input of material properties. Three types of contacts were modeled: contact between the connected plates, contact between the bolt shank and the bolt hole, and contact between the bolt nuts and the connected plates. The 'hard contact' feature in ABAQUS was used to reproduce the normal behaviour of each contact and to eliminate penetration; for the tangential contact behaviour, the

friction coefficient of 0.33 was applied to capture the frictional response. In the simulations, the movements of the two ends were coupled to the two reference points through kinematic coupling, RF1 and RF2, respectively. The axial loading was realised by fixing RF2 and enforcing displacement of RF1 along the longitudinal axis of the brace. For more details about the numerical model, please refer to [21].

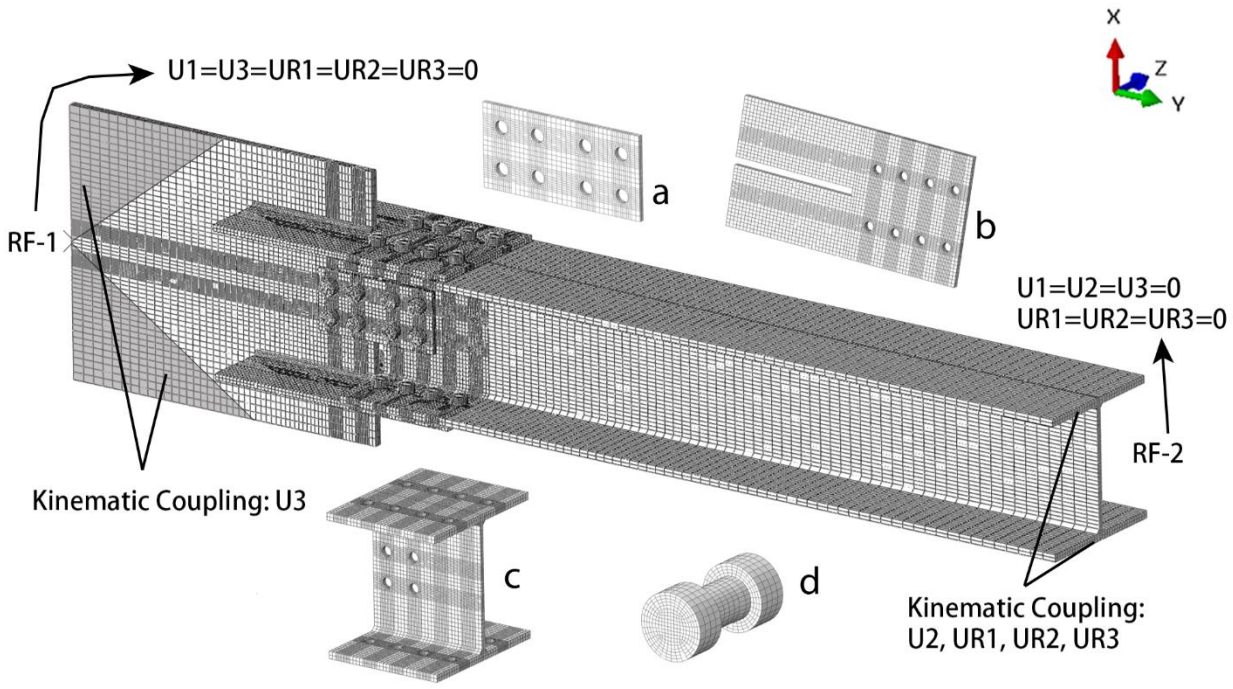

Figure 4.3: FE model of the brace and connection assembly by Wang et al. [21]: (a) web lap plate; (b) flange lap plate; (c) brace end with refined mesh; (b) bolt

The accuracy of the model was validated through comparison with the experimental test results [21]. The comparison of the experimental and simulated loading responses for two representative specimens is presented in Figure 4.4. Based on the numerical simulation results, the force transfer mechanism was studied. In order to prevent bolt shear rupture and weld fracture, which are known to have little deformation capacity, it was recommended to design the bolts and welds in the flange and web branches based on the ultimate strength of the branch, so as to achieve more ductile limit

states such as bearing or yielding of the lap plates. The study also revealed a nonuniform shear force distribution within bolt groups and an eccentric loading condition for the welds connecting the flange lap plates to the gusset plates. Recommendations were also made that these effects be explicitly accounted for in design to avoid premature failure of the bolts and welds. Moreover, the validated numerical procedure laid the foundation for this parametric study on the flange lap plate brace connection.

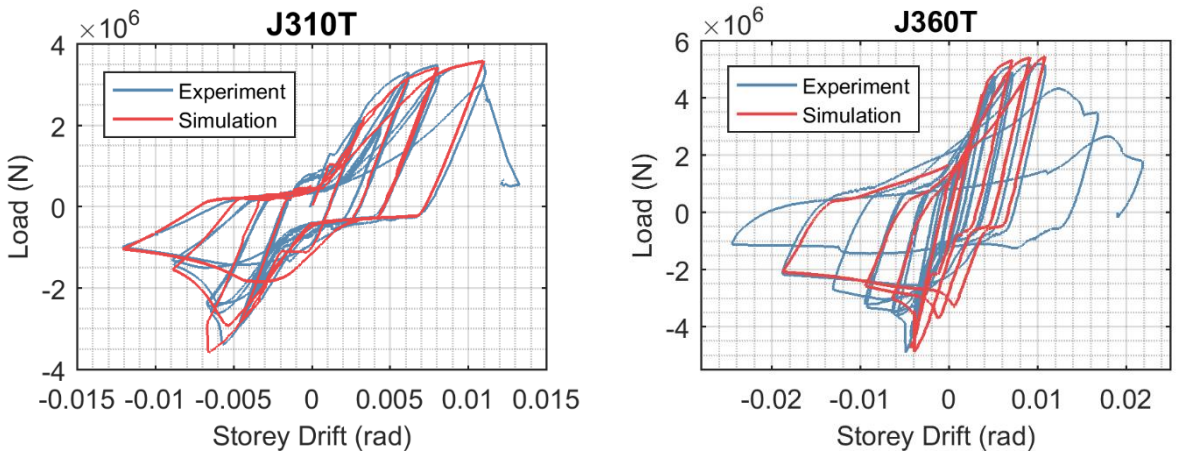

Figure 4.4: Comparison of experimental and simulated load vs. corresponding storey drift hysteretic curves [21]

4.3. PARAMETRIC STUDY

Based on the validated FE model of the brace and connection assembly (Figure 4.3) by Wang et al. [21], a parametric study was conducted and presented herein. Please note that the length of the brace-connection assemblies was extracted from a prototype one-bay one-storey braced frame that was 3.75 m high and 5.5 m wide. For direct perception of the axial deformation level of the brace-connection assembly, the deformations were expressed as the corresponding storey drifts of the prototype braced frame throughout this paper. The “load” hereafter refers to the axial load applied on the brace-connection assembly.

4.3.1. Flange plate connection study matrix

As shown in Figure 4.5, the studied brace connection consists of three types of plates: flange lap plate (FLP), web lap plate (WLP), and gusset plate. In realistic designs, the relative strengths vary among the three parts, which might result in different failure modes. To study the effect of the relative strength variation, three parameters (namely, the gusset plate thickness, the FLP thickness, and the WLP thickness) were varied individually in this parametric study. The two models by Wang et al. [21] served as the reference cases, and are labeled as J310-REF and J360-REF, respectively. Four variations were considered for each parameter: 50%, 75%, 125%, and 150% relative to the quantity in the reference models. Due to the fact that the 50% variations of gusset plate thickness caused numerical convergence problems, the 65% and 60% variations were instead adopted for gusset plate thickness with respect to J310-REF and J360-REF, respectively. Therefore, twenty-six numerical models were created in this parametric study as listed in Table 4.1.

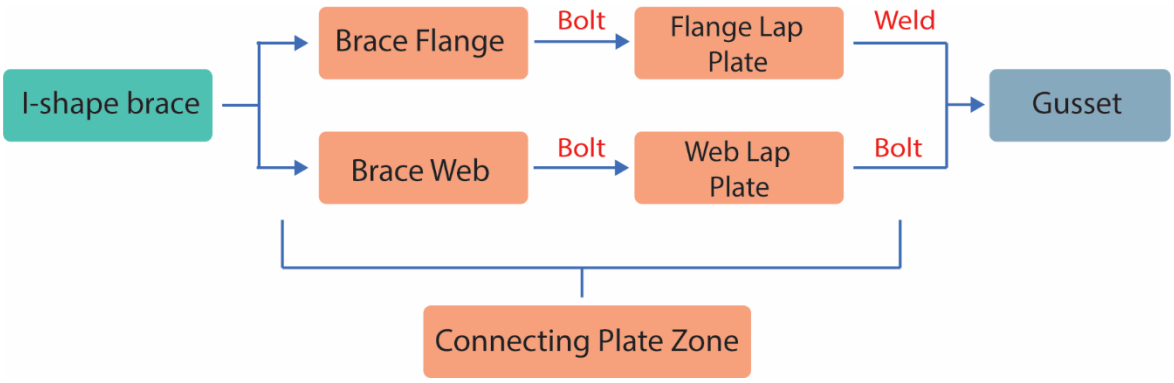

Figure 4.5: Main component and load path of I-shape brace flange plate connections

For the model labelling scheme, the first part indicates the reference model on which the new model was built. This is followed by letter ‘G’, ‘F’, or ‘W’ to indicate the component for which the thickness was varied: gusset plate, flange lap plate, or web lap plate, respectively. The final three-digit number denotes the ratio (in percentage) of the component’s thickness to that of the

control model. For instance, ‘J310-F-125’ corresponds to the model that was built on J310-REF but with the flange lap plate thickness 125% to that of the reference model.

Table 4.1: Flange plate connection parametric study list

Model ID	Brace Section	Bolt Grade and Size (in.)	Gusset Thickness (mm)	Flange Lap Plate Thickness (mm)	Web Lap Plate Thickness (mm)
J310-REF	W310×97	A325 (7/8)	15.9	15.9	9.53
J310-G-065	W310×97	A325 (7/8)	10.3	15.9	9.53
J310-G-075	W310×97	A325 (7/8)	11.9	15.9	9.53
J310-G-125	W310×97	A325 (7/8)	19.8	15.9	9.53
J310-G-150	W310×97	A325 (7/8)	23.8	15.9	9.53
J310-F-050	W310×97	A325 (7/8)	15.9	7.94	9.53
J310-F-075	W310×97	A325 (7/8)	15.9	11.9	9.53
J310-F-125	W310×97	A325 (7/8)	15.9	19.8	9.53
J310-F-150	W310×97	A325 (7/8)	15.9	23.8	9.53
J310-W-050	W310×97	A325 (7/8)	15.9	15.9	4.76
J310-W-075	W310×97	A325 (7/8)	15.9	15.9	7.14
J310-W-125	W310×97	A325 (7/8)	15.9	15.9	11.9
J310-W-150	W310×97	A325 (7/8)	15.9	15.9	14.3
J360-REF	W360×134	A490 (1)	19.1	15.9	9.53
J360-G-060	W360×134	A490 (1)	11.4	15.9	9.53
J360-G-075	W360×134	A490 (1)	14.3	15.9	9.53
J360-G-125	W360×134	A490 (1)	23.8	15.9	9.53
J360-G-150	W360×134	A490 (1)	28.6	15.9	9.53
J360-F-050	W360×134	A490 (1)	19.1	7.94	9.53
J360-F-075	W360×134	A490 (1)	19.1	11.9	9.53
J360-F-125	W360×134	A490 (1)	19.1	19.8	9.53
J360-F-150	W360×134	A490 (1)	19.1	23.8	9.53
J360-W-050	W360×134	A490 (1)	19.1	15.9	4.76
J360-W-075	W360×134	A490 (1)	19.1	15.9	7.14
J360-W-125	W360×134	A490 (1)	19.1	15.9	11.9
J360-W-150	W360×134	A490 (1)	19.1	15.9	14.3

4.3.2. Material properties

To prevent bolt rupture and weld fracture, the previous study [21] recommended the following: the bolts and welds in the flange branch of the brace connection be designed based on the ultimate tensile strength of the flange branch; the bolts in the web branch be designed based on the ultimate tensile strength of the web branch. This recommendation was subsequently proved to be effective

to keep the bolts essentially elastic [21]. The parametric study presented in this paper assumes this recommendation has been implemented in the brace connection design, and hence bolts and welds would remain essentially elastic. Therefore, in this parametric study, the bolts and welds were modeled as elastic for the sake of time-saving and better numerical convergence.

For all the other parts, material nonlinearity was modelled. In order to ensure the modelling accuracy at large deformation levels, nonlinear steel strain hardening was taken into account through the implementation of the nonlinear kinematic hardening model provided in ABAQUS 6.14 [22]. Within the material plasticity model, the backstress, α, describes the translation of the yield surface with the plastic strain (ε^{pl}) in the stress-strain space. In this study, three backstresses were used to collectively model the steel kinematic hardening (Equation 4.1 and 4.2).

$$\alpha_k = \frac{C_k}{\gamma_k}\left(1 - e^{-\gamma_k \varepsilon^{pl}}\right) \tag{4.1}$$

$$\alpha = \sum_1^3 \alpha_k \tag{4.2}$$

The data obtained from unidirectional tension coupon tests [18] were utilised to calibrate the coefficients, C_k and γ_k, for each backstress. The values that provided the best correlation with the experimental data were adopted.

4.3.3. Loading protocol and analysis technique

All models were loaded monotonically both in compression and in tension. A maximum compressive deformation of 60 mm, approximately corresponding to 2% storey drift for the prototype frame (5.5 m wide and 3.75 m high), was applied for all models, during which inelastic buckling behaviour occurred. Either 60 mm or 110 mm displacement was enforced in tension to

reach the tensile ultimate limit states. The applied deformation covers and exceeds the range of deformation anticipated for CCBFs under design level earthquakes.

Different numerical solving techniques were implemented for compression and tension loading simulations based on their capability and efficiency. For the compression simulations, the implicit dynamic method was used to ease convergence in the post-buckling range. For assemblies loaded in tension, the simpler general static approach was employed.

4.4. RESULTS AND DISCUSSION

4.4.1. Compressive behaviour

Effect of gusset plate thickness

The compressive load-deformation curves of simulations with gusset plate thickness variation are plotted in Figure 4.6. The legend of Figure 4.6, and of the following figures of the same type, contain values after lines of different colours that correspond to the third part of the Model ID listed in Table 4.1; the title of the sub-figure corresponds to the first two parts of the Model ID specified in Table 4.1. For instance, the yellow line followed by '075' in the sub-figure with the title of 'J310-G', refers to the model with the Model ID 'J310-G-075' defined in Table 4.1. The two shapes (diamond and circle) denote the two compressive buckling modes, brace buckling and gusset buckling, respectively.

Inelastic buckling with degrading compressive strength in the post-buckling range occurred in all models, in the form of either gusset plate buckling or out-of-plane brace buckling. As shown in Figure 4.7, the reference models J360-REF and J310-REF exhibited gusset buckling and out-of-plane overall minor-axis brace buckling, respectively, which matched with the laboratory test observations [18,19]. This drastic difference in response is expected for CCBFs as current code

provisions do not stipulate a preferred buckling mode nor do they contain design rules to ensure a certain buckling mode. Hence, either form of buckling can occur, depending on the selection and detailing of the brace and its connections, as the buckling mode is determined by the relative compressive strength of the two components. The results of the FE simulations in Figure 4.6 show that the buckling mode was clearly affected by the gusset plate thickness: for both braces studied, the buckling mode shifted from gusset buckling to overall minor-axis brace buckling when the gusset plate thickness was increased. For specimens with brace section W310×97, the buckling mode changed from gusset buckling to overall minor-axis brace buckling with the gusset plate thickness changed from 11.9 mm to 15.9 mm; the same buckling mode shift occurred for specimens with brace section W360×134 as gusset plate thickness increased from 19.1 mm to 23.8 mm.

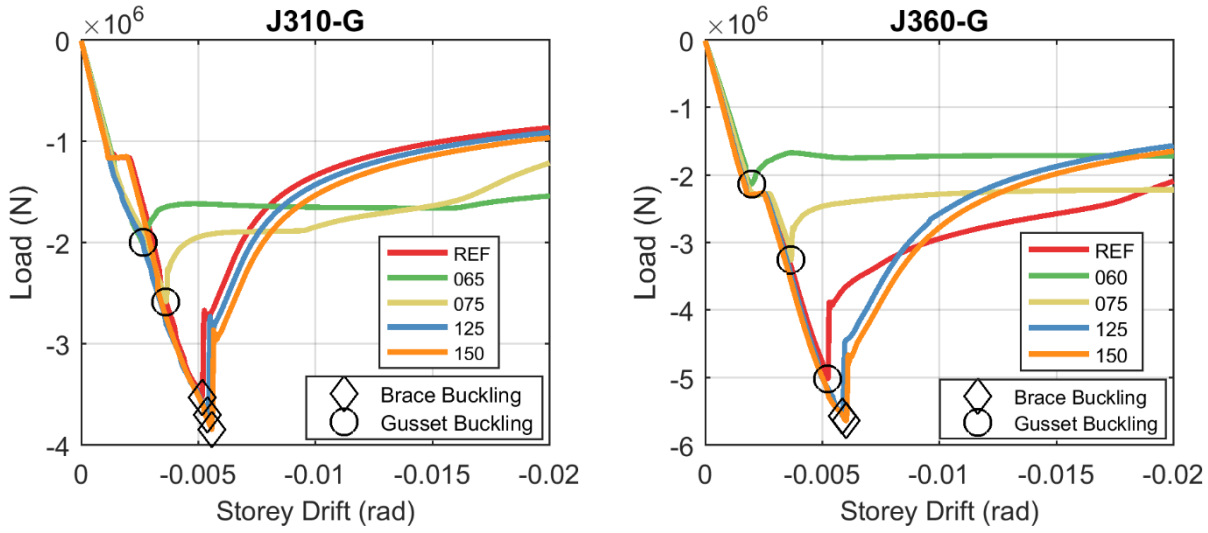

Figure 4.6: Compressive load-deformation curves of models with varying gusset plate thicknesses

The gusset buckling resistance was significantly affected by its thickness, which is consistent with numerous past studies on the gusset plate compressive resistance, e.g. Yam et al. [23,24]. For instance, compared to that of J360-G-060, the gusset plate buckling resistance increased by 52.6% and 135% in J360-G-075 and J360-REF, respectively. Likewise, an increase of 15.4% in gusset

plate thickness resulted in a 29.3% increase in the gusset buckling resistance in the analysis of J310-G-065 and J310-G-075.

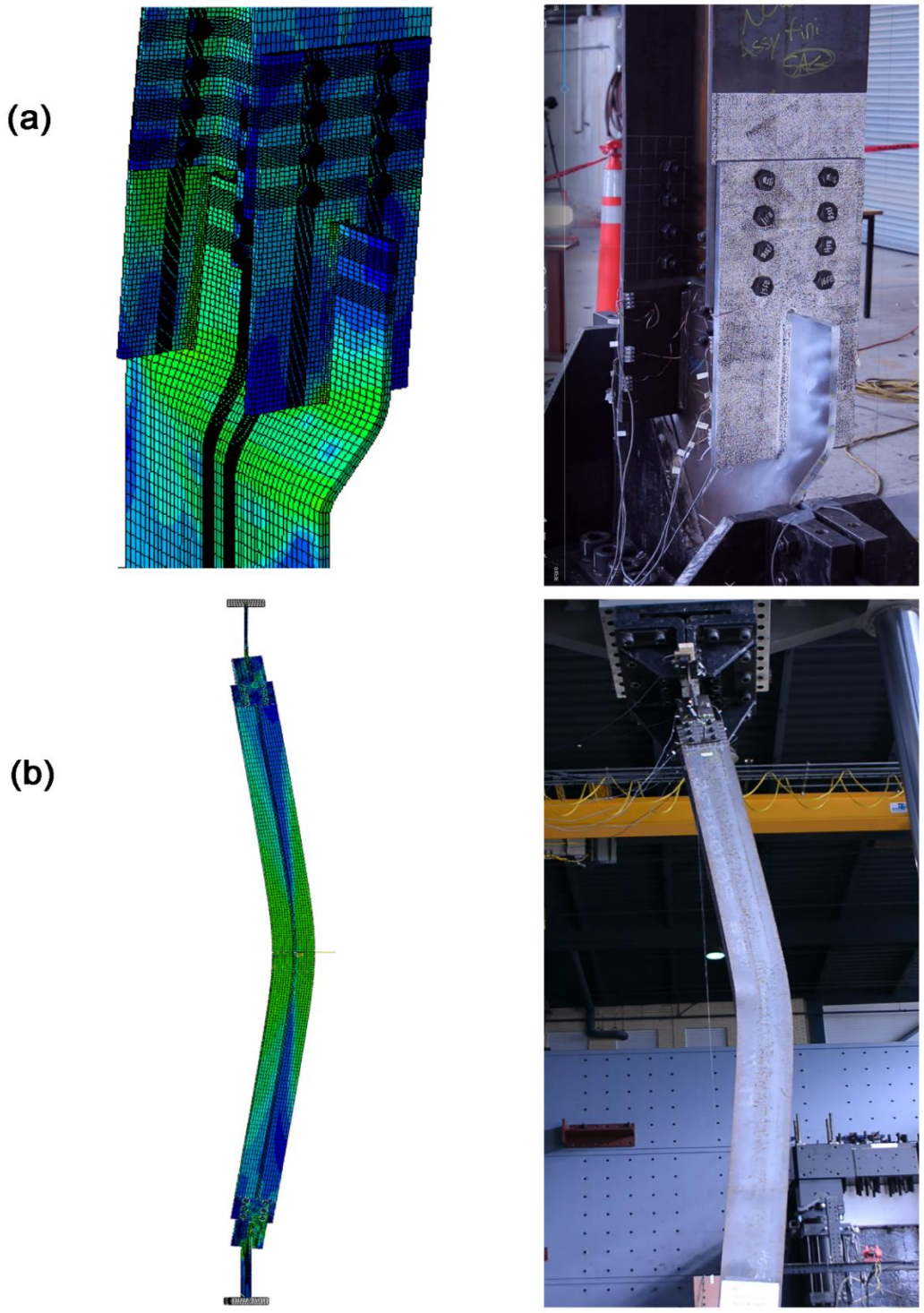

Figure 4.7: (a) gusset buckling in J360-REF; (b) overall minor-axis brace buckling in J310-REF

On the other hand, in the case of brace buckling, the variation of the gusset plate thickness had a less significant, yet still noticeable impact on the brace buckling resistance. For instance, the buckling resistance increased by 9.4% when changing the gusset plate thickness from 15.9 mm in J310-REF to 23.8 mm in J310-G-150. This is attributed to the increased rotational restraint provided by the greater gusset plate bending stiffness mobilized upon brace buckling [25], which will be further discussed.

Brace buckling versus gusset buckling

For CBFs other than the CCBF studied in this paper, the seismic design codes generally require that energy dissipation be facilitated by the buckling of the braces in compression, along with the yielding of the braces in tension, e.g. SCBFs and OCBFs in AISC 341-16 [26] and type MD and LD CBFs in CSA S16 [17]. Gusset plate buckling is explicitly not permitted in such CBFs. However, for CCBFs, specifically the R=3 CBF system in ASCE/SEI 7-16 and type CC CBFs in CSA S16 [17], there exist no requirements with respect to the compression buckling mode, and as such, either form of instability could occur.

The results of the parametric study indicate that brace buckling should be the preferred buckling mode in order to improve CCBF seismic performance for two main reasons. Firstly, smaller plastic strain will be introduced in components by brace buckling compared to gusset buckling, resulting in a longer low-cycle fatigue life. In the case of brace buckling, axial compression deformations of the brace-connection assembly are accommodated by the bending of the brace over its entire length. In contrast, when gusset plate buckling occurs, compression deformations concentrate in the short laterally unsupported region of the gusset plate. As shown in Figure 4.8, at the same axial compression deformation level corresponding to 2% storey drift, the maximum plastic strain

induced by gusset buckling is more than two times that imposed by brace buckling. Note, all comparisons with percent storey drift herein are based on the prototype frame (5.5 m wide and 3.75 m high) considered by Rudman et al. [19] in their brace test program.

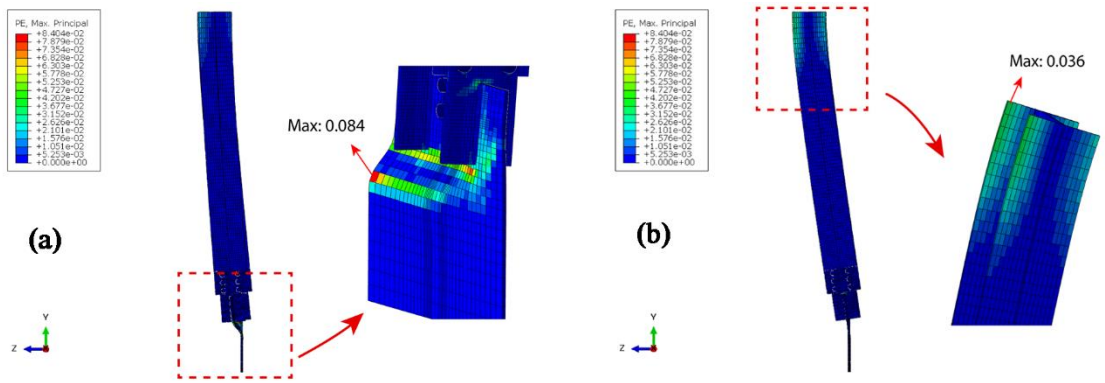

Figure 4.8: Maximum equivalent plastic strains induced by buckling: (a) gusset buckling in J310-G-075; (b) brace buckling in J310-REF

Secondly, gusset plate buckling is expected to occur at one end of the brace despite the nominally identical design at both ends. The variability in the buckling resistances offered by the gusset plates at the two ends of the brace, due to unavoidable differences in material properties, geometric dimensions, etc., is sufficient to trigger buckling of only one gusset plate. The subsequent compressive strength degradation will limit the force imposed on the other gusset, which results in the inelastic demands being concentrated in the gusset plate where buckling first occurred.

Walbridge et al. [27] reported on the energy absorption characteristics of gusset buckling, and proposed that the gusset plates in braced frames be the weak element in compression, rather than the braces. They observed the post-buckling resistance of the gusset plates to be stable, whereas the post-buckling resistance of the braces showed substantial degradation. However, this recommendation for weak gusset plate design did not account for the longer low-cycle fatigue life and larger axial deformation capacity characteristic of overall brace buckling. In the context of improving the seismic performance of CCBFs, it is believed that the cyclic fracture life and the

inelastic deformation capacity are more critical response parameters than the energy dissipation efficiency, suggesting that brace buckling should represent the preferred inelastic mechanism under compression for this system.

Effect of flange lap plate thickness

The variability in the flange lap plate thickness seems not to have an impact on the buckling mode of the brace-connection assembly (Figure 4.9), as long as premature buckling does not occur in the flange lap plates. The models of the J310 series (J310-F-075, J310-F-125, and J310-F-150) all exhibited brace buckling. Similarly, varying the flange lap plate thickness did not change the buckling mode in the J360 series: gusset buckling occurred in J360-REF, J360-F-075, J360-F-125, and J360-F-150. However, the thinner flange lap plates failed by buckling, as shown in Figure 4.10. Such a buckling behaviour prevents the assembly from developing its full compressive resistance potential, which is not desirable and should be avoided.

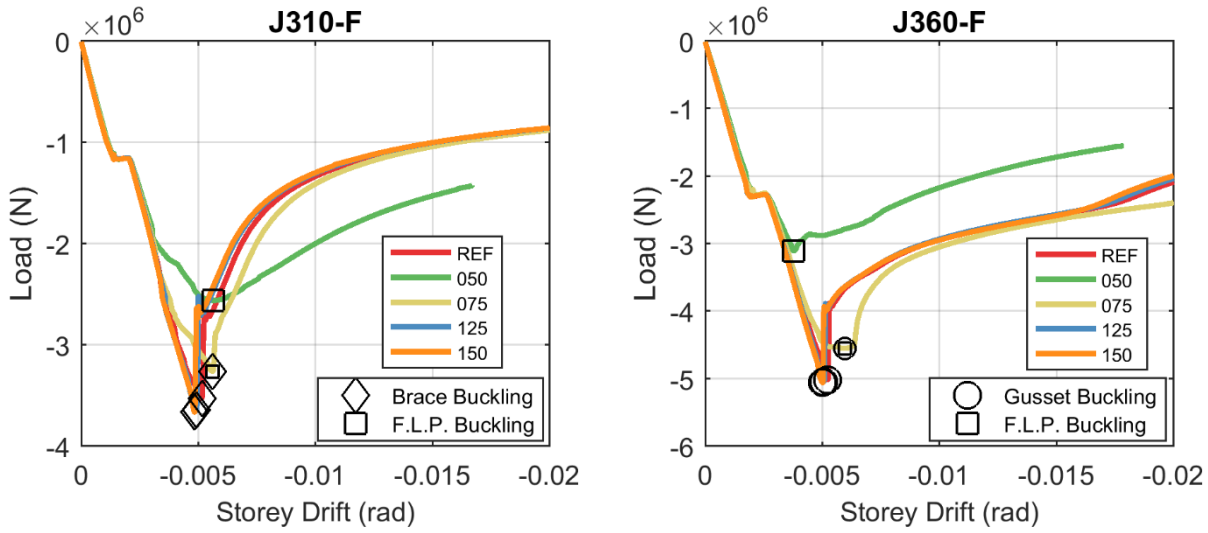

Figure 4.9: Compressive load-deformation curves of models with varying flange lap plate thicknesses

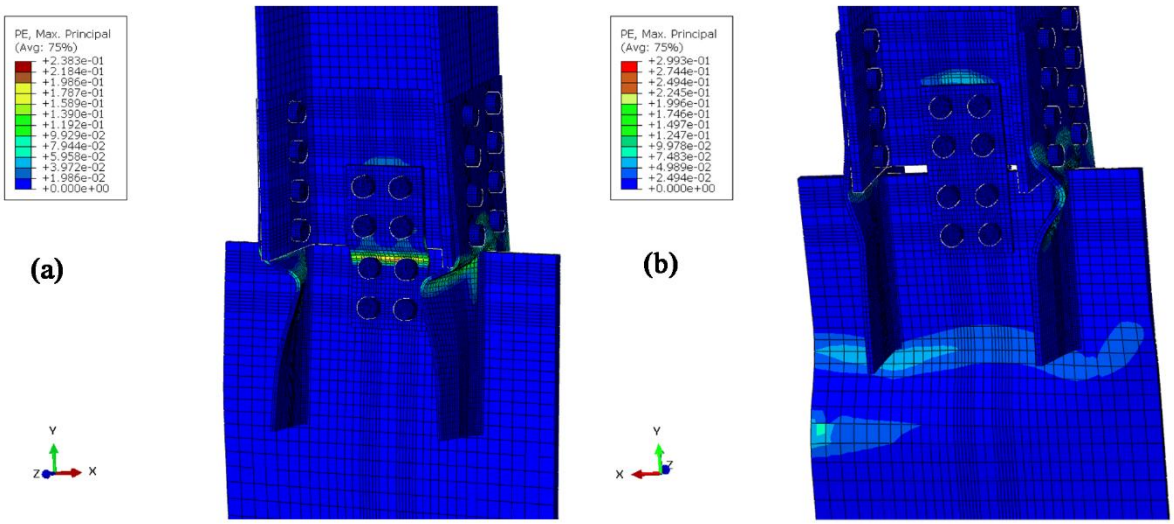

Figure 4.10: Compressive failure of flange lap plates: (a) flange lap plate buckling in J360-F-050; (b) Both gusset and flange lap plate buckling in J360-F-075

In terms of buckling resistance for the whole assembly, the flange lap plate thickness had different effects for the cases of brace buckling and gusset plate buckling. As shown in Figure 4.9, increasing the flange plate thickness led to a noticeable increase in the minor axis brace buckling resistance in the small thickness range, with values increasing from 3260 kN for J310-F-075 to 3530 kN to J310-REF; but this beneficial effect reached a plateau when thicker plates were used, with values of 3650 kN in J310-F-125 and 3660 kN in J310-F-150. Flange lap plates contribute to the end rotational restraint for the I-shape braces by means of their in-plane bending. The thicker the flange lap plates, the more restraint that is provided, and the higher the corresponding minor axis brace buckling resistance. A comparison of the plastic strain distribution in the flange lap plates at brace buckling is provided in Figure 4.11. The reduction of the plastic strains and the resulting greater rotational end restraint explain the increase in brace buckling resistance. Nevertheless, at a certain thickness the flange lap plates remain essentially elastic at brace buckling, as in the case of J310-F-125. Further strengthening of the flange lap plates then has limited effect on the brace buckling resistance, as in the case of J310-F-150.

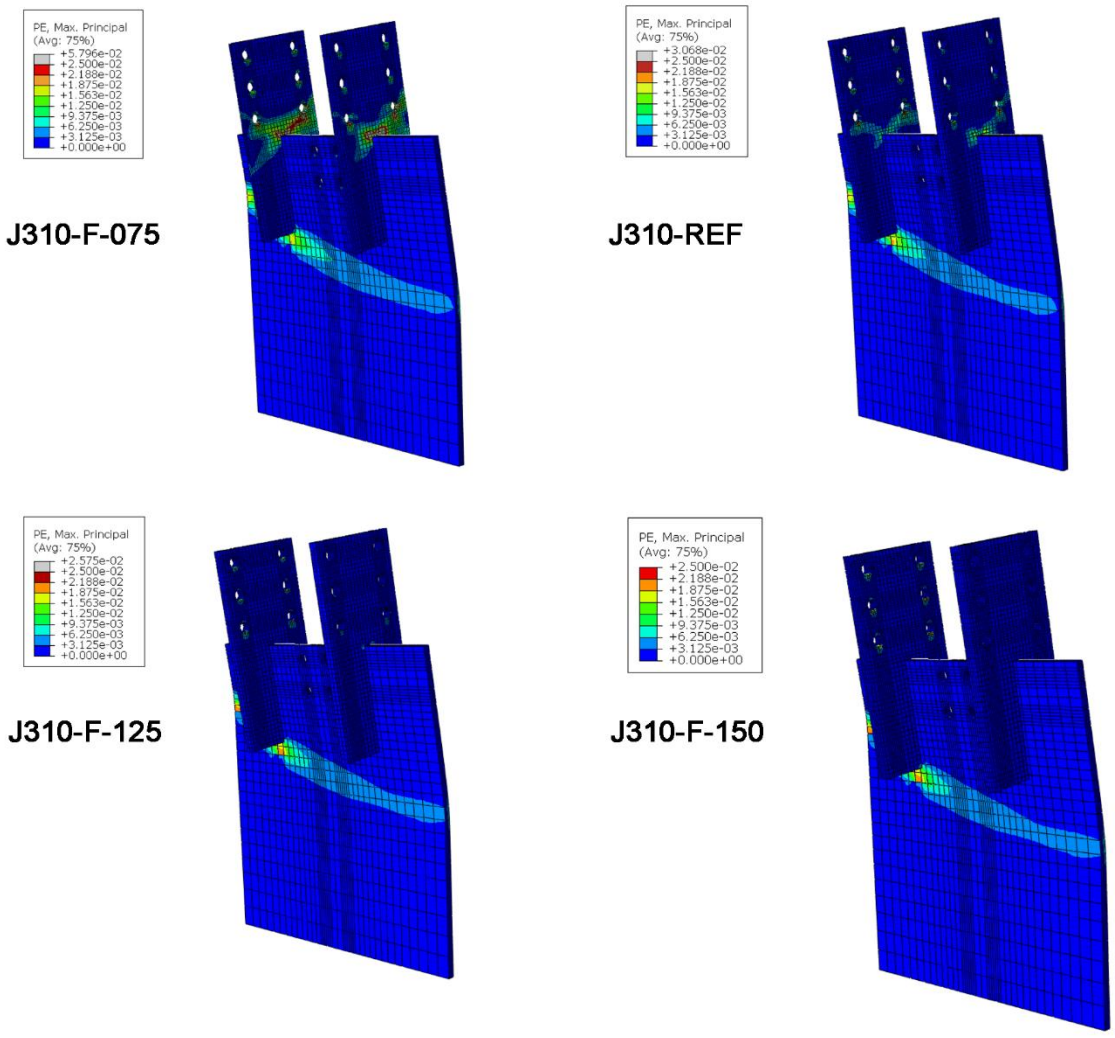

Figure 4.11: Comparison of plastic strains in flange lap plates at brace buckling

In the case of gusset plate buckling, the buckling resistance was not significantly affected by the thickness of the flange lap plates when flange lap plate buckling did not occur. Compressive resistances of 5015 kN, 5043 kN, and 5061 kN were obtained for J360-REF, J360-F-125, and J360-F-150, respectively. In these cases, the flange lap plates served more as orthogonal stiffeners, and the gusset plate buckling strength was determined mainly by their unstiffened lengths [28].

Brace effective length factor

Due to the unique geometry characteristics of the flange plate connection, the minor axis of the I-shape brace is aligned with the plane of the braced frame, and therefore, brace buckling occurs out of the plane of the frame. The analyses described in previous sections have revealed that the gusset plate and the flange lap plates collectively provide boundary rotational restraint for minor axis buckling of the brace. In design practice, the brace effective length (KL) is generally estimated assuming that the brace ends are pin-connected (K=1.0), and the length is taken as the distance between the expected hinge locations, L_H, as shown in Figure 4.12(a). However, this assumption is more suitable for the case where a distinct hinge zone is created in the gusset plate by leaving a clear distance equal to two times the thickness of the gusset ($2\ t_g$) at the end of connecting elements, as shown in Figure 4.12(b). Such a brace connection detail has been shown to offer small rotational restraint for the brace, and can safely accommodate the rotational demand that develops upon brace buckling [25].

However, the current design provisions for CCBFs do not require this type of clear hinge zone in the gusset plate. Practicing engineers usually discard this connection detail to achieve more compact and more economical gusset plate designs, as shown in Figure 4.12(c). Without the ability to accommodate brace end rotation, the brace end connections provide more substantial rotational restraint for minor axis brace buckling. Not accounting for this brace end restraint in design can lead to a low estimation of the brace buckling resistance, which may be problematic if brace buckling is the desired inelastic mechanism in compression, instead of gusset buckling. In this situation, it is possible for gusset buckling to occur during a seismic event because the braces are stronger in compression than predicted in design.

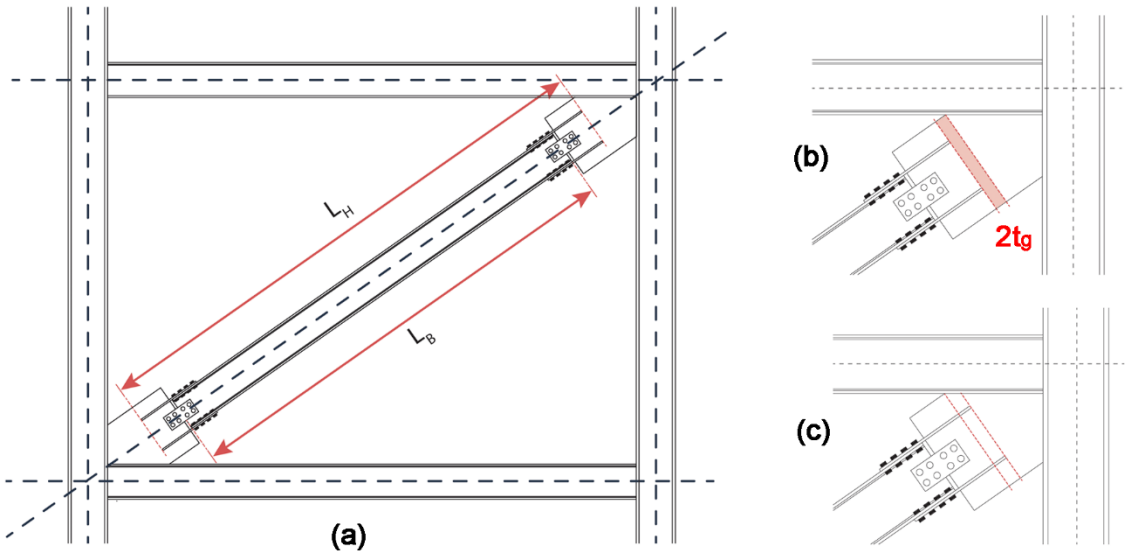

Figure 4.12: Gusset plate design with and without clearance in the flange plate connection

Therefore, actual support conditions of I-shape braces in CCBFs should be accounted for in the determination of the brace effective length (KL). Currently, the brace factored compressive resistance, C_r, in CSA S16-19 [17] for overall flexural buckling is calculated from:

$$C_r = \phi A F_y (1 + \lambda^{2n})^{-1/n} \tag{4.3}$$

in which, the brace slenderness, λ, is defined as:

$$\lambda = \frac{KL}{r}\sqrt{\frac{F_y}{\pi^2 E}} \tag{4.4}$$

where ϕ is the resistance factor, A is the area of the cross section, F_y is the yield stress, n is a coefficient associated with the buckling curve, K is the effective length factor, L is the buckling length, r is the radius of gyration and E is Young's modulus. Using these equations, the effective length factor, K_{CSA}, was back-calculated using the brace buckling resistances obtained from the FE simulations. In that calculation, L was taken equal to the I-shape brace length, L_B, as shown in Figure 4.12(a), and the resistance factor ϕ was set equal to 1.0. The calculations were repeated using the equations for the compressive strength of members in the AISC 360 Specification [29]

to obtain the effective length factor, referred to as K_{AISC}. Input for these calculations and the resulting K factors are presented in Table 4.2.

Table 4.2: Effective length factors from brace buckling resistances obtained in FE analysis

Model ID	F_y (MPa)	E (MPa)	r_y (mm)	L_B (mm)	C_r (kN)	K_{CSA}	K_{AISC}
J310-REF	352	224000	77	5334	3530	0.74	0.80
J310-G-125	352	224000	77	5334	3700	0.67	0.70
J310-G-150	352	224000	77	5334	3850	0.59	0.61
J310-F-075[a]	352	224000	77	5334	3260	0.86	0.94
J310-F-125	352	224000	77	5334	3650	0.69	0.73
J310-F-150	352	224000	77	5334	3660	0.68	0.73
J360-G-125	355	197000	94	5067	5570	0.63	0.62
J360-G-150	355	197000	94	5067	5640	0.59	0.58

[a] Brace buckling was accompanied by flange lap plate buckling in this analysis .

As shown, the calculated brace effective length factors K_{CSA} range from 0.59 to 0.86 with a mean value of 0.68. When using the AISC 360 equations, the effective length factors K_{AISC} vary between 0.58 and 0.94 with a mean value of 0.71. Clearly, current design practice for CCBFs may lead to a significant underestimation of the minor axis brace buckling resistance. To achieve the preferred minor axis brace buckling inelastic mechanism under seismic events, it is recommended that the gusset plate be designed to resist the brace compressive resistance determined with consideration of the actual brace end conditions. Further research is needed to quantify brace effective length factors as a function of the geometrical properties of typical flange plate connections used in CCBFs.

Effect of web lap plate thickness

As shown in Figure 4.13, the FE simulations revealed that the thickness of the web lap plate had almost no impact on the buckling resistance of either the gusset plate or the brace. For the models in which brace buckling was observed, the web lap plate was bent about its minor axis. Therefore, their limited flexural stiffness and strength provided little restraint for brace buckling. In the cases

where gusset plate buckling occurred, out-of-plane displacement developed in the laterally unsupported region of the gusset; this region was usually defined by the location of the flange lap plates. Because web lap plates are generally short and do not extend into the unsupported region of the gusset plates, they also have little influence on the compressive strength associated with gusset plate buckling.

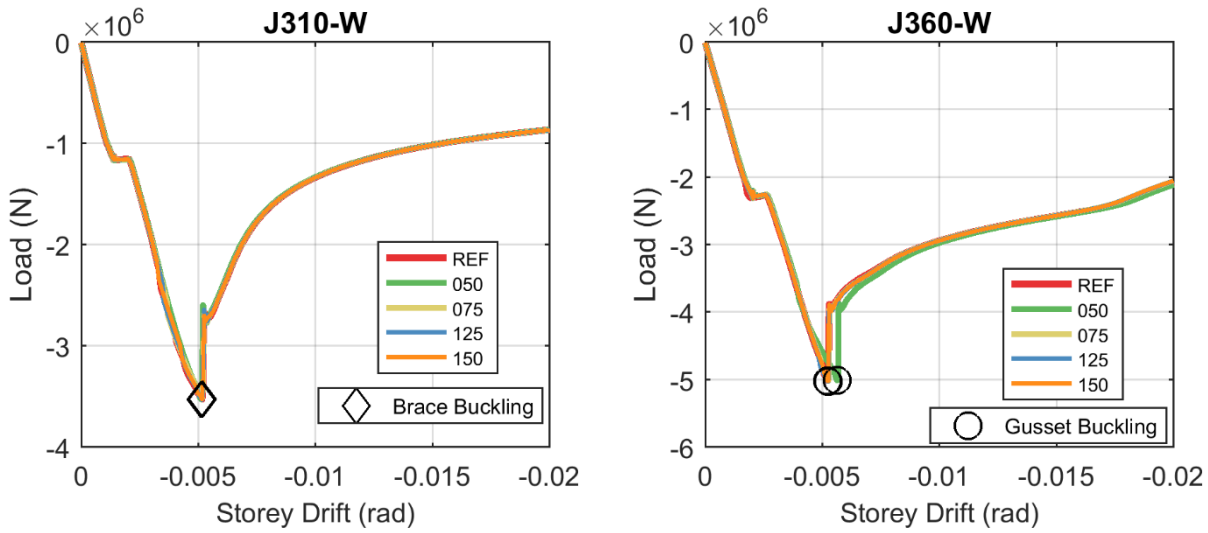

Figure 4.13: Compressive load-deformation curves of models with varying web lap plate thicknesses

4.4.2. Tensile behaviour

Effect of gusset thickness

The tensile load-deformation curves of all models with varying gusset plate thicknesses are plotted in Figure 4.14. The ultimate tensile resistances of each model, calculated in accordance with CSA S16 [17] using measured material properties and a resistance factor equal to 1.0, are also plotted for comparison (dashed lines). The failure occurred either in the gusset plate (gross section fracture) or in the connecting plate zone (net-section fracture of the flange lap plates and block shear failure of the brace web, as shown in Figure 4.15). The calculated CSA S16 resistances match well the ultimate tensile resistances predicted by FE simulations, except that the CSA S16 equations gave

lower values than the FE simulations for cases where failure occurred in the connecting plate zone. Those cases will be discussed in detail in the following section.

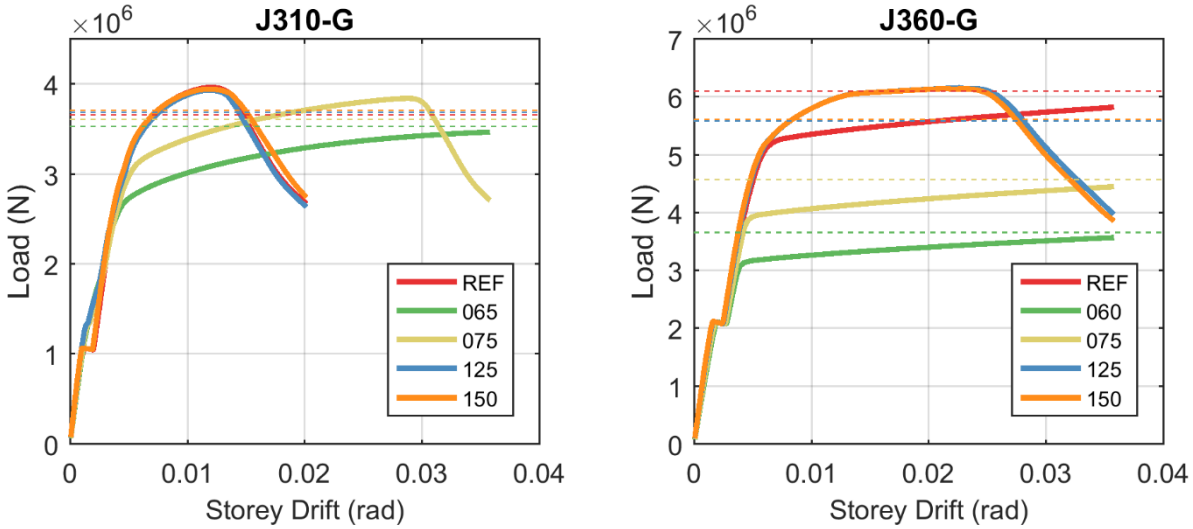

Figure 4.14: Tensile load-deformation curves of models with varying gusset plate thicknesses

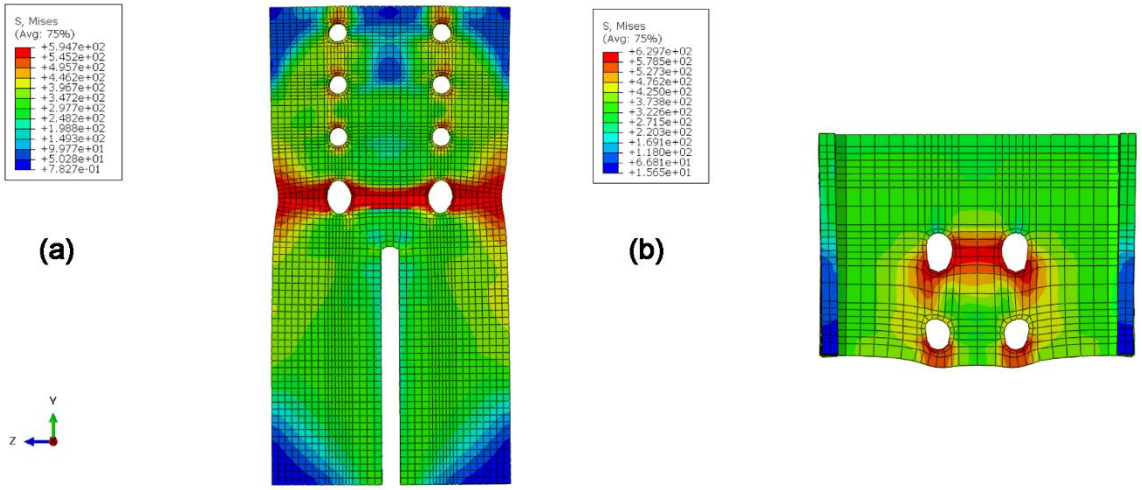

Figure 4.15: Failure modes in the connecting plate zone: (a) net-section fracture of flange lap plate; (b) brace web block shear

The ultimate tensile strength was governed by the connecting plate zone in J310-G-075 and J310-REF. However, for these two models, the resistance began to deteriorate at deformations corresponding to storey drifts of 1.3% and 2.8%, respectively, due to the necking of the flange lap plates. If the deformation at which resistance degradation starts due to necking of the plate is taken

as the deformation capacity of the assembly, which is reasonable since there is little deformation reserve beyond that, model J310-G-075 had better deformation capacity than J310-REF. This is because the ultimate tensile strength of the connecting plate zone was larger than the yield strength of the gusset plate in model J310-G-075. As such, the gusset plate yielded before the connecting plate zone reached its ultimate strength, which contributed substantially to the global deformation of the assembly. In contrast, the gusset plate remained essentially elastic in model J310-REF, contributing little to the global deformation; almost all deformation concentrated in the connecting plate zone. The gusset plates also remained elastic in models J310-G-125 and J310-G-150, which explains why these two models showed almost the same global deformation as J310-REF. Therefore, from the perspective of deformation capacity of the CCBFs, having stronger gusset plates is not necessarily beneficial, as it may force the plastic deformations to concentrate in the connecting plate zone.

J360-G-150 and J310-G-150 shared two similarities: their ultimate tensile strengths were governed by the connecting zone and almost all deformations concentrated in the connecting plate zone due to very strong gusset plates. However, the tensile resistance declined at deformation levels corresponding to storey drifts of 2.6% and 1.3% in models J360-G-150 and J310-G-150, respectively, due to necking in the flange lap plates. The assembly deformation at which the resistance starts to decline is indicative of the ductility of the assembly. The large difference in the tensile deformation capacities for these two models can be due to differences in the flange lap plate properties, such as the bolt gauge, the end edge distance, and the net-to-gross area ratio in the net section. Further research is needed to better understand the relation between the flange lap plate deformation capacity and its geometrical properties.

Effect of flange lap plate thickness

The tensile load-deformation curves (solid lines) and the calculated ultimate tensile strengths (dashed lines) according to CSA S16 [17] using measured material properties [18] and a resistance factor equal to 1.0 are provided in Figure 4.16. For models J310-F-125 and J310-F-150, the dashed lines represent the gross section yield strength of the brace. The code-compliant strength predictions matched well with the ultimate tensile strengths in general; nonetheless, again, for all models that failed in the connecting plate zone (J-310-REF, J-310-F-50, J-310-F-75, J-360-F-50, and J-360-F-75), the ultimate strengths calculated with CSA S16 underestimated the maximum forces developed in these models.

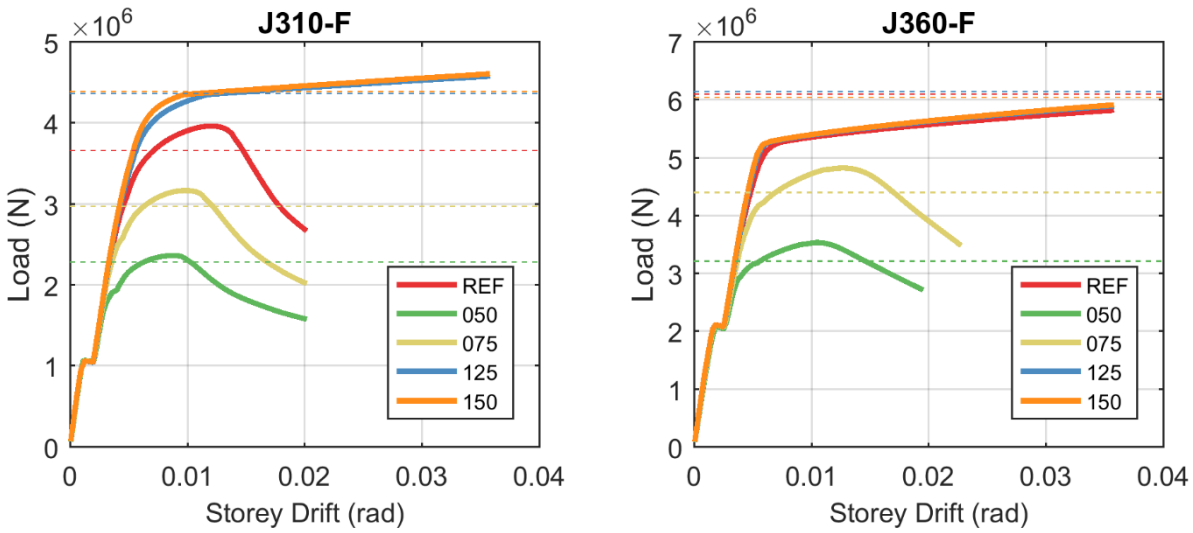

Figure 4.16: Tensile load-deformation curves of models with varying flange lap plate thicknesses

In the models J360-F-050 and J310-F-050, the governing failure modes were flange lap plate net-section fracture and block shear of the brace web. For these models, almost all the plastic deformations occurred in the connecting plate zones, and the lowest deformation capacities were observed.

When the flange lap plate thickness was increased, the resulting increase in the tensile resistance of the connecting plate zone forced other parts to engage plastically and to contribute more to the global deformation capacity. For instance, the ultimate tensile resistance was still governed by the

connecting plate zone in J310-F-125 and J310-F-150. However, their ultimate tensile resistances were larger than the yield strength of the brace. Therefore, before these two assemblies reached their ultimate tensile strengths, the braces yielded and contributed to the global deformation, greatly improving the deformation capacity of the whole assembly.

Similarly, models J360-F-125 and J360-F-150 exhibited better deformation capacities compared to J360-F-075 because strengthening of the flange lap plates made the tensile failure shift from the connecting plate zone to the gusset plates. The plastic deformations in the gusset plates improved the deformation capacity of the brace-connection assembly; and necking of the gusset plate was not observed even when the deformation had reached a value corresponding to 3.5% storey drift. However, one must note that plastic strains introduced by tensile stretching of the gusset plates may have detrimental effects on the low-cycle fatigue life of the gusset plate if the compressive failure mode is gusset buckling. In that case, inelastic tensile strains would add to plastic straining induced upon gusset buckling, which can promote premature fracture of the gusset plate. This behaviour was observed in the test J-360-T by Rudman et al. [19]. In that test, buckling of the gusset plate took plate in compression; tearing failure developed soon thereafter on a tension excursion at a relatively low deformation level in the region of the gusset plate where the buckling-induced deformations had occurred, as a result of the cumulative reversed plastic strains.

Overstrength of flange lap plates

As noted earlier in the text, when tension failure occurred in the connecting plate zone in the FE simulations, the strength values calculated with CSA S16 [17] always underestimated the tensile strength predicted by the FE models. A subsequent examination of the force development within the two branches of the connecting plate zone revealed that the code underestimation mainly came

from the strength prediction of the flange lap plates. The CSA S16 predicted strengths of the flange lap plates (T_{u_CSA}) and the strengths obtained through FE simulation (T_{u_FEA}), as well as the resulting overstrength ratios (T_{u_FEA}/T_{u_CSA}), are given in Table 4.3 for models in which net-section fracture occurred in the flange lap plates.

The stress distribution within the flange lap plates under tension loading was investigated in detail. The typical distribution of all stress components when the applied load reached its maximum in the flange lap plate is shown in Figure 4.17. The stresses along the primary loading direction of the flange lap plate (σ_{yy}) are significant across the whole net section. In addition, substantial tensile stresses in the transverse direction (σ_{zz}) exist in the net section, between the two bolt holes. In the σ_{zz} distribution, there is also a coexisting zone (blue colour) at the upper edge of the flange plate where significant compressive transverse stresses develop. The combination of these transverse stresses results in an in-plane moment acting on the symmetry plane of the flange lap plate, over the length of the bolt group, as shown in Figure 4.18. This moment is caused by the eccentricity that exists between the bolt lines and the welds connecting the flange lap plate to the gusset plate.

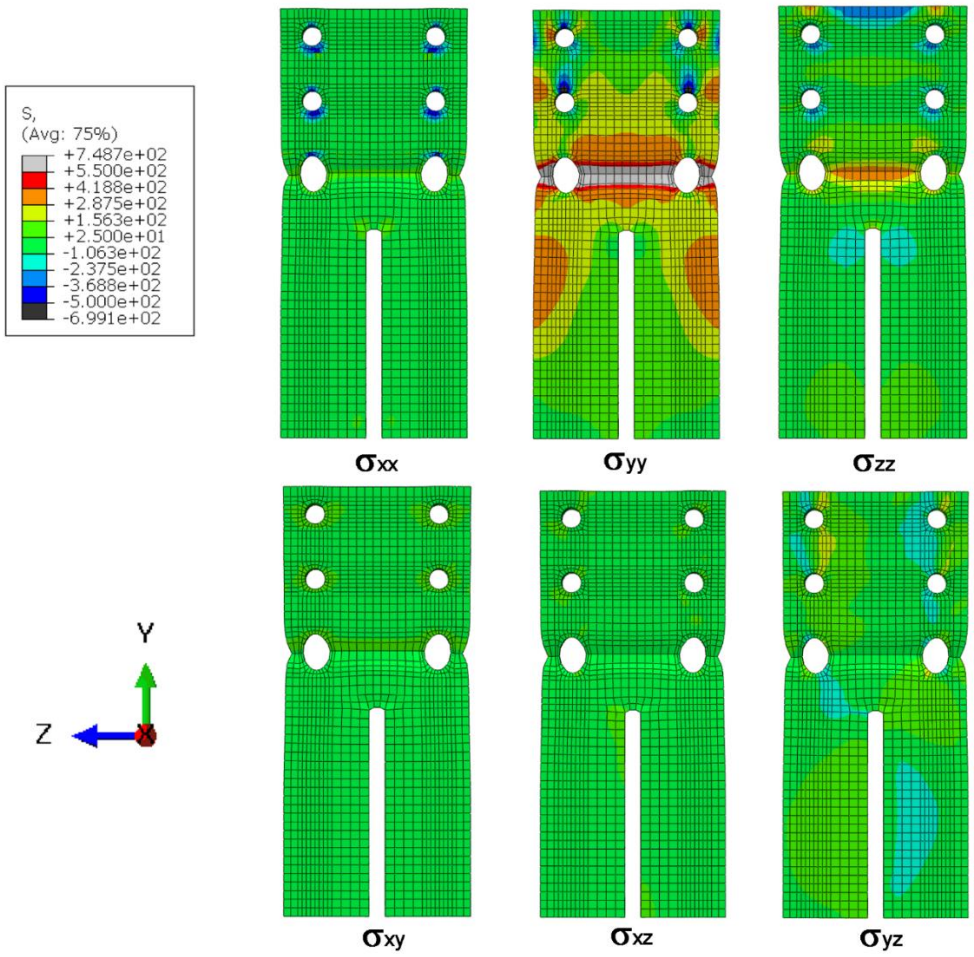

Figure 4.17: Stress components within the flange lap plates at the maximum tension loading

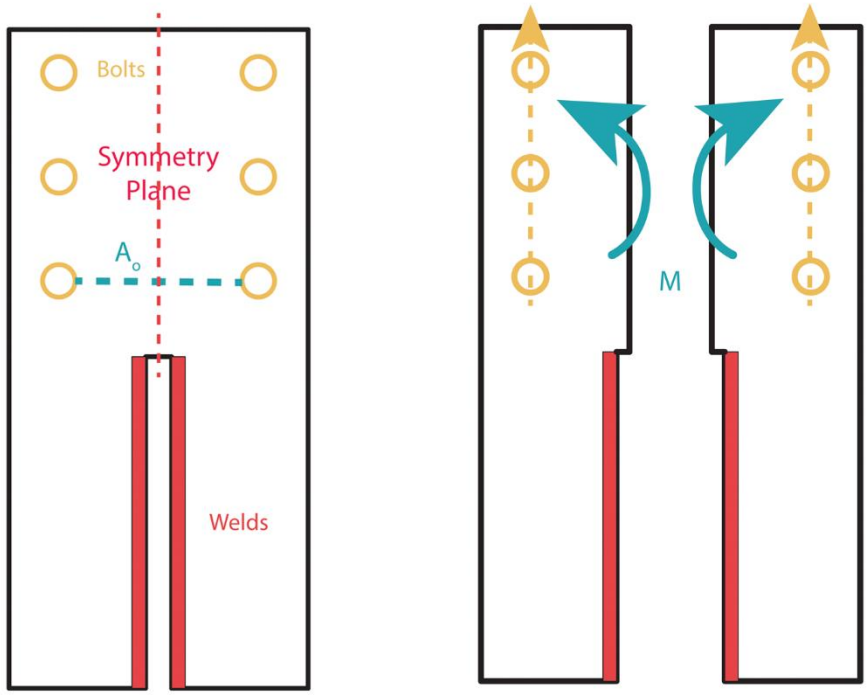

Figure 4.18: Schematic illustration of moment in the symmetry plane of flange lap plate

The four other stress components along the net cross section are negligible. Hence, stresses in the critical net section can be expressed as a planar bi-axial stress condition with principal stresses equal to σ_y and σ_z in accordance with the coordinate system in Figure 4.17. According to the von Mises yield criterion, the equivalent stress in this case is:

$$\sigma_e = \sqrt{{\sigma_y}^2 - \sigma_y \sigma_z + {\sigma_z}^2}. \tag{4.5}$$

For a steel with a given ultimate stress F_u, the existence of a tensile stress (+) in the Z direction (σ_z) therefore leads to an increase of the stress required in the Y direction (σ_y) to reach F_u. This increase in longitudinal stress (σ_y) at rupture on the net section due to the bi-axial stress condition is seen as the cause for the overstrength associated with net section rupture that was observed in the FE simulations compared to CSA S16 predictions. To quantify the increase of the stress, σ_y, it is assumed that the stress condition between the bolt holes is:

$$\sigma_z = x\sigma_y \tag{4.6}$$

Equation 4.5 then changes to:

$$\sigma_e = \sigma_y\sqrt{1 - x + x^2} \tag{4.7}$$

The square root term in Equation 4.7 takes a minimum value of 0.866 when x = 0.5, which means that σ_y can attain a maximum value of 1.15 σ_e when $\sigma_z = 0.5\sigma_y$. For this condition, it is possible to determine an upper bound for the ultimate strength for net section rupture of the flange lap plates assuming that the stress σ_y at rupture is equal to 1.15 F_u on the portion A_o of the plate net section between the bolt holes (Figure 4.18) and F_u on the remaining of the net section $(A_n - A_o)$. Based on this assumption, the tensile overstrength ratio for the flange lap plate net section rupture, denoted herein by α_o, with respect to CSA S16 prediction, can be obtained from:

$$\alpha_o = \frac{1.15A_o + (A_n - A_o)}{A_n} \tag{4.8}$$

where A_n is the net section area, and A_o is the area between the bolt holes in the net section as shown in Figure 4.18. The ratio A_o/A_n for the J310 and J360 series of models is equal to 0.67 and 0.44, respectively. Using Equation 4.8, the overstrength ratios α_o for these two series are 1.10 and 1.07, respectively. These two values match well with the overstrength ratios obtained through FE simulations (Table 4.3).

In the previous study by Wang et al. [21], to avoid bolt shear rupture and premature weld fracture in the connection, the authors recommended that the bolts and welds of the flange lap plates be designed to resist a load equal to the tensile resistance of the flange branch. In view of this, the

overstrength ratio, α_o, calculated based on Equation 4.8 is recommended to be used in the tensile resistance determination of the flange lap plate, which should be considered in the design of bolts and welds in the flange branch.

Table 4.3: Net-section overstrength of flange lap plates

Model ID	T_{u_CSA} (kN)	T_{u_FEA} (kN)	Ratio (T_{u_FEA}/ T_{u_CSA})	α_o
J310-J-075	1032	1181	1.14	1.10
J310-G-075	1377	1555	1.13	1.10
J310-G-100	1377	1572	1.14	1.10
J310-G-125	1377	1549	1.13	1.10
J310-G-150	1377	1552	1.13	1.10
J360-J-075	1779	1915	1.08	1.07
J360-G-100	2372	2465	1.04	1.07
J360-G-125	2372	2547	1.07	1.07
J360-G-150	2372	2529	1.07	1.07

Effect of web lap plate thickness

The tensile loading simulation results for the web lap plate thickness variation are plotted in Figure 4.19.

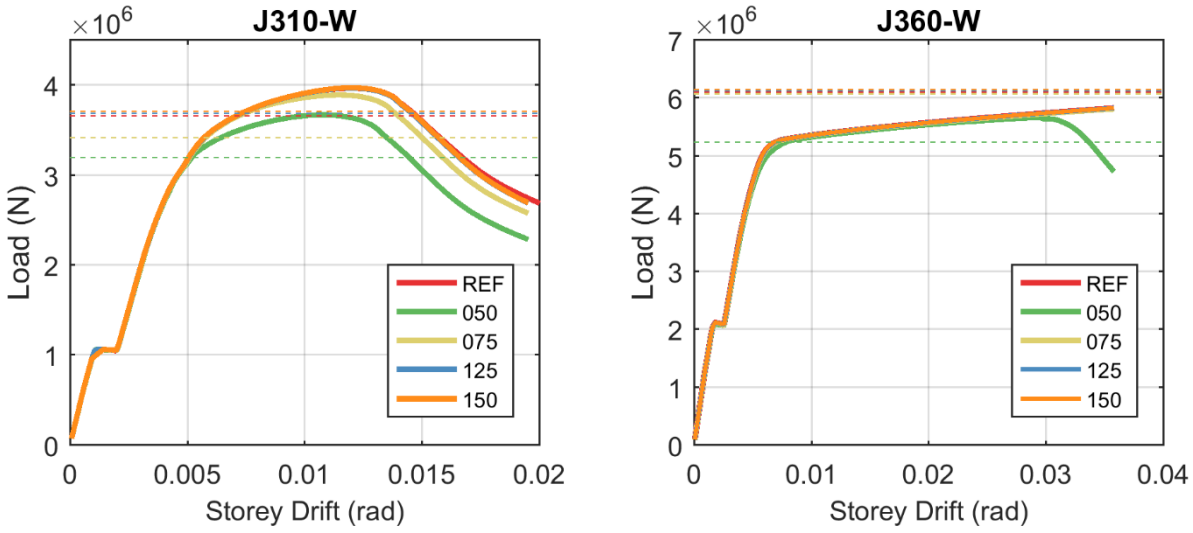

Figure 4.19: Tensile load-deformation curve comparison with varying web lap plate thicknesses

In the FE simulations for models J310-REF and J360-REF, block shear failure was observed in the web of the brace, as occurred in the tests by Rudman et al. [19]. When reducing the web lap plate thickness in the simulations, the failure mode shifted to net-section fracture of the web lap plates, as shown in Figure 4.20. Moreover, with the decrease of the web lap plate thickness, the ultimate tensile strength of the connecting plate zone decreased, and other parts (the brace and gusset plate) became relatively stronger. At the point where the ultimate strength of the brace-connection assembly was reached, the contribution of the brace and gusset plate deformations to the global deformation was therefore reduced. This explained why the resistance degradation in J310-REF and J310-W-050 occurred at deformations of 47 mm and 42 mm, equal to storey drifts of 1.5% and 1.4%, respectively. This 5 mm difference in global deformations all came from the brace and gusset plate because the flange lap plates were the same in both models. The same trend occurred in the J360 series, for which the resistance decline happened earlier in J360-W-050 than in J360-REF.

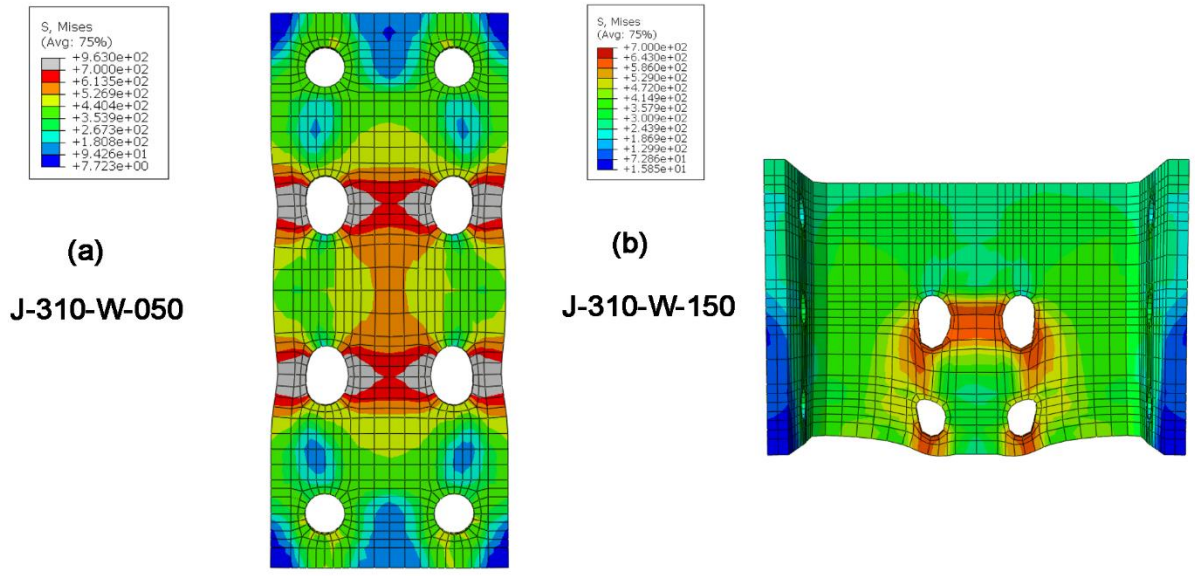

Figure 4.20: Failure mode shift: (a) net-section fracture in J-310-W-050; (b) brace web block shear in J-310-W-150

The tensile behaviour of models J310-W-125 and J310-W-150 was almost identical to that of J310-REF. This is because the strengthening of only the web lap plate did not change the failure modes in the web branch. Therefore, neither the tensile strength nor the deformation was changed. The same behaviour was observed when modifying the thickness of the web lap plate in the J360 model series.

4.5. CONCLUSIONS AND DESIGN RECOMMENDATIONS

A parametric study of the behaviour of the flange plate connection for I-shape braces, a configuration commonly used in CCBFs, was conducted based on a validated numerical simulation procedure. Three parameters, the gusset plate thickness, the flange lap plate thickness, and the web lap plate thickness, were varied for two different brace connection assemblies replicating specimens previously tested by Rudman et al. [19]. Both tensile loading and compressive loading were simulated monotonically. The response was examined up to large deformations exceeding the level expected under the design level seismic demand, with the focus on failure modes and deformation capacities. The primary conclusions are as follows:

1. In CCBFs with I-shape braces designed in accordance with current practice, either the gusset plates or the braces can buckle when subjected to compression. Gusset plate buckling could lead to inferior seismic performance for two reasons: a) gusset plate buckling will impose much larger plastic strains at the buckling position than brace buckling, which may lead to diminished low-cycle fatigue life for the assembly; b) gusset plate buckling is expected to occur at only one brace end due to inherent variations in material and geometric properties, which will increase further the plastic strains in areas of buckling.

2. Flange lap plates provide end restraint for both the gusset plates and the I-shape braces when subjected to compression, yet in different ways. The flange lap plates work as stiffeners for the gusset plates while offering rotational restraint through in-plane bending stiffness for the I-shape braces. Therefore, varying the flange lap plate thickness was found not to have an impact on the gusset buckling compressive resistance. However, for overall brace buckling, the use of thicker flange lap plates leads to shorter brace effective lengths and higher brace compressive resistances.
3. The end rotational restraint for the I-shape braces as collectively provided by the gusset plates and the flange lap plates can be significant in CCBFs as there is no requirement for minimum clearance to form a hinge zone in the gusset plates to accommodate the brace end rotation. The current design assumption that braces have pinned end connections can lead to a significant underestimation of the brace compressive resistance, which could result in gusset plate buckling during a seismic event.
4. Opting for a strong gusset plate design is not necessarily beneficial for the global deformation capacity because it can force plastic deformations to concentrate in the connecting plate zone. An alternative approach consisting of using thicker flange lap plates to increase the tensile resistance of the connecting plate zone will cause other components of the assembly (gusset plates or braces) to participate more in the plastic deformation in tension, which may result in higher global deformation capacities.
5. The FE simulations revealed the presence of significant transverse tensile stresses in the critical net section of the flange lap plates, which can cause an increase in the longitudinal tensile strength of these plates.

6. Modifying the thickness of the web lap plates had no impact on the compressive behaviour of the brace-connection assembly. Nonetheless, tensile failure may change from block shear of the brace web to net section failure of the web lap plates when thinner web lap plates are used."

In view of the conclusions drawn from the parametric study, the following design recommendations are proposed in order to obtain improved seismic performance of CCBFs with I-shape braces and flange plate brace connections:

1. Overall minor-axis brace buckling should be the governing buckling mode rather than gusset plate buckling.
2. The actual brace end conditions should be considered when determining the gusset plate resistance required to achieve the desired brace buckling response in compression, rather than assuming braces are pinned at both ends.
3. The connecting plate zone should be designed for a tensile axial load corresponding to the yield strength of either the gusset plate or the brace, whichever is lower.
4. The derived tensile overstrength ratio in Equation 4.8 should be used in the tensile resistance determination of the flange lap plates.

ACKNOWLEDGEMENTS

The work was funded by the Natural Sciences and Engineering Research Council of Canada (NSERC), the Fonds de recherche du Québec - Nature et technologies (FRQ-NT) and the Centre d'études interuniversitaire des structures sous charges extremes (CEISCE). The financial and technical support from DPHV Structural Consultants and the ADF Group Inc. is gratefully acknowledged. The first author is supported in part through the China Scholarship Council (CSC).

The numerical simulations were conducted on the supercomputer cluster Graham of Compute Canada, which is funded by the Canada Foundation for Innovation (CFI).

REFERENCES

[1] American Society of Civil Engineers/Structural Engineering Institute (ASCE/SEI) 7-16. (2016). Minimum Design Loads and associated criteria for buildings and other structures. Reston, Virginia, USA.

[2] National Research Council of Canada (NRCC). (2015). National Building Code of Canada (NBCC) (13th ed.). Ottawa, ON, Canada.

[3] Mitchell, D., Tremblay, R., Karacabeyli, E., Paultre, P., Saatcioglu, M., & Anderson, D. (2003). Seismic force modification factors for the proposed 2005 edition of the national building code of canada. Canadian Journal of Civil Engineering, 30(2), 308-327. doi:10.1139/l02-111

[4] Brunet, F., Tremblay, R., Richard, J., & Lasby, M. (2019). Improved canadian seismic provisions for steel braced frames in heavy industrial structures. Journal of Constructional Steel Research, 153, 638-653. doi:10.1016/j.jcsr.2018.11.008

[5] ICBO. (1988). Uniform building code, 1988 ed. In Proc., Int. Conf. of Building Officials. Whittier, Calif.: International Conference of Building Officials.

[6] Canadian Standards Association. (1989). CSA S16. 1-M89. Steel structures for buildings—Limit states design. Rexdale, ON, Canada.

[7] Sen, A., Swatosh, M., Ballard, R., Sloat, D., Johnson, M., Roeder, C., Berman, J. (2017). Development and evaluation of seismic retrofit alternatives for older concentrically braced frames. Journal of Structural Engineering, 143(5), 04016232-04016232. doi:10.1061/(ASCE)ST.1943-541X.0001738

[8] Chakrabarti, S., & Bjorhovde, R., F. ASCE. (1985). Tests of full-size gusset plate connections. Journal of Structural Engineering, 111(3), 667-684. doi:10.1061/(ASCE)0733-9445(1985)111:3(667)

[9] Lehman, D., Roeder, C., & Herman, D. (2008). Improved seismic performance of gusset plate connections. Journal of Structural Engineering, 134(6), 890-901. doi:10.1061/(ASCE)0733-9445(2008)134:6(890)

[10] Fang, C., Yam, M., Cheng, J., & Zhang, Y. (2015). Compressive strength and behaviour of gusset plate connections with single-sided splice members. Journal of Constructional Steel Research, 106, 166-183. doi:10.1016/j.jcsr.2014.12.009

[11] Astaneh-Asl, A. (1998). Seismic behavior and design of gusset plates. Structural Steel Educational Council.

[12] Sen, A., Roeder, C., Lehman, D., Berman, J., Sloat, D., Ballard, R., & Johnson, M. (2016). Experimental evaluation of the seismic vulnerability of braces and connections in older concentrically braced frames. Journal of Structural Engineering, 142(9). doi:10.1061/(ASCE)ST.1943-541X.0001507

[13] Tremblay, R., Filiatrault, A., Timler, P., & Bruneau, M. (1995). Performance of steel structures during the 1994 northridge earthquake. Canadian Journal of Civil Engineering, 22(2), 338-360. doi:10.1139/l95-046

[14] Tremblay, R., Filiatrault, A., Bruneau, M., Nakashima, M., Prion, H., & DeVall, R. (1996). Seismic design of steel buildings: Lessons from the 1995 hyogo-ken nanbu earthquake. Canadian Journal of Civil Engineering, 23(3), 727-756. doi:10.1139/l96-885

[15] Bradley, C., Fahnestock, L., Sizemore, J., & Hines, E. (2017). Full-scale cyclic testing of low-ductility concentrically braced frames. Journal of Structural Engineering, 143(6). doi:10.1061/(ASCE)ST.1943-541X.0001760

[16] Sizemore, J., Fahnestock, L., Hines, E., & Bradley, C. (2017). Parametric study of low-ductility concentrically braced frames under cyclic static loading. Journal of Structural Engineering, 20170601. doi:10.1061/(asce)st.1943-541x.0001761

[17] Canadian Standards Association (CSA) S16-19. (2019). Design of steel structures. Toronto, ON, Canada.

[18] Rudman, A. (2018) Testing of conventional construction W-shape brace members and their bolted end connections undergoing reversed cyclic loading. Master's thesis, Department of Civil Engineering, McGill University, Montreal, QC, Canada.

[19] Rudman, A., Tremblay, R., Rogers, C.A. (2021). Conventional I-shape brace member bolted connections under seismic loading: Laboratory study. Journal of Constructional Steel Research, 184, 106795.

[20] Wang, C., González Ureña, A., Afifi, M., Rudman, A., Tremblay, R., Rogers, C. A. (2020) "Conventional construction steel braces with bearing plate energy dissipation", 17th World Conference on Earthquake Engineering, Sendai, Japan

[21] Wang, C., Rudman, A., Tremblay, R., Rogers, C.A. (2021). Numerical investigation into I-shape brace connections of conventional concentrically braced frames. Engineering Structures (in press).

[22] Systèmes, Dassault. (2014). Abaqus 6.14 Documentation. Providence, RI: Dassault Systèmes.

[23] Yam, M., & Cheng, J. (2002). Behavior and design of gusset plate connections in compression. Journal of Constructional Steel Research, 58(5), 1143-1159. doi:10.1016/S0143-974X(01)00103-1

[24] Yam, M., Hu, S., & Cheng, J., Member, ASCE. (1994). Elastic buckling strength of gusset plate connections. Journal of Structural Engineering, 120(2), 538-559. doi:10.1061/(ASCE)0733-9445(1994)120:2(538)

[25] Goel, S., Astaneh-Asl, A., A. M. ASCE, & Hanson, R., Members, ASCE. (1985). Cyclic out-of-plane buckling of double-angle bracing. Journal of Structural Engineering, 111(5), 1135-1153. doi:10.1061/(ASCE)0733-9445(1985)111:5(1135)

[26] American Institute of Steel Construction (AISC) 341-16. (2016). Seismic provisions for structural steel buildings. Chicago, IL, USA.

[27] Walbridge, S., Grondin, G., & Cheng, J. (2005). Gusset plate connections under monotonic and cyclic loading. Canadian Journal of Civil Engineering, 32(5), 981-995. doi:10.1139/l05-045

[28] Thornton, W. A. (1984). Bracing connections for heavy construction. Engineering Journal, 21(3), 139-148.

[29] American Institute of Steel Construction (AISC) 360-16. (2016). Specification for Structural Steel Buildings. Chicago, IL, USA.

FOREWORD TO CHAPTER 5

As brace connections are considered to be the weak links in Conventional Concentrically Braced Frames (CCBFs), the accurate modeling of their nonlinear force-deformation hysteretic behaviour and fracture is crucial for reliable numerical analyses of the entire system. The high-fidelity numerical study presented in Chapters 3 and 4 revealed various possible failure modes and identified the deformation mechanisms of the bolted brace connection. However, the high-fidelity finite element (FE) modelling method is not feasible for nonlinear analyses of the entire system under seismic loading, as it is too computationally demanding and time consuming. In Chapter 5, an efficient nonlinear numerical modeling method using OpenSees, comprising the component-based modeling concept, is proposed for the bolted brace connection. A set of organized springs was used to model the response of the brace connection to loading. Each spring is relied upon to replicate the behaviour of the various deformation mechanisms identified in Chapters 3 and 4.

Subsequently, a case study, consisting of eight single-storey archetype buildings, with variation in locations, site classes, beam orientation, and brace connection strength levels, was conducted. For each building, the two-bay CCBFs with the symmetric diagonal bracing configuration were adopted as the seismic force resisting system. The component-based modelling of the bolted brace connections was incorporated into the numerical models of the eight CCBFs. The structural behaviour of CCBFs with I-shape braces and bolted brace connections was studied through nonlinear static analyses and nonlinear response history analyses (NRHAs).

It is worth noting that, in this chapter, the steel plate bearing behaviour was simplified as bi-linear in the numerical models using the elastic-perfectly plastic gap material. However, as presented in Appendix A, an attempt was made and recorded to model the steel plate bearing behaviour more

accurately using the hyperbolic gap material element. This element, which can reproduce the non-linear response, was adopted for all the bearing components in the bolted brace connections.

CHAPTER 5: COMPONENT-BASED MODEL FOR BOLTED BRACE CONNECTIONS IN CONVENTIONAL CONCENTRICALLY BRACED FRAMES

Submitted to journal Engineering Structures.

Chen Wang, Robert Tremblay, Colin A. Rogers

ABSTRACT

In low and moderate seismic regions, low-ductility concentrically braced frames (CBFs) are widely used as the seismic force-resisting system for steel structures. The capacity-based design method is not required for such systems, i.e. no individual component in the lateral load carrying path is explicitly designated to sustain plastic deformations under seismic loading. Such CBFs are referred to as conventional CBFs (CCBFs) in this paper. Prior studies have revealed that, in CCBFs, the brace-to-gusset connections are inherently weaker in tension than the adjoining braces and gusset plates. Therefore, the accurate numerical modelling of the brace connections is critical for the reliable seismic evaluation of CCBFs. However, few research publications address the inelastic bolted brace connection modelling necessary for the structural analyses of these braced frame systems. In this paper, an efficient inelastic numerical modelling method, comprising the component-based modelling concept, is proposed for bolted brace connections. The accuracy of the numerical model is validated through comparison with laboratory test results of full-scale I-shape brace connection specimens. Eight single-storey CCBFs with the symmetric diagonal bracing configuration were designed and modeled. The nonlinear static and dynamic analyses revealed that: 1) although the buckling of the middle column at small storey drifts resulted in substantial lateral strength deterioration, a secondary seismic mechanism provided stable resistance to prevent collapse; 2) when loaded in tension, the brace connections deformed more

than the braces; 3) stronger brace connections resulted in higher structural lateral stiffness and triggered earlier buckling of the middle column; 4) stronger brace connections possessed higher frictional energy-dissipating capacity which reduced the maximum storey drift.

Keywords: low ductility, concentrically braced frame, bolted brace connection, component-based model, nonlinear dynamic analysis

5.1. INTRODUCTION

Concentrically braced frames (CBFs) are often used as seismic force-resisting systems because they are effective in providing structural lateral stiffness and strength. A variety of seismic design methods for CBFs with different levels of expected system ductility have been developed. In areas of low and moderate seismic hazard, low-ductility CBFs are permitted in many countries. Such CBFs are designed using a simple approach: the member forces are first calculated using linear elastic structural analysis; the structural members and connections are then designed to resist the obtained member forces. Capacity-based design and additional seismic detailing are not required. Such low-ductility CBFs are referred to as Conventional CBFs (CCBFs) in this study. Due to the expected low structural deformation capacity, CCBFs are typically designed for higher seismic loads as compared to more ductile lateral bracing systems.

Owing to the exemption for capacity-based design and additional seismic detailing, CCBFs are generally more economical than their more ductile counterparts. As such, CCBFs are widely used in low and moderate seismic regions in many countries. Each country may have its own designation and design requirements for the CCBF. In Canada, a low-ductility type of CBF, i.e. Type Conventional Construction (CC), is permitted as per CSA S16 [1]. Capacity-based design and seismic detailing are not required for structural members of Type CC CBFs, but the resistance of the brace connections must be increased by 1.5 if the expected connection failure mode is not proven to be ductile. In the USA, CBFs categorized as "Systems not specifically detailed for seismic resistance" in ASCE/SEI 7-16 [2] are prevalent in regions of low and moderate seismic hazard. To account for the modest expected structural deformation, a response modification factor, R=3, is assigned to such systems. In Europe, CBFs can be designed based on the concept of low dissipative structural behaviour with low structural ductility (DCL) per Eurocode 8 [3]. Structural

members and connections are simply required to resist the seismic loads calculated on the basis of an elastic global analysis, without any additional requirements. A behaviour factor (q) ranging from 1.5 to 2 is specified for design. In New Zealand, an elastic system with minimal structural displacement ductility demand (i.e. Category 4 system) is permitted in NZS 3404 [4]. A structural ductility factor (μ) of 1 is assigned. Furthermore, a performance factor (S_p) of 1.0 is specified for connections, compared to 0.9 for structural members, which effectively increases the design force demand on the connections.

In CCBFs, the brace-to-gusset connections tend to be inherently weaker than the adjoining braces and gusset plates. This is because, under the CCBF design framework, the brace-to-gusset connection, and the adjoining brace and gusset plate, are designed to resist the same forces. Braces and gusset plates are typically selected based on their respective compressive buckling resistances which are usually smaller than their respective tensile resistances, while brace-to-gusset connections are designed based on the tensile resistances. As such, both braces and gusset plates generally possess greater tensile resistances than the brace-to-gusset connections. This point has been verified both experimentally and numerically in prior studies. Sen et al. [5,6] experimentally studied CBFs that were built in the past without capacity-based design. Fracture of the brace-to-gusset welds was observed at low storey drifts. They concluded that the brace-to-gusset connection is of high priority in terms of retrofit of older CBFs. Bradley et al. [7] and Sizemore et al. [8,9] studied the seismic performance of low-ductility CBFs in the USA (including the R=3 CBFs) through full-scale system tests and numerical structural simulations. They found that the brace-to-gusset weld fracture was the dominant limit state; the as-built weld overstrength significantly affected the damage locations. To obtain insight into the seismic performance of CCBFs with I-shape braces and bolted brace connections, Rudman et al. [10] and Wang et al. [11] conducted a

series of full-scale tests of I-shape brace and bolted connection assemblies under reversed cyclic loadings. Wang et al. [12] subsequently developed high-fidelity finite element models to extend their experimental findings. Their studies revealed that significant plasticity and failure occurred in the brace-to-gusset connections when the specimens were loaded in tension, which confirmed that the bolted brace-to-gusset connection was weaker in tension than the adjoining braces and gusset plates.

Therefore, accurate modelling of the plastic behaviour and fracture of the brace connections is critical for the reliable seismic performance evaluation of CCBFs. Efforts have been taken to attain accurate brace connection modelling in previous studies. Hsiao et al. [13] developed a rotational spring model to account for the non-linear out-of-plane rotational restraint provided by brace connections. To account for the additional stiffness due to the presence of gusset plates, Qu et al. [14,15] modelled gusset plates as rigid, and added force-based fiber elements at the ends of braces to capture the rotational restraints. To represent the brace-to-gusset weld fracture, Hsiao et al. [16] implemented a translational spring at the brace end that had a linear-elastic response and a fracture displacement limit. In Sizemore et al. [8, 9], a translational spring was adopted to model the brace-to-gusset weld, and fracture was initiated based on a force limit. Moreover, in the modelling of their test frame, Sizemore et al. [8] used a gap-contact element to capture the reengagement between the brace and gusset plate after the brace-to-gusset weld fracture. Sen et al. [17] provided a framework for modelling welded gusset plate connections, in which the modelling of the gusset plate yielding, brace-to-gusset weld fracture, and gusset-plate interface weld fracture were covered. To model the bolted single shear lap connection, which are traditionally used for hollow structural section bracing members, Tremblay and Davaran [18] developed two OpenSees models. In the first model, the lap plates were modelled using the beam-column elements individually, with truss

elements with compression-only material placed between the lap plates to mimic the contact. In the second model, a single beam-column element with end plastic hinges was used for the entire connection.

However, it is noted that most previous studies on brace connection modelling were focused on welded brace connections. Limited research exists for the modelling of bolted brace connections. The high-fidelity continuum finite element analysis method could capture the bolted brace connection behaviour accurately, but such an approach is extremely computationally demanding and not practical for nonlinear dynamic structural analyses under earthquake loading, especially when extensive geometric and material nonlinearities are involved. There is a need to develop an accurate and computationally efficient numerical modelling method to capture the full behaviour range of bolted brace connections for reliable structural analyses of CCBFs.

The objective of this paper is to develop an accurate and efficient modelling method for bolted brace connections, specifically, the bolted flange plate brace connection. The component-based modelling concept was adopted in this study. This method first models each of the main components that constitute the brace connection, and then aggregates them as appropriate to reproduce the full behaviour of the connection. The ability of this method to characterize the force-deformation hysteretic behaviour and to predict the onset of fracture is then validated through comparison with experimental results. In the last section of this paper, the seismic performance of eight archetype buildings was evaluated through inelastic static (Pushover) analyses and Nonlinear Response History Analyses (NRHAs) with the brace connections modeled using the proposed component-based method.

5.2. OVERVIEW OF THE BOLTED FLANGE PLATE BRACE CONNECTION

I-shape sections are widely used as the bracing members in CCBFs, as they are available with a wider range of sizes compared to other section types. Bolted connections are usually adopted to connect I-shape braces with other framing members, which avoids expensive on-site welding and expedites the construction process. A typical I-shape connection configuration is the flange plate connection shown in Figure 5.1.

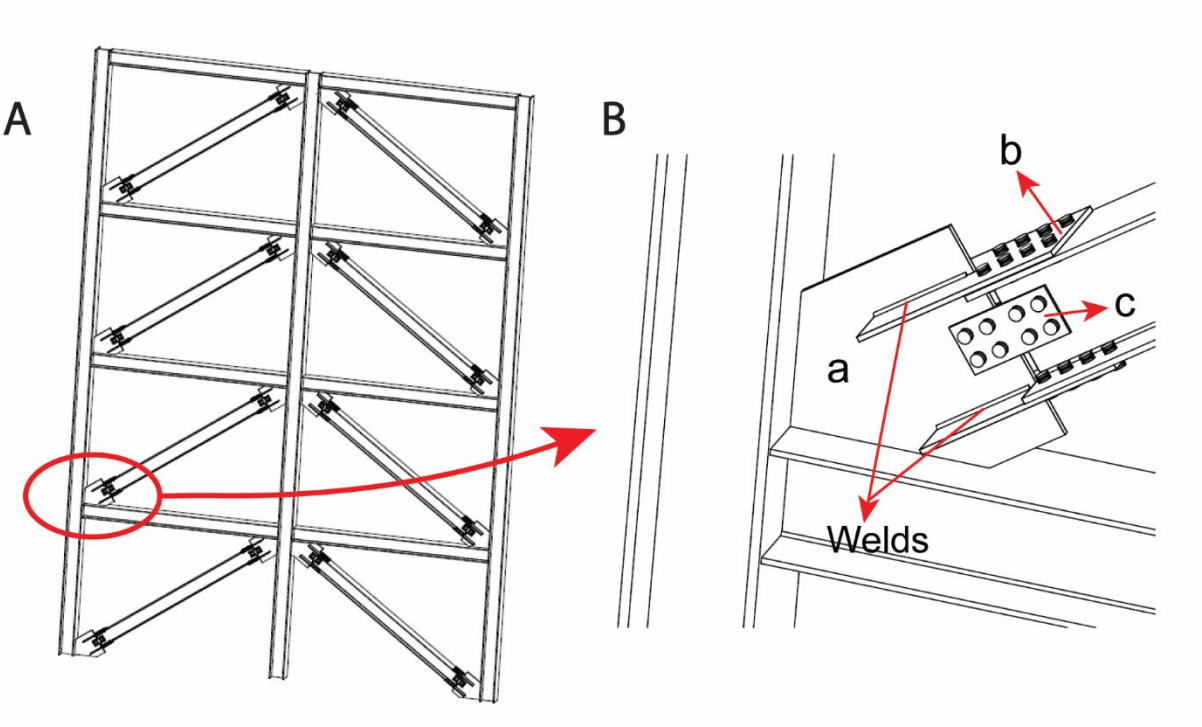

Figure 5.1: Schematic of CCBF with I-shape braces and flange plate brace connection: a) gusset plate, b) flange lap plate (FLP), c) web lap plate (WLP)

The behaviour of the flange plate brace connection was evaluated in previous studies both experimentally [10,11] and numerically [12]. The force transfer mechanism under reversed cyclic loading was characterized, and the force flow path through individual components of the flange plate connection was identified (Figure 5.2).

In this paper, the flange plate brace connection is used to illustrate the implementation of the component-based modelling method to construct numerical models for bolted brace connections; the experimental results serve the validation of the method.

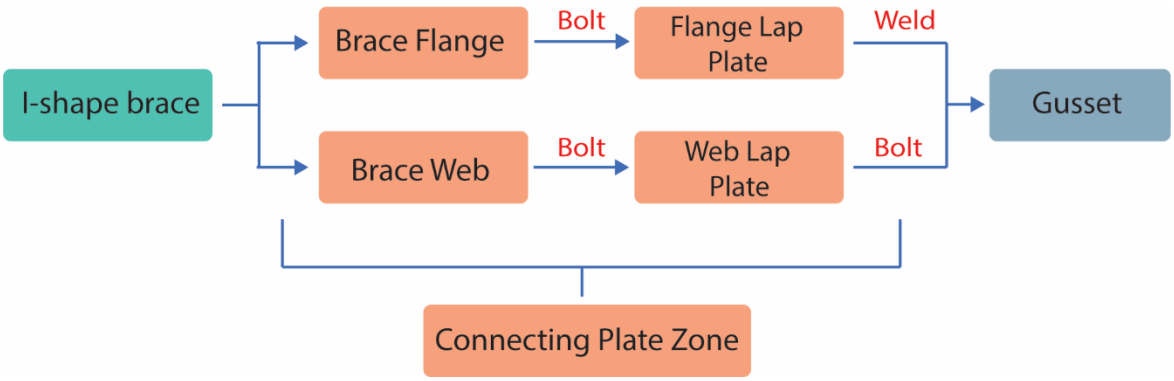

Figure 5.2: Components and force paths of the flange plate brace connection

5.3. COMPONENT-BASED BRACE CONNECTION MODELING METHOD

The component-based modelling concept provides a flexible numerical framework to model the response of complex connections, especially when there is no general model available to capture the full-range of behaviour of the connection [19,20]. Rather than attempting to extract one general model for the whole connection, the component-based method discretizes the connection into individual components that contribute to the global behaviour. Each component is modeled by a spring with the characteristic behavioural properties; the interactions between the components are captured by arranging springs either in parallel or in series, as appropriate.

There is no prescribed yielding/failure hierarchy in the bolted flange plate brace connection in CCBFs, as explained by Wang et al. [12]; therefore, any one of the components illustrated in Figure 5.2 could dominate the behaviour, and should be incorporated in the numerical model. For the multi-bolted component, e.g. the bolted flange lap plate, it is further discretized into individual

single-bolted components, which comprise a bolt and two bearing plates (Figure 5.3), as utilized by Weigand [21]. The description and modelling of individual components involved in the flange plate connection are elaborated in the following sections. Note that the component-based method is not limited to the flange plate brace connection, it can easily be extended to other bolted brace connection configurations based on the same philosophy, by changing the constituting components, as appropriate.

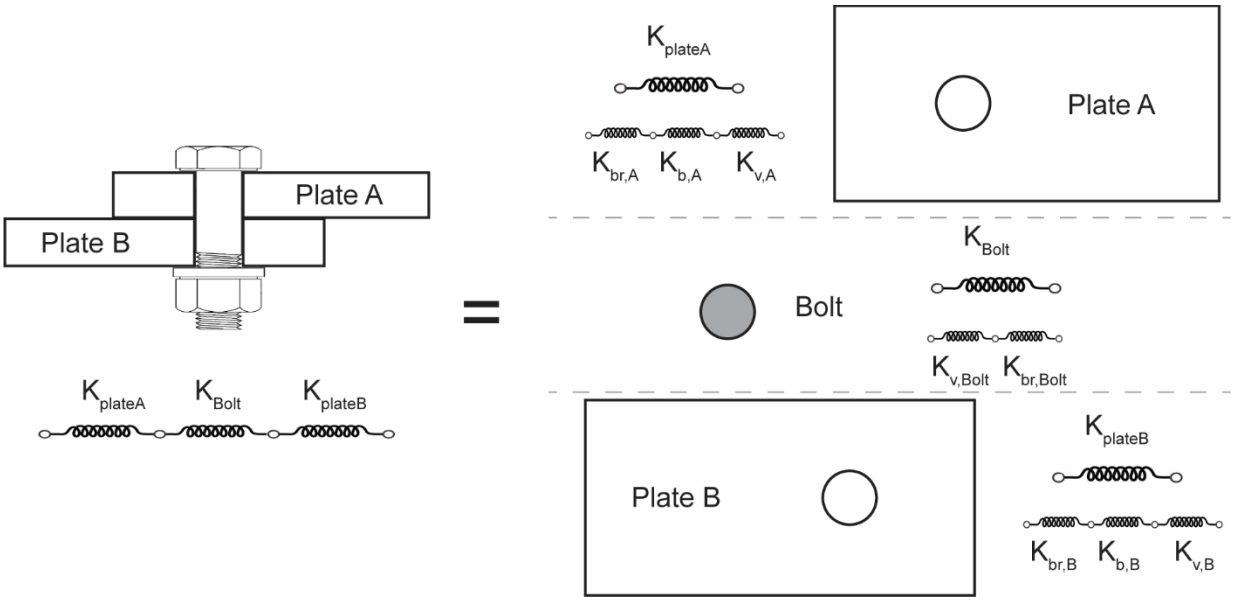

Figure 5.3: Disaggregation of the single-bolted component

5.3.1. Bearing Behaviour

The bearing behaviour of the plate was analytically established by Rex and Easterling [22], who performed 46 tests of a single bolt bearing against a single plate with various edge distances, plate thicknesses, bolt diameters, plate widths, and edge conditions. They adopted the equation proposed by Richard and Abbott [23], commonly known as the Richard equation, and calibrated the equation parameters based on their experimental results using a nonlinear least-square regression technique. The load-deformation relationship in bearing is:

$$\frac{\mathrm{R}}{\mathrm{R_n}} = \frac{(\alpha_{kb} - \alpha_{kp})\overline{\Delta}}{\left[1 + \left|\frac{(\alpha_{kb} - \alpha_{kp})\overline{\Delta}}{\alpha_{rb}}\right|^{n}\right]^{\frac{1}{n}}} + \alpha_{kp}\overline{\Delta} = \frac{1.74\overline{\Delta}}{\left(1 + \overline{\Delta}^{\frac{1}{2}}\right)^{2}} - 0.009\overline{\Delta} \tag{5.1}$$

where R = bearing load, R_n= plate ultimate bearing strength, $\overline{\Delta}$ = normalized bearing deformation, with $\alpha_{kb} = 1.731$, $\alpha_{kp} = -0.009$, $\alpha_{rb} = 1.740$, and $n = 0.5$.

There are several limits available in different standards in terms of the ultimate plate bearing strength. The model for predicting the plate ultimate bearing/tearing strength (F_b) developed by Fisher and Struik [24] was adopted in this study:

$$F_b = 1.4F_u\left(\frac{L_e}{d_b} - \frac{1}{2}\right) \leq 3.0F_u \tag{5.2}$$

where F_u = ultimate stress of the steel material, L_e = end distance of the bolt, d_b = bolt diameter.

The normalized deformation $\overline{\Delta}$ is equal to $\Delta\beta K_i/R_n$, where Δ = hole elongation, β = steel correction factor (taken as one for typical steels), K_i = initial stiffness. Through experimental tests and numerical simulations Rex and Easterling [22] found the initial stiffness depended on three primary stiffness mechanisms in the plate—bearing, bending, and shearing. The model that accounts for these three stiffnesses is:

$$K_i = \frac{1}{\frac{1}{K_{br}} + \frac{1}{K_b} + \frac{1}{K_v}} \tag{5.3}$$

where K_{br} = bearing stiffness, K_b = bending stiffness, K_v = shearing stiffness, and they are quantified as:

$$K_{br} = 120 t_p F_y \left(\frac{d_b}{25.4}\right)^{0.8} \tag{5.4}$$

$$K_b = 32 E t_p \left(\frac{L_e}{d_b} - \frac{1}{2}\right)^3 \tag{5.5}$$

$$K_v = 6.67 G t_p \left(\frac{L_e}{d_b} - \frac{1}{2}\right) \tag{5.6}$$

with t_p = thickness of the plate.

5.3.2. Bolt behaviour

The shear force-deformation behaviour of the bolt can also be described by means of the Richard equation, as done by Weigand [21]:

$$R_{bolt} = \frac{\left(K_{i,bolt} - K_{p,bolt}\right)\Delta}{\left[1 + \left|\frac{\left(K_{i,bolt} - K_{p,bolt}\right)\Delta}{R_{v,bolt}}\right|^2\right]^{\frac{1}{2}}} + K_{p,bolt}\Delta \tag{5.7}$$

where R_{bolt} = shear force, Δ = shear deformation, $K_{i,bolt}$ = bolt initial stiffness, $K_{p,bolt}$ = bolt plastic stiffness, and $R_{v,bolt}$ = bolt shear capacity.

The initial stiffness of the bolt, $K_{i,bolt}$, is primarily affected by bearing and shearing in the bolt shank, and therefore is calculated by assuming two springs in series as:

$$K_{i,bolt} = \frac{1}{\frac{1}{K_{br,bolt}} + \frac{1}{K_{v,bolt}}} \tag{5.8}$$

where $K_{br,bolt}$ = bolt bearing stiffness and $K_{v,bolt}$ = bolt shearing stiffness.

Nelson et al. [25] proposed a model for bolt bearing stiffness based on their experimental work,

$$K_{br,bolt} = \frac{1}{1 + 3\beta_b} \frac{t_p t_w E_{bolt}}{2(t_p + t_w)} \tag{5.9}$$

where t_w is the thicknesses of the connected plate, and β_b is a correction factor that represents the fraction of the total bending moment on the bolt that is reacted by the nonuniform bearing stresses across the thickness of the connected plate. Many factors may affect the value of β_b, e.g., the bolt geometry and bolt pretension, the size of nuts and washers, the ratio of bolt diameter to plate thickness, among others. The value of β_b could vary from a maximum of 1.0 for simple shear pin, to a very small value for bolted connections with large washers and a large ratio of bolt diameter to plate thickness. It is worth noting that limited data are available to calibrate the value of β_b for bolted joints in steel structures. A value of β_b = 0.7 was adopted by Weigand [21] in models for 13 steel shear connections, in which bolts of two grades (A325 and A490) and various diameters (19-22 mm) were used. Good agreement between the predicted connection stiffness with the experimental ones reported in Weigand and Berman [26] was obtained. In this study, the same bolt

grades (A325 and A490) and similar bolt diameters (16-20 mm) were used, and the same value of β_b = 0.7 was adopted.

The bolt shearing stiffness is determined by assuming that the bolt acts as a prismatic Timoshenko beam with circular cross section and fixed ends,

$$K_{v,bolt} = \frac{12E_{bolt}I_{bolt}}{L_{bolt}^3(1+\Phi)} \tag{5.10}$$

where E_{bolt} = bolt modulus of elasticity, $I_{bolt} = \frac{\pi d_b^4}{64}$ = moment of inertia of the bolt shaft cross section, $L_{bolt} = t_p + t_w$ = bolt length, and

$$\Phi = \frac{12E_{bolt}I_{bolt}}{G_{bolt}\kappa A_{bolt}L_{bolt}^2} \tag{5.11}$$

is a term that accounts for the relative importance of shear deformation to bending deformation in Timoshenko beam theory [27]. In equation (5.11), $G_{bolt} = \frac{E}{2(1+\nu)}$ is the bolt shear modulus, A_{bolt} is the bolt cross section area, and κ is the shear coefficient for a circular cross section

$$\kappa = \frac{1}{\frac{7}{6} + \frac{1}{6}\left(\frac{\nu}{1+\nu}\right)^2} \tag{5.12}$$

Based on the bolt shear test data [28], the bolt shear capacity was taken as

$$R_{v,bolt} = 0.62 A_{bolt} F_{u,bolt} \tag{5.13}$$

and the bolt plastic stiffness $K_{p,bolt}$ was calculated as 2% of the bolt initial stiffness $K_{i,bolt}$.

5.3.3. Weld behaviour

In the bolted flange plate brace connection, the flange lap plates (FLPs) are connected to the gusset plate by fillet welds that are parallel to the line of action of the brace force (Figure 5.1). The expression developed by Lesik and Kennedy [29] for load-deformation response of welds loaded longitudinally, i.e. at an angle of 0°, was therefore adopted:

$$P = P_0 f(\rho) \tag{5.14}$$

where P_0 is the ultimate strength of the longitudinal weld. The function $f(\rho)$ gives the variation of load with respect to deformation, and is defined as:

$$f(\rho) = 8.234\rho; \qquad 0 < \rho < 0.0325$$

$$f(\rho) = -13.29\rho + 457.32\rho^{\frac{1}{2}} - 3385.9\rho^{\frac{1}{3}} + 9054.29\rho^{\frac{1}{4}} - 9952.13\rho^{\frac{1}{5}} + 3840.71\rho^{\frac{1}{6}}; \quad \rho > 0.0325 \tag{5.15}$$

In equation (5.15), ρ is the normalized deformation with respect to the deformation at ultimate strength,

$$\rho = \frac{\Delta}{\Delta_u} = \frac{\Delta}{0.209 \times 2^{-0.32} D} \tag{5.16}$$

where Δ and *D* are the weld deformation and fillet weld size in the same units, respectively.

By using the weld resistance equation in Clause 13.13.2.2 of CSA S16 [1], the ultimate strength of a longitudinally loaded weld is calculated as

$$P_0 = 0.67 \phi A_W X_u \tag{5.17}$$

where A_W is the effective throat area of the fillet weld, X_u is the ultimate strength of the weld metal, and the resistance factor ϕ was taken as one to obtain a realistic estimate of the strength.

5.3.4. Brace connection modeling in OpenSees

The component-based brace connection modelling was implemented in OpenSees [30]. The spring model structure for the flange plate brace connection, with each spring representing one constituting component of the connection, is schematically shown in Figure 5.4.

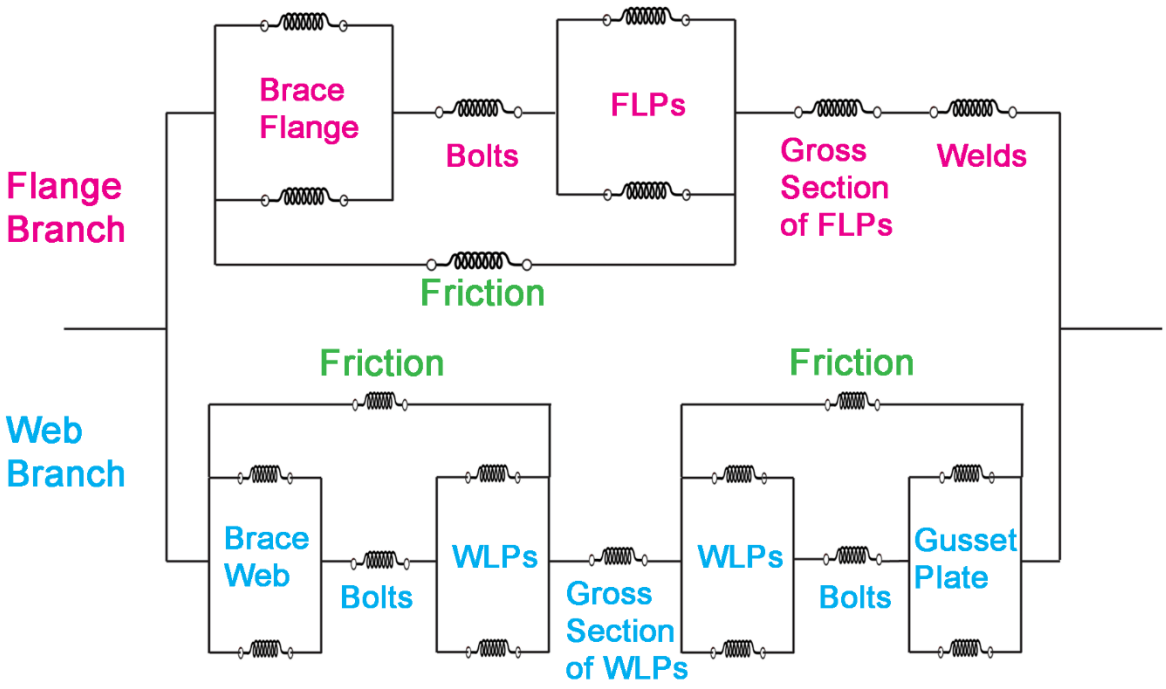

Figure 5.4: Spring model structure of the bolted flange plate brace connection in OpenSees

Bolt slippage plays a significant role in the cyclic response of bolted brace connections. In order to capture the pronounced bolt slippage behaviour, a pair of Elastic-Perfectly Plastic Gap (EPPG) elements were selected for each bearing component, with one for tensile bearing and the other for compressive bearing behaviour. Before the specified gap is taken up, the EPPG element provides zero resistance. It was assumed that the bolt hole diameter was 1.6 mm (1/16 in.) greater than the bolt diameter, and all the bolts were initially in the middle of the bolt holes. As such, the initial gap values were set as 0.8 mm and -0.8 mm for the tensile bearing element and the compressive bearing element, respectively. Moreover, for each gap element, the ‘damage’ option was turned on so that the gap value would grow with the plastic deformation of the bolt hole to account for the bolt hole elongation phenomenon. Frictional forces were reported to decrease upon cyclic loading [10,11]; at the final phase of the tests, a mean value of 17% was obtained for the ratio of the frictional force to the force based on which the brace connection was designed. In the OpenSees

model, the friction was modelled by placing an Elastic-Perfectly Plastic (EPP) element parallel to the EPPG elements, with the frictional force set equal to 17% of the force based on which the brace connection was designed. The bearing behaviour after the gap was closed was determined by the analytical method described in Section 5.3.1, and simplified as bilinear with the ratio of post-yield stiffness to initial stiffness set as 0.04.

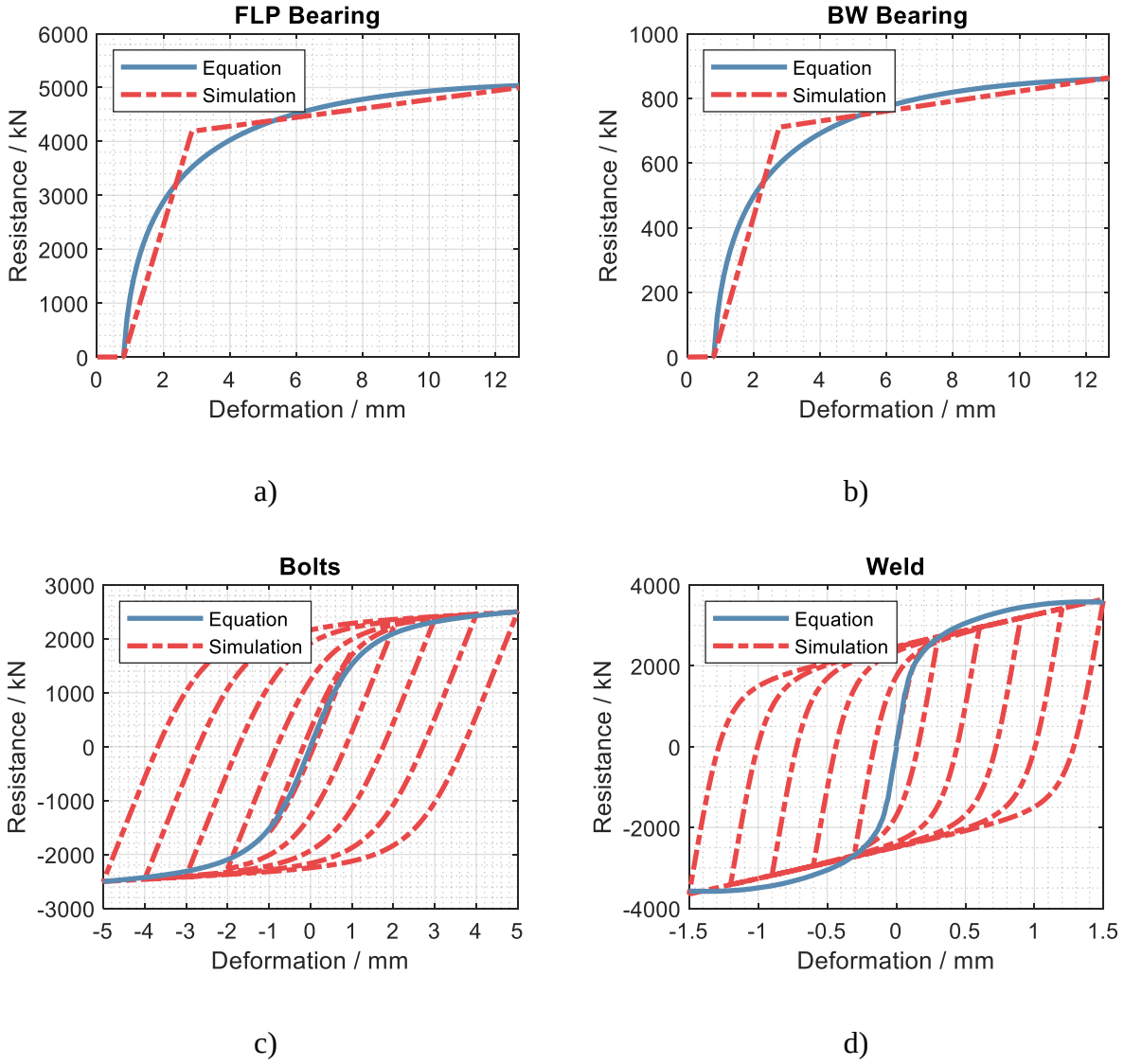

Figure 5.5: Comparison of simulated and numerically predicted behaviour of typical components: a) FLP bearing, b) Brace web bearing, c) Bolts in the brace flange, and d) Welds

The bolt and weld behaviours were modelled using the Steel02 material in OpenSees [31]. The Steel02 material parameters were determined to make the backbone curve of the force-deformation hysteretic loops match with the response curve predicted in accordance with the equations in Section 5.3.2 and Section 5.3.3: R0=4, cR1=0.01 and cR2=0.01 for bolts, and R0=3, cR1=0.01 and cR2=0.01 for welds. Figure 5.5 shows a comparison between the behaviours predicted by the equations and the response provided by the OpenSees model for typical components of the tested specimen J310-T by Rudman et al. [10]. They are representative of the simulation of tensile bearing behaviour, cyclic bolt shear behaviour, and cyclic weld behaviour.

5.3.5. Fracture criteria

To capture the fracture that could be caused by various mechanisms, fracture criteria were introduced to individual components in the OpenSees model. The bolt shear tests reported by Wallaert & Fisher [32] and Weigand [28] indicated that the high-strength bolt (e.g., grade A325 and A490 bolts) generally failed in shear at 5 mm (0.2 in.) deformation, which was selected as the bolt deformation limit. The MinMax material in OpenSees was adopted to introduce the maximum deformation limit. If the deformation fell above the prescribed limit, the element was assumed to have failed and values of zero were returned for the stiffness and strength.

Likewise, fillet welds loaded longitudinally were reported to reach their ultimate strength at a deformation approaching 0.2D (D is the fillet weld size), after which they lost their strength quickly [29]. In the model, the weld deformation limit was set to 0.2D. The plate bearing failure was defined when the bearing deformation exceeded 12.7 mm (0.5 in.), as done by Rex and Easterling [22]. In some cases, fracture may occur along the net section of the FLPs and WLPs. In view of the limited deformation capacity associated with net section fracture, the force-based limit was set to model the net section fracture, with the value determined by:

$$T_u = A_n R_t F_u \tag{5.18}$$

where A_n = area of net section, R_t = the ratio of the expected tensile ultimate strength to the minimum tensile ultimate strength of the steel.

5.3.6. Validation

To verify the validity of the component-based brace connection modelling method, numerical models were built in OpenSees for the tested full-scale brace-connection assemblies reported in Rudman et al. [10] and Wang et al. [11]. Knowing that the numerical models described herein were not developed to capture gusset plate buckling, only the test specimens that exhibited brace buckling in compression were modeled, specifically specimens J-310-C and J-310-T in Rudman et al. [10] and specimen J360-P in Wang et al. [11].

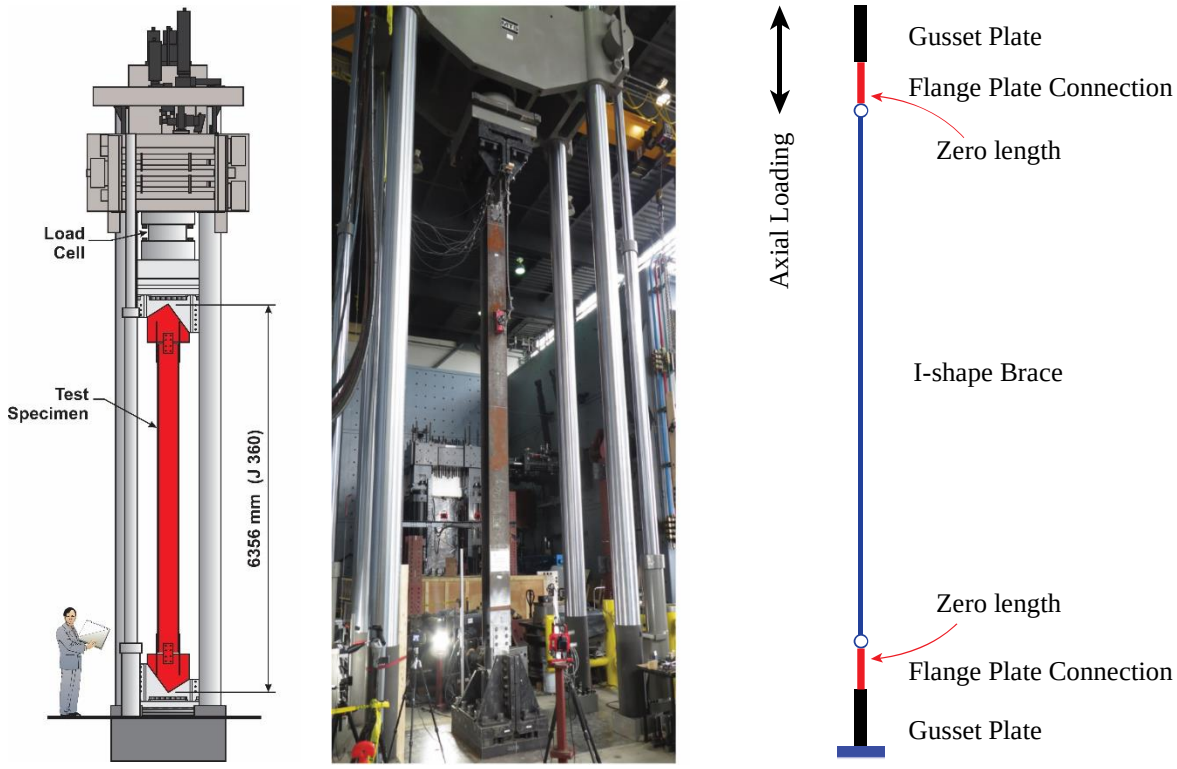

Figure 5.6: Modelling of tested full-scale brace-connection assemblies in OpenSees: a) test set-up [10,11]; b) OpenSees model

As shown in Figure 5.6, the tested specimens contained three parts: gusset plates, flange plate connections, and I-shape brace. The flange plate connections were modeled following the approach in Section 5.3.4, and the modelling parameters of each component were calculated based on the measured geometric and material properties [10,11]. For each brace, ten displacement-based beam-column elements with five integration points in each element were used. The fiber-based section, with 10 fibers along flange width/web height and 4 fibers through flange thickness/web thickness, was assigned to each element. This discretization scheme is slightly more stringent than that recommended by Karamanci & Lignos [33]. An initial out-of-straightness of 1/1000 times brace length following a half sine wave distribution was introduced. Due to the configuration of the flange plate brace connection, the end rotation restraint about the I-shape brace minor axis is far smaller than that about its major axis. As such, the initial out-of-straightness was only introduced for the minor axis of the I-shape braces because they were expected to buckle about this axis. The brace was pin connected to the gusset plate through the flange plate connection. The Steel02 material was used for braces, with the yield strength, initial elastic tangent, and strain-hardening ratio (b=0.29%) determined based on the tension coupon test results reported in Rudman [34]. Other parameters in the model were R0=15, cR1=0.925, and cR2=0.15 as recommended in Mazzoni et al. [35]. Previous research has been conducted to capture the low-cycle fatigue rupture behaviour [15,36]. However, due to the fact that in CCBFs braces are not expected to experience low-cycle fatigue rupture, this failure mode was not modelled in this study.

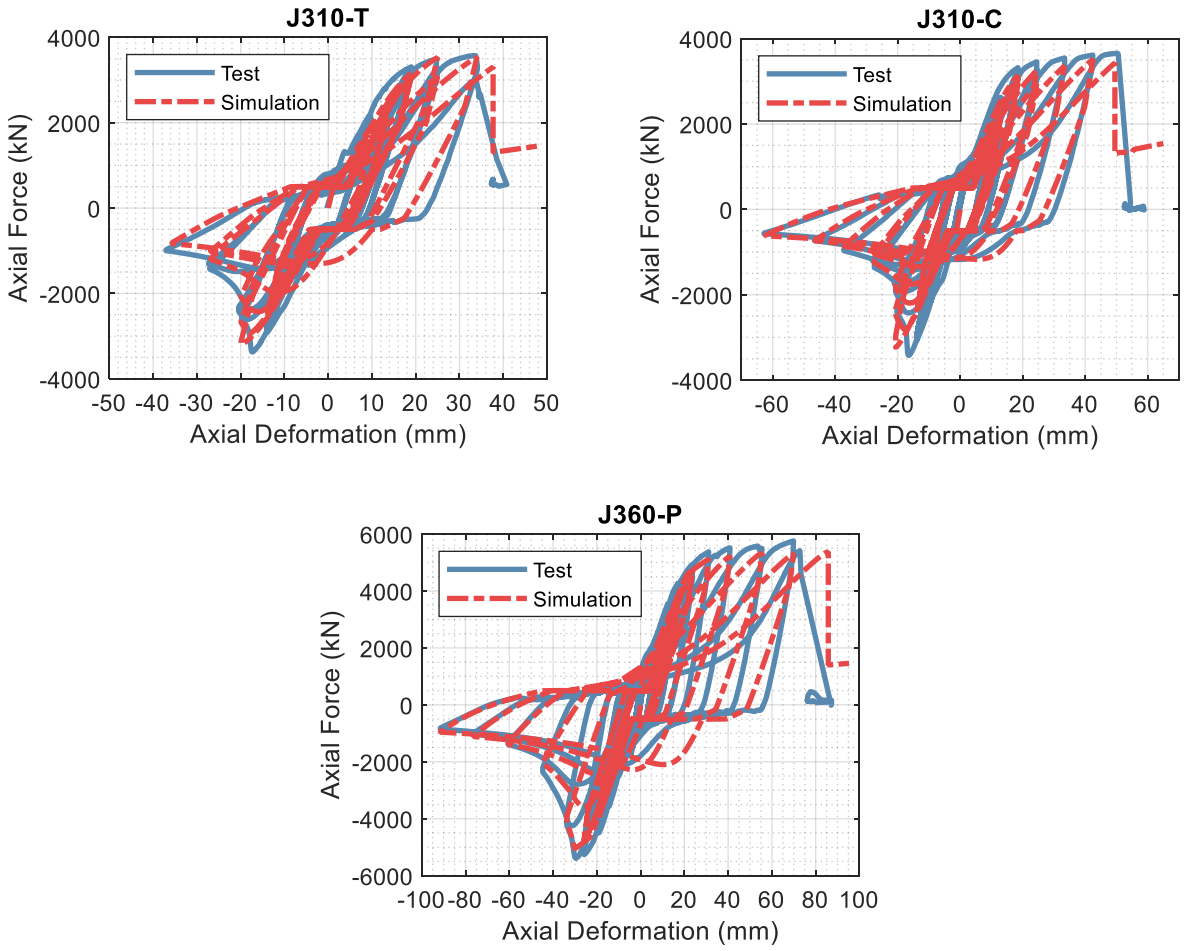

Figure 5.7: Comparison of simulated and experimental [10] axial force-deformation responses of the brace-connection assembly

In CCBFs with I-shape braces and bolted brace connections, the bolted brace-to-gusset connection is weaker than the adjoining brace and gusset plate, especially when loaded under tension. This is because, under the non-capacity design framework, the brace-to-gusset connection, and the adjoining brace and gusset plate, are designed to resist the same force demand calculated through elastic structural analysis. Braces and gusset plates are typically selected and designed based on their respective compressive buckling resistances, which are usually smaller than their respective tensile resistances. However, brace-to-gusset connections are typically designed based on their tensile resistances, as compressive buckling is not expected to occur in the connections. As such,

when loaded under tension, the brace-to-gusset connection is weaker than the adjoining brace and gusset plate; plastic deformations leading to failure are expected to occur in the brace-to-gusset connection rather than in the gusset plate. This has been verified experimentally through full-scale tests of brace and bolted brace connection assemblies by Rudman et al. [10] and Wang et al. [11], and numerically by Wang et al. [12,37]. Therefore, the gusset plates were modelled as rigid bodies in this study, by using a displacement-based beam-column element assigned with a very large section (more than 1000 times larger than the brace section) and the brace material.

Reversed cyclic loading was simulated following the loading protocols used in the laboratory tests [10,11]. The axial force-deformation results obtained from the numerical simulations were compared with those acquired from the tests [10,11], as shown in Figure 5.7. These force-deformation hysteretic curves exhibited good agreement, and the numerical models accurately predicted the connection failure mode (bolt shear rupture) at similar deformation levels to those reported in the tests, indicating the capability of the proposed component-based brace connection modelling method to capture the cyclic behaviour and failure of the connections.

In addition, the brace connection axial deformation histories at one end of the brace, excluding the brace axial deformation, were extracted from the numerical simulations and compared with those measured during the tests [10,11], as shown in Figure 5.8. A generally good match was obtained, which further validated the accuracy of the component-based brace connection model.

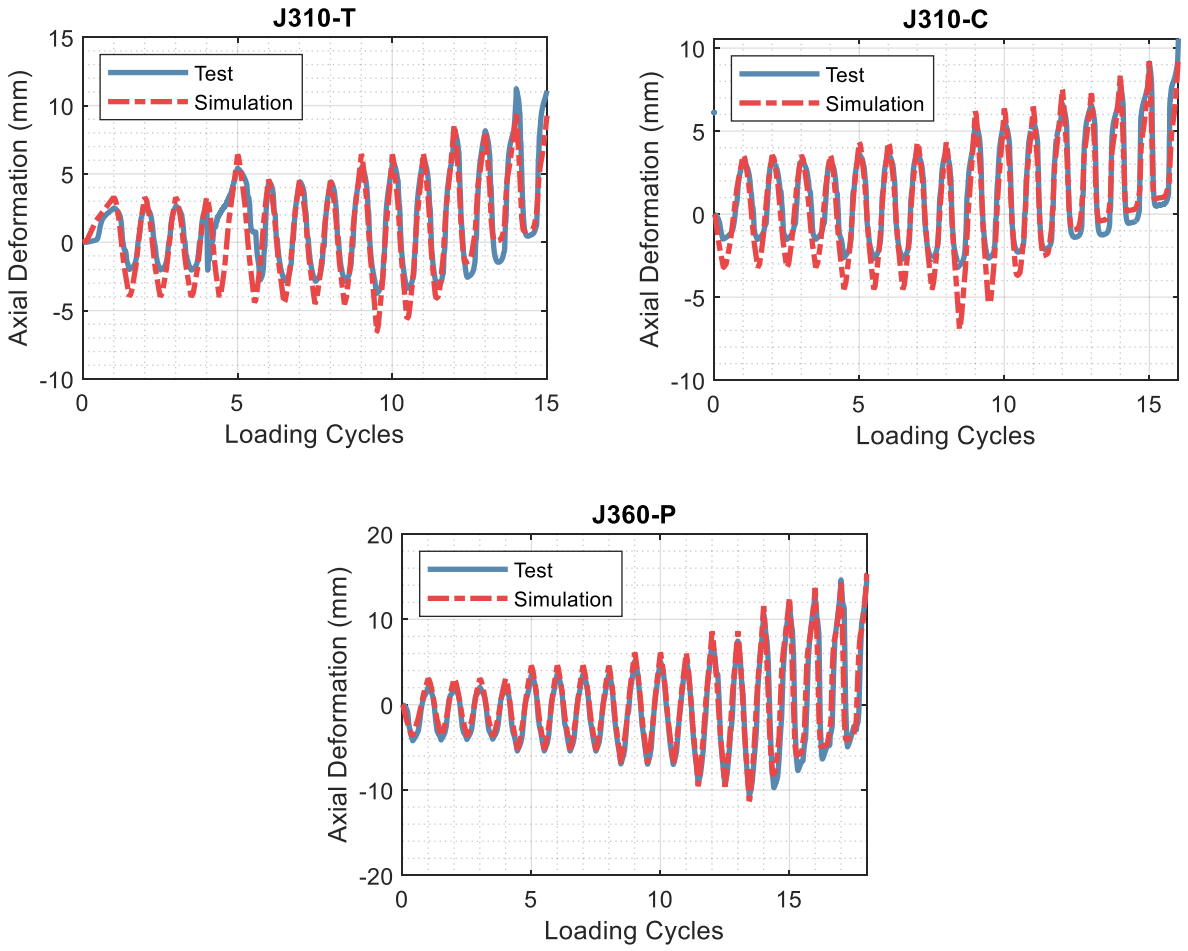

Figure 5.8: Comparison of simulated and experimental [10,11] axial deformation histories of one brace connection

5.3.7. Significance of modelling bolted brace connections

The deformation histories of the brace connections at both ends of the brace, the brace, and the entire specimen, for the three validation models, are compared in Figure 5.9. Before brace buckling occurred, most deformation developed in the brace connections under both tension and compression loadings. After brace buckling had occurred, due to the sudden degradation of the brace compressive resistance, most deformation concentrated in the brace under compression loading; however, when loaded under tension loading, the deformation from the brace connections

still constituted a significant portion of the total deformation. For all three specimens, ultimate failure occurred in the brace connections.

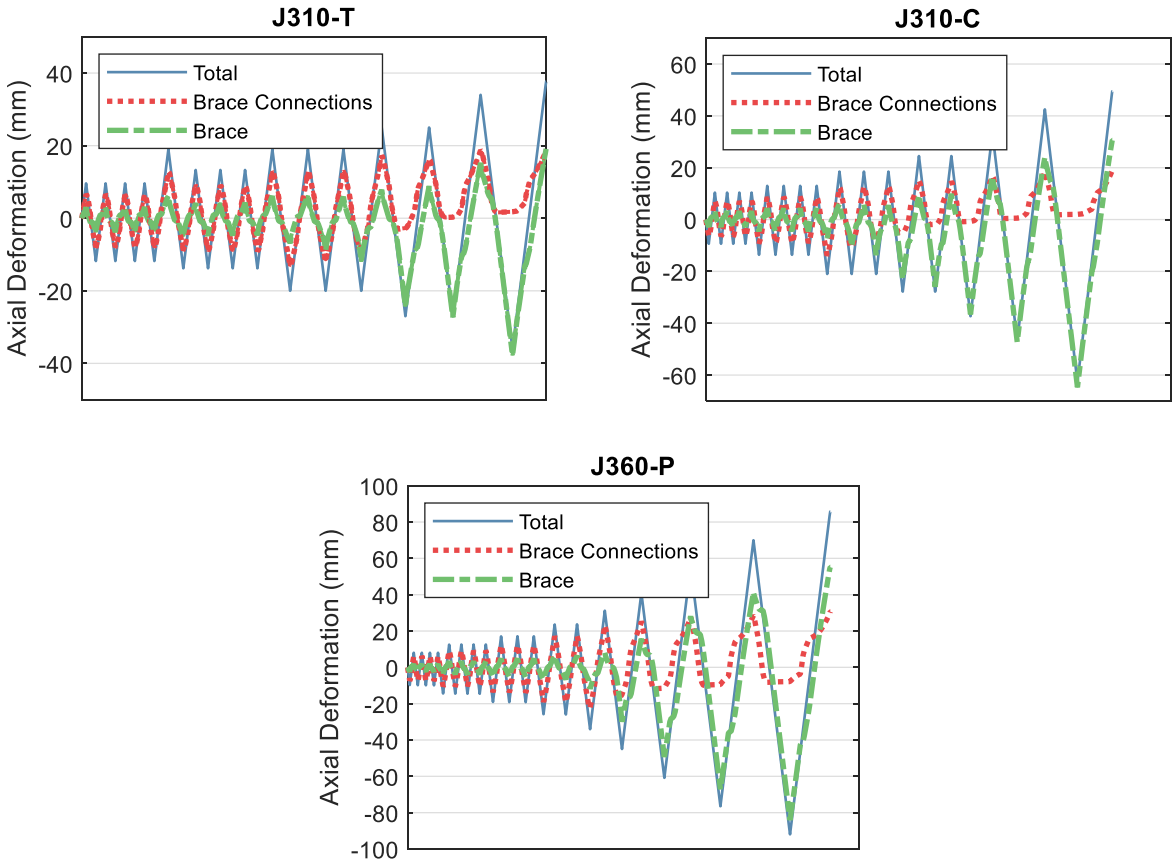

Figure 5.9: Comparison of deformation histories between brace and brace connections

Moreover, simulations were conducted in which the brace connections were not modelled, while all the other aspects (other elements, boundary conditions, loading protocols, etc.) were maintained. In Figure 5.10, the force-deformation hysteretic response results are compared between the models with and without the brace connections.

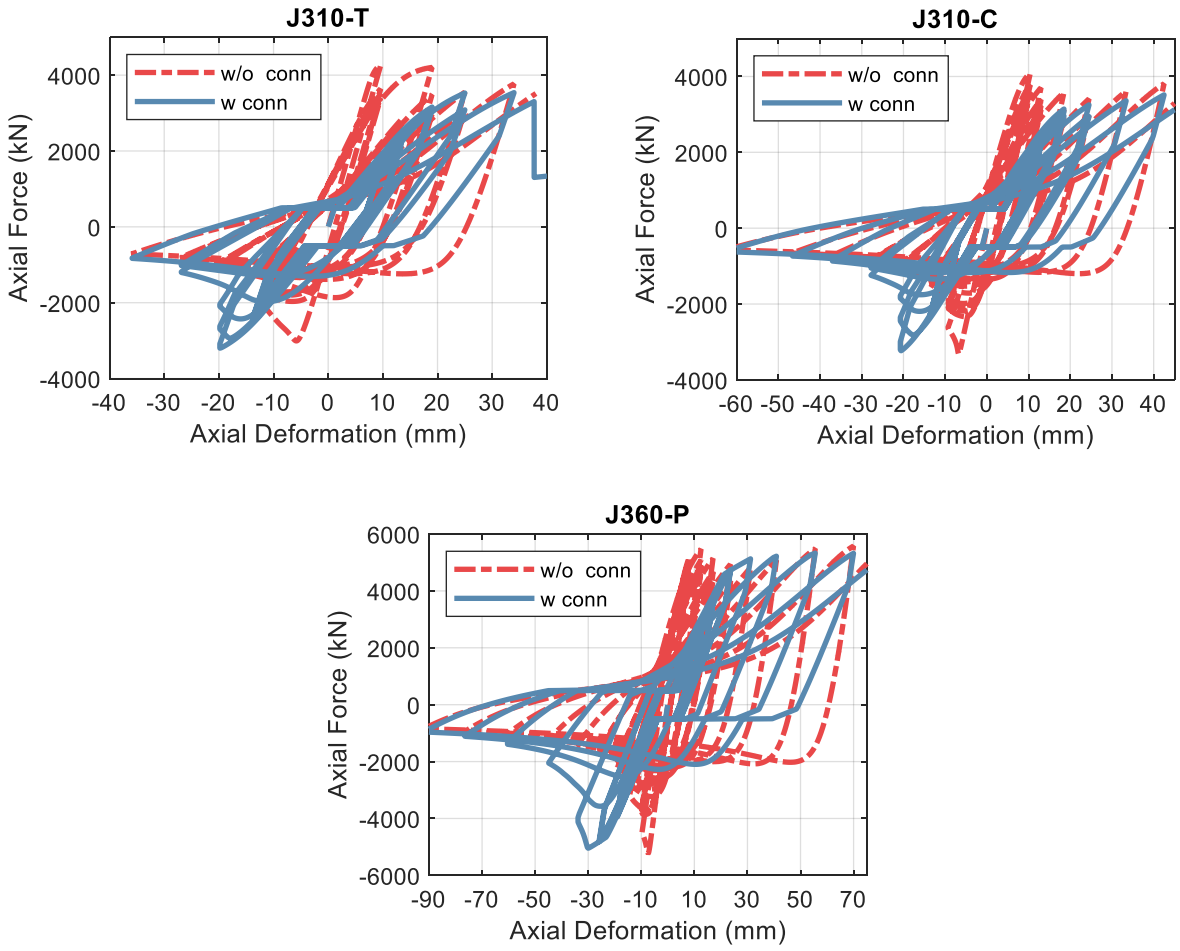

Figure 5.10: Response comparison between models with (w) and without (w/o) the brace connections

The behaviour of the bolted brace connections significantly affected the response of the brace and brace connection assembly. Firstly, the axial stiffness of the assembly was noticeably reduced with the incorporation of the brace connections. Secondly, as explained in Section 5.3.6, the tensile strength of the assembly was usually controlled by the tensile strength of the brace connections in CCBFs. Without modelling the brace connections, the tensile strength of the brace controlled, which resulted in a greater tensile strength for the assembly. Thirdly, significant axial deformation occurred in the bolted brace connections, including slip, bolt hole elongation, and deformation of other components, which substantially affected the force-deformation hysteresis of the assembly. When loaded under compression, the abrupt strength loss due to brace buckling occurred at a much

larger deformation level when the brace connections were modeled. When loaded under tension, the assemblies developed much higher strength at small deformation levels when the brace connection deformation was not accounted for. Moreover, whenever the load was reversed, the slip in the bolted brace connections, which increased in magnitude over the course of the loading protocol due to bolt hole elongation, resulted in a plateau in the axial force-deformation response and pinched hysteresis loops. This was not captured when the brace connections were not modelled.

5.4. CASE STUDY

To study the effect of brace connection behaviour on the seismic response of CCBFs, eight archetype buildings located in areas of different seismic hazard levels in Canada were designed and analyzed. Two brace connection strength levels and two beam orientations were considered. The validated component-based modelling approach described in Section 5.3 was adopted for all the brace connection modelling in the analyses.

5.4.1. Archetype building design

Eight single-storey buildings with CCBF seismic systems were designed. The building dimensions and building plans with different beam orientations are shown in Figure 5.11. A two-bay symmetric diagonal bracing configuration, with braces connected at the top end of the middle column, was adopted for the CCBF. For one-storey CCBFs with such bracing configuration, the braces will not impose large forces on other structural members under the elastic structural response, and economical design can usually be achieved. Loading was applied to the buildings in the EW direction. They are located either on a site class E (soft soil) in Vancouver, BC, representing regions of high seismic hazard, or on a site class C (firm ground) in Montreal, QC,

representing regions of moderate seismic hazard. Other design parameters including loads, load combinations, and structural materials, are listed in Table 5.1.

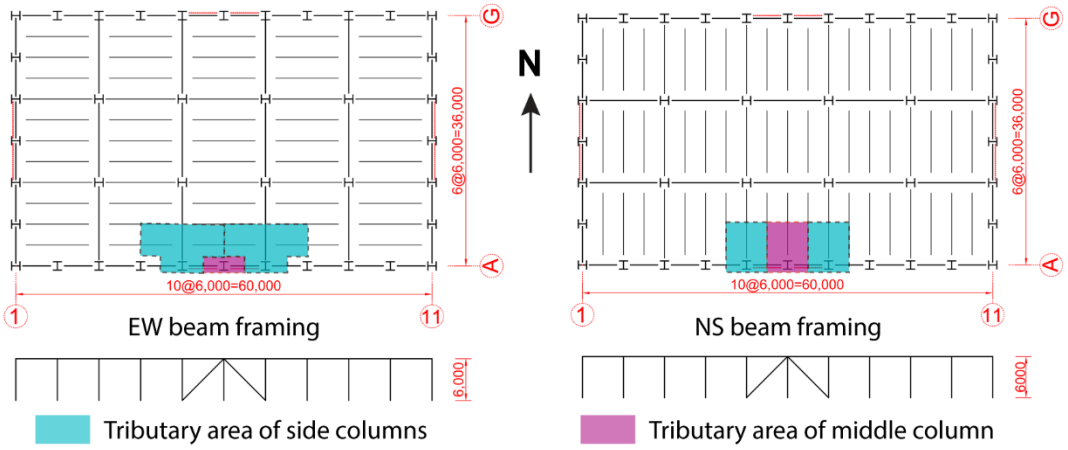

Figure 5.11: Building plans with different secondary beam orientations (dimensions in mm)

Table 5.1: Building design parameters

Loads	Roof dead load: 0.98 kPa Roof live load: 1 kPa Wall: 4.94 kPa Snow load: 1.64 kPa (Vancouver) and 2.48 kPa (Montreal)
Load combinations	1.4D 1.25D+1.5L+1.0S 1.25D+1.0L+1.5S 1.0 E+1.0D+0.5L+0.25S
Structural materials	W sections: A572 Grade 50 Plates: A572 Grade 50 Bolts: A490/A325 Welds: E49

The CCBFs were designed following the Equivalent Lateral Force Procedure with the design base shear calculated as per the National Building Code of Canada (NBCC) [38]. The required strengths

for structural components and connections were subsequently determined through a linear elastic structural analysis without consideration of the capacity-based design principle. The two adjacent braces were assumed to equally resist the seismic load and their contribution to resist gravity loads was not considered. It is worth mentioning that the unbalanced force resulting from brace buckling was not accounted for in the linear elastic structural analysis. The columns (both the middle column and side columns) were only designed to carry gravity loads. The orientation of the secondary beams in the East-West direction (referred to as the EW orientation) resulted in a larger tributary area for the middle column and a smaller tributary area for the side columns compared to the NS orientation (Figure 5.11), which resulted in stronger middle columns and weaker side columns (EW orientation).

Table 5.2: Studied archetype buildings and design of CCBFs

CCBF ID	Location	Site Class	Secondary Beam Orientation	Brace Connection Strengthening (%)	Brace	Beam	Middle Column	Side Column
VE-EW-100	Vancouver	E	EW	100	W250×73	W310×28	W150×18	W200×36
VE-EW-150	Vancouver	E	EW	150	W250×73	W310×28	W150×18	W200×36
VE-NS-100	Vancouver	E	NS	100	W250×73	W360×33	W130×28	W130×28
VE-NS-150	Vancouver	E	NS	150	W250×73	W360×33	W130×28	W130×28
MC-EW-100	Montreal	C	EW	100	W200×52	W250×18	W100×19	W200×42
MC-EW-150	Montreal	C	EW	150	W200×52	W250×18	W100×19	W200×42
MC-NS-100	Montreal	C	NS	100	W200×52	W360×33	W150×30	W150×30
MC-NS-150	Montreal	C	NS	150	W200×52	W360×33	W150×30	W150×30

The archetype building matrix and the design results of CCBFs are listed in Table 5.2. With regard to the CCBF ID, the first term indicates the location and site class of the building, with VE meaning Vancouver and site class E, and MC meaning Montreal and site class C; the second term denotes

the secondary beam orientation; and the last term represents different brace connection designs, which will be described further in the next section.

5.4.2. Brace connection design

Two brace connection designs were studied: one based on the seismic force demand obtained through the linear elastic structural analysis, the other based on the force demand amplified by 1.5. Such variation was intended to evaluate the different specifications for the brace connection design force in different seismic codes. In the USA and Europe, there is no seismic design force amplification requirement for brace connections in CCBFs (i.e. the R=3 CBF in ASCE/SEI 7-16 [2] and the DCL CBF in Eurocode 8 [3]). In contrast, in Canada, the seismic design forces of brace connections are required to be amplified by 150% for CCBFs (i.e. the Type CC CBF in CSA S16 [1]), if the brace connections are not shown to be ductile. In the CCBF ID listed in Table 5.2, the terms "100" and "150" indicate the brace connection designs based on the normal force demand (i.e. 100%) and the 1.5-times amplified force demand (i.e. 150%), respectively.

Table 5.3: Design of brace connections

CCBF ID	Design Force (kN)	Bolt				FLP		WLP		Gusset		Weld	
		Grade	Size	n_F	n_W	t	w	t	w	t	w*	D	L
VE-EW-100	974	A490	16	8	2	12	150	10	110	10	392	8	100
VE-NS-100	974	A490	16	8	2	12	150	10	110	10	392	8	100
MC-EW-100	427	A325	20	4	1	10	120	10	60	8	295	6	60
MC-NS-100	427	A325	20	4	1	10	120	10	60	8	295	6	60

Note: dimensions in mm; n_F = number of bolts in the flange branch; n_W = number of bolts in the web branch; t = thickness; w = width; D = fillet weld size; L = weld length

*Whitmore width

As shown in Figure 5.2, the flange plate brace connection consists of two force paths, namely, the flange branch and the web branch. In design practice, engineers usually assume that the ratio of

the force in the flanges to the force in the web is equal to the ratio of the brace flange area to the brace web area. This assumption was adopted in the brace connection design in this study to allow the design to match the procedures commonly used in practice. The design results of the brace connections that were designed based on the non-amplified design forces are listed in Table 5.3. The modelling of the brace connections that were designed based on the 1.5-times amplified design forces was achieved by multiplying the stiffnesses and strengths of the corresponding non-strengthened ones by 1.5.

5.4.3. OpenSees modeling of CBFs

All studied CCBFs were modeled in OpenSees (Figure 5.12). Both the in-plane and out-of-plane degrees of freedom were considered for all nodes to account for the possible out-of-plane deformation of structural members. The braces, brace connections and gusset plates were modelled following the validated approach described in Sections 5.3.4 to 5.3.6. The expected material strengths (the expected yield strength, R_yF_y, and the expected tensile strength, R_tF_u) calculated as per AISC 341-16 [39], were used to define the material properties and to calculate the material related parameters. Similar to the modelling of the braces, the beams and columns were also modeled using ten displacement-based beam-column elements with five Integration Points. The fiber-based section, with 10 fibers along the flange width/web height and 4 fibers through the flange thickness/web thickness, was assigned to each element. The Steel02 material was used for the braces, beams and columns, with the same parameters as those specified in Section 5.3.6, except that the yield strength was set as the expected yield strength (R_yF_y) calculated in accordance with AISC 341-16 [39]. For the columns, an initial out-of-straightness imperfection of 1/1000 the member length following a half sine wave distribution was introduced about the minor axis. The columns were pin connected to the foundation. Two types of beam-column connections exist in

the CBF, one with gusset plates, the other without. For beam-column connections without the gusset plate, a spring with the force-deformation hysteretic model proposed by Liu and Astaneh-Asl [40] was used to model the rotational behaviour. The rotational hysteretic behaviour reported by Stoakes and Fahnestock [41] was adopted to define the rotational spring for the beam-gusset-column connection. The seismic masses (calculated based on the load combination 1.0D+0.25S) tributary to the studied CBF, i.e. placed on half of the plan view of the building, were applied at the top end of the two side columns. To account for the gravity loads and the vertical dynamic effect, the tributary gravity masses (calculated based on the load combination 1.0D+0.5L+0.25S) were applied at the top end of the three CBF columns, and a constant gravity acceleration was imposed throughout each dynamic analysis. Rayleigh damping of 2% was assigned to the first two modes of vibration of the structure.

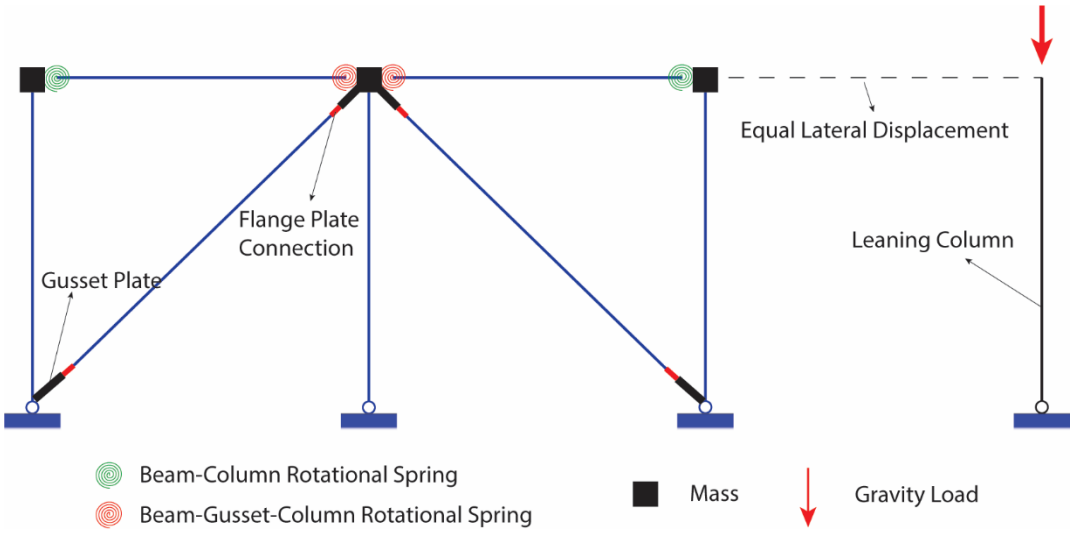

Figure 5.12: OpenSees model of CCBFs

In recognition of the lateral support for the beam provided by the steel roof deck or roof joists, beam deformations were confined to the CBF plane in the model. Moreover, to account for the global P-delta effect, an elastic leaning column was incorporated in the model. The leaning column

was pinned at the base and horizontally linked to the CBF at the roof level. The gravity load on half of the building (plan view), subtracting the portion directly resisted by the CBF, calculated based on the load combination 1.0D+0.5L+0.25S, was applied at the top of the leaning column throughout the analyses.

5.5. NONLINEAR STATIC ANALYSES (PUSHOVER)

The nonlinear static (Pushover) analyses of the archetype building CCBFs were first conducted to gain insight on the structural behaviour and limit state progression under seismic loading. All the CCBFs were pushed laterally at the roof level until significant lateral resistance loss. The base shear-storey drift curves are shown in Figure 5.13, with limit state progression marked along the loading process. The title of the sub-figure (e.g. "VE-EW") corresponds to the first two parts of the CCBF ID listed in Table 5.2, and the legend ("100" or "150") corresponds to the third part.

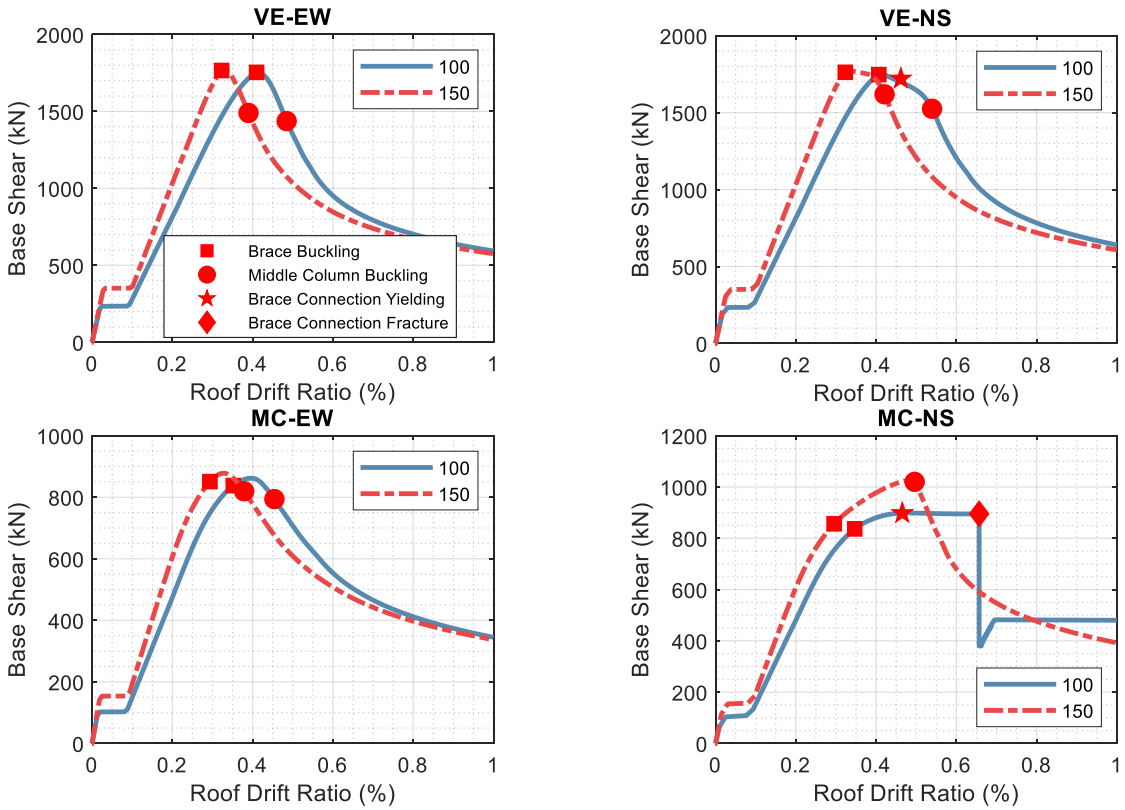

Figure 5.13: Roof drift-base shear curves of Pushover analyses

5.5.1. Limit state identification

The studied single-storey CCBFs followed similar limit state progression patterns to that shown in Figure 5.14. At the start of lateral loading, the two braces worked elastically (one in tension, the other in compression). As the lateral load increased, frictional slippage occurred in the bolted brace connections, resulting in a plateau in the base shear-storey drift curves. With increased lateral force, the compression brace buckled, resulting in a rapid and pronounced deterioration of its compressive strength. A significant unbalanced force was subsequently imposed on the middle column by the post-buckling force in the compression brace and the force in the adjacent tension brace. As the lateral drift increased, the force in the tension brace increased, as did the unbalanced force on the middle column. Depending on the brace connection strength, yielding can occur in the tension brace connections at this stage. As the middle column was only designed to resist gravity loads, the unbalanced force triggered the buckling of the middle column in most cases, except for MC-NS-100. In the MC-NS-100 model, yielding concentrated in the tension brace connections, where fracture eventually occurred.

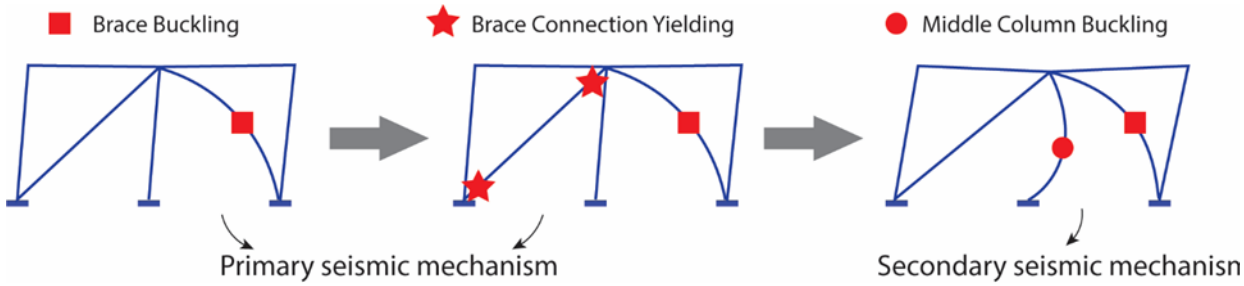

Figure 5.14: Progression of limit states to secondary seismic mechanism

After the middle column buckled, the lateral resistance of the studied CCBFs deteriorated substantially. However, as the lateral drift continued, the stable reserve lateral resistance was attained through the secondary seismic mechanism. In this mechanism, the tension brace and the

adjoining column and beam worked as a rigid body, and the buckled brace and middle column provided support for the rigid body. Therefore, the failure of the local components may not result in the overall system failure of CCBFs, as secondary seismic mechanisms may form to provide lateral resistance. This phenomenon has also been demonstrated experimentally and numerically in previous studies on CCBFs by Simpson & Mahin [42] and Sizemore et al. [9].

5.5.2. Effect of brace connections

The plateaus in the base shear-storey drift curves in Figure 5.13 resulted from the frictional slippage in the bolted brace connections. Stronger brace connections resulted in connection slippage at higher frictional force levels, indicating the higher frictional energy-dissipating capacity under cyclic loadings. After slippage occurred, the structures with stronger brace connections exhibited larger structural lateral stiffness and developed brace buckling at lower storey drifts compared to their counterparts with relatively weaker brace connections. In the case of MC-NS-100 (Figure 5.13), the yielding of the brace connection in tension resulted in a substantial loss in lateral stiffness of the structure, and notably affected the continued increase of lateral strength, as compared to MC-NS-150.

Moreover, stronger brace connections always triggered buckling of the middle column at smaller storey drifts. As explained by Wang et al. [12], the brace connection is the weakest compared to the adjoining brace and gusset plate in terms of tensile strength in CCBFs. As such, the brace connection determines the possible maximum force that is transferred by the braces to the middle column. After the compression brace buckles, a stronger brace connection imposes a larger unbalanced force on the middle column than a weaker brace connection at the same storey drift, which can trigger earlier middle column buckling.

5.5.3. Effect of beam orientation

Figure 5.13 shows that the CCBFs designed for buildings with the NS secondary beam orientation maintained their primary lateral resistance to larger storey drifts compared to the corresponding CCBFs of buildings with the EW secondary beam orientation. As discussed in Section 5.5.1, the buckling of the middle column resulted in significant structural lateral strength deterioration, which indicated the beginning of the secondary seismic mechanism. The stronger middle columns associated with the NS secondary beam orientation helped the structure maintain the primary seismic mechanism by delaying or eliminating buckling of the middle column.

5.6. NONLINEAR RESPONSE HISTORY ANALYSES (NRHAS)

5.6.1. Selection and scaling of ground motion (GM) records

The ground motion (GM) records were selected and scaled to be representative of the seismotectonic environment and the geotechnical conditions at the location of the building. The selection and scaling were conducted following the guidelines provided in the NBCC [38], with reference to a target response spectrum corresponding to a probability of exceedance of 2% in 50 years (a return period of 2475 years). For buildings in Montreal, eleven GMs, divided into two suites (listed in Table 5.4) to cover the range of periods that contribute significantly to the seismic response of the building, were selected. Due to the absence of recorded GM data for this region of the country, simulated GM time histories were used [43]. For buildings in Vancouver, three suites of five GM records (listed in Table 5.5) were selected and scaled to represent the three seismic sources for this region—shallow crustal, subduction interface and subduction intra-slab earthquakes. The notation “S1G1” is used to denote GM 1 in suite 1, and so on. The mean response spectra of the individual suites and the corresponding targeted response spectra are shown in Figure 5.15.

Table 5.4: Ground motions for building in Montreal

ID.	Event Name	Magnitude	Distance (km)	Class Site	Scale Factor
S1G1	M6c2-1	6.0	24.8	C	1.55
S1G2	M6c1-1	6.0	17.0	C	0.80
S1G3	M6c2-1	6.0	25.6	C	1.49
S1G4	M6c2-8	6.0	26.1	C	1.78
S1G5	M6c2-1	6.0	25.6	C	1.51
S2G1	M7c2-4	7.0	50.3	C	1.63
S2G2	M7c2-1	7.0	47.8	C	1.50
S2G3	M7c2-6	7.0	62.6	C	2.15
S2G4	M7c2-8	7.0	69.9	C	1.92
S2G5	M7c2-3	7.0	45.2	C	0.93
S2G6	M7c2-1	7.0	41.6	C	1.19

Note: All the listed are simulated ground motion records from the source Engineering Seismology Toolbox of Canada (https://www.seismotoolbox.ca/index.html).

Table 5.5: Ground motions for building in Vancouver

ID.	Event Name	Magnitude	Record Station	Distance (km)	Class Site	Scale Factor
S1G1	Superstition Hills-02	6.5	Imperial Valley Wildlife Liquefaction Array	23.85	E	1.80
S1G2	Superstition Hills-02	6.5	Kornbloom Road (temp)	18.48	D	3.55
S1G3	Loma Prieta	6.9	Hollister Differential Array	24.82	D	1.70
S1G4	Darfield_ New Zealand	7.0	Christchurch Resthaven	19.48	E	1.50
S1G5	Victoria_ Mexico	6.3	Chihuahua	18.96	D	2.80
S2G1	Japan, Geiyo	6.8	IYO	47	D	1.94
S2G2	El Salvador,	7.7	San Miguel	109	D	3.76
S2G3	Japan, Geiyo	6.8	TOHWA	56	D	1.58
S2G4	El Salvador,	7.7	Armenia	90.48	E	0.81
S2G5	El Salvador,	7.7	Ahuachapán	137	D	2.26
S3G1	Japan, Tohoku	9.1	KYONAN	227	E	1.91
S3G2	Japan, Tohoku	9.1	MISAKI	190	E	2.13
S3G3	Japan, Tohoku	9.1	INAGE	179	D	1.99
S3G4	Japan, Tohoku	9.1	URAYASU	186	E	1.93
S3G5	Japan, Tohoku	9.1	TSUGAWA	203	D	3.29

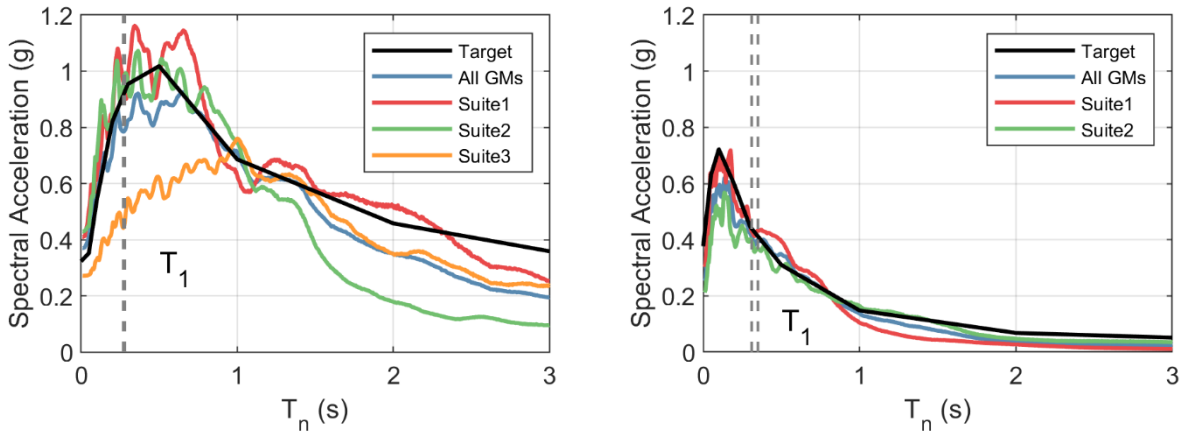

Figure 5.15: Mean response spectrum of GMs and target response spectrum: (a) Vancouver Site Class E; (b) Montreal Site Class C

5.6.2. Dynamic responses under selected ground motion

The nonlinear response history dynamic analyses showed that all buildings in Montreal exhibited low levels of maximum storey drifts and maintained their primary seismic mechanism under all selected GMs. In contrast, the CCBF systems for buildings in Vancouver developed the secondary seismic mechanism under some GMs. The responses of the VE-EW-100 and VE-EW-150 under GM S1G3 are representative of the seismic responses with the secondary seismic mechanism, which are shown in Figures 5.16 and 5.17, respectively. The storey drift response history, the base shear, and the response of each component were presented. It is noted that the axial deformation of the brace connection in Figures 5.16 and 5.17 referred to the total value of the two brace connections in one bay.

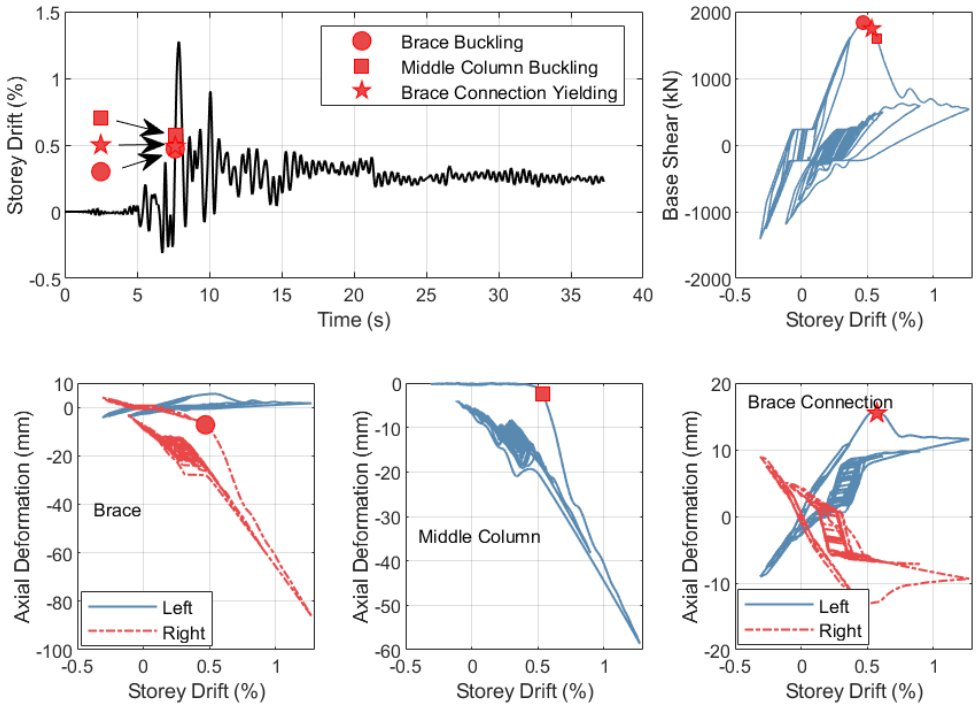

Figure 5.16: Seismic response of VE-EW-100 under S1G3

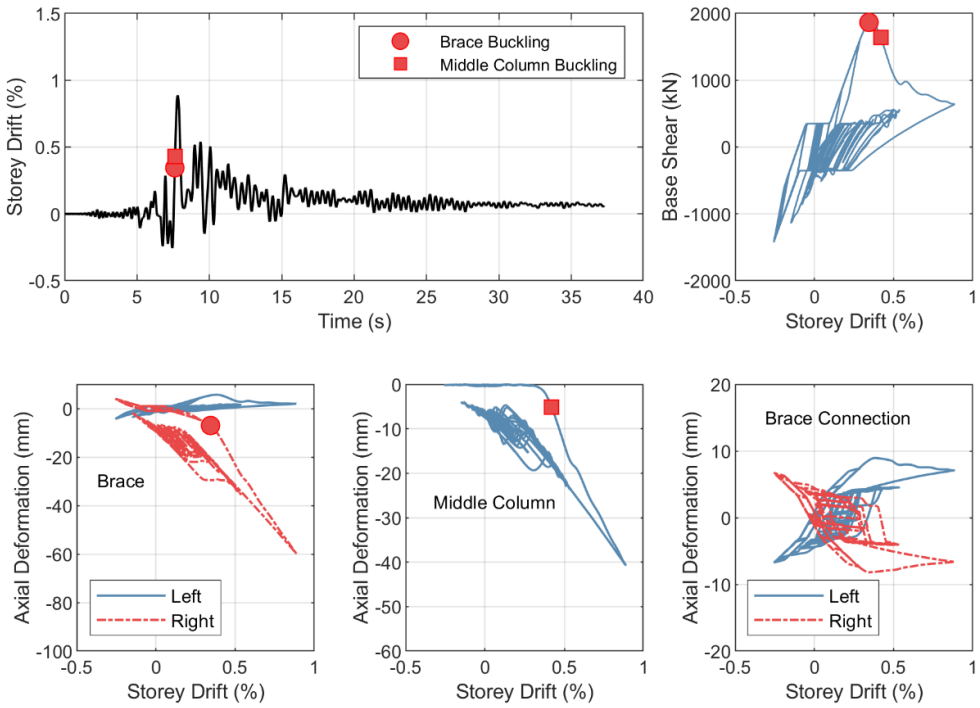

Figure 5.17: Seismic response of VE-EW-150 under S1G3

During the first 7.5 s of the GM shaking, both the CBFs remained elastic and cyclic frictional slippage occurred in the bolted brace connections. As the brace connection frictional resistance in VE-EW-150 is higher than in VE-EW-100, the plateaus in the base shear-storey drift curve were at higher base shear levels, which resulted in higher energy dissipation. Starting at the time of around 7.5 s, there was a large monotonic increase in the storey drift in the right direction. During this large storey drift excursion, the compression brace in the right bay buckled. As the storey drift increased further, the post-buckling resistance of the compression brace decreased and the force in the tension brace increased. As such, the axial compression force imposed on the middle column increased.

It is noted that before the middle column buckled, yielding occurred in the tension brace connections of the VE-EW-100. The maximum tensile deformation of the two brace connections in the left bay reached 15.6 mm, which was 2.82 times more than that of the tension brace, 5.5 mm. Even though all brace connections in the VE-EW-150 remained elastic throughout the analysis, the maximum tensile deformation of the two brace connections (8.9 mm) in the left bay was 1.56 times more than that of the brace (5.7 mm).

As the axial compression force increased, the middle columns in the two systems buckled. The base shear subsequently dropped substantially. However, structural instability did not occur as lateral resistance was provided through the secondary seismic mechanism, in which the unbuckled brace and the adjoining column and beam worked elastically as a rigid body, and the buckled brace and middle column provided support for the rigid body.

5.6.3. Maximum storey drift

The maximum storey drift ratios under individual GMs are plotted in Figure 5.18, with the mean value denoted by the dashed line for each CCBF. The CCBFs in Vancouver exhibited higher levels of maximum storey drifts than those in Montreal. For Vancouver, the maximum storey drifts were still quite low, with the maximum of 1.36% in VE-EW-100 under GM S1G3, compared to the NBCC limit of 2.5%. No structural instability occurred, indicating the satisfactory collapse-preventing performance of the single-storey CCBFs in both Montreal and Vancouver. Stronger brace connections led to smaller maximum storey drifts in most cases. This is believed to be attributed to the higher frictional energy-dissipation capacity of the stronger brace connections.

Compared with CCBFs with the EW secondary beam orientation, CCBFs designed with the NS secondary beam orientation exhibited lower maximum storey drifts. This is because stronger middle columns delayed the buckling of themselves and enabled the CCBF to maintain the primary lateral resistance until relatively larger storey drifts. The result indicated the potential of preventing middle column buckling for improved seismic performance of CCBFs with the studied bracing configuration, which could be attained by designing the middle column for the unbalanced brace forces. However, more direct analyses and evidence are needed to substantiate this design recommendation.

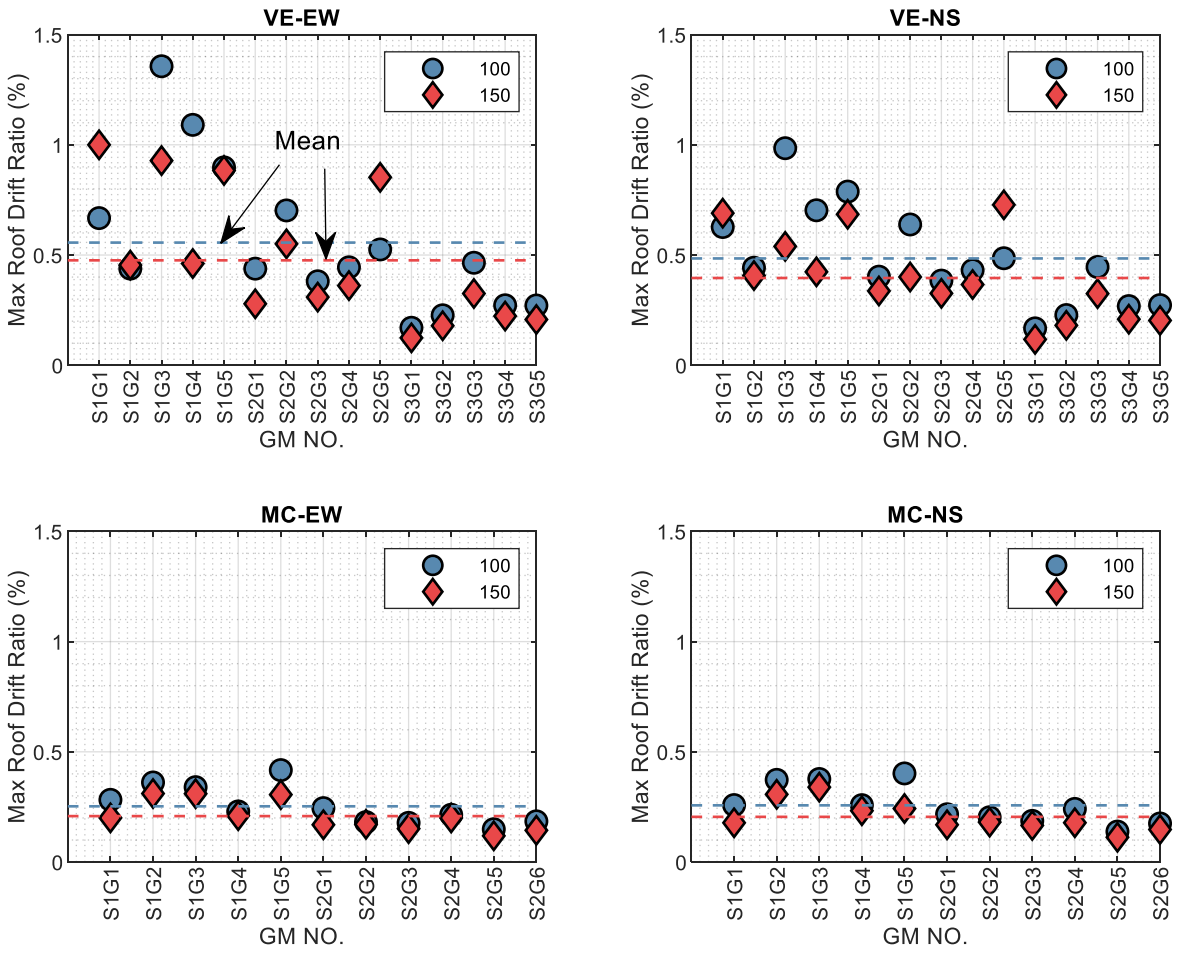

Figure 5.18: Maximum storey drifts

5.6.4. Brace connection deformation

As discussed in Section 5.6.1, when loaded in tension, the two brace connections contributed more deformation than the brace members themselves. Previous experimental studies [10,11] have witnessed the failure of brace connections designed for CCBFs. Therefore, the quantification of brace connection deformation demand is critical to establish the acceptance criteria for the brace connection ductility of CCBFs.

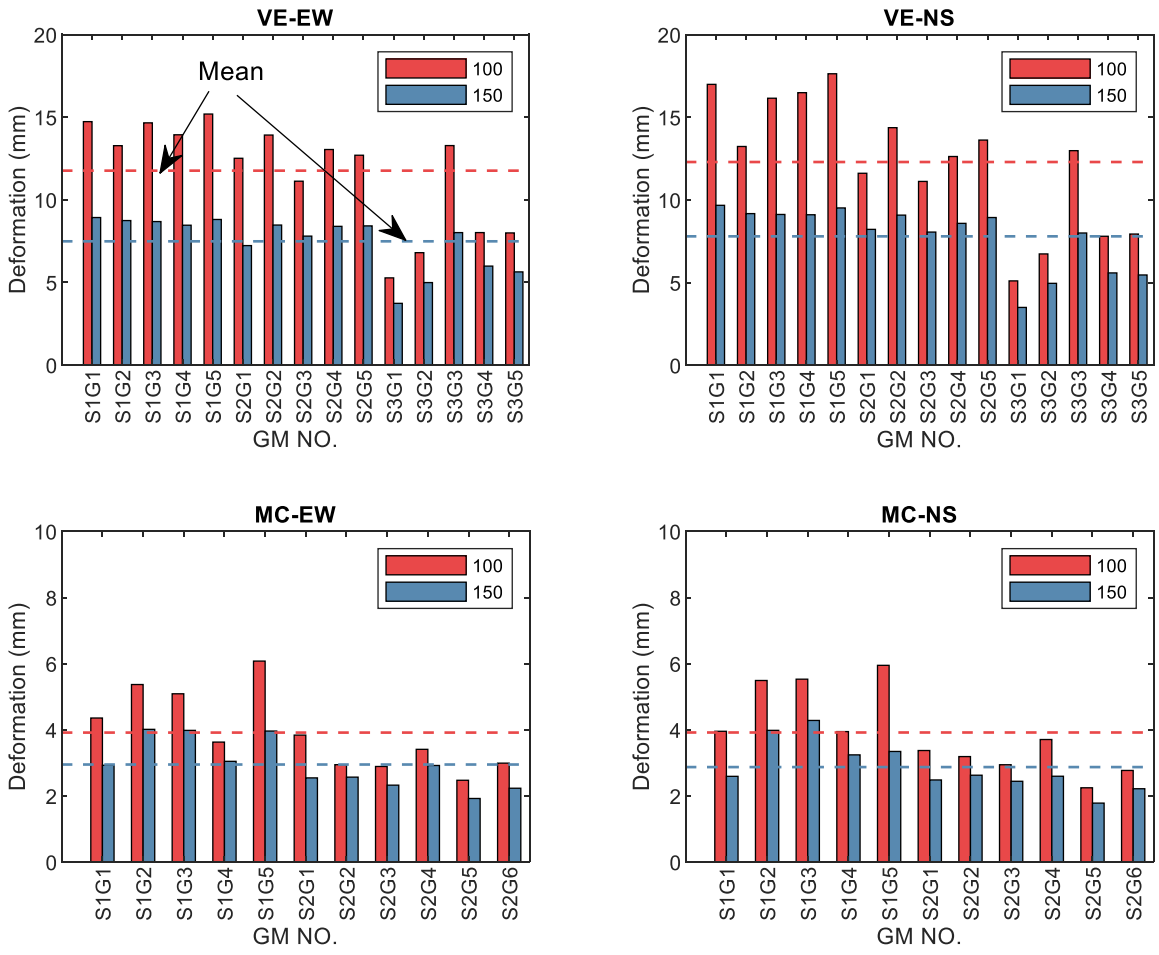

Figure 5.19: Maximum brace connection deformation

The maximum brace connection deformations under individual GMs are plotted in Figure 5.19. It is noted that the deformation amount is for only one brace connection. The brace connection deformation demands for CCBFs in Montreal were smaller than those of CCBFs in Vancouver, indicating a lower demand of brace connection ductility for CCBFs in areas of lower seismic hazard.

Strengthening of the brace connections proved to be an effective way to reduce the deformation demand on the brace connections, which justified the seismic provision for brace connection design of CCBFs in the CSA S16 Standard [1]: “the seismic design force has to be amplified by

1.5 unless the brace connection is proved to be ductile". The secondary beam orientation had a negligible effect on the brace connection deformation demand. Even though buildings with the NS secondary beam orientation exhibited lower levels of maximum storey drifts, the associated stronger middle column increased the tensile deformation demand by delaying the secondary seismic mechanism.

When interpreting the brace connection deformation demands presented in Figure 5.19, caution has to be taken as they were derived from the study on the single-storey CBFs with the symmetric diagonal bracing configuration with middle columns. Further studies are needed to quantify the brace connection deformation demand for CCBFs of different numbers of storeys and various bracing configurations, which is the topic of the ongoing research by the authors.

5.7. CONCLUSION

Brace connections in conventional CBFs (CCBFs) are expected to sustain inelastic deformations under strong earthquakes, and therefore, accurate numerical modelling of brace connections is critical for the reliable assessment of the seismic performance of CCBFs. In this paper, an efficient numerical model was proposed for the bolted flange plate brace connection by applying the component-based modelling method. The numerical model was validated to be able to capture the brace connection force-deformation hysteretic behaviour and the onset of fracture with high accuracy.

Eight single-storey CCBFs with the symmetric diagonal bracing configuration were designed and analyzed. Through the nonlinear static analyses and nonlinear dynamic analyses, the main findings are:

1. The buckling of the middle column can result in significant lateral strength deterioration. However, the secondary seismic mechanism can provide stable remaining lateral resistance to prevent global structural instability.
2. When loaded in tension, the brace connections may deform (including the slippage) much more than the brace members themselves. The brace connection deformation demand is higher in areas of high seismic hazard. Strengthening brace connections is an effective way of reducing the deformation demand.
3. Stronger brace connections will lead to greater lateral stiffness of the structure and trigger earlier buckling of middle columns.
4. Stronger brace connections possess higher frictional energy-dissipating capacity, which can reduce the maximum storey drift.
5. Stronger middle columns will reduce the maximum storey drift, but have a negligible effect on the brace connection deformation demand.

It is noted that the conclusions are only applicable to the studied single-storey CCBFs with the symmetric diagonal bracing configuration. Further research is needed for CCBFs having different bracing configurations and a larger number of storeys.

ACKNOWLEDGEMENTS

The work was funded by the Natural Sciences and Engineering Research Council of Canada (NSERC), the Fonds de recherche du Québec-Nature et technologies (FRQ-NT) and the Centre d'études interuniversitaire des structures sous charges extremes (CEISCE). The financial and technical support from DPHV Structural Consultants and ADF Group Inc. is gratefully acknowledged. Assistance with the ground motion selection and scaling from Mr. Bashar Hariri at Polytechnique Montréal is greatly appreciated. The first author is supported in part through the China

Scholarship Council (CSC). The numerical simulations were conducted on the supercomputer cluster Graham of Compute Canada, which is funded by the Canada Foundation for Innovation (CFI).

REFERENCES

[1] Canadian Standards Association (CSA) S16-19. (2019). Design of steel structures. Toronto, ON, Canada.

[2] American Society of Civil Engineers/Structural Engineering Institute (ASCE/SEI) 7-16. (2016). Minimum Design Loads and associated criteria for buildings and other structures. Reston, Virginia, USA.

[3] EN 1998-1. (2004). Eurocode 8: Design of Structures for Earthquake Resistance – Part 1: general Rules, Seismic Actions and Rules for Buildings. Brussels: European Committee for Standardization.

[4] Standards New Zealand (NZS). (2007). NZS 3404 Part 1:1997, Steel Structures Standard Incorporating Amendment No. 1 and Amendment No. 2., Wellington, NZ.

[5] Sen, A., Roeder, C., Lehman, D., Berman, J., Sloat, D., Ballard, R., & Johnson, M. (2016). Experimental evaluation of the seismic vulnerability of braces and connections in older concentrically braced frames. Journal of Structural Engineering, 142(9). doi:10.1061/(ASCE)ST.1943-541X.0001507

[6] Sen, A., Swatosh, M., Ballard, R., Sloat, D., Johnson, M., Roeder, C., Berman, J. (2017). Development and evaluation of seismic retrofit alternatives for older concentrically braced frames. Journal of Structural Engineering, 143(5), 04016232-04016232. doi:10.1061/(ASCE)ST.1943-541X.0001738

[7] Bradley, C., Fahnestock, L., Sizemore, J., & Hines, E. (2017). Full-scale cyclic testing of low-ductility concentrically braced frames. Journal of Structural Engineering, 143(6). doi:10.1061/(ASCE)ST.1943-541X.0001760

[8] Sizemore, J., Fahnestock, L., Hines, E., & Bradley, C. (2017). Parametric study of low-ductility concentrically braced frames under cyclic static loading. Journal of Structural Engineering, 20170601. doi:10.1061/(asce)st.1943-541x.0001761

[9] Sizemore, J., Fahnestock, L., & Hines, E. (2019). Seismic performance assessment of low-ductility concentrically braced frames. Journal of Structural Engineering, 145(4). doi:10.1061/(ASCE)ST.1943-541X.0002276

[10] Rudman, A., Tremblay, R., & Rogers, C. A. (2021). Conventional I-shape brace member bolted connections under seismic loading: Laboratory study. Journal of Constructional Steel Research, 184, 106795.

[11] Wang, C., González Ureña, A., Afifi, M., Rudman, A., Tremblay, R., Rogers, C. A. (2020) "Conventional construction steel braces with bearing plate energy dissipation", 17th World Conference on Earthquake Engineering, Sendai, Japan

[12] Wang, C., Rudman, A., Tremblay, R., Rogers, C.A. (2021). Numerical investigation into I-shape brace connections of conventional concentrically braced frames. Engineering Structures 236: 112091.

[13] Hsiao, P.-C., Lehman, D. E., & Roeder, C. W. (2012). Improved analytical model for special concentrically braced frames. Journal of Constructional Steel Research, 73, 80–94.

[14] Qu, B., Sanchez-Zamora, F., & Pollino, M. (2014). Mitigation of inter-story drift concentration in multi-story steel concentrically braced frames through implementation of rocking cores. Engineering structures, 70, 208-217.

[15] Qu, B., Sanchez-Zamora, F., & Pollino, M. (2015). Transforming seismic performance of deficient steel concentrically braced frames through implementation of rocking cores. Journal of Structural Engineering, 141(5), 04014139.

[16] Hsiao, P. C., Lehman, D. E., Berman, J. W., Roeder, C. W., & Powell, J. (2014). Seismic vulnerability of older braced frames. Journal of Performance of Constructed Facilities, 28(1), 108-120.

[17] Sen, A. D., Roeder, C. W., Lehman, D. E., & Berman, J. W. (2019). Nonlinear modeling of concentrically braced frames. Journal of Constructional Steel Research, 157, 103-120.

[18] Tremblay, R., & Davaran, A. (2020). Design of Bolted Single Shear Lap Connection with Different Thicknesses of Splice Plates. Journal of Structural Engineering, 146(3), 04020004.

[19] Shen, J., & Astaneh-Asl, A. (2000). Hysteresis model of bolted-angle connections. Journal of Constructional Steel Research, 54(3), 317–343. https://doi.org/10.1016/S0143-974X(99)00070-X

[20] Rassati, G. A., Noè S, & Leon, R. T. (2004). Component modeling of partially restrained composite joints under cyclic and dynamic loading. Journal of Structural Engineering, 130(2), 343–351. https://doi.org/10.1061/(ASCE)0733-9445(2004)130:2(343)

[21] Weigand, J. M. (2016). Component-based model for single-plate shear connections with pretension and pinched hysteresis. Journal of Structural Engineering, 143(2), 04016178–04016178.

[22] Rex, C. O., & Easterling, W. S. (2003). Behavior and modeling of a bolt bearing on a single plate. Journal of Structural Engineering, 129(6), 792-800. doi:10.1061/(asce)0733-9445(2003)129:6(792)

[23] Richard, R. M., & Abbott, B. J. (1975). Versatile elastic-plastic stress-strain formula. Journal of the Engineering Mechanics Division, 101(4), 511-515.

[24] Fisher, J. W., & Struik, J. H. A. (1974). Guide to design criteria for bolted and riveted joints. Wiley.

[25] Nelson, W. D., Bunin, B. L., & Hart-Smith, L. J. (1983). Critical joints in large composite aircraft structure (No. DP-7266). McDonnell Douglas Corp., Long Beach, CA.

[26] Weigand, J. M., & Berman, J. W. (2014). Integrity of steel single plate shear connections subjected to simulated column removal. Journal of Structural Engineering, 140(5), 04013114.

[27] Thomas, D. L., Wilson, J. M., & Wilson, R. R. (1973). Timoshenko beam finite elements. Journal of Sound and Vibration, 31(3), 315–330. https://doi.org/10.1016/S0022-460X(73)80276-7

[28] Weigand, J. M. (2014). The integrity of steel gravity framing system connections subjected to column removal loading. Ph.D. dissertation, Univ. of Washington, Seattle.

[29] Lesik, D. F., & Kennedy, D. J. L. (1990). Ultimate strength of fillet welded connections loaded in plane. Canadian Journal of Civil Engineering, 17(1), 55-67. doi:10.1139/l90-008

[30] McKenna, F., Fenves, G. L., Scott, M. H., & Jeremić, B. (2000). Open system for earthquake engineering simulation (http://opensees.berkeley.edu)

[31] Filippou, F. C., Popov, E. P., & Bertero, V. V. (1983). Effects of bond deterioration on hysteretic behavior of reinforced concrete joints. University of California Press, Berkeley, CA

[32] Wallaert, J. J., & Fisher, J. W. (1964). Shear strength of high-strength bolts. Fritz Laboratory Reports. 1822. https://preserve.lehigh.edu/engr-civil-environmental-fritz-lab-reports/1822

[33] Karamanci, E., & Lignos, D. G. (2014). Computational approach for collapse assessment of concentrically braced frames in seismic regions. Journal of Structural Engineering, 140(8), A4014019.

[34] Rudman, A. (2018). Testing of conventional construction W-shape brace members and their bolted end connections undergoing reversed cyclic loading. Master's thesis, Department of Civil Engineering, McGill University, Montreal, QC, Canada.

[35] Mazzoni, S., McKenna, F., Scott, M. H., and Fenves, G. L. (2006). OpenSees command language manual. Pacific Earthquake Engineering Research (PEER) Center, Berkeley, CA.

[36] Uriz, P., and Mahin, S. A. (2008). Toward earthquake-resistant design of concentrically braced steel-frame structures. PEER Rep. No. 2008/08, Univ. of California, Berkeley, Berkeley, CA.

[37] Wang, C., Tremblay, R., & Rogers, C. A. (2021). Parametric study on the I-shape brace connection of conventional concentrically braced frames. Journal of Constructional Steel Research, 182, 106669.

[38] National Research Council of Canada (NRCC). (2015). National Building Code of Canada (NBCC) (13th ed.). Ottawa, ON, Canada.

[39] American Institute of Steel Construction (AISC) 341-16. (2016). Seismic Provisions for Structural Steel Buildings. Chicago, IL: American Institute of Steel Construction.

[40] Liu, J., & Astaneh-Asl, A. (2004). Moment–rotation parameters for composite shear tab connections. Journal of Structural Engineering, 130(9), 1371–1380. https://doi.org/10.1061/(ASCE)0733-9445(2004)130:9(1371)

[41] Stoakes, C. D., & Fahnestock, L. A. (2011). Cyclic flexural testing of concentrically braced frame beam-column connections. Journal of Structural Engineering, 137(7), 739–747. https://doi.org/10.1061/(ASCE)ST.1943-541X.0000326

[42] Simpson, B. G., & Mahin, S. A. (2018). Experimental and numerical evaluation of older chevron concentrically braced frames with hollow and concrete-filled braces. Journal of Structural Engineering (United States), 146(1). https://doi.org/10.1061/(ASCE)ST.1943-541X.0001988

[43] Atkinson G. (2009). Earthquake time histories compatible with the 2005 NBCC uniform hazard spectrum. Canadian Journal of Civil Engineering, 36(6):991–1000.

CHAPTER 6: SUMMARY AND CONCLUSIONS

6.1. SUMMARY

Conventional concentrically braced frames (CCBFs), designed using the conventional linear elastic method without additional seismic proportioning and detailing requirements, are widely adopted as the seismic force-resisting systems in low and moderate seismic regions. The capacity-based design method is not required for such systems, i.e. no individual component is explicitly designated to sustain plastic deformation under seismic loading. In CCBFs, brace connections are inherently weaker than the adjoining brace and gusset plate, and therefore, are critical for the seismic behaviour of the entire system. However, CCBFs and their brace connections have received little research attention, and hence, their seismic behaviour and performance are not well understood at a fundamental level. The primary objective of this research was to evaluate the seismic performance of CCBFs with I-shape braces and bolted flange plate connections, which is a common choice in design practice. This study was carried out mainly through two-level numerical simulations.

Firstly, high-fidelity finite element (FE) models were created for the bolted flange plate connections and validated through comparison with experimental test results. The force transfer mechanism within the two branches of the brace connection was characterized. Based on the validated FE modeling procedure, a parametric study was performed. Three key design parameters, namely, the gusset plate thickness, the flange lap plate thickness, and the web lap plate thickness, were varied to study their effects on both the compressive and tensile behaviour of the brace and connection assembly. Various possible failure modes were revealed both in compression and in

tension. Design recommendations were proposed with regards to preventing brittle failure and attaining better connection deformation capacity.

Secondly, to incorporate the brace connection into the system-level simulation of CCBFs, a component-based modeling method was developed for the bolted flange plate connection and validated against experimental test results. Eight prototype single-storey CCBFs with the symmetric diagonal bracing configuration were designed and modeled. Two seismic hazard levels, two brace connection seismic design force levels, and two beam orientations were considered. Nonlinear response history analyses were conducted for each prototype building subjected to a suite of ground motion records. The seismic behaviour and performance of the studied CCBFs were analyzed, and the deformation demand on the brace connections was quantified.

6.2. CONCLUSIONS

6.2.1. Seismic behaviour of the flange plate connection

- In the flange plate connection, brace axial forces are transferred from the brace to the gusset by the flange lap plates (flange branch) and the web lap plates (web branch) acting in parallel. The analyses revealed that three stages exist for the force transfer mechanism within the connecting plate zone: 1) before major bolt slippage occurs, the force is entirely transferred by means of friction resistance between all components; 2) following the first major bolt slippage, the flange lap plates start to develop their ultimate strength by bolt bearing, while the force in the web branch is still transferred by friction; and 3) not until the flange branch deforms to accommodate all bolt slippage in the web branch, will the ultimate bearing condition be attained in the web branch.

- In CCBFs, gusset plates and braces are typically chosen based on their compressive resistance, and therefore possess significant overstrength in tension. Connecting lap plates in the connections are designed for tensile resistance and, hence, the connecting plate zone is usually the weakest part compared to the gusset plate and the I-shape brace in terms of tensile strength.
- Both the flange branch and the web branch of the connecting plate zone are expected to develop their ultimate tensile strength. In order to avoid premature bolt shear rupture and weld fracture, and to develop minimum ductility, it is recommended that the bolts and welds along the flange branch be designed based on the ultimate tensile strength of this branch (most likely the ultimate tensile strength of the flange lap plates). Likewise, the bolts in the web lap plates are recommended to be designed to resist a force equal to the ultimate tensile strength of the web branch (either the ultimate tensile strength of the web lap plates or the block shear strength of the I-shape brace web or gusset plate).
- The tests and the numerical simulations revealed a non-uniform distribution of the shear forces within the bolt group connecting the flange lap plates to the brace flanges, even if the connection length is short. The ratios of maximum to minimum shear forces in the studied four specimens ranged between 1.21 and 1.23. This phenomenon may have detrimental consequences on the shear strength of the bolt group due to the 'unbuttoning response'; this effect should be taken into account in the bolt design to achieve ductile connection response.
- The study also showed that a pronounced loading eccentricity exists on the fillet welds connecting the flange lap plates to the gusset plate. As the distance between the bolts and welds of the flange lap plates is short, a significantly nonuniform stress distribution occurs between the bolt group and weld group. Although the resultant force passes through the centroid of the weld group due to symmetry, each weld leg is subjected to noticeable eccentric

loading. For design of the welds, conservatively, the magnitude of the eccentricity can be taken as the larger of the distance between the weld-to-gusset plate interface and the centerline of bolts and the distance between the weld-to-gusset plate interface and the centerline of the leg of the flange lap plates.

6.2.2. Effect of different connection parameters

- In CCBFs with I-shape braces designed in accordance with current practice, either the gusset plates or the braces can buckle when subjected to compression. For better seismic performance, it is recommended that the connection be designed such that brace buckling occurs rather than gusset plate buckling for the following reasons: a) gusset plate buckling is expected to impose larger plastic strains than brace buckling, which may lead to diminished low-cycle fatigue life for the assembly; b) gusset plate buckling is expected to occur at only one brace end due to inherent uncertainties in material and geometric properties, which will increase further inelastic deformation demand in the gusset plates.
- Flange lap plates provide end restraint for both the gusset plates and the I-shape braces when subjected to compression, yet in different ways. The flange lap plates work as stiffeners for the gusset plates while offering rotational restraint through their in-plane bending for the I-shape braces. Therefore, varying the flange lap plate thickness was found not to have an impact on the gusset buckling compressive resistance, provided that local buckling of the flange lap plates was prevented. However, for overall out-of-plane buckling of the brace, the use of thicker flange lap plates leads to shorter brace effective lengths and higher brace compressive resistances.
- The end rotational restraint for the I-shape braces as collectively provided by the gusset plates and the flange lap plates can be significant in CCBFs as there is no requirement for minimum

clearance to form a hinge zone in the gusset plates to accommodate the brace end rotation. The current design assumption that braces are pin connected can lead to significant underestimation of the brace compressive resistance, which could result in the undesirable gusset plate buckling during a seismic event. It is therefore recommended that the actual brace end conditions be considered when estimating the brace compressive buckling strength.

- The connecting plate zone is usually the weakest link along the brace-connection load path in terms of tensile resistance. Opting for a strong gusset plate design is not necessarily beneficial for the global deformation capacity because it can force plastic deformations to concentrate in the connecting plate zone. An alternative approach consisting of using thicker flange lap plates to increase the tensile resistance of the connecting plate zone will cause other components of the assembly (gusset plates or braces) to contribute more to the plastic deformation in tension, which may result in higher global deformation capacities. Therefore, it is recommended that the connecting plate zone be designed for a tensile axial load corresponding to the yield strength of either the gusset plate or the brace, whichever is lower.
- The FE simulations revealed the presence of significant transverse tensile stresses in the critical net section of the flange lap plates, which can cause an increase of the longitudinal tensile strength of these plates. The tensile overstrength ratio was derived based on the von Mises yielding criterion. It was recommended that the bolts and welds be designed based on the tensile resistance of the flange branch to avoid bolt rupture and weld fracture. It is further recommended that the derived tensile overstrength ratio should be used in the tensile resistance determination of the flange lap plates.
- Modifying the thickness of the web lap plates had no impact on the compressive behaviour of the brace-connection assembly. It may however affect its tensile response as failure may

change from block shear failure of the brace web to net section failure of the web plates when thinner web plates are sued.

6.2.3. Seismic performance of CCBFs and deformation demand on brace connections

- In the nonlinear static analyses, the studied single-storey CCBFs followed similar limit state progression patterns. After the compression brace buckled, a significant unbalanced force was imposed on the middle column by the post-buckling force in the compression brace and the force in the adjacent tension brace. As the middle column was only designed to resist the gravity load, the unbalanced force triggered the buckling of the middle column in most cases.
- The buckling of the middle column would result in a substantial loss in the structural lateral resistance. However, as the lateral drift continued, the stable reserve lateral resistance was attained through the secondary seismic mechanism. In the secondary mechanism, the tension brace and the adjoining column and beam worked as a rigid body, and the buckled brace and middle column provided support for the rigid body.
- The nonlinear response history analyses showed that all buildings in Montreal exhibited low levels of maximum storey drifts and maintained their primary seismic mechanism under all selected ground motions. In contrast, the CCBF systems for buildings in Vancouver developed the secondary seismic mechanism under some ground motions and experienced higher levels of maximum storey drifts than buildings in Montreal. Nonetheless, all studied buildings exhibited satisfactory collapse prevention performance under the hazard level corresponding to a probability of exceedance of 2% in 50 years (a return period of 2475 years).
- Stronger brace connections would trigger buckling of the middle column at smaller storey drifts. This is because the brace connection determines the maximum force that could be transferred by the braces to the middle column. After the compression brace buckles, the

stronger brace connections could impose larger unbalanced forces on the middle column than the weaker brace connections at the same storey drift. However, stronger brace connections led to smaller maximum storey drifts in the nonlinear response history analyses under most ground motions. This is believed to be attributed to the higher frictional energy-dissipation capacity of stronger brace connections.

- When loaded in tension, the two brace connections contributed much more deformation than the brace member itself. The statistics of brace connection maximum deformations revealed that the brace connection deformation demands for CCBFs in Montreal were smaller than those of CCBFs in Vancouver, indicating a lower demand of brace connection ductility for CCBFs in areas of lower seismic hazard.
- Strengthening of the brace connections proved to be an effective way to reduce the deformation demand on the brace connections, which justified the seismic provision for brace connection design of CCBFs in the CSA S16-19 (CSA, 2019): “the seismic design force has to be amplified by 1.5 unless the brace connection is proved to be ductile”.
- The studied structures with stronger middle columns exhibited lower maximum storey drifts. This is because stronger middle columns delayed their buckling and enabled the CCBFs to maintain their primary lateral resistances until relatively larger storey drifts. The result indicated the potential of preventing middle column buckling for improved seismic performance of CCBFs with the studied bracing configuration, which could be attained by designing the middle column for the unbalanced brace forces. However, more direct analyses and evidence are needed to substantiate this design recommendation.

6.3. LIMITATIONS AND SUGGESTIONS FOR FUTURE WORK

This section summarizes the limitations of this thesis and recommendations for future work, as follows:

- Significant non-uniform distribution of the shear forces within the bolt group in the flange lap plates was revealed. However, the extent of the non-uniform distribution was not quantified. Further studies are required to identify factors that might affect the bolt shear force distribution and quantify those effects so as to propose design guidelines for the bolt design.
- The flange plate connection was shown to provide notable end rotation restraint for the I-shape braces. The assumption that braces are pinned at both ends (i.e. the boundary condition coefficient K=1.0) in design will result in conservative estimates for the brace compressive capacity, which may in turn trigger detrimental gusset plate buckling. Further studies are required to quantify the end rotation restraint and develop recommended values for the boundary condition coefficient to reflect the realistic restraint.
- In this thesis, only one common brace connection configuration was studied, i.e. the bolted flange plate connection. The findings and derived design recommendations are, hence, only applicable to this connection configuration. Other brace connection configurations commonly used in practice should be studied, and separate design recommendations should be explored.
- For the study of the brace connection behaviour, only the brace and brace connections were considered. The effect of frame action, i.e. the beam-column joint opening and closing, on the brace connection was not included. Future studies including the frame action are required to simulate the realistic loading condition of brace connections. This could be conducted through experimental tests or numerical simulations of single-bay single-storey braced frames.

- The developed component-based numerical model is not capable of capturing the gusset plate buckling. Since this study revealed that in CCBFs gusset plate buckling might occur and have an entirely different response compared to brace buckling, refinement of the numerical model to incorporate gusset plate buckling is needed.
- For the component-based modelling of the bolted brace connections in the prototype building models, the response parameters were calculated based on the nominal material and geometric properties. Given the closeness of resistances of different failure modes in CCBFs, the variability in both the material and geometric properties is expected to have a significant influence on the behaviour of the brace connections, especially on the failure mode. Further studies are recommended to study the effect of the variability in the material and geometric properties through Monte Carlo simulations.
- The bolts in brace connections may sustain extensive plastic deformations and even rupture under cyclic shear loading. To the best knowledge of the author, no tests of bolts subjected to cyclic shear loading in the plastic range have been reported. Such tests are needed to characterize the behaviour of bolts under cyclic loading in the plastic range, which is needed in the component-based model to accurately define the bolt response.
- In the nonlinear numerical models of the CCBFs, the concrete floor slabs and the composite action were not modeled. In future work, the composite effect should be included in the model to reflect the realistic structural condition.
- Gravity frames in the building could provide significant lateral resistance and might have an impact on the collapse prevention performance. In future structural analyses of CCBFs, the effect of gravity frames should be properly accounted for.

- Only single-storey CCBFs with the symmetric diagonal bracing configuration were studied in this thesis. For a more comprehensive evaluation of CCBFs, prototype CCBFs having different bracing configurations and a larger number of storeys should be studied.
- The system-level behaviour of CCBFs with I-shape braces and bolted connections was only studied numerically. System-level experimental tests of such systems are needed to provide data to calibrate the numerical models.

APPENDIX A

For the modelling of steel plate bearing behaviour in OpenSees in Chapter 5, the elastic-perfectly plastic gap material was adopted, in which the bearing behaviour was simplified as bi-linear, as illustrated in Figure 5.5. An attempt was made, and presented herein, to model the steel plate bearing behaviour more accurately using the hyperbolic gap material. This material, which can reproduce the non-linear response, was adopted for all the bearing components in the bolted brace connections.

A.1 MATERIAL PROPERTY DETERMINATION BY DATA FITTING

The equation that determines the behaviour back-bone curve of the hyperbolic gap material is

$$F(x) = \frac{x}{\frac{1}{K_{max}} + R_f \frac{x}{F_{ult}}} \tag{A.1}$$

where $F(x)$ = the resistance

x = the deformation

K_{max} = initial stiffness

R_f = failure ratio

F_{ult} = ultimate (maximum) passive resistance

Under reversed cyclic loading, the parameter, K_{ur}, determines the unloading/reloading stiffness.

In this study, the unloading/reloading stiffness, K_{ur}, was set equal to the initial stiffness, K_{max}. The failure ratio, R_f, was set as 0.7. The values of K_{max} and F_{ult} were determined through data

fitting with the aim of obtaining a good match between the behaviours predicted by equation A.1 and equation 5.1. Figure A.1 shows the comparison of the bearing responses predicted by equation A.1 and equation 5.1 for different plates of the specimen J310-T and J310-C (Rudman et al., 2021). As shown, the hyperbolic gap material can yield responses that are closer to those predicted by equation 5.1, as compared to the elastic-perfectly plastic gap material.

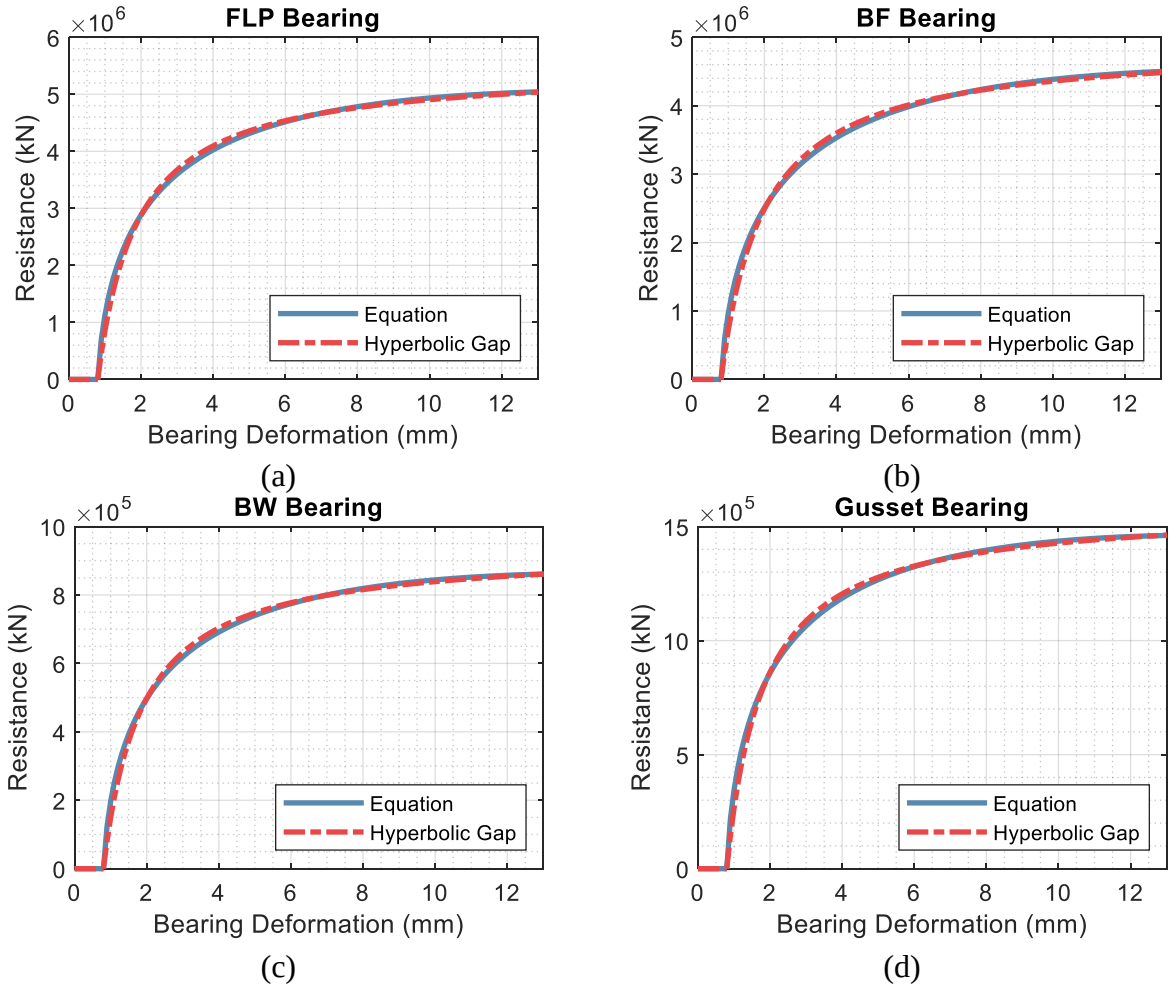

Figure A.1: Comparison between the behaviours predicted by the hyperbolic gap material (equation A.1) and equation 5.1: (a) flange lap plate (FLP) bearing; (b) brace flange (BF) bearing; (c) brace web (BW) bearing; (d) gusset plate bearing

A.2 ADOPTION OF THE HYPERBOLIC GAP MATERIAL IN THE CONNECTION MODELLING

Following the same modelling procedure described in Section 5.3.6, numerical models were constructed in OpenSees for the previously tested brace-connection assemblies, specifically, specimens J310-T and J310-C reported in Rudman et al. (2021) and the specimen J360-P reported in Wang et al. (2020). For the component-based modelling of the bolted brace connections, the same modelling technique as elaborated in Sections 5.3.4 and 5.3.5 was used, except that the hyperbolic gap material was adopted for all the bearing components. The same loading protocols as those in the experimental tests were adopted.

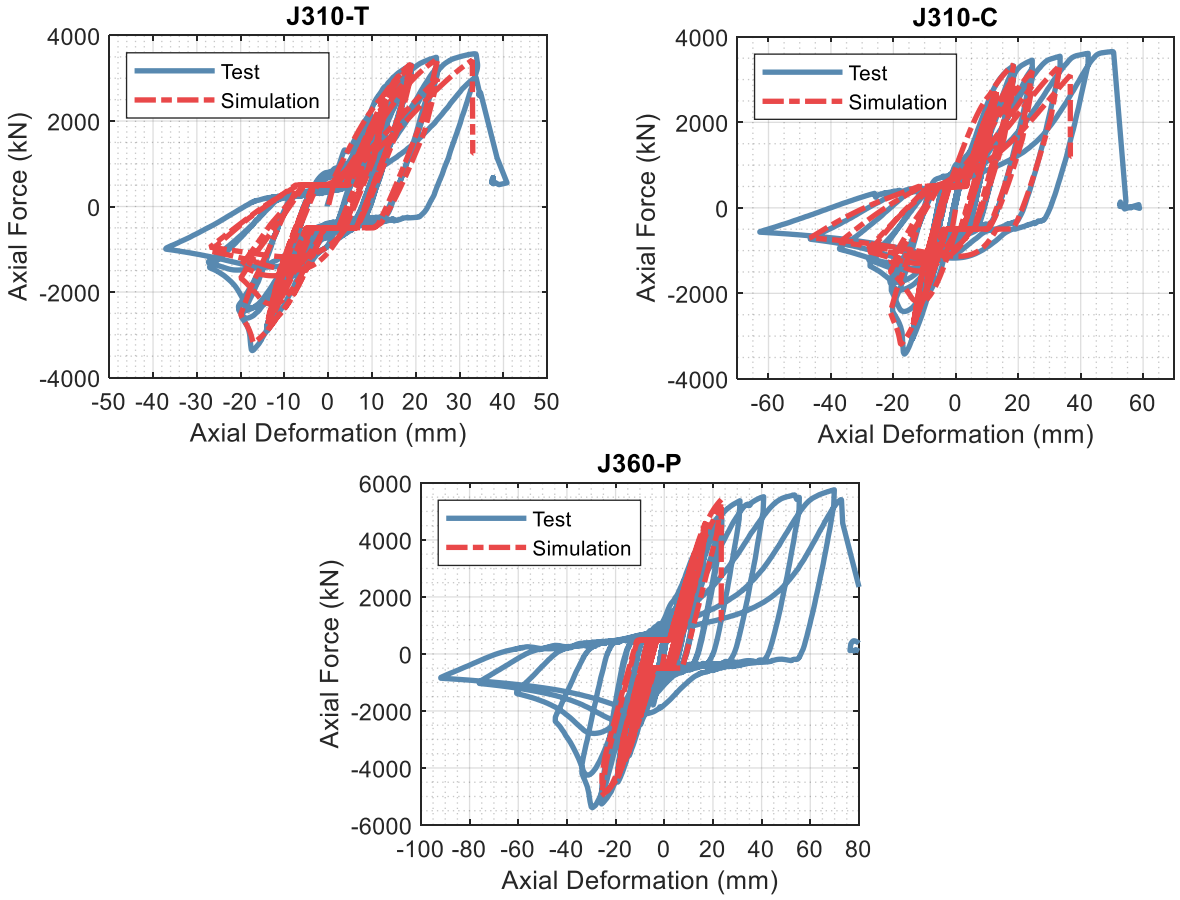

Figure A.2: Comparison of numerical and experimental axial force-deformation responses of the brace-connection assembly

In Figure A.2, the axial force-deformation responses obtained through the numerical simulations were compared with those obtained through the experimental tests. It was found that the numerical results did not match well with the experimental results.

A detailed examination of the behaviour of each element in the numerical models revealed that the mismatch originated from the result that the hyperbolic gap material did not work in the intended way. Figure A.3 shows the response of the hyperbolic gap material representing the brace flange bearing of the specimen J310-T on one side of the bolt holes, which was typical of the response of all the hyperbolic gap materials adopted in the component-based modelling of the bolted brace connections.

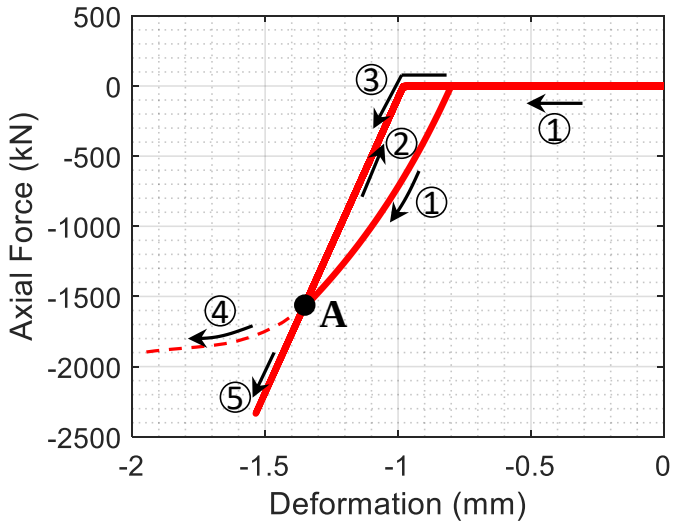

Figure A.3: Response of the hyperbolic gap material representing the brace flange bearing of the specimen J310-T

As illustrated by branch ① in Figure A.3, after the gap was closed, the bearing response followed the curve determined by equation A.1. Upon loading reversal, the unloading response was linear with the stiffness equal to K_{ur} until zero resistance was returned; see branch ②. When reloaded, the response first followed the path of the previous unloading until the point where the previous unloading started, i.e., Point A; see branch ③. However, it is noted that, beyond Point A, instead

of following the dotted curve, which is the intended response (branch ④), the response followed the extended line with the stiffness of K_{ur} (branch ⑤). The departure from the intended behaviour upon reloading resulted in the stiffer and stronger bearing behaviour, which explained the earlier rupture of bolts in the numerical responses and the mismatch between the numerical and experimental responses illustrated in Figure A.2. Further studies are needed to investigate why the hyperbolic gap material did not respond in the intended way under cyclic loading in this case.

REFERENCES

Rudman, A., Tremblay, R., & Rogers, C. A. (2021). Conventional I-shape brace member bolted connections under seismic loading: Laboratory study. Journal of Constructional Steel Research, 184, 106795.

Wang, C., González Ureña, A., Afifi, M., Rudman, A., Tremblay, R., Rogers, C. A. (2020) Conventional construction steel braces with bearing plate energy dissipation, 17th World Conference on Earthquake Engineering, Sendai, Japan

MASTER LIST OF REFERENCES

Abaqus 6.14 Documentation. (2014). Systèmes Dassault Simulia Corp., Providence, RI, USA.

Abaqus Analysis User's Guide. (2016). Systèmes Dassault Simulia Corp., Providence, RI, USA.

American Institute of Steel Construction (AISC) 341-05. (2005). Seismic Provisions for Structural Steel Buildings. Chicago, IL: American Institute of Steel Construction.

American Institute of Steel Construction (AISC) 341-10. (2010). Seismic Provisions for Structural Steel Buildings. Chicago, IL: American Institute of Steel Construction.

American Institute of Steel Construction (AISC) 341-16. (2016). Seismic Provisions for Structural Steel Buildings. Chicago, IL: American Institute of Steel Construction.

American Institute of Steel Construction (AISC) 360-16. (2016). Specification for Structural Steel Buildings. Chicago, IL, USA.

American Institute of Steel Construction (AISC). (1990). Seismic Provisions for Structural Steel Buildings. Chicago, IL: American Institute of Steel Construction.

American Society for Testing and Materials (ASTM) A370-17. (2017). Standard Test Methods and Definitions for Mechanical Testing of Steel Products. West Conshohocken, PA: ASTM International.

American Society for Testing and Materials (ASTM) A6/A6M-17. (2017). Standard Specification for General Requirements for Rolled Structural Steel Bars, Plates, Shapes, and Sheet Piling. West Conshohocken, PA: ASTM International.

American Society of Civil Engineers (ASCE). (2007). “Seismic Rehabilitation of Existing Buildings.” ASCE Standard Number ASCE/SEI 41-06, American Society of Civil Engineers, Reston, VA.

American Society of Civil Engineers (ASCE). (2016). ASCE/SEI 7-16, Minimum Design Loads and associated criteria for buildings and other structures. Reston, Virginia, USA.

Architectural Institute of Japan (AIJ). (2012). Recommendation for Design of Connections in Steel Structures. [in Japanese]

Asada, H., Sen, A. D., Li, T., Berman, J. W., Lehman, D. E., & Roeder, C. W. (2020). Seismic performance of chevron configured special concentrically braced frames with yielding beams. Earthquake Engineering & Structural Dynamics, (20200721). https://doi.org/10.1002/eqe.3320

Astaneh-Asl, A. (1986). A Report on the Behavior of Steel Structures During September 19,1985 Earthquake of Mexico. Proceedings, Annual Technical Session of Structural Stability Research Council, April.

Astaneh-Asl, A., Bolt, B., McMullin, K., Donikian, R. R., Modjtahedi, D. and Cho, S.W. (1994). Seismic performance of steel bridges during the 1994 Northridge Earthquake. Report No. UCB/CEESteel-94/01, Department of Civil Engineering, University of California, Berkeley, April.

Astaneh-Asl, A. (1998). Seismic behavior and design of gusset plates. Structural Steel Educational Council.

Astaneh-Asl, A., & Goel, S. C. (1984). Cyclic in-plane buckling of double angle bracing. Journal of Structural Engineering, 110(9), 2036-2055.

Astaneh-Asl, A., Cochran, M., & Sabelli, R. (2006). Seismic detailing of gusset plates for special concentrically braced frames. Structural steel educational council.

Astaneh-Asl, A., Goel, S. C., & Hanson, R. D. (1985). Cyclic out-of-plane buckling of double-angle bracing. Journal of structural Engineering, 111(5), 1135-1153.

Astaneh-Asl, A., Goel, S. C., and Hanson, R. D. (1982). “Cyclic behavior of double angle bracing members with end gusset plates”, Report no. UMEE 82R7, University of Michigan, Ann Arbor.

Atkinson G. (2009). Earthquake time histories compatible with the 2005 NBCC uniform hazard spectrum. Canadian Journal of Civil Engineering, 36(6):991–1000.

Bagheri Sabbagh, A., Petkovski, M., Pilakoutas, K., & Mirghaderi, R. (2013). Cyclic behaviour of bolted cold-formed steel moment connections: FE modelling including slip. Journal of Constructional Steel Research, 80, 100-108. doi:10.1016/j.jcsr.2012.09.010

Bendigo, R. A., Hansen, R. M., & Rumpf, J. L. (1963). Long bolted Joints. Journal of the Structural Division, Vol. 89, ST6.

Bradley C. R., Fahnestock L. A., Hines E. M., Sizemore J. G. (2015). Full-Scale Cyclic Testing of an Ordinary Concentrically-Braced Frame. Structures Congress 2015, Portland, OR: American Society of Civil Engineers. DOI: 10.1061/9780784479117.061.

Bradley, C. R., Fahnestock, L. A., Hines, E. M., & Sizemore, J. G. (2017). Full-Scale Cyclic Testing of Low-Ductility Concentrically Braced Frames. Journal of Structural Engineering, 143(6). doi:10.1061/(ASCE)ST.1943-541X.0001760

Brunet, F., Tremblay, R., Richard, J., & Lasby, M. (2019). Improved canadian seismic provisions for steel braced frames in heavy industrial structures. Journal of Constructional Steel Research, 153, 638-653. doi:10.1016/j.jcsr.2018.11.008

Bursi, O. S., & Jaspart, J. P. (1998). Basic issues in the finite element simulation of extended end plate connections. Computers & Structures, 69(3), 361-382. doi:10.1016/s0045-7949(98)00136-9

Callister, J. T., & Pekelnicky, R. G. (2011). Seismic evaluation of an existing low ductility braced frame building in California. In Structures Congress 2011 (pp. 2756-2767).

Canadian Standards Association (CSA) G40.20-13/G40.21-13. (2013). General requirements for rolled or welded structural quality steel/Structural quality steel. Toronto, ON: Canadian Standards Association.

Canadian Standards Association (CSA) S16-19. (2019). Design of steel structures. Toronto, ON, Canada.

Canadian Standards Association (CSA). (1989). CSA S16. 1-M89. Steel structures for buildings—Limit states design. Rexdale, ON, Canada.

Chakrabarti, S. K., & Bjorhovde, R. F. A. (1985). Tests of Full‐Size Gusset Plate Connections. Journal of Structural Engineering, 111(3), 667-684. doi:10.1061/(ASCE)0733-9445(1985)111:3(667)

Cheng, J. J. R., Yam, M. C. H., & Hu, S. Z. (1994). Elastic buckling strength of gusset plate connections. Journal of Structural Engineering, 120(2), 538–559. https://doi.org/10.1061/(ASCE)0733-9445(1994)120:2(538)

Chu X., Sause R., Ricles J. M. (2018). Seismic collapse performance assessment of low-ductility concentrically braced frames incorporating modeling uncertainty. Proceedings of the 11th National Conference in Earthquake Engineering, Earthquake Engineering Research Institute, Los Angeles, CA.

Chu X. (2017). Probabilistic Seismic Performance Assessment of Low-Ductility Concentrically Braced Frames in East Coast U.S.. Ph.D. Dissertation. Department of Civil and Environmental Engineering, Lehigh University.

Citipitioglu, A. M., Haj-Ali, R. M., & White, D. W. (2002). Refined 3D finite element modeling of partially-restrained connections including slip. Journal of Constructional Steel Research, 58(5-8), 995-1013. doi:10.1016/s0143-974x(01)00087-6

Clark K. A. (2009). Experimental performance of multi-story X-brace systems, a thesis submitted in partial fulfillment of the MS degree. Seattle: University of Washington.

Del Gobbo, G. M., Williams, M. S., & Blakeborough, A. (2018). Seismic performance assessment of Eurocode 8-compliant concentric braced frame buildings using FEMA P-58. Engineering Structures, 155, 192-208.

Elliott, M. D., & Teh, L. H. (2019a). Whitmore Tension Section and Block Shear. Journal of Structural Engineering, 145(2), 04018250.

Elliott, M. D., & Teh, L. H. (2019b). Ultimate Tensile Resistance of Bolted Gusset Plates. Practice Periodical on Structural Design and Construction, 24(4), 04019030.

Elliott, M. D., & Teh, L. H. (2020). Bolted Gusset Plate Yielding in Special Concentrically Braced Frames. Journal of Structural Engineering, 146(4), 04020031.

EN 1993. (2005). Eurocode 3: Design of Steel Structures. Brussels: European Committee for Standardization.

EN 1998-1. (2004). Eurocode 8: Design of Structures for Earthquake Resistance – Part 1: general Rules, Seismic Actions and Rules for Buildings. Brussels: European Committee for Standardization.

Fang, C., Yam, M., Cheng, J., & Zhang, Y. (2015). Compressive strength and behaviour of gusset plate connections with single-sided splice members. Journal of Constructional Steel Research, 106, 166-183. doi:10.1016/j.jcsr.2014.12.009

Faytarouni, M., Seker, O., Akbas, B., & Shen, J. (2019). Seismic assessment of ductile concentrically braced frames with HSS bracings. Engineering Structures, 191, 401-416.

Federal Emergency Management Agency (FEMA). (2009). Quantification of building seismic performance factors. FEMA P695. Washington, DC: FEMA.

Filippou, F. C., Popov, E. P., & Bertero, V. V. (1983). Effects of bond deterioration on hysteretic behavior of reinforced concrete joints. University of California Press, Berkeley, CA

Fisher, J. W., & Kulak, G. L. (1968). Tests of bolted butt splices. Journal of the Structural Division, ASCE, Vol. 94, ST11.

Fisher, J. W., & Rumpf, J. L. (1965). Analysis of bolted butt joints. Journal of the Structural Division, ASCE, Vol. 91, ST5.

Fisher, J. W., & Struik, J. H. A. (1974). Guide to design criteria for bolted and riveted joints. Wiley.

GB50017-2017. (2017). Standards for Design of Steel Structures. Beijing, China: Ministry of Housing and Urban-Rural Development of the People's Republic of China. [in Chinese]

Goel, S., Astaneh‐Asl, A., A. M. ASCE, & Hanson, R., Members, ASCE. (1985). Cyclic out‐of‐plane buckling of double‐angle bracing. Journal of Structural Engineering, 111(5), 1135-1153. doi:10.1061/(ASCE)0733-9445(1985)111:5(1135)

Gross, J. L. (1990). "Experimental study of gusseted connections." AISC Engrg. J., (3rd Quarter), 89–97.

Hardash, S. G., & Bjorhorde, R. (1985). New design criteria for gusset plates in tension. Engineering journal, 22(2).

Herman D. (2006). Further improvements on and understanding of SCBF systems, a thesis submitted in partial fulfillment of the MS degree. Seattle: University of Washington.

Hines, E. M., M. E. Appel, and P. J. Cheever. (2009). “Collapse performance of low-ductility chevron braced steel frames in moderate seismic regions.” Eng. J. 46 (3): 149.

Hsiao, P. C., Lehman, D. E., & Roeder, C. W. (2013). A model to simulate special concentrically braced frames beyond brace fracture. Earthquake engineering & structural dynamics, 42(2), 183-200.

Hsiao, P. C., Lehman, D. E., & Roeder, C. W. (2012). Improved analytical model for special concentrically braced frames. Journal of Constructional Steel Research, 73, 80–94. https://doi.org/10.1016/j.jcsr.2012.01.010

Hu, S. Z., and Cheng, J. J. R. (1987). Compressive behavior of gusset plate connections. Structural Engineering Rep. No.153, Univ. of Alberta, Alberta, Canada.

Huns, B., Grondin, G., & Driver, R. (2006). Tension and shear block failure of bolted gusset plates. Canadian Journal of Civil Engineering, 33, 395–408.

International Conference of Building Officials (ICBO). (1988). Uniform building code, Whittier, CA.

Johnson S. (2005). Improved seismic performance of special concentrically braced frames, a thesis submitted in partial fulfillment of the MS degree. Seattle: University of Washington.

Kazemzadeh Azad, S., Topkaya, C., & Astaneh-Asl, A. (2017). Seismic behavior of concentrically braced frames designed to AISC 41 and EC 8 provisions. Journal of Constructional Steel Research, 133, 383–404. https://doi.org/10.1016/j.jcsr.2017.02.026

Koduru, S. D., & Driver, R. G. (2014). Generalized component-based model for shear tab connections. Journal of Structural Engineering, 140(2), 04013041.

Kotulka, B. A. (2007). Analysis for a design guide on gusset plates used in special concentrically braced frames, a thesis submitted in partial fulfillment of the MS degree. Seattle: University of Washington.

Kulak, G. L. (1967). The Analysis of Constructional Alloy Steel Bolted Plate Splices. Ph.D. Dissertation, Lehigh University, Bethlehem, Pennsylvania.

Kulak, G. L., Fisher, J. W., & Struik, J. H. (2001). Guide to Design Criteria for Bolted and Riveted Joints Second Edition. Chicago, IL: AISC.

Lehman, D. E., Roeder, C. W., & Herman, D. (2008). Improved Seismic Performance of Gusset Plate Connections. Journal of Structural Engineering, 134(6), 890-901. doi:10.1061/(ASCE)0733-9445(2008)134:6(890)

Lesik, D. F., & Kennedy, D. J. L. (1990). Ultimate strength of fillet welded connections loaded in plane. Canadian Journal of Civil Engineering, 17(1), 55-67. doi:10.1139/l90-008

Li, G., Dong, Z. Q., & Li, H. N. (2018). Simplified collapse-prevention evaluation for the reserve system of low-ductility steel concentrically braced frames. Journal of Structural Engineering, 144(7), 04018071.

Lignos, D. G., Chung, Y., Nagae, T., & Nakashima, M. (2011). Numerical and experimental evaluation of seismic capacity of high-rise steel buildings subjected to long duration earthquakes. Computers & Structures, 89(11-12), 959-967.

Liu, J., & Astaneh-Asl, A. (2004). Moment–rotation parameters for composite shear tab connections. Journal of Structural Engineering, 130(9), 1371–1380. https://doi.org/10.1061/(ASCE)0733-9445(2004)130:9(1371)

Lumpkin, E. J. (2009). Enhanced seismic performance of multi-story special concentrically brace frames using a balanced design procedure, a thesis submitted in partial fulfillment of the MS degree. Seattle: University of Washington.

Ma, L., & Bocchini, P. (2019). Hysteretic Model of Single-Bolted Angle Connections for Lattice Steel Towers. Journal of Engineering Mechanics, 145(8), 04019052.

McKenna, F., Fenves, G. L., Scott, M. H., & Jeremić, B. (2000). Open system for earthquake engineering simulation (http://opensees.berkeley.edu)

Miazga, G. S., & Kennedy, D. L. (1989). Behaviour of fillet welds as a function of the angle of loading. Canadian Journal of Civil Engineering, 16(4), 583-599.

Mitchell, D., Tremblay, R., Karacabeyli, E., Paultre, P., Saatcioglu, M., & Anderson, D. (2003). Seismic force modification factors for the proposed 2005 edition of the national building code of canada. Canadian Journal of Civil Engineering, 30(2), 308-327. doi:10.1139/l02-111

Motallebi, M., Lignos, D. G., & Rogers, C. A. (2018). Behaviour of stiffened extended shear tab connections under gravity induced shear force. Journal of Constructional Steel Research, 148, 336-350.

National Institute for Land and Infrastructure Management & Building Research Institute. (2015). Manual for Structural Regulations for Building Design. All Japan Official Gazette Inc. [in Japanese]

National Research Council of Canada (NRCC). (2015). National Building Code of Canada (NBCC) (13th ed.). Ottawa, ON, Canada.

Nelson, W. D., Bunin, B. L., & Hart-Smith, L. J. (1983). Critical joints in large composite aircraft structure (No. DP-7266). McDonnell Douglas Corp., Long Beach, CA.

New Zealand Standard (NZS). (2007). NZS 3404 Part 1:1997, Steel Structures Standard Incorporating Amendment No. 1 and Amendment No. 2., Wellington, NZ.

New Zealand Standard (NZS). (2004). NZS 1170.5. Structural design actions Part 5: earthquake actions – New Zealand.

Okazaki, T., Hikino, T., Kajiwara, K., & Lignos, D. G. (2013). Dynamic response of a chevron concentrically braced frame. Journal of Structural Engineering (United States), 139(4), 515–525. https://doi.org/10.1061/(ASCE)ST.1943-541X.0000679

Powell, J. A. (2010). Evaluation ofspecial concentrically braced frames for improved seismic performance and constructability, a thesis submitted in partial fulfillment of the MS degree. Seattle: University of Washington.

Prathuangsit, D., Goel, S. C., & Hanson, R. D. (1978). Axial hysteresis behavior with end restraints. Journal of the Structural Division, 104(6), 883-896.

Rabinovitch, J. S., and Cheng, J. J. R. (1993). Cyclic behaviour of steel gusset plate connections. Department of Civil and Environmental Engineering, University of Alberta, Edmonton, Alta. Structural Engineering Report no. 191.

Rassati, G. A., Noè S, & Leon, R. T. (2004). Component modeling of partially restrained composite joints under cyclic and dynamic loading. Journal of Structural Engineering, 130(2), 343–351. https://doi.org/10.1061/(ASCE)0733-9445(2004)130:2(343)

Rex, C. O., & Easterling, W. S. (2003). Behavior and modeling of a bolt bearing on a single plate. Journal of Structural Engineering, 129(6), 792-800. doi:10.1061/(asce)0733-9445(2003)129:6(792)

Richard, R. M., & Abbott, B. J. (1975). Versatile elastic-plastic stress-strain formula. Journal of the Engineering Mechanics Division, 101(4), 511-515.

Roeder, C. W., Lumpkin, E. J., & Lehman, D. E. (2011). A balanced design procedure for special concentrically braced frame connections. Journal of Constructional Steel Research, 67(11), 1760-1772. doi:10.1016/j.jcsr.2011.04.016

Rudman, A. (2018). Testing of conventional construction W-shape brace members and their bolted end connections undergoing reversed cyclic loading. Master's thesis, Department of Civil Engineering, McGill University, Montreal, QC, Canada.

Rudman, A., Tremblay, R., & Rogers, C. A. (2021). Conventional I-shape brace member bolted connections under seismic loading: Laboratory study. Journal of Constructional Steel Research, 184, 106795.

Sarraj, M. (2007). The behaviour of steel fin plate connections in fire. Ph.D. thesis. University of Sheffield.

Sen, A. D., Roeder, C. W., Lehman, D. E., Berman, J. W., Sloat, D., Ballard, R., & Johnson, M. M. (2016). Experimental evaluation of the seismic vulnerability of braces and connections in older concentrically braced frames. Journal of Structural Engineering (United States), 142(9). doi:10.1061/(ASCE)ST.1943-541X.0001507

Sen, A. D., Swatosh, M. A., Ballard, R., Sloat, D., Johnson, M. M., Roeder, C. W., Berman, J. W. (2017). Development and Evaluation of Seismic Retrofit Alternatives for Older Concentrically

Braced Frames. Journal of Structural Engineering, 143(5), 04016232. doi:10.1061/(ASCE)ST.1943-541X.0001738

Shen, J., & Astaneh-Asl, A. (2000). Hysteresis model of bolted-angle connections. Journal of Constructional Steel Research, 54(3), 317–343. https://doi.org/10.1016/S0143-974X(99)00070-X

Shen, J., Rou, W., Akbas, B., Seker, O., & Uckan, E. (2015). Near-collapse behavior of steel buildings with non-ductile concentrically braced frames. Journal of Constructional Steel Research, 113, 101-114.

Sheng, N., Yam, C. H., & Iu, V. P. (2002). Analytical investigation and the design of the compressive strength of steel gusset plate connections. Journal of Constructional Steel Research, 58(11), 1473-1493.

Simpson, B., Mahin, S. A., & Lai, J. W. (2013). Summary of Test Results for Non-Seismic Concentric Braced Frame Specimen at NEES Berkeley Laboratory. Berkeley, Ca.

Simpson, B. G., & Mahin, S. A. (2018). Experimental and numerical evaluation of older chevron concentrically braced frames with hollow and concrete-filled braces. Journal of Structural Engineering (United States), 146(1). https://doi.org/10.1061/(ASCE)ST.1943-541X.0001988

Sizemore, J. (2017). Inelastic behavior and seismic collapse prevention performance of low-ductility steel braced frames. Ph.D. dissertation, Dept. of Civil and Environmental Engineering, Univ. of Illinois at Urbana-Champaign.

Sizemore, J. G. S. M. A., Bradley, C. R. S. M. A., Fahnestock, L. A. P. D., & Hines, E. M. P. D. (2017). Parametric Study of Low-Ductility Concentrically Braced Frames under Cyclic Static Loading. Journal of Structural Engineering, 143(6). doi:10.1061/(ASCE)ST.1943-541X.0001761

Sizemore, J. G., Fahnestock, L. A., & Hines, E. M. (2019). Seismic Performance Assessment of Low-Ductility Concentrically Braced Frames. Journal of Structural Engineering, 145(4). doi:10.1061/(ASCE)ST.1943-541X.0002276

Sizemore, J. G., Fahnestock, L. A., Hines, E. M., Bradley, C. R. (2015). Full-Scale Cyclic Testing of a Low-Ductility Concentrically-Braced Frame. 8th International Conference on Behavior of Steel Structures in Seismic Areas, Shanghai, China.

Sloat, D. A. (2014). Evaluation and retrofit of non-capacity designed braced frames. M.S. thesis, Univ. of Washington, Seattle.

Stoakes, C. D. (2012). Beam-column connection flexural behavior and seismic collapse performance of concentrically braced frames. Ph.D. dissertation, Dep. of Civil Engineering, Univ. of Illinois at Urbana-Champaign, IL.

Stoakes, C. D., & Fahnestock, L. A. (2011). Cyclic flexural testing of concentrically braced frame beam-column connections. Journal of Structural Engineering, 137(7), 739-747.

Stoakes, C. D., & Fahnestock, L. A. (2012). Cyclic flexural analysis and behavior of beam-column connections with gusset plates. Journal of Constructional Steel Research, 72, 227-239.

Swanson, J. A., and R. T. Leon. (2000). Bolted steel connections: Tests on T-stub components. J. Struct. Eng. 126 (1): 50–56. https://doi.org/10 .1061/(ASCE)0733-9445(2000)126:1(50).

Tan, Q., Lehman, D. E., Roeder, C. W., Berman, J. W., Sen, A. D., & Wu, B. (2021). Design-parameter study on seismic performance of chevron-configured SCBFs with yielding beams. Journal of Constructional Steel Research, 179, 106561.

Thomas, D. L., Wilson, J. M., & Wilson, R. R. (1973). Timoshenko beam finite elements. Journal of Sound and Vibration, 31(3), 315–330. https://doi.org/10.1016/S0022-460X(73)80276-7

Thornton, W. A. (1984). Bracing connections for heavy construction. Engineering Journal, 21(3), 139-148.

Tousignant, K., & Packer, J. A. (2017). Numerical Investigation of Fillet Welds in HSS-to-Rigid End-Plate Connections. Journal of Structural Engineering, 143(12). doi:10.1061/(asce)st.1943-541x.0001889

Tremblay, R., Filiatrault, A., Bruneau, M., Nakashima, M., Prion, H., & DeVall, R. (1996). Seismic design of steel buildings: Lessons from the 1995 hyogo-ken nanbu earthquake. Canadian Journal of Civil Engineering, 23(3), 727-756. doi:10.1139/l96-885

Tremblay, R., Filiatrault, A., Timler, P., & Bruneau, M. (1995). Performance of steel structures during the 1994 northridge earthquake. Canadian Journal of Civil Engineering, 22(2), 338-360. doi:10.1139/l95-046

Walbridge, S., Grondin, G., & Cheng, J. (2005). Gusset plate connections under monotonic and cyclic loading. Canadian Journal of Civil Engineering, 32(5), 981-995. doi:10.1139/l05-045

Wallaert, J. J., & Fisher, J. W. (1964). Shear strength of high-strength bolts. Fritz Laboratory Reports. 1822. https://preserve.lehigh.edu/engr-civil-environmental-fritz-lab-reports/1822

Wang, C., González Ureña, A., Afifi, M., Rudman, A., Tremblay, R., Rogers, C. A. (2020) Conventional construction steel braces with bearing plate energy dissipation, 17th World Conference on Earthquake Engineering, Sendai, Japan

Wang, C., Rudman, A., Tremblay, R., & Rogers, C. A. (2021). Numerical investigation into I-shape brace connections of conventional concentrically braced frames. Engineering Structures, 236, 112091.

Wang, M., Shi, Y., Wang, Y., & Shi, G. (2013). Numerical study on seismic behaviors of steel frame end-plate connections. Journal of Constructional Steel Research, 90, 140-152. doi:10.1016/j.jcsr.2013.07.033

Weigand, J. M. (2014). The integrity of steel gravity framing system connections subjected to column removal loading. Ph.D. dissertation, Univ. of Washington, Seattle.

Weigand, J. M. (2016). Component-based model for single-plate shear connections with pretension and pinched hysteresis. Journal of Structural Engineering, 143(2), 04016178–04016178. https://doi.org/10.1061/(ASCE)ST.1943-541X.0001662

Wen, R., Akbas, B., & Shen, J. (2013). Practical moment–rotation relations of steel shear tab connections. Journal of Constructional Steel Research, 88, 296-308.

Whitmore, R. E. (1952). Experimental investigation of stresses in gusset plates. MS thesis, Univ. of Tennessee, Knoxville, Tenn.

Yam, M. C. H., & Cheng, J. J. R. (2002). Behavior and design of gusset plate connections in compression. Journal of Constructional Steel Research, 58(5), 1143–1159. https://doi.org/10.1016/S0143-974X(01)00103-1

Yam, M. C. H., and Cheng, J. J. R. (1993). Experimental investigation of the compressive behavior of gusset plate connections. Struct. Eng. Rep. No.194, Univ. of Alberta, Alberta, Canada.

Yam, M., & Cheng, J. (2002). Behavior and design of gusset plate connections in compression. Journal of Constructional Steel Research, 58(5), 1143-1159. doi:10.1016/S0143-974X(01)00103-1

Yu, H., Burgess, I. W., Davison, J. B., & Plank, R. J. (2009). Experimental investigation of the behaviour of fin plate connections in fire. Journal of Constructional Steel Research, 65(3), 723-736.